Semiconductor technology for detection of DNA methylation based biomarkers in early screening of cancer

by

Melpomeni Kalofonou

October 2013

A thesis submitted for
the degree of Doctor of Philosophy of Imperial College London

Department of Electrical and Electronic Engineering
Imperial College of Science, Technology and Medicine

Declaration of Originality

I hereby declare that this thesis and the work described is my own and that everything else is appropriately referenced and attributed.

Copyright Declaration

The copyright of this thesis rests with the author and is made available under a Creative Commons Attribution Non-Commercial No Derivatives licence. Researchers are free to copy, distribute or transmit the thesis on the condition that they attribute it, that they do not use it for commercial purposes and that they do not alter, transform or build upon it. For any reuse or redistribution, researchers must make clear to others the licence terms of this work.

Abstract

The role of DNA methylation based biomarkers in several stages of cancer development is a rapidly advancing area of research. The aberrancies on the methylation profile of gene promoters play a critical role in gene silencing, thus contributing in different phases of tumour initiation, progression and recurrence, also associated with predicting the response to chemotherapeutic agents, therefore leading to a better assessment of the clinical effectiveness of cancer therapies and so of better prognosis. The need for detection of DNA methylation has become one of the most important assays in early cancer screening.

This work introduces the use of semiconductor technology for detection of DNA methylation based biomarkers in CMOS for early screening of cancer using the Ion-Sensitive Field-Effect Transistor (ISFET). This enables label-free detection of DNA methylation in gene markers of interest associated with tumour development in different organs, ultimately enabling a Point-of-Care (PoC) system for early cancer diagnosis. Towards this goal, we introduce the concept of ratiometric detection using the "Methylation Cell" which allows continuous computation of the DNA methylation ratio. This was demonstrated through a Lab-on-Chip (LoC) system using low power current-mode translinear circuits fabricated in unmodified CMOS.

Complementary to this, a novel implementation of the "Gilbert Gain Cell" integrated with ISFET sensors was proposed, referred to as the ISFET based Chemical Gilbert Cell, a current-mode circuit for differential reaction monitoring of pH signals derived from DNA methylation reactions. The Cell achieves elimination of common non-idealities of ISFETs such as drift reduction and temperature variations, while achieving gain tunability.

Contents

1 Introduction **4**

1.1 Motivation 4

1.2 Technological vision 7

1.3 Research objectives 8

1.4 Overview 9

1.4.1 Epigenetics and DNA methylation in cancer 9

1.4.2 The Ion-Sensitive Field-Effect Transistor 10

1.4.3 DNA methylation detection using ISFETs 10

1.4.4 An analogue ratiometric method for DNA methylation detection . . 11

1.4.5 A current-mode approach for differential DNA methylation detection 11

1.4.6 Conclusion 12

2 Epigenetics and DNA methylation in cancer **15**

2.1 Introduction 15

2.2 Epigenetics in cancer 18

2.3 DNA methylation 19

2.3.1 Gene methylation in cancer 22

2.4 Methods for DNA methylation detection 27

2.4.1 Restriction enzyme based methods 28
2.4.2 Affinity based methods 30
2.4.3 Sodium bisulfite based methods 30
2.5 DNA methylation ratio in DNA methylation computational analysis 33
2.5.1 Other approaches for DNA methylation detection 36
2.6 Summary 40

3 The Ion-Sensitive Field-Effect Transistor 54

3.1 Introduction 55
3.2 Solid-state chemical sensing 55
3.3 Label-free DNA detection in CMOS 58
3.4 The Ion-Sensitive Field-Effect Transistor (ISFET) 60
3.4.1 ISFET operation 61
3.4.2 pH sensitivity 63
3.5 ISFETs fabricated in CMOS 67
3.5.1 Device characteristics in weak inversion 69
3.5.2 Non-ideal effects 72
3.6 Summary 73

4 DNA methylation detection using ISFETs 79

4.1 Introduction 79
4.2 DNA base pair incorporation detection 81
4.3 DNA methylation detection using pH-PCR 84
4.3.1 Materials and Methods 85
4.3.2 Results 97

4.4 DNA methylation detection using pH-LAMP 101
4.4.1 Materials and Methods 102
4.4.2 Results 106
4.5 Summary 111

5 An analogue ratiometric method for DNA methylation detection 117
5.1 Introduction 117
5.2 The translinear principle 120
5.2.1 The translinear "Methylation Cell" 122
5.3 Simulation results 126
5.4 Fabricated system 128
5.5 Measured results 131
5.5.1 Measured results using epoxy encapsulation 132
5.5.2 Measured results on Lab-on-Chip set-up 137
5.5.3 Validation based on real methylated data 141
5.6 Summary 145

6 A current-mode approach for differential DNA methylation detection 150
6.1 Introduction 150
6.2 Differential CMOS ISFET topologies 152
6.2.1 Voltage-mode topologies 153
6.2.2 Current-mode topologies 157
6.3 Gilbert Gain Cell 159
6.4 Chemical Gilbert Cell 161
6.4.1 Simulation results 163

6.5 Fabricated system 166
6.6 Measured results 166
6.6.1 DC characteristics 168
6.6.2 pH change 170
6.6.3 Tunable gain 172
6.6.4 Drift 177
6.6.5 Power consumption 179
6.6.6 Temperature stability 179
6.7 Summary 182

7 Conclusion **189**
7.1 Contributions 190
7.2 Recommendations for Future Work 191
7.2.1 Large scale arrays for DNA methylation detection 192
7.2.2 Clinical validation of the system 192
7.2.3 ISFET based Chemical Gilbert Cell arrays 193

A Publications arising from this thesis **194**

B Fabricated Chips **196**

C CMOS ISFET Experimental set-up **198**

D The multichannel pH-sensing SoC platform **203**

E DNA based methods **204**

F Encapsulation Procedures **206**

G Supplementary Material **207**

G.1 Chemical Gilbert Cell: Supplementary Experiments 207

G.2 Ratiometric method: Supplementary Experiments 209

G.2.1 Voltage-mode switching 209

G.2.2 I_{ratio} computation during pH 7-9 211

List of Figures

1.1 The future scene of a closed-loop strategy towards cancer management using semiconductors for DNA methylation detection. 6

1.2 Future technological vision for early cancer screening 7

2.1 Epigenetic changes are influenced by both environmental stimuli and genetic changes. This means that our phenotype is determined by our genotype, the genetic information we are carrying, and our epigenotype, all the inherited and acquired epigenetic changes. In case of cancer development, disruptions in both genetic and epigenetic mechanisms occur, with DNA methylation, a key epigenetic modification, to play an important role in detection strategies of cancer. The fact that DNA methylation changes, associated with a primary tumour source, can be detected in blood circulation makes it a very attractive cancer biomarker [9–11]. 16

2.2 DNA methylation disruptions in promoter gene regions in the cases of a normal cell (top) and a cancer cell (bottom). A CpG island of a promoter region of a tumour suppressor gene in a normal cell and a cancer cell is represented, with hypermethylation or aberrant DNA methylation patterns to change the molecular environment of the cell leading to gene silencing. Figure adapted from [6]. 20

2.3 DNA methylation: It is the addition of a methyl group, CH_3, to the 5th position of the cytosine ring, C. 21

2.4 Principles for DNA methylation analysis and detection. Figure obtained and adapted from [42]. 29

2.5 The principle behind bisulfite conversion: DNA strands are chemically treated with sodium bisulfite so that unmethylated cytosines are converted to uracils whereas methylated cytosines remain unaltered and preserved through chain extension. Through bisulfite conversion, DNA is modified in a methylation-dependent way before amplification of the selected loci starts and so DNA methylation information is not erased, letting specific genetic regions be examined for their levels of methylation. 31

3.1 Potentiometric measurement set-up using an ISE 57

3.2 The Ion-Sensitive Field-Effect Transistor (ISFET) 60

3.3 Shift in the I_D-V_{GS} characteristic for variable pH 62

3.4 Site-binding model at a SiO_2-solution interface. Figure adapted from [22]. . 64

3.5 Charge and potential distribution of electrolyte-insulator (SiO_2) interface. The ionic distribution on the surface of the ISFET together with the formation of the Helmholtz plane and the Gouy-Chapman layer is illustrated. . . 65

3.6 ISFET behavioural macromodel [29] 67

3.7 (a) CMOS ISFET structure, (b) behavioural macromodel. 68

3.8 ISFET I_DV_{GS} characteristics (left) and transconductance (right) at pH 7, with the operational range of weak inversion to be highlighted. 70

3.9 CMOS ISFET behavioural macromodel [49] 71

4.1 Biochemical mechanism for H^+ release following nucleotide incorporation. Figure obtained and adapted from [6]. 81

4.2 ISFETs can be used as pH sensors to detect methylated DNA (M) and distinguish it from unmethylated DNA (U) due to the presence of hydrogen ions (H^+) resulting from an extension reaction taking place in the presence of methylated DNA. For this to happen, the process of *bisulfite conversion* (method explained in Section 2.4, Chapter 2) is applied, which differentiates M from U. DNA strands are treated with sodium bisulfite so that methylated cytosines remain preserved through a DNA chain extension reaction whereas unmethylated cytosines are converted to uracils. This is a methylation dependent pre-amplification modification that is applied to the targeted genetic areas so that DNA methylation information is kept unaltered throughout the process. 82

4.3 Map of pUC19. Visible are the areas of antibiotic resistance (Ap^R, where Ap stands for the antibiotic Ampicillin), the origin of plasmid replication (*ori*) and the multiple cloning sites including the actual coding sequence (*lac*) [14, 21]. Restriction sites are also shown in bold and regular font. . . . 86

4.4 Forward and reverse primers designed to amplify the target DNA fragment of methylated pUC19 plasmid DNA using PCR and pH-PCR. 91

4.5 Synthesis of a 322-bp fragment of pUC19 DNA used for the demonstration of the initial steps of a PCR reaction which includes *denaturation* of the DNA template, *hybridisation* of the primers on the DNA template, also referred to as the *annealing* step, followed by *elongation* of the DNA template with the aid of the DNA polymerase enzyme and of dNTPs, a step also called *DNA extension* or *DNA replication*. The figure shows the sequence of events during 2 PCR cycles which is continued in Fig. 4.6 for the completion of 3 cycles. 93

4.6 Continuation of Fig. 4.5 resulting in the accumulation of the resulting 322-bp DNA template, while the PCR amplification exponentially continues. 94

4.7 Map of pUC19. The location of amplification by the methylation-specific primer pair $p19.F6/p19.R6$, Table 4.2, which performs a 100% match with the target pUC19 template is displayed together with the location for the primer pair $p19.F4/p19.R4$, Table 4.4, used for positive control, performing 100% match with the "parent" template as well. 95

4.8 DNA cleavage using the restriction enzymes $MvaI$ and $EcoRII$ on dcm^+/dcm^- pUC19. 98

4.9 Gradient PCR using the primer set $p19.F6/p19.R6$ for 6 different temperature values using pUC19 as a DNA template. The primer set $p19.F4/p19.R4$ was used as positive control. 99

4.10 Methylation-specific pH-PCR in-tube: (a) average pH drop from 3 trials of triplicates in the cases of methylated/unmethylated pUC19. Error bars are also adapted in both charts based on the standard deviation of the pH recordings, (b) results of DNA extension reaction in triplicates for methylated pUC19 DNA (M1, M2, M3) compared to no extension reactions taking place for unmethylated pUC19 DNA (U1, U2, U3). Non-Template Control (NTC) was also clear showing no contamination of the reaction. 100

4.11 Principle of LAMP method adapted from [11]. Steps 1-8 represent the starting points of LAMP amplification, with DNA synthesis starting with the primer FIP (F2+F1c) (step 1) whereby the region F2 anneals to the complementary F2c on the DNA target, initiating DNA extension, with the process to continue with the primer BIP (B2+B1c) (step 4). Primer F3 anneals to the complementary F3c targeted region, initiating strand displacement and DNA synthesis (steps 2, 3), while the 5'-3' single strand is being released (step 3), forming the first loop structure, creating a "dumbbell" shape (step 5). The cycling amplification step then starts with the structure of step 5 being used as the template for DNA synthesis, to continue with primer FIP annealing to a single strand from the 3' end of the F1 region to the F2c region (step 6, 7), creating a loop structure. Through step 8, this leads to step 9 where one more "dumbbell" shape is produced, complementary to the one of step 5 [11]. 104

4.12 ISFETs in CMOS for real-time detection of methylated DNA versus unmethylated DNA using pH-LAMP in the 3-chamber SoC with (a,i) indicating the integration of a microfluidic assembly in chambers interfacing with CMOS ISFETs and (a,ii) showing the area where CMOS ISFETs, temperature sensors, digital IO and ADCs are embedded. Image of the fabricated CMOS die in 0.35μm process on (b) indicates the 3 reaction chambers and location of ISFET sensors. 105

4.13 Methylation-specific pH-LAMP in-tube: triplicates of pH-LAMP for isothermal assays designed to detect $DAPK1_M$ (a) and $p16_M$ (b). Results of DNA chain extension reactions are shown in both (a) and (b) due to the presence of methylated DNA (M1, M2, M3). No extension reactions take place due to the presence of unmethylated DNA (U1, U2, U3). Non-template control also came clear showing no contamination or any nonspecific amplification in the reaction. A bar chart on the right hand side reveals the average pH drop from 10 trials of triplicates, in the cases of methylated DNA ($DAPK1_M$, $p16_M$) as a result of amplification happening in both DAPK1 and p16 assays. No significant pH change was detected in cases of unmethylated DNA ($DAPK1_U$, $p16_U$). Error bars are also adapted in both charts based on the standard deviation measured values of the pH recordings. 107

4.14 Real-time methylation-specific pH-LAMP on-chip together with gel electrophoresis validation for (a) DAPK1 gene and (b) p16 gene 109

4.15 Chip statistics from real-time pH-LAMP results for both assays as has been shown in Fig. 4.14 for $DAPK1$ (a) and $p16$ (b) genes. Chip statistics indicate the average differential voltage change for $DAPK1_M$ and $p16_M$ (blue) versus $DAPK1_U$ and $p16_U$ (red) respectively. Results from 7 chips are displayed for $DAPK1$ and $p16$ assays. Methylated products are inserted in Chamber 1 and unmethylated products in Chamber 3 of the SoC. Chamber 2 was used as a negative control chemical reference. 110

5.1 System level block diagram of the ratiometric computation method towards the detection of DNA methylation 119

5.2 Translinear loop consisted of four diodes 121

5.3 ISFET based translinear current divider using voltage-mode switching . . . 123

5.4 ISFET based translinear current divider using current-mode switching . . . 125

5.5 Transient response of the translinear "Methylation Cell" with voltage-mode switching 128

5.6 Translinear circuit voltage-mode switching at different incremental percentages of I_{perc} 129

5.7 Transient response of the translinear "Methylation Cell" with current-mode switching 129

5.8 Top: Microphotograph of the floorplan of the fabricated die, highlighting in black the relevant circuit area. Bottom: Magnification of the "Methylation Cell" and of the two ISFETs connected to it. 130

5.9 Single ISFET sensor with pixel dimensions. Left: Chemical sensing area of the ISFET. Right: Electrical dimensions of the gate. 131

5.10 (a) ISFET based CMOS microchip mounted and encapsulated on pcb with microfluidic assembly adapted on top. (b) Magnification of the manifold and the two microfluidic chambers. An Ag/AgCl reference electrode is passing through the chambers, creating a stable potential to the solution added in chambers. (c) ISFETs visible in both chambers integrated in the manifold area. The two chambers were spaced at 300μm from each other. 132

5.11 Measured I_D-V_{GS} sweep of a pMOS ISFET for pH buffer solutions of 4, 7 and 10 showing the relationship between the drain current, the source gate voltage and the shift in the threshold voltage for strong inversion (left) and weak inversion (right). 133

5.12 Measured transient response of the "Methylation Cell": shown are (a) variations in I_{meth} for constant I_{unmeth} resulting in I_{ratio} in (c) and (b) variations in I_{unmeth} for constant I_{meth} resulting in I_{ratio} in (d). 135

5.13 Transient response of the "Methylation Cell" illustrating the current loops between I_{ratio} and I_{meth} in (a) and between I_{ratio} and I_{unmeth} in (b) during increasing and decreasing values of I_{meth} and I_{unmeth} as shown in Fig. 5.12. 136

5.14 Measured response of I_{ratio} for varying values of I_{gain} while both I_{meth} and I_{unmeth} are set at 100nA. 137

5.15 I_{out} vs I_{ratio} during 1 pH change for I_{perc}=50nA and I_{gain}=50nA 138

5.16 I_{out} vs I_{ratio} during 1 pH change for I_{perc}=56nA and I_{gain}=100nA 138

5.17 Transient response of I_{meth} and absolute I_{ratio} during decremental pH steps 140

5.18 Average values of two repeats of I_{ratio} with respect to the range of pH values 7-9 and 5-7. The red line illustrates the average of $I_{ratio_{avg}}$ values collected from the data during decremental ascending and descending pH steps for pH 7-9 in (a) and pH 5-7 in (b) drawn as dashed lines. The best linear fit equations are displayed in both figures, with the one in (a) to overlap with the average of I_{ratio} of both ascending and descending pH values and the one in (b) to overlap with the blue line representing the response of the average values of I_{ratio} during incremental pH steps. 142

5.19 Transient response of absolute I_{ratio} of two repeats during (a) a pH step change from 8.8 to 6.8 and (b) a pH step change from 6.8 to 8.8. 143

5.20 Transient response of the current comparator I_{out} and absolute I_{ratio} of two consecutive repeats during an incremental and decremental pH step change of 6.9 to 7.9. 144

5.21 Absolute I_{ratio} and I_{out} of two repeats with respect to time, during a pH step change from 8.8 to 6.8 and a preset I_{perc} value during descending (a) and ascending (b) directions of the pH step change, followed by the values of I_{perc} for a reaction to take place (YES) or not (NO). 144

6.1 A differential ISFET/REFET measuring system [15] 153

6.2 Differential ISFET interface for measurement of sensors [20] 154

6.3 Differential circuit schematic [23] 154

6.4 A differential ISFET/REFET read-out using switched capacitors [21] 155

6.5 Schematic of the ISFET amplifier used in the differential read-out circuit [24] 156

6.6 CMOS ISFET differential read-out system architecture [22] 157

6.7 CMOS based differential ISFET/REFET read-out [17] 158

6.8 The Gilbert Gain Cell 160

6.9 The ISFET based Chemical Gilbert Gain Cell. $ISFET1$ is sensing $pH1$ generated from the reaction chamber (Ch 1) and $ISFET2$ is sensing $pH2$ generated from the buffer chamber (Ch 2). 162

6.10 Transient response of the Chemical Gilbert Cell 163

6.11 Parametric analysis on I_{gain} at 5 steps, from 1nA to 50nA 164

6.12 Temperature variation at 11 steps, from 0 °C to 100 °C 165

6.13 Monte Carlo analysis 165

6.14 Top: Microphotograph of the floorplan of the fabricated die, highlighting in black the relevant circuit area. Bottom: Magnification of the ISFET based Chemical Gilbert Cell and of the two ISFETs connected to it. 167

6.15 Single ISFET sensor with pixel dimensions. Left: Chemical sensing area of the ISFET. Right: Electrical dimensions of the gate. 167

6.16 Measured I_D-V_{GS} sweep of the two pMOS ISFETs for pH buffer solution of 7, showing the relationship between the drain current and the applied source gate voltage. 169

6.17 Transconductance with respect to source gate voltage for pH buffer solution of 7. The operational area of linear weak inversion range is highlighted. . . 169

6.18 Transient response of 15 repeats over the course of two days of the Chemical Gilbert Cell's differential output I_{out} during a pH step change from 8.15 to 6.83 for I_{gain} at 10nA. Standard deviation bars of the pH recordings are also displayed for all repeats, seconds before the pH jump and towards the end of the recording. 170

6.19 pH sensitivity of the Chemical Gilbert Cell showing the transient response of the differential output I_{out} for I_{gain}=10nA during four steps of pH change. 171

6.20 Experimental analysis on I_{gain} from 10nA to 200nA during a transient response of the Chemical Gilbert Cell's differential output I_{out} for a pH step change from 8.15 to 6.83. 3 repeats were performed per pH change. 173

6.21 Transient response of the Chemical Gilbert Cell's differential output I_{out} for different values of I_{gain} following 4 pH step changes. In both chambers a buffer of pH 7 was initially induced giving a differential output current of 0nA, followed by a step change of pH when pH buffers of 5, 6, 8 and 9 were induced. The experimental results shown are confirmed after two repeats. The average value is also displayed as a dotted line. 174

6.22 Experimental analysis on the differential output I_{out} in the range of four pH values. 175

6.23 Gain variability for four pH steps change in the range of incremental current gains. The average value of two repeats is also displayed as a dotted line. . 176

6.24 Single-ended drift I_{ISFET} in comparison to differential drift I_{out} for pH 7. Drift values are indicated for both current outputs. 177

6.25 Single-ended drift I_{ISFET} in comparison to differential drift I_{out} for pH 7 corresponding to figure indicators (1) and (3) and pH 9 corresponding to figure indicators (2) and (4). Drift values are indicated for both current outputs. 178

6.26 Temperature stability for a single ISFET in comparison to the differential output I_{out} for (a) ascending temperature from 32^{o}C to 42^{o}C and (b) descending temperature from 42^{o}C to 32^{o}C. 181

B.1 Chips fabricated during the course of this thesis. 197

C.1 Set-up for electrical characterisation of ISFETs using a glass beaker filled with pH buffer solution. 198

C.2 Instrumentation set-up for electrical characterisation of ISFETs in a buffer solution. 199

C.3 Set-up for electrical characterisation of ISFETs using a microfluidic assembly in a Lab-on-Chip set-up. 199

C.4 Temperature stability experimental set-up 200

D.1 The IC mounted on a test card (a) connected to an electronic analyser (b) [3] 203

G.1 Transient response of the Chemical Gilbert Cell's differential output I_{out} for different values of I_{gain} following 4 pH step changes. In both chambers a buffer of pH 7 was initially induced giving a differential output current of 0nA, followed by a step change of pH when pH buffers of 5, 6, 8 and 9 were induced. The experimental results shown are confirmed after three repeats. The average value is also displayed as a dotted line. 208

G.2 Transient response of the voltage output, V_{out}, of the inverter and the current output, I_{ratio}, of the translinear cell in pH 7, for varying ascending values of I_{perc} starting from 1nA up to 10nA. 209

G.3 Transient response of the voltage output, V_{out}, of the inverter and the current output, I_{ratio}, of the translinear cell in pH 7, for varying descending values of I_{perc} starting from 10nA down to 1nA. 210

G.4 Transient response of the voltage output, V_{out}, of the inverter and the current output, I_{ratio}, of the translinear cell in pH 7, while I_{meth} is electrically tuned from 10nA to 40nA and back to 10nA, for a given I_{unmeth}=10nA for an I_{gain} of 10nA. 210

List of Tables

2.1 Frequently hypermethylated genes silenced in several cancer cases 23

2.2 Detection of cancer in circulation using DNA methylation as a biomarker . 25

2.3 Comparison of commonly used DNA methylation analysis techniques 34

2.4 Comparison of main optically and electrically based DNA methylation techniques 38

3.1 Solid-state electrochemical sensing methods for DNA detection in CMOS . 59

3.2 Comparison of CMOS ISFET arrays over the last decade 69

4.1 Restriction digestion protocol set-up for validation of methylated and unmethylated pUC19 plasmid DNA using $EcoRII$ and $MvaI$ restriction enzymes. 89

4.2 Primers designed for methylated pUC19 91

4.3 Thermal cycling program for a 55-66^{o}C temperature annealing investigation 92

4.4 Primers designed for positive control for the temperature gradient PCR investigation 92

4.5 pH-PCR thermal cycling program 96

4.6 pH average values between 5 and 40 cycles of pH-PCR (3 trials) for methylated pUC19 DNA (M) vs unmethylated pUC19 DNA (U) together with resulting ΔpH and standard deviation values for both reaction mixtures. . 100

4.7 pH average values at 180s and 2100s of pH-LAMP in-tube (10 trials) for $DAPK1_M$ vs $DAPK1_U$ together with resulting ΔpH and standard deviation values for both reaction mixtures. 106

4.8 pH average values at 180s and 2100s of pH-LAMP in-tube (10 trials) for $p16_M$ vs $p16_U$ together with resulting ΔpH and standard deviation values for both reaction mixtures. 106

4.9 Average values of differential signal change, ΔV (mV), during pH-LAMP on the SoC platform (7 trials) for $DAPK1_M$ vs $DAPK1_U$ together with standard deviation values for both reaction mixtures. 111

4.10 Average values of differential signal change, ΔV (mV), during pH-LAMP on the SoC platform (7 trials) for $p16_M$ vs $p16_U$ together with standard deviation values for both reaction mixtures. 111

5.1 Cut-off point of the CMOS inverter and voltage/current output of the translinear cell 126

5.2 I_{ratio} for different I_{meth} values and I_{unmeth}=23.59±0.63(nA) 135

5.3 I_{ratio} for different I_{unmeth} values and Imeth=18.14±2.75(nA) 135

5.4 Average values with standard deviation results of I_{ratio} and I_{meth} for given I_{unmeth} values for two repeats during ascending and descending pH steps from pH 7 to pH 9 for I_{gain}=100nA. 140

5.5 Average values with standard deviation results of I_{ratio} and I_{meth} for given I_{unmeth} values for two repeats during ascending and descending pH steps from pH 5 to pH 7 for I_{gain}=100nA. 141

5.6 System properties and performance characteristics 145

6.1 ΔI_{out} for I_{gain}=$10nA$ during four pH step changes 171

6.2 Average values of three repeats of ΔI_{out} for different I_{gain} values as seen in Fig. 6.20 with standard deviation results 172

6.3 Average values of two repeats of ΔI_{out} in nA for different I_{gain} values as seen in Fig. 6.22 for each pH step 175

6.4 System properties and performance characteristics 183

G.1 Results of average and standard deviation values of two repeats of I_{ratio}, I_{meth} under given I_{unmeth} values during ascending and descending pH steps from pH 7 to pH 9 showing the effect of drift on I_{ratio}. 211

List of Abbreviations

ADC	Analog-to-Digital Converter
APC	adenomatous polyposis coli
BJT	Bipolar Junction Transistor
bp	base pair
BRCA1	breast cancer-1
CCND2	cyclin-D2
CDH1	cadherin-1
CDH13	cadherin-13
CDKN2A/p16-INK4	cyclin-dependent kinase inhibitor-2A
CDKN2B/p15-INK4B	cyclin-dependent kinase inhibitor-2B
CHARM	Comprehensive High-throughput Arrays for Relative Methylation
CHEMFET	Chemical Field-Effect Transistor
ChIP	Chromatin immunoprecipitation
CMOS	Complementary Metal-Oxide Semiconductor
COBRA	Combined Bisulfite Recognition Analysis
CpG	Cytosine-phosphodiester bond-Guanine
DAPK1	death-associated protein kinase-1
DKK1	Dickkopf-related protein-1
DMH	Differential Methylation Hybridisation
DNA	Deoxyribonucleic acid
DNMT	DNA methyltransferase
dNTP	deoxynucleotide
EnFET	Enzyme Field-Effect Transistor
ER	oestrogen receptor
ESR1	oestrogen receptor-1
ESR2	oestrogen receptor-2
GSTP1	glutathione S-transferase protein-1
HELP	HpaII tiny fragment Enrichment by Ligation-mediated PCR
IC	Integrated Circuit
IO	Input-Output
ISE	Ion-Selective Electrode
ISFET	Ion-Sensitive Field-Effect Transistor
LAMP	Loop-Mediated Isothermal Amplification

LoC	Lab-on-Chip
MeDIP	Methyl-DNA immunoprecipitation
MGMT	O^6-methylguanine-DNA methyltransferase
MLH1	mutL homologue-1
MOSFET	Metal-Oxide-Semiconductor Field-Effect Transistor
MRE-seq	Methylation-sensitive Restriction Enzyme sequencing
MS-MLPA	Methylation-Specific Multiplex Ligation dependent Amplification
MS-SNuPE	Methylation-Sensitive Single Nucleotide Primer Extension
MSP	Methylation-Specific PCR
NSCLC	Non-Small Cell Lung Cancer
OTA	Operational Amplifier
PCDH10	protocadherin-10
PCR	Polymerase Chain Reaction
PECVD	Plasma Enhanced Chemical Vapour Deposition
PoC	Point-of-Care
RARβ	retinoic acid receptor-β
RASSF1A	Ras association domain family member-1
RB1	retinoblastoma protein-1
REFET	Reference Field-Effect Transistor
RLGS	Restriction Landmark Genomic Scanning
RNA	Ribonucleic acid
SEPT9	septin-9
SNP	Single Nucleotide Polymorphism
SoC	System-on-Chip
TMS1	target of methylation-induced silencing-1
TP73	Tumor Protein P73

Dedicated to my parents, my sister and my beloved ones

Acknowledgements

First and foremost I would like to express my gratitude to my supervisor Professor Chris Toumazou, for his constantly infusing inspiration and continuous support during this research journey. He taught me the valuable skill of looking not only at the microscopic angle of a research question but also at the macroscopic and holistic view of it. It is there, where novel ideas can truly change the world. Professor Toumazou's ability to motivate and support me throughout the course of my Ph.D. has been exemplary. I am deeply honoured to have been his Ph.D. student and part of his team at the Centre for Bio-Inspired Technology at the Institute of Biomedical Engineering.

I also have to express special thanks to Dr. Pantelis Georgiou for being a continuous source of innovative ideas and insightful advice as well as an excellent motivator. From the engineering community, I would also like to thank Dr. Timothy Constandinou for being a role model in this group, always kind and supportive, to whom our group owes a lot.

From the biochemical community that played an equally important role in this work, I would like to thank Dr. Marian Rehak for all the very constructive and helpful insight during the challenges of designing the basic chemical framework for this research and Dr. Chung-Pei Ou for allowing me to learn from his knowledge and long experience in the field of biology and biochemistry, making the design of the proof-of-principle method for DNA methylation detection become real. He taught me to always be patient when biology proves how powerfully challenging it can be, proving to me that engineers can gain the skills required to become independent in a wet lab and even obtain the abilities to design protocols and investigate the secret paths of biology. I would like to thank my friend and colleague Dr. Zhaolei Lang as well for really useful advice in protocol planning in biochemistry, in acquiring lab skills and troubleshooting in my final year when the dream of developing a robust DNA methylation based platform at a higher level came true.

Moreover, I would like to express my gratitude to Ms Maria Khaleeq from the Department of Physics for her warmth, supportive aura and willingness to help in any chip-related post processing step.

Special mention must go to DNA Electronics Ltd. for broadening my horizons towards seeing my research taking a commercial orientation. I would like to thank DNAe's staff for the knowledge I gained while working with them, especially Mr. Pantelis Athanasiou for helping me merge biochemistry and electronics with microfluidics while contributing in creating a novel microfluidic platform as part of this research.

I would like to thank my dear friends and colleagues Alex, Mohammadreza, Mohamed, Peter, Pau, Mat, Yan, Yuanqi, Song, Christina, Olive, Irina, Abdul, Ian, Konstantin, Ali, Virginia, Amir, Themis, Sivylla, Orada, Tanasit and Melissa for their unique presence, support and endless discussions about mind-breaking matters and all my group from the Centre for Bio-Inspired Technology for creating a warm and maturing environment during all these years. Last but not least, Ms. Gifty Kugblenu, Ms. Wiesia Hsissen, Ms. Iza Wojcicka and Ms. Sandra Lock deserve a big thanks for always being so kind and helpful, looking after us in every step of the Ph.D.

Finally, this journey would not have reached its destination without the love, ongoing and unconditional support, encouragement and strength infusion of my family in Greece. My loving grandparents who taught me how to walk, my wonderful parents and academic pillars, who blossomed and inspired me as an individual and researcher, teaching me ethics and life principles, encouraging me to aim high both in life and in science and my beloved sister Fotini, my friend and co-pilot in life who has always been next to me, creating our unique cocoon of trust and friendship. This thesis is dedicated to you.

Chapter 1

Introduction

1.1 Motivation

We are living in an era that has experienced significant technological revolutions as well as advances in medicine and health management, improving our quality of life and giving us the opportunity to be the protagonists of a personalisation trend. Personalised technology and its applications in the world of healthcare has brought remarkable advances and novel solutions in early detection, real-time monitoring and therapy of disease, bridging the gap between the biological problem and methods for a solution.

Over the past few years, bio-inspired technology in combination with the integration of semiconductors in biomedical applications has created a fertile ground for the development of methods for offering novel solutions to these problems. These include nanofabrication of electrode based systems for neural recording with interfacing capabilities to the brain periphery [1] as well as significant advances in the field of genetic technology [2], with Point-of-Care diagnostics and on-the-spot testing to be the future of drastically effective monitoring of critical biological markers and of the personalised application of therapeutic schemes. These examples reveal that such technologies have been engineered according to the demands required for therapy and diagnosis.

Never before have we been in this unique position to be able to apply technology so effectively for treatment of disease. The biggest being the war against cancer.

Cancer, a prominent cause of death worldwide, is exponentially increasing in numbers, an observation that can be correlated with the genetic predisposition of the individual

towards the disease as well as the epigenetic inheritance passed by our ancestors and our environmental influences. Historically, the very first remark on the term *epigenetics* was given in 1939 by Conrad Waddington [3], introducing a new perspective on the classification of biological events that do not influence the genetic code and thus cannot be described by genetic principles. It was the first time a connection between genetic information and phenotype was conceived [4], allowing for further definitions of the term to be presented in the following years. Epigenetics has been established as highly influential in the activity and expression of key regulatory genes due to its role in applying heritable changes in them without altering the genetic sequences themselves [5–8].

The field of epigenetics has seen explosive interest in the last decade especially due to its powerful role in the initiation and progression of various cancer types [9, 10], being considered as a central driving force in tumour development. One of the key epigenetic factors and most common epigenetic events in the human genome, playing a critical role in the mechanisms behind the regulation of genetic functions and of gene expression is *DNA methylation*, a chemical modification that can be inherited while keeping the genetic information unaltered during cell differentiation. DNA methylation has emerged as a highly promising biomarker[1], been actively studied in multiple cancer types, with the methylation profile to be possible to distinguish tumour types and even predict the response to chemotherapeutic agents [12–15].

It has been shown by a large number of studies that disruptions in DNA methylation, in particular genetic regions known as "CpG islands" can be responsible for aberrations in key regulatory areas of genes, such as their promoter regions, leading to inappropriate gene expression and thus chromosomal instability [16]. Such changes may lead to gene silencing by forcing the switching mechanisms, responsible for normal gene expression to turn "off" instead of "on". These certain disruptions that can be the consequence of aberrancies in the methylation levels of such areas are implicated in several steps of tumour development, progression and recurrence, intricately interacting in the pathogenesis of cancer [17, 18]. This can be validated by the observation that aberrancies in DNA methylation patterns in the genome of cancer cells can exhibit abnormal transformations, leading to inactivation of tumour suppressor genes, promotion of oncogenes, deregulation of cell death, DNA repair irregularities, direct or indirect consequences of epigenetic deregulation [19].

[1] In cancer research, a *biomarker* refers to a substance or process that is indicative of the presence of signs of cancer in the body. It might be either a molecule secreted by a malignancy itself, or a specific response of the body to the presence of cancer [11].

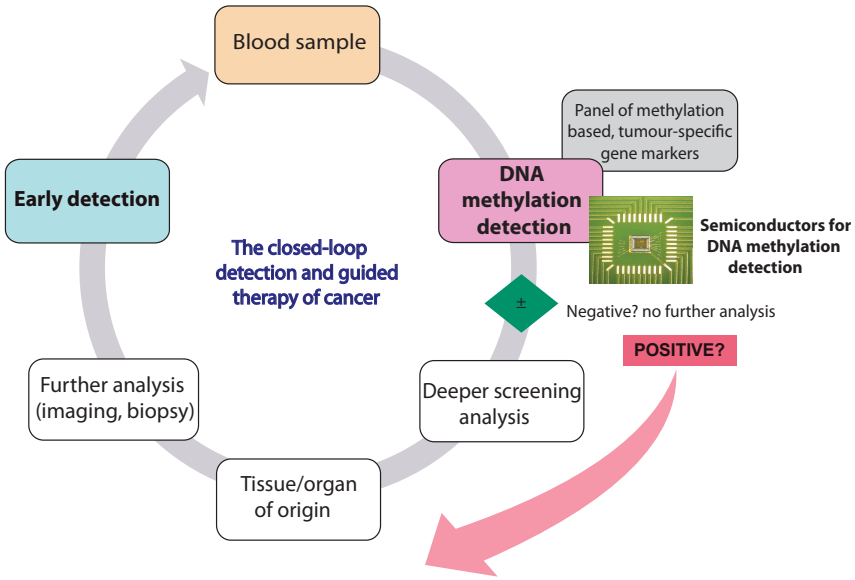


Figure 1.1: The future scene of a closed-loop strategy towards cancer management using semiconductors for DNA methylation detection.

If cancer cannot be entirely prevented, then the earlier it is detected the more the chances for an effective and well-personalised treatment to the patient, better risk assessment and thus clinical outcome [20, 21]. For certain cancer types, the patient's survival rate may drop dramatically once it is diagnosed with the current diagnostic and screening methods, leading to higher risks taken by the oncologists for a targeted treatment based on the stage of the disease progression, affecting the efficiency of the therapy as well as the patient's quality of life. Consequently, cancer early detection needs to be reshaped through the development of assays using well-studied epigenetic biomarkers, such as DNA methylation, that could offer more sensitive prediction and more accurate prognosis during the stages of cancer progression.

Since mass population early screening of cancer may still be a challenging topic for the healthcare sector, early detection systems based on semiconductor technology can be a promising approach. This could be part of a scheme whereby the epigenetic description of a tumour could provide the clinician with the initial information about the organ of origin or the stage of cancer progression through a deeper screening analysis, dependent on the DNA methylation analysis result. We may call these systems *closed-loop detection systems*, as shown in Fig. 1.1.

These systems may ultimately contribute in the monitoring process of cancer and the

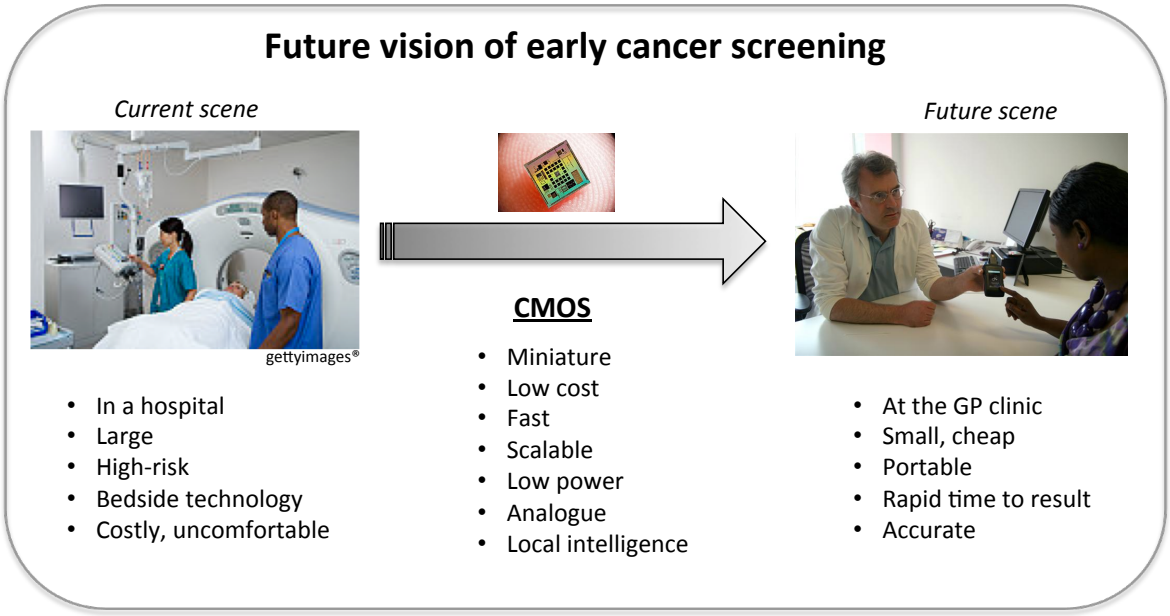


Figure 1.2: Future technological vision for early cancer screening

clinical implications behind cancer management by helping individuals keep track of their health progression regarding any malignancies that may unexpectedly arise, providing with an approach for a more precise detection of disease, better prognosis and a closer to the patient's profile therapeutic model. For that goal, developing assays that would serve that need could form an attractive territory for the new generation of early detection systems, putting semiconductor technology at the centre of attention.

1.2 Technological vision

We believe that genetic testing using DNA methylation as the biomarker for early screening of cancer will yield a more accurate result for early detection over current methods which require imaging and possible invasive intervention for diagnosis. The future vision for the work in this thesis is depicted in Fig. 1.2, whereby the screening methods of cancer would gradually converge from bulky, slow and expensive which are located in a hospital to portable, miniaturised, cheap and with local intelligence which can be made available for the GP clinic, expanding its use to a wider population.

The realisation of this vision is enabled with the use of CMOS technology which brings

the potential for miniaturisation and low cost, due to the economies of scale of silicon which over the last few decades have been following Moore's law, in addition to rapid label-free DNA detection which has proven to be feasible in under an hour [22].

With CMOS, we demonstrate the first DNA methylation detection system which enables this vision for early screening of cancer. For this, an integrated CMOS based chemical sensor is required, with the ability to be developed into a biochemical processing platform. The ISFET (Ion-Sensitive Field-Effect Transistor) is the sensor that will be used in this research, allowing a label-free approach for DNA methylation detection which can be miniaturised and give a rapid result.

Implementing in CMOS consequently has additional benefits which are explored in this thesis. We show that through utilising local intelligence on the chip, we can combine ISFET sensors and current-mode circuits to provide building blocks for large scale sensing arrays to be used in parallel detection of DNA methylation in multiple genetic targets. This will ultimately reduce the need for large data bandwidth of large scale arrays by reduction of the output of the circuit to a simple YES/NO answer, which can be defined using 1 bit of information and therefore can ultimately allow further scaling of ISFET arrays.

1.3 Research objectives

This research focuses on the application of semiconductor technology for detection of DNA methylation based biomarkers for early screening of cancer using solid state based ion sensors known as Ion-Sensitive Field-Effect Transistors (ISFETs). The aim is to develop a Lab-on-Chip (LoC) system forming a link between the CMOS based ISFET technology and a DNA methylation based platform as a first attempt to detect electrically early signs of genetic markers associated with tumour growth. This opens up a very promising area of research in the field of semiconductor technology applied in cancer screening.

This work also introduces the interaction of a specifically applied biochemical platform with an electronic interface, implemented using ISFET sensors for DNA methylation detection. The signal acquisition (pH change) obtained from the DNA samples will be the measured output of the ISFETs, whose sensed information is dependent on the instrumentation chosen for the DNA analysis. This will be designed in CMOS which utilises intelligent sensor design due to the integrative capability of ISFETs with standard well-known circuit techniques and provides the ability of real-time continuous detection and processing,

paving the way for the next generation of real-time DNA methylation specific assays for early screening and further monitoring of cancer.

The main axons to be explored in this thesis are:

- Development of a proof-of-concept method to determine and validate DNA methylation based biomarkers in genetic assays using the pH sensitive ISFET technology, with the objective to form the chemical front-end of a label-free based system for DNA methylation detection.
- Demonstration of a label-free based method for DNA methylation detection in CMOS in under an hour.
- Formation of the electrical front-end of the system using ISFETs in standard CMOS by exploiting circuit techniques to perform analogue computation in addition to enhancing the signal generated from DNA based reactions (thermocycling/isothermal reaction) and reducing the amount of data to be transmitted. Main objective here is to develop low power interfaces, avoiding common non-idealities found in ISFET sensors and in parallel by highlighting a DNA based computational path that can compute ratios of DNA methylation, which have been identified as a potential mechanism for DNA methylation analysis of heterogeneous DNA methylation profiles.
- Development of a Lab-on-Chip system which includes fully integrated chemical and electrical front-ends with real-time monitoring of input pH signals and local intelligence capable of giving a YES/NO answer based on a ratiometric detection of DNA methylation.

1.4 Overview

The structure of the thesis can be divided in the following chapters with an overview for each one presented as below:

1.4.1 Epigenetics and DNA methylation in cancer

This chapter introduces a comprehensive literature review, covering the recent developments in the field of epigenetics and specifically in their involvement in cancer, focusing on

the most common and well-studied epigenetic event, DNA methylation. The importance of DNA methylation as a powerful cancer biomarker is also highlighted as well as its role in aberrancies in genetic silencing and instability in gene expression, contributing in cancer development, emphasising on the significant role of such biomarker in early detection strategies as well as in cancer prognosis and therapy. The methylation profile of genes that show epigenetic alterations, contributing in tumorigenesis is also presented, with cases of highly methylated genes used as good examples associated with certain tumour types. Finally, the current methods and latest technological revolutions for detecting and analysing DNA methylation are presented, stating the advantages but also the limiting factors of such approaches. The chapter concludes by setting the scene for the next generation of systems for early cancer screening using CMOS based technologies for large scale, high-density DNA methylation detection.

1.4.2 The Ion-Sensitive Field-Effect Transistor

This chapter presents the fundamental elements needed for an integrated DNA base pair incorporation detection system which can be used for DNA methylation detection. A brief review of solid-state chemical sensors is introduced together with their chemical sensing mechanisms and the introduction of the Ion-Sensitive Field-Effect Transistor (ISFET), the primary sensor used in this work. The principles of operation of the ISFET sensor is described and its macromodel is shown. ISFET characteristics and the theory behind the pH sensitivity that primarily describes it as a sensor are presented. Emphasis is given on the devices' CMOS implementation which is shown to have advantages, especially in applications related to DNA detection. Specific focus is then given on the weak inversion region of operation which has been chosen for its low power and computational capability.

1.4.3 DNA methylation detection using ISFETs

This chapter presents the development of the chemical front-end of the system required for DNA methylation detection. This consists of a first proof-of-concept method of primarily determining and validating the methylation status of a DNA template and additionally using a commercially available Sentron ISFET microelectrode to detect pH changes during extension reactions of the DNA template, with known levels of methylation, as a sensitive as well as specific method for the basis of DNA methylation detection. Through this, the proof-of-concept of DNA methylation detection using ISFETs was proven. Following

on from this, the first use of ISFETs in CMOS was demonstrated in real-time using an optimised biochemical assay at isothermal conditions in a System-on-Chip (SoC) platform. This proves that DNA methylation can be detected on-chip enabling potential development of a fully integrated miniaturised system.

1.4.4 An analogue ratiometric method for DNA methylation detection

This chapter presents a ratiometric computation method that can be used for DNA methylation detection. In particular, the concept of the translinear "Methylation Cell" is introduced, using a novel ISFET based readout for the calculation of the ratio between aberrantly methylated DNA of a gene site possibly correlated to pathogenesis and to unmethylated DNA of the same gene site showing no aberrancies, therefore corresponding to the normal status of it. This circuit technique is based on the "translinear principle" to implement current division of sensed biochemical signals and aims to formulate a process of using the ratio between methylated and unmethylated DNA as an indication of the level of aberrancy of methylation existent in tumour suppressor genes of interest. Analysis of such ratiometric markers will be based upon the proportion of methylated sites presented above a pre-defined threshold value, sensed using ISFETs in standard CMOS. Further to this effort of introducing the ratiometric approach, a fabricated system consisting of both ISFET sensors and circuitry to compute the ratio is presented in a typical 0.35μm CMOS process, integrated in a Lab-on-Chip (LoC) set-up. Experimental results are presented, proving that pH changes associated with DNA methylation can be detected in CMOS and that the ratio can be computed reliably in hardware.

1.4.5 A current-mode approach for differential DNA methylation detection

In this chapter, an alternative current-mode approach was developed leading to the development of an ISFET based Chemical Gilbert Cell, capable for differential amplification of current signals originated from biochemical reactions of DNA amplification, allowing stable drift reduction of continuously recording pH signals. It also achieves gain tunability and low power consumption. The concept was designed and fabricated in a typical 0.35μm CMOS process, with both biochemical and electrical front-ends been fully integrated in a Lab-on-Chip (LoC) setup. Experimental results and analysis on the capabilities of the system follows with the advantages that such configuration can bring to applications where

ISFETs are integrated at a large scale.

1.4.6 Conclusion

Finally, concluding remarks of this thesis are summarised together with the contributions of this research. Recommendations for future work are also proposed.

References

[1] A. Jackson and J. Zimmermann, "Neural interfaces for the brain and spinal cord-restoring motor function," *Nature Reviews Neurology*, vol. 8, no. 12, pp. 690–699, 2012.

[2] D. Garner, H. Bai, P. Georgiou, T. Constandinou, S. Reed, L. Shepherd, W. Wong, K. Lim, and C. Toumazou, "A multichannel DNA SoC for rapid point-of-care gene detection," *IEEE Conference on Solid-State Circuits (ISSCC)*, pp. 492–493, 2010.

[3] C. Waddington, "An introduction to modern genetics.," *An Introduction to Modern Genetics.*, 1939.

[4] C. Waddington, "The epigenotype," *Endeavor*, vol. 1, pp. 18–20, 1942.

[5] R. Holliday, "DNA methylation and epigenetic mechanisms," *Cell Biochemistry and Biophysics*, vol. 15, no. 1, pp. 15–20, 1989.

[6] S. Baylin, "DNA methylation and gene silencing in cancer," *Nature Clinical Practice Oncology*, vol. 2, pp. S4–S11, 2005.

[7] A. Feinberg, R. Ohlsson, and S. Henikoff, "The epigenetic progenitor origin of human cancer," *Nature Reviews Genetics*, vol. 7, no. 1, pp. 21–33, 2006.

[8] A. Goldberg, C. Allis, E. Bernstein, *et al.*, "Epigenetics: a landscape takes shape," *Cell*, vol. 128, no. 4, p. 635, 2007.

[9] P. Jones and S. Baylin, "The epigenomics of cancer," *Cell*, vol. 128, no. 4, pp. 683–692, 2007.

[10] M. Esteller, "Epigenetics in cancer," *New England Journal of Medicine*, vol. 358, no. 11, pp. 1148–1159, 2008.

[11] P. Laird, "Principles and challenges of genome-wide DNA methylation analysis," *Nature Reviews Genetics*, vol. 11, no. 3, pp. 191–203, 2010.

[12] P. Das and R. Singal, "DNA methylation and cancer," *Journal of Clinical Oncology*, vol. 22, no. 22, pp. 4632–4642, 2004.

[13] J. Espada and M. Esteller, "DNA methylation and the functional organization of the nuclear compartment," *Seminars in Cell & Developmental Biology*, vol. 21, no. 2, pp. 238–246, 2010.

[14] F. Carmona and M. Esteller, "DNA methylation in early neoplasia," *Cancer Biomarkers*, vol. 9, no. 1-6, pp. 101–111, 2011.

[15] H. Heyn and M. Esteller, "DNA methylation profiling in the clinic: applications and challenges," *Nature Reviews Genetics*, vol. 13, no. 10, pp. 679–692, 2012.

[16] M. Esteller, "CpG island hypermethylation and tumor suppressor genes: a booming present, a brighter future.," *Oncogene*, vol. 21, no. 35, p. 5427, 2002.

[17] P. Laird, "The power and the promise of DNA methylation markers," *Nature Reviews Cancer*, vol. 3, no. 4, pp. 253–266, 2003.

[18] H.-C. Tsai, H. Li, L. Van Neste, Y. Cai, C. Robert, F. Rassool, J. Shin, K. Harbom, R. Beaty, *et al.*, "Transient low doses of DNA-demethylating agents exert durable antitumor effects on hematological and epithelial tumor cells," *Cancer Cell*, vol. 21, no. 3, pp. 430–446, 2012.

[19] M. Lambert and Z. Herceg, "Epigenetics and cancer, 2nd IARC meeting, Lyon, France, 6 and 7 December 2007.," *Molecular Oncology*, vol. 2, no. 1, p. 33, 2008.

[20] A. Feinberg and B. Tycko, "The history of cancer epigenetics," *Nature Reviews Cancer*, vol. 4, no. 2, pp. 143–153, 2004.

[21] Z. Herceg, "Epigenetics and cancer: towards an evaluation of the impact of environmental and dietary factors," *Mutagenesis*, vol. 22, no. 2, pp. 91–103, 2007.

[22] C. Toumazou, L. Shepherd, S. Reed, G. Chen, A. Patel, D. Garner, C.-J. Wang, C.-P. Ou, K. Amin-Desai, *et al.*, "Simultaneous DNA amplification and detection using a pH-sensing semiconductor system," *Nature Methods*, vol. 10, no. 7, pp. 641–646, 2013.

Chapter 2

Epigenetics and DNA methylation in cancer

2.1 Introduction

There has been an explosive interest in the field of epigenetics, with recent advances changing the understanding of many biological phenomena and complex diseases, such as cancer, a disease that was traditionally viewed as genetic in origin [1]. Cancer is a result of a multistep process in which aberrant genetic changes such as gene mutations, gene deletions and chromosomal translocations accumulate, resulting in the transformation of a normal cell into an invasive or metastatic[1] tumour cell [3, 4]. Growing evidence has shown that acquired epigenetic abnormalities together with genetic alterations participate in processes of cancer development, Fig. 2.1, causing disruptions in the regulatory mechanisms of genes. Epigenetic changes are involved in aberrant activation or inactivation of genes, participating in mechanisms that may influence the homeostasis of gene expression, the disruption of which is intricately prevalent in the pathogenesis of cancer [5–8].

The growing interest in cancer epigenetics has been derived from the fact that epigenetic changes are involved in various steps of tumour development and progression being further augmented by the recent realisation that such changes can be exploited as a powerful tool in the clinic and as a novel approach for early cancer diagnosis, prediction of clinical outcome, risk assessment and targeted therapy [7, 12–15]. Epigenetics has evolved as a rapidly developing area of research, referring to heritable and potentially reversible alterations in gene

[1] A metastatic tumour is defined as one formed at a location in the body, the cells of which have been transported from a primary tumour located elsewhere in the body [2].

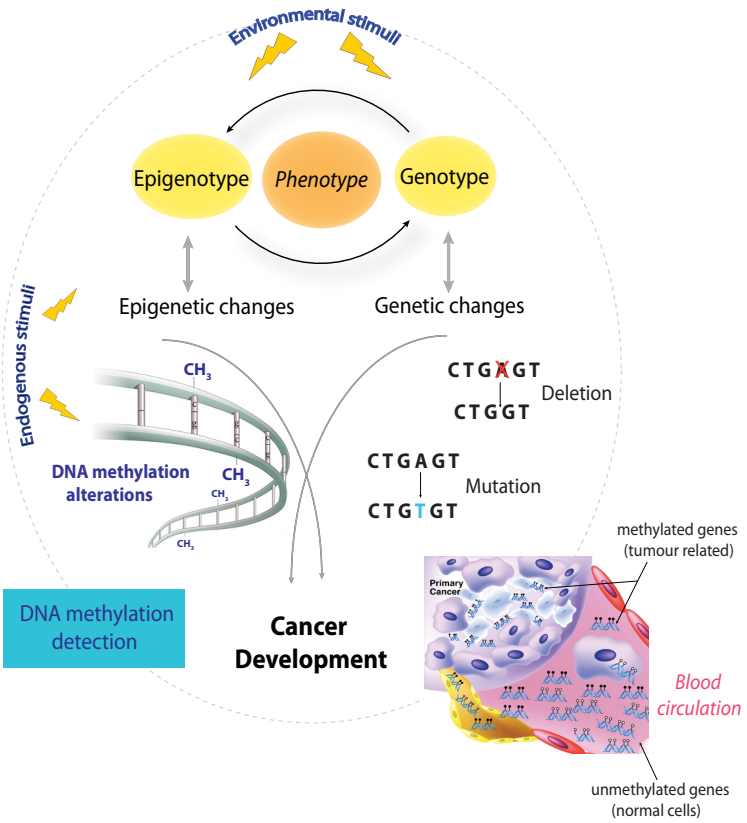


Figure 2.1: Epigenetic changes are influenced by both environmental stimuli and genetic changes. This means that our phenotype is determined by our genotype, the genetic information we are carrying, and our epigenotype, all the inherited and acquired epigenetic changes. In case of cancer development, disruptions in both genetic and epigenetic mechanisms occur, with DNA methylation, a key epigenetic modification, to play an important role in detection strategies of cancer. The fact that DNA methylation changes, associated with a primary tumour source, can be detected in blood circulation makes it a very attractive cancer biomarker [9–11].

expression that are not coded in the DNA sequence itself. The epigenome of cancer cells has been extensively studied, having shown that a large number of potential biomarkers has been identified, specifically DNA methylation, Fig. 2.1, a highly promising molecular biomarker, one of the most frequent alterations that occur in human malignancies and one of the most common epigenetic events in the human genome. This plays a critical role in regulating the mechanisms of gene expression [5, 6, 16, 17].

DNA methylation, a dynamically spreading chemical modification, has been studied in multiple cancer types, with abnormalities in its patterns identified in particular gene

regions known as *CpG islands*, rich in the content of CG bases [13, 14]. The majority of CpG islands are located in the promoter regions of the genes, areas responsible for the gene's transcription and the controlling mechanisms that regulate gene expression, generally unmethylated in normal cells. Aberrant hypermethylation occurring in the promoter regions of tumour suppressor genes has been reported to play a significant role in several cellular mechanisms disrupted or silenced at different stages of cancer progression [13, 17, 18]. Aberrancies during cellular events including phases of cell cycle, cellular apoptosis (process of programmed cell death), cell differentiation and DNA repair mechanisms are considered as some of the main causes of inappropriate transcriptional silencing of the genes. These may result in loss of gene function directly linked to early stages of tumorigenesis in several cancer cases such as breast, lung, prostate, colorectal, bladder, head and neck, cervical, ovarian, lymphoma, leukemia, hepatocellular, thyroid, liver and esophageal, correlating with the malignant progression or tumour burden (referring to the size of the tumour or the number of cancer cells), as well as to the recurrence of cancer or they may affect whether or not certain drugs are effective on an individual patient [1, 14, 17, 19].

Therefore, the need for detection of DNA methylation in tumour suppressor genes associated with the initiation of neoplasias[2] in certain organs appears to be of significant importance for screening and monitoring of cancer at an early stage of tumour development, when symptoms have not yet arisen for a diagnosis to be made. That is the time when an intervention needs to be made and methylation-specific assays need to be developed to enable systems for early detection, giving a better guidance to a patient, allowing early diagnosis and patient-centralised screening towards a personalised cancer therapy.

This chapter provides an overview of the rapidly advancing area of epigenetics focusing on its significant involvement in cancer development. The role of one of the most researched epigenetic events in tumourigenesis, DNA methylation, is further reviewed, followed by the effect of aberrancies of DNA methylation in gene inactivation using examples of where hypermethylated genes have been used as diagnostic markers in several types of cancer, based on their DNA methylation profile changes during tumour progression. A brief analysis on the methods and technologies used for DNA methylation detection is then presented, including single-loci based and genome-wide approaches, with the chapter concluding with the description of electrical analysis techniques and computational approaches, setting the scene for semiconductor based methods developed later in this thesis.

[2]Neoplasia refers to a benign or malignant tumour composed of cells with an abnormal appearance or an aberrant proliferation pattern [2].

2.2 Epigenetics in cancer

Cancer is exponentially increasing in numbers, an observation that is not only correlated with the *genetic* predisposition of the individual towards the disease but also with the *epi-genomic* or *epigenetic* inheritance passed by our ancestors in combination with our environmental influences. The term *epigenetics* was first conceived by Waddington in the early 1940s, originally introducing the concept of the "epigenetic landscape" to describe the studies of "the interactions of genes with their environment that bring the phenotype into being" [20, 21], with a further meaning of a "causal analysis of development", translated as to how the developmental decisions are made while the genetic information is converted into phenotypic traits [22, 23]. The definition of epigenetics ever since its introduction has however experienced a transient evolution, with a variety of biological events having been classified of epigenetic origin when no changes to DNA sequences are involved [9, 24].

Epigenetic phenomena have been historically linked to mechanisms that initiate and regulate heritable patterns of gene function, bridging the gap between the *genotype* and the *phenotype*, playing a critical role in maintaining the normality in events related to the development of organisms. They also contribute in establishing the regulation of cell processes while keeping cellular differentiation well-controlled, enabling the cells to carry the same genetic information but express a different phenotypic behaviour [9, 25, 26]. An example of this feature may explain why twins with identical genotypes can be phenotypically different given the distinct environmental stimulus that may have grown under [26].

While epigenetic mechanisms occur at a higher frequency than genetic changes, they have a direct effect on the way genes are expressed, allowing the formation of suitable gene expression patterns without affecting the primary nucleotide sequences as mutations do. Aberrancies in epigenetic mechanisms can result in inappropriate activation of key regulatory genes leading to their abnormal expression or to genetic silencing by inhibiting signal pathways [5, 6, 8, 24]. Screening studies have revealed that most of the critical processes found in cancer cells, such as silencing of tumour suppressor genes, activation of oncogenes, aberrant cell cycle processes, defects in DNA repair and dysregulation of cell death can be triggered directly or indirectly by epigenetic aberrancies. These series of events can be detrimental for the homeostasis of the cellular regulatory mechanisms, forming a driving force in the initiation and progression of tumourigenesis [8, 26, 27].

Epigenetic mechanisms comprise three main categories: DNA methylation, histone mod-

ifications and RNA-mediated gene silencing [28]. The two major epigenetic modifications are those occurring at a DNA level (DNA methylation) and at a chromatin level (chromatin remodelling), both of which are considered to be associated with silencing of critical tumour suppressor genes and activation of oncogenes involved in cancer development. DNA methylation in particular, is a widespread epigenetic modification that plays a critical role in the regulation of gene expression and thus the genomic stability during development, differentiation but also diseases such as multiple sclerosis, diabetes, schizophrenia and multiple types of cancer [23].

The disruption of normal methylation patterns resulting in genomic instability and chromosomal aberrations has been recognised as one of the most common molecular alterations in human neoplasia, with advances in the processes taking part to have brought great awareness to the role of epigenetics as an alternative or complementary mechanism to mutational events in oncogenesis [29, 30]. Therefore, the fact that epigenetic events are increasingly recognised for their contribution to oncogenesis, either by occurring in the early stages of tumour progression or by actually being the initiating events, opens up an exciting new avenue of research with potential impact in cancer prevention, early detection and treatment through the development of accurate and sensitive methods to detect changes in DNA methylation patterns [14, 31].

2.3 DNA methylation

DNA methylation is a key epigenetic factor, one of the earliest studied epigenetic modifications in eukaryotes, the disruption of which has been proposed as one of the causes of inactivation of a variety of genes, studied in various cancer types [13]. It has been characterised as a stably inherited chemical modification, playing a critical role in the mechanisms behind genetic functions and gene expression [13]. Disruptions in key areas responsible for gene regulation such as the gene promoter regions, which are responsible for their normal expression, may lead in their inhibition by turning those genes from “on” to “off”, as can be seen in Fig. 2.2. These certain disruptions that are the consequence of aberrancies in the methylation levels of such areas may significantly influence the mechanisms behind the initiation as well as the progression or recurrence of cancer or they may affect whether or not certain drugs are effective as parts of a therapy scheme on an individual patient [14, 32].

DNA methylation or more specifically cytosine methylation is a complex enzyme-driven

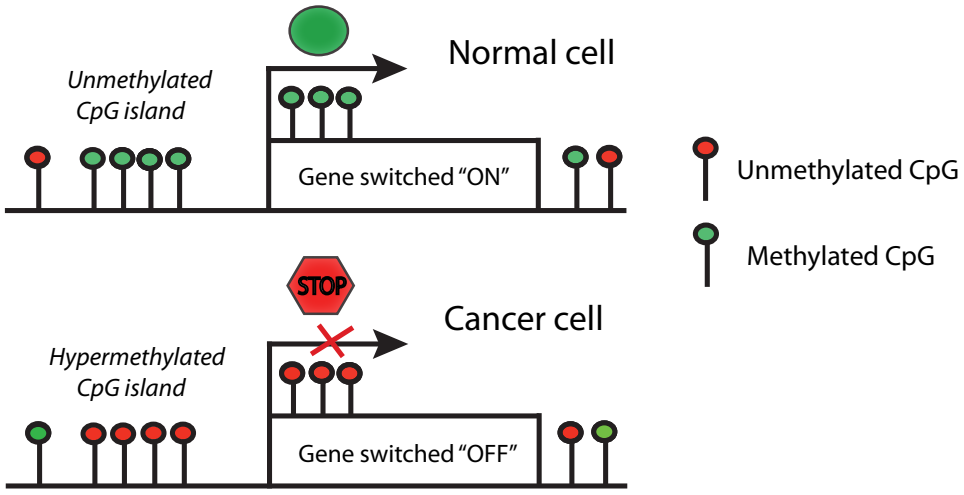


Figure 2.2: DNA methylation disruptions in promoter gene regions in the cases of a normal cell (top) and a cancer cell (bottom). A CpG island of a promoter region of a tumour suppressor gene in a normal cell and a cancer cell is represented, with hypermethylation or aberrant DNA methylation patterns to change the molecular environment of the cell leading to gene silencing. Figure adapted from [6].

chemical modification occurring almost exclusively at the cytosine DNA base, including the addition of a methyl group (CH_3) to the carbon 5-position of the cytosine ring, as shown in Fig. 2.3. This is performed by enzymes called $DNA\ methyltransferases$ ($DNMTs$) [33], which are responsible for the maintenance of DNA methylation during DNA replication, the activity of which increases progressively during the initiation of cancer and also along with the advancement of the tumour stage of different kinds of cancers [34].

DNA methylation takes place in areas when a guanine base follows a cytosine in clusters of CG dinucleotides (CpGs), regions well-known as $CpG\ islands$[3] [35–37] which are found most often in gene promoters, areas responsible for controlling the expression of a gene. The presence of methylation in these areas may lead to hypermethylated genetic traits of a gene promoter, a well-known feature of many tumour suppressor genes that remain silenced during cancer development [28]. Also, DNA hypermethylation (aberrant methylation reaching higher than normal levels) which occurs mostly in CpG islands, is present at higher percentages in tumours than genetic mutations do, resulting in higher sensitivity of detection

[3]CpG islands were originally identified as short regions of CpG-rich DNA, referred to, in 1985 by Bird et al., as "HTF islands" which contained sites that could generate the action of the methylation-sensitive restriction enzyme HpaII. They are known as areas of GC-rich dinucleotides, associated with gene silencing and in general with the ability to provide a way towards the challenge of mapping methylation throughout the genome [35].

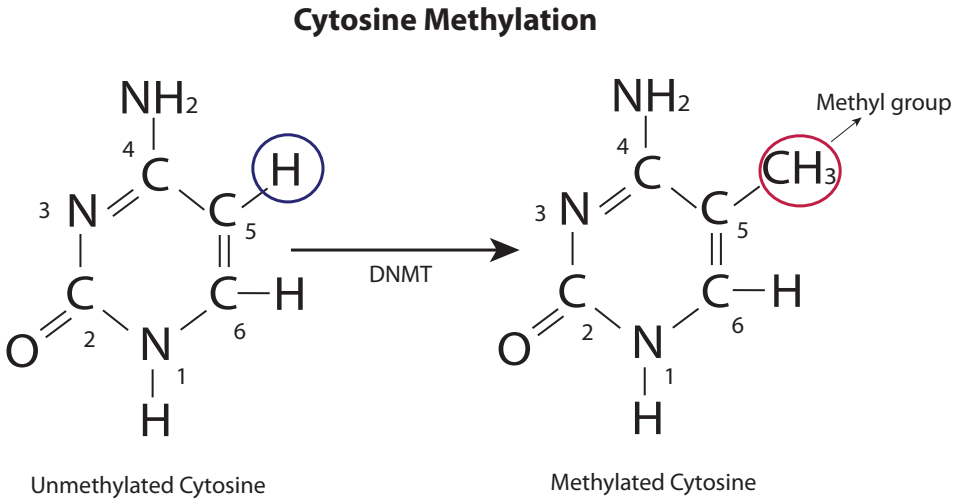


Figure 2.3: DNA methylation: It is the addition of a methyl group, CH_3, to the 5th position of the cytosine ring, C.

strategies when used as a biomarker for early screening of cancer [38, 39].

CpG islands are not equally distributed in the human genome, occurring in frequency of 1 in 80 dinucleotides in half of the human gene promoter regions (length of 500 base pairs to several thousand base pairs). Latest criteria on the definition of a CpG island given by [28, 40] proposed that a genomic region of $\geq$ 500 base pairs with a G+C content $\geq$ 55% and an observed/expected CpG ratio $\geq$ 0.65 could estimate the existence of a CpG island. It has been estimated that around 60% to 90% of CpG sequences in GC-rich regions are methylated in mammalian genomes. In normal cells the majority of CpG regions are unmethylated before the onset of cancer, so the associated genes in the promoter regions located in the CpG islands can be expressed normally [40]. However, in cancer cells, abnormal DNA methylation patterns occurring in one or several CpG islands of the gene promoter can cause loss of gene expression leading to the suppression of the gene's transcription resulting in gene silencing [8, 17] with some of the genes been hypermethylated in over 90% of cancer cases. Although the most significant proportion of CpG islands is located in the 5' region, occupying around 60% of the human gene promoters [41] (for a gene's orientation defined as 5' to 3'), certain CpG islands can occasionally be found within the body or at the 3' end of a gene. CpG islands in these locations are more prone to methylation occurence, contributing in the disruption of the regulatory mechanisms of gene expression.

2.3.1 Gene methylation in cancer

Abnormal DNA methylation at specific transcription sites can result in epigenetic silencing of genes that protect against tumour formation or that repair DNA, with the disruption of both to play an important role in tumour initiation [12, 28, 29]. As compared with normal cells, malignant cells show major disruptions in their DNA methylation patterns, with global levels of DNA methylation becoming hypomethylated[4] in conjunction with DNA hypermethylation of gene promoters of the CpG islands and increased rate of mutations at methylated CpG dinucleotides, both ways through which DNA methylation can contribute to cancer due to the blocked expression of a gene that would otherwise be expressed [1, 16, 17, 30].

DNA hypomethylation is a significant alteration observed in cancer with 20% to 60% loss of overall methylation being present [23]. Genomic hypomethylation usually involves repeated DNA sequences and has been hypothesised to contribute to cancer progression being responsible for the overexpression of proto-oncogenes, the protein products of which are involved in cancer cell proliferation, invasion and metastasis, leading to elevated mutation rates by destabilising the genome through the promotion of chromosomal instability [29, 30, 42]. Given the significance that DNA hypomethylation may have as an epigenetic alteration, the exact reasons of its origin at a genome-wide level still remain unclear, with its diagnostic use to be limited given the nature of the detectable signal, since the loss of DNA methylation is to be detected rather than the gain (i.e. DNA hypermethylation) [39]. On the other hand, regional hypermethylation of CpG islands within or around the promoter region of tumour suppressor genes has been the most extensively studied area of research of DNA methylation in cancer and has been characterised as a well-recognised epigenetic change that occurs in virtually every type of human neoplasia, participating not only in precancerous stages but also in the malignant progression, having prognostic impact on patients with cancer [17, 30, 34, 42].

In the past years there has been a substantial growth of the number of genes known to undergo CpG promoter hypermethylation in cancer, affecting different molecular pathways and cellular processes, including cell-cycle regulation ($CDKN2A/p16$-$INK4$ ($p16$), $CDKN2B/p15$-$INK4B$, $CCND2$, $RB1$), DNA repair ($MGMT$, $BRCA1$, $MLH1$), apoptosis ($DAPK1$, $TMS1$, $TP73$), metastasis ($CDH1$, $CDH13$, $PCDH10$), detoxification

[4]DNA hypomethylation: A decreased level of DNA methylation in a DNA sample (CpG site or group of CpG sites) relative to a reference DNA sample of a normal tissue [14].

Table 2.1: Frequently hypermethylated genes silenced in several cancer cases

Hypermethylated gene	Gene function	Cancer type
CDKN2A/p16-INK4	Cell cycle control	Lung, breast, prostate, pancreatic, colorectal, head and neck, bladder, renal, esophageal, lymphoma
RASSF1A	Cell cycle, DNA repair	Breast, ovarian, lung, prostate, colorectal, bladder, renal, head and neck, thyroid, cervical, liver
DAPK1	Control of programmed cell death (apoptosis)	Lung, bladder, head and neck, colorectal, breast, gastric, cervical, lymphoma
GSTP1	DNA repair	Prostate, breast, liver, lung, bladder, renal
APC	Regulation of cellular processes and chromosomal stability	Colorectal, prostate, lung, bladder, breast, esophageal
MGMT	DNA repair	Glioma, colorectal, lung, prostate, renal, lymphoma, head and neck, gastric
SEPT9	Cell cycle control	Colorectal
BRCA1	DNA damage response	Breast, ovarian
ER	Hormonal resistance	Breast, prostate
CDH1	Cell adhesion	Breast, bladder, gastric, lung, leukemia
CDH13	Cell adhesion	Lung, head and neck
MLH1	DNA repair	Colorectal, gastric, endometrial, ovarian, stomach
CDKN2B/p15-INK4B	Cell cycle control	Leukemia, lymphoma, liver
RARβ	Cell cycle control	Lung, breast, prostate, kidney, bladder, colorectal
ESR1	Estrogen receptor signalling	Breast, leukemia, prostate, lung, thyroid

Data summarised by [1, 17, 39, 42]. Abbreviations with sequence of appearance: $CDKN2A/p16\text{-}INK4$, cyclin-dependent kinase inhibitor-2A; $RASSF1A$, Ras association domain family member-1; $DAPK1$, death-associated protein kinase-1; $GSTP1$, glutathione S-transferase protein-1; APC, adenomatous polyposis coli; $MGMT$, O^6-methylguanine-DNA methyltransferase; $SEPT9$, septin-9; $BRCA1$, breast cancer-1, early onset; ER, oestrogen receptor; $CDH1$, cadherin-1, type-1, E-cadherin; $CDH13$, cadherin-13, H-cadherin (heart); $MLH1$, mutL homologue-1; $CDKN2B/p15\text{-}INK4B$, cyclin-dependent kinase inhibitor-2B; $RAR\beta$, retinoic acid receptor-β; $ESR1$, oestrogen receptor-1.

($GSTP1$), hormonal regulation ($ESR1$, $ESR2$), *Ras* signalling[5] ($RASSF1A$) and *Wnt* signalling[6] (APC, $DKK1$) [17, 38, 42]. The profiles of hypermethylated tumour suppressor genes, which are specific to cancer types [38], create a unique "hypermethylome" per tumour type, as has been proposed by Esteller [1]. According to the cancer methylation database PubMeth [43], the most often reported cancer types associated with DNA hypermethylation are lung, breast, colorectal, prostate, head and neck, gastric, leukemia, lymphoma and liver, the occurrence of which indicating that the frequency of disruption in DNA methylation patterns is potentially present in the majority of cancer types as well [42, 43]. Table 2.1 summarises the most frequently reported genes that are silenced by DNA methylation.

DNA hypermethylation of some genes, such as $CDKN2A/p16$-$INK4$, $RASSF1A$ and $MGMT$, may be frequently observed in multiple cancer types allowing the detection of a subset of them, while it may be limited to a particular cancer type. $GSTP1$ gene can be used as an example, since it has been found hypermethylated in more than 90% of prostate cancers but is largely unmethylated in acute myeloid leukemia [17, 44].

DNA methylation of several genes (i.e. $CDKN2A/p16$-$INK4$, $DAPK1$, $RASSF1A$, $MGMT$, APC) has been detected most commonly in serum or plasma of blood samples using minimally invasive methods and also in sputum as well as in samples derived from the corresponding primary tumours (i.e. biopsy). The first studies to show that DNA methylation changes could be detected in serum DNA of cancer patients were reported by Esteller et al. [45] in NSCLC (Non-Small Cell Lung Cancer) patients and by Wong et al. [46] demonstrating $p16$ methylation in plasma and serum of liver cancer patients. What is more, a considerable number of studies has evaluated the potential of circulating tumour DNA methylation in serum and plasma for the molecular diagnosis and early detection of a variety of cancer types [11, 45–50], showing that tumour-specific DNA methylation patterns can be detected in tumour-derived free circulating DNA from the bloodstream of cancer patients coming from DNA derived from the primary tumour source of the patient.

Table 2.2 summarises some highly methylated genes investigated in blood circulation for cancer types such as breast, lung, prostate, colorectal and liver cancer. Even more interestingly, it has been found that the mean concentration of DNA in plasma samples from control subjects has been estimated to be around 10 to 18 times less than that from

[5]Ras signalling: Signalling system that is controlled by *Ras* proteins, regulators of several aspects of normal cell growth and malignant transformation [2].

[6]Wnt signalling: Independent signalling system that can be regulated by proteins involved in the *Wnt* pathway, associated with cellular metabolism processes [2].

Table 2.2: Detection of cancer in circulation using DNA methylation as a biomarker

Tumour Type	Gene	Serum/ Plasma	Methylation (%)	Ref.
Breast cancer	$RASSF1A$	S/P	75%	[51]
Non-small cell lung cancer (NSCLC)	$p16$, $DAPK1$	S/P	73%	[45]
	$MGMT$, $GSTP1$	S/P	73%	[45]
Prostate cancer	$GSTP1$	S/P	72%	[52]
Colorectal cancer	$CDKN2A/p16\text{-}INK4$	S	71%	[53]
Liver cancer	$CDKN2B/p15\text{-}INK4B$	S/P	81%	[54]

patients within different cancer type groups [47]. Different methods of analysis have been used by several research groups, as referenced, through the collection and analysis of plasma or serum samples, showing that the methylation profile of cancer cells detected in the blood of cancer patients, while avoiding invasive methods of sample acquisition such as biopsies, offers a very promising application for a Point-of-Care approach towards the early detection of cancer [48].

Examples of one of the most frequently studied cancer types, lung cancer, have given significant insight in the methylation levels of tumour suppressor genes as being at a considerably higher degree of alteration in DNA methylation patterns of the cancerous cases compared to healthy subjects. Of the various genes studied, the commonly hypermethylated ones, as reported in Table 2.2, included: $CDKN2A/p16\text{-}INK4$ (the most frequently methylated gene among the majority of the genes studied in various cancer types [13]), $DAPK1$ and $RASSF1A$, with a prognostic significance by associating their methylation status dependent on the stage of cancer progression, with overall survival rates of patients compared to non-cancerous samples [55–59]. Combination of the DNA hypermethylation profile of more than one genes in most of the cases resulted in higher sensitivity and specificity of detection reducing the number of false positives.

Although in many studies the frequency of DNA methylation in serum or plasma samples has been reported to be lower compared to the same observation in primary tumours, the levels of methylation were significantly higher in cancerous samples opposed to non-cancerous ones, reinforced by the fact that most often if DNA methylation is detected in

serum or plasma then the primary tumour will also be positive for the same alteration [60, 61]. Exceptions to this have been reported in small number of cases [47]. Additionally to the diagnostic potential that DNA methylation profiling could give for lung cancer detection, it could provide information on disease prognosis, whereby a panel of hypermethylation genes ($CDKN2A/p16\text{-}INK4$, $RASSF1A$, APC, $CDH13$) could predict the early recurrence of cancer as reported by Brock et al. [62]. One example of combinatorial schemes of DNA hypermethylated biomarkers used to detect prostate and lung cancer reported by [62, 63] showed high sensitivities of detection of cancer cells in the case of prostate cancer and good accuracy in prediction of tumour progression in the case of lung cancer.

Similarly, in breast cancer, DNA methylation has been proposed as one of the causes of inactivation of a variety of genes which have been hypermethylated, the most highly methylated of which were $CDKN2A/p16\text{-}INK4$, associated with increased susceptibility to breast cancer [64], $RASSF1A$, a tumour-specific biomarker frequently found as hypermethylated in relevant studies [51, 65, 66] which in combination with $GSTP1$, APC and $DAPK1$, as the results shown in Table 2.2 confirm, detected primarily in blood [67, 68], may enhance the sensitivity of early detection of breast cancer, given its presence in all grades and stages. DNA methylation profiling could also provide important information on disease metastasis, with examples reported by Muller et al. [69] and Graff et al. [70], showing a strong connection between hypermethylation of $RASSF1A$, $BRCA1$ and $E-cadherin$ genes, with disease prognosis being closely related to metastatic behaviour.

In several other cancer cases, the DNA hypermethylation status of genes under investigation was determined, together with its clinical significance as they may be used to indicate the disease progression. In addition to this, the level of DNA methylation of tumour suppressor genes identified in plasma/serum was reported to increase during the late stages of tumour development compared to early stages of diagnosis, an observation also made for cases of recurrence of the disease after curative surgery or chemotherapy applied [71–74]. The frequency of methylation events also varied, depending on the patient (genetic profile, age, medical history) and the cancer type, highlighting the great potential of using DNA hypermethylation as a biomarker for the personalised evaluation of early detection of cancer, diagnosis as well as for prognosis, recurrence and response to treatment [1, 62]. It is therefore apparent that there is a need for accurate methods for DNA methylation detection that could provide multiple information on the status of DNA hypermethylation of several genes related to cancer cases under investigation, while managing the variation in DNA methylation in between the individual subjects. The methods used for DNA methylation

detection, together with the challenges which exist, given the demand for high-throughput approaches in epigenetic screening, are to be presented in the following section.

2.4 Methods for DNA methylation detection

Over the past few decades, the number of studies on the role of DNA methylation in cancer development has grown dramatically with several DNA methylation assays developed for the examination and analysis of gene-specific or genome-wide levels of DNA methylation. Much effort has been put into the development of early-detection strategies. DNA methylation changes have been reported to occur early in carcinogenesis and therefore are potentially good early indicators of the status of the existing disease, or they may even contribute to the risk assessment of the future development of the disease. For many types of malignancies, symptoms often do not arise until after the primary tumour has metastasised, contributing to high mortality rates. Therefore, the development of cancer biomarker assays and the evaluation of potential markers using standardised techniques, testing their limit of detection as well as their specificity and sensitivity, would be of great need for early detection strategies used for screening and thus improving the clinical evaluation and outcome.

The samples used for analysis of DNA methylation biomarkers usually contain high concentrations of background DNA from the tumour. However, tumour-derived DNA is difficult to be detected because it is often present in very low concentrations and can be contaminated substantially with the DNA from the healthy cells. Moreover, DNA methylation is not evenly distributed across the genome. Thus, methods with sensitive detection capabilities are often needed to identify aberrantly methylated tumour-derived DNA in body fluids [6, 75]. As has been summarised by [31, 39, 42, 76], the combination of different types of pre-treatment of sample DNA, followed by different analytical steps, has resulted in a plethora of techniques available for determining DNA methylation patterns and profiles at a genome-wide level.

The main principles for DNA methylation analysis, as shown in Fig. 2.4, are based on three main approaches followed:

- *Restriction enzyme digestion*: methylated DNA is digested by methylation-sensitive restriction enzymes.
- $Affinity\ enrichment$: methylated DNA is enriched with methylation-specific binding

proteins or antibodies.

- *Sodium bisulfite treatment*: DNA is treated with *sodium bisulfite*, also regarded as the gold standard for DNA methylation detection.

Treatment with one of these methods allows for further processing of the samples using powerful techniques, such as high density DNA methylation microarray analysis [77–79], which has shown great promise on DNA methylation pattern profiling or bisulfite sequencing, resulting in a single base pair resolution of detection [80, 81]. Also, other approaches based on optical or electrical methods of detection have been reported as potential ways for DNA methylation analysis. The principles of the most-widely applied methods for DNA methylation analysis together with their merits and trade-offs are further discussed in the following sections.

2.4.1 Restriction enzyme based methods

Restriction enzyme based methods use sequence-specific restriction enzymes with the ability to "digest" only genetic areas where DNA methylation is present, with *HpaII* and *SmaI* to be the most widely used methylation-sensitive restriction enzymes [31]. DNA methylation analysis was first conducted by methylation-sensitive restriction enzymes using Southern blot analysis for visualisation of methylated sites as reported by [82]. Southern blot analysis was further replaced by methylation-specific polymerase chain reaction (PCR) based methods i.e. Methylation-Specific Multiplex Ligation dependent Amplification (MS-MLPA) [83], providing high-throughput (number of samples that can be analysed per run) of the average ratio of methylated over unmethylated sites.

Several approaches have been developed ever since the first application of methylation-sensitive restriction based analysis, with the most popular being the Restriction Landmark Genomic Scanning (RLGS) [84], reported as the first technique for DNA methylation analysis at a genome-wide scale, followed by array based Differential Methylation Hybridisation (DMH) [85], which combines array based analysis with restriction digestion, offering a new approach on differential methylation hybridisation. Moreover, adaptations on DMH and the array design introduced the method of Comprehensive High-throughput Arrays for Relative Methylation (CHARM) [86], providing high-density array readouts for genome wide methylation, allowing methylation discrimination at a CpG locus level. Also the method of HpaII tiny fragment Enrichment by Ligation-mediated PCR (HELP) [87] was further

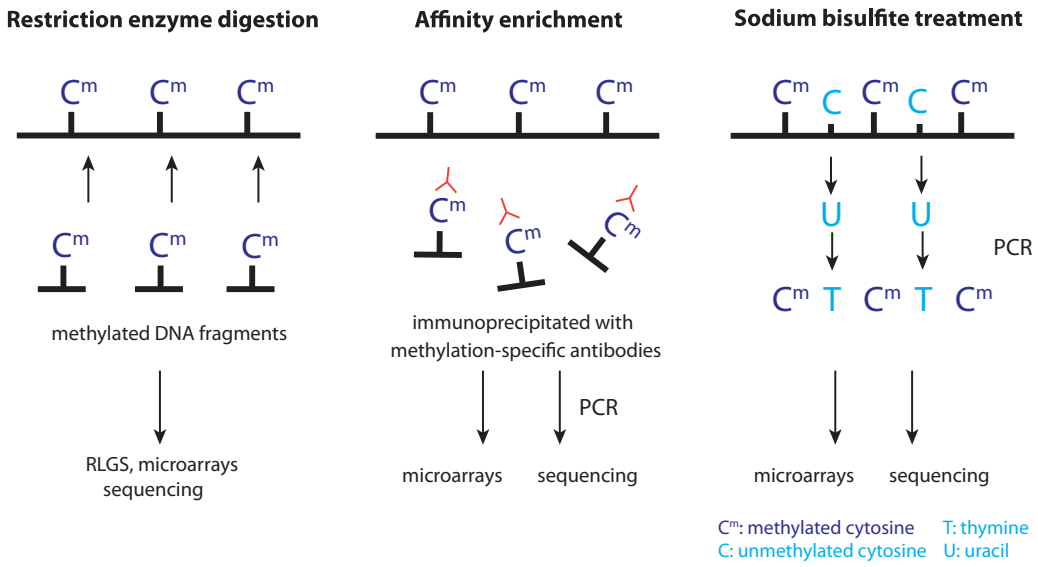


Figure 2.4: Principles for DNA methylation analysis and detection. Figure obtained and adapted from [42].

proposed, fundamentally based on PCR amplification of restriction fragments followed by array hybridisation, providing information on the distribution of cytosine methylation in the genomic regions [42]. What is more, advances in sequencing approaches have brought further adaptations on the restriction enzyme methods, developing restriction based assays capable for providing sequence-specific analysis, allowing allele-specific DNA methylation analysis, an example of which is the integration of the HELP assay with next-generation sequencing analysis [88].

Although restriction enzyme based methods are highly reliable for analysis of large amounts of methylated sites, however the use of restriction enzymes can be a limiting factor especially when global methylation analysis is required, given that restriction enzymes are dependent on given restriction sites, therefore being unable for large CpG regions coverage for DNA methylation analysis. Restriction digestion is also prone to generate false positives in the case of insufficient enzyme cleavage, also lacking to provide methylation information at a sequence-specific level. Also the requirements for large amounts of DNA for digestions can be quite challenging especially when the amount of DNA recovered from remote media is generally low in copy numbers [31, 42].

2.4.2 Affinity based methods

Chromatin immunoprecipitation (*ChIP*) based or $affinity$ enrichment methods are protein based, useful for the identification of methylated regions in tumours through the interaction between methyl-binding proteins or antibodies specific to methylated cytosines [31]. MeDIP (Methyl-DNA immunoprecipitation) [89] is an affinity based approach whereby methylation analysis is achieved by methylated DNA immunoprecipitation, where antibodies specific to methylated cytosines are used to capture methylated sites, followed by hybridisation using genomic microarrays, allowing for identification of methylated CpG loci. MeDIP, coupled with sequencing analysis on the results, introduced MeDIP-seq [90, 91], bringing the advantage of genome-wide sequence-specific analysis of methylated CpG sites [39], even quantitatively in the case of Methylation-sensitive Restriction Enzyme sequencing (MRE-seq) [92], allowing for fast genome-wide analysis while providing sequence-specific information on a CpG or sequence level [31, 81].

Although the combination of sequencing in the affinity based methods brings certain advantages compared to the array based approaches, the use of proteins or antibodies to attach to defined methylated sites adds certain limitations given that they cannot provide a single-base pair resolution regarding the methylation targets and are difficult to be standardised. Also the levels of complexity of the method increases considerably when extra amplification steps are required after the antibodies attachment [81].

2.4.3 Sodium bisulfite based methods

Sodium $bisulfite$ based methods are based on the use of $bisulfite\ conversion$ to distinguish methylated from unmethylated cytosines, being considered as a gold-standard approach for DNA methylation detection. Bisulfite conversion was first introduced by [93], opening a new era for gene based DNA methylation analysis, allowing methylated DNA to be bisulfite-treated and then amplified and detected in conjunction with PCR based approaches and sequencing [94], methods of choice when detection at a single base pair resolution is desired, allowing methylation information to be preserved after the DNA sample is amplified [75], independent of the need for restriction enzymes, following a label-free approach [95]. Bisulfite treatment of the genomic DNA, derived from a collection of cells which may vary in their DNA methylation patterns, is useful for mapping the normal and aberrant patterns of methylation, leading to the conversion of unmethylated cytosines to uracils (U), which

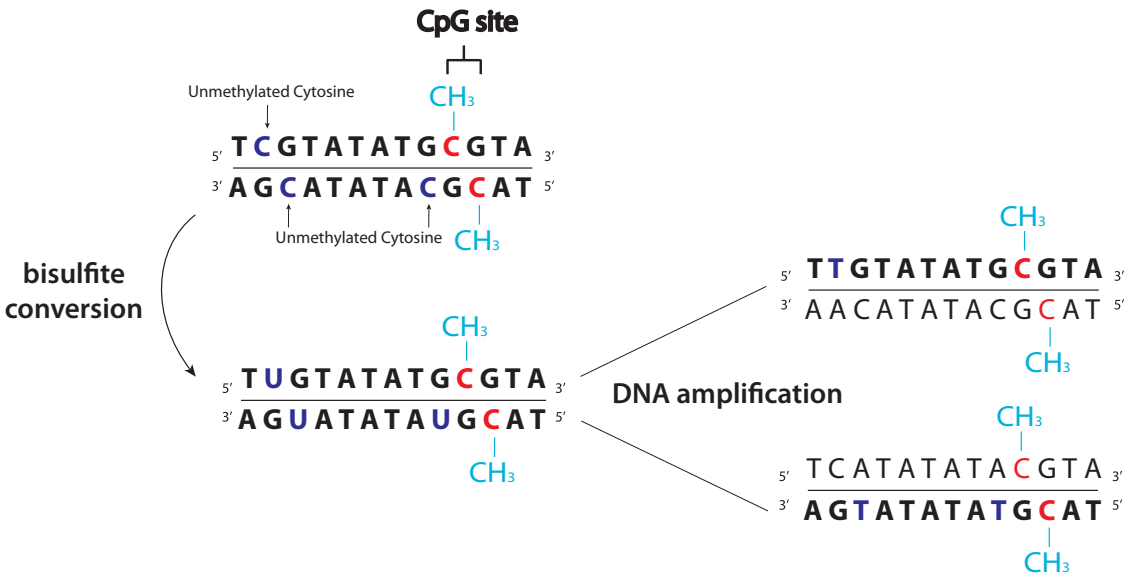


Figure 2.5: The principle behind bisulfite conversion: DNA strands are chemically treated with sodium bisulfite so that unmethylated cytosines are converted to uracils whereas methylated cytosines remain unaltered and preserved through chain extension. Through bisulfite conversion, DNA is modified in a methylation-dependent way before amplification of the selected loci starts and so DNA methylation information is not erased, letting specific genetic regions be examined for their levels of methylation.

are amplified as thymines (T) by PCR amplification, leaving only the methylated cytosines unaltered, as can be seen in Fig. 2.5, therefore transforming the epigenetic information into a genetic difference, enabling the use of DNA methylation detection techniques to be further applied for analysis of read-outs [14, 42]. The requirements for large-scale sequencing, based on the original bisulfite sequencing technique by [93], can be a computational mapping challenge, with millions of bisulfite reads to be processed and compared to a reference genome in conjunction with the need for control tests and multiplexing.

Various approaches using bisulfite conversion have been further developed, given the advantage of the method to be applied on a large DNA spectrum of different origin and varying amount [96]. One broadly used approach for DNA methylation analysis is Methylation-Specific PCR (MSP), introduced by Herman et al. [97] as a qualitative method, with the ability to study DNA methylation at a single CpG locus level. MSP combines the modification of DNA using sodium bisulfite followed by a subsequent amplification using primers that are specific to the methylated genomic region of interest versus the equivalent unmethylated one. MSP allows fast and sensitive detection of the methylation status of a

DNA target during the course of methylation-specific PCR amplification without requiring subsequent analysis of the final products, been considered as a widely applied prognostic tool in the clinic. It is known for its high analytical sensitivity, which can provide a complete overview of a base-pair resolution of the CpG methylation levels with the ability for further integration with next-generation sequencing technologies for deeper methylation data analysis [39, 80]. MSP's efficacy can however be influenced by the primer design of the methylation-sensitive areas and the number of PCR cycles. Thus, there is a risk of false positive results arising as a result of incomplete DNA bisulfite conversion, which is claimed to be one of the most significant problems when using the methylation technology in early screening of cancer [6, 75]. Nevertheless, the applicability of the method and the advantage of high specificity that it provides establishes it as one of the highly preferred techniques for DNA methylation analysis.

The method of Combined Bisulfite Recognition Analysis (COBRA) was further introduced as a method by Xiong et al. [98], with the ability to differentiate methylated from unmethylated sequences with the aid of restriction digestion of DNA products combined with bisulfite conversion and amplification of methylated sequences of a single CpG site, adding an internal control of the digested products through the use of bisulfite conversion, limited however by the dependence on the restriction enzymes. The technique of Methylation-Sensitive Single Nucleotide Primer Extension (MS-SNuPE) also followed [99], as a quantitative method for assessing the differences in DNA methylation of specific CpG sites based on bisulfite treatment of DNA and a two-steps amplification of the bisulfite treated sample, resulting in quantifying the level of DNA methylation in the initial DNA sample, requiring however well-aligned sets of primers for every step of amplification, adding up in complexity of the process as well as in the consistency of the results. Moreover, quantitative PCR based methods on gene-specific analysis such as MethyLight [100], which combines treatment of small amounts of DNA with sodium bisulfite and DNA amplification using fluorescent based real-time PCR, generating real-time quantitative data on CpG sites of interest or pyrosequencing for DNA methylation analysis [101], which provides a sequential information on the amount of methylation of multiple CpG loci by substituting the restriction analysis that COBRA is using with the quantitative pyrosequencing reaction [102], have contributed in enabling a quantitative in addition to qualitative analysis of DNA methylation levels, with the step of bisulfite sequencing to add an extra step of confirmation of the DNA methylation analysis result.

In addition to the previous methods analysed, the genome-wide profile of DNA methyla-

tion sites can be determined using CpG-specific array based technologies, which can access the methylation status of a large number of genes of the entire genome. These can be applied in conjunction with bisulfite based analysis methods, allowing for in parallel profiling of multiple DNA methylation patterns at a lower cost compared to sequencing based approaches. The GoldenGate BeadArray technology by Illumina is one of the examples of DNA methylation arrays used for multiplexed methylation detection of samples after bisulfite treatment and amplification steps are completed, with the products being hybridised to bead arrays containing 30 beads per CpG site, while utilising DNA probes unique for the methylated or unmethylated CpG state [103], adaptations which led to the development of the Infinium platform (Illumina) [104] with the latest DNA methylation array, HumanMethylation 450 BeadChip assay (Illumina), been developed for genome-wide DNA methylation analysis of 450,000 CpGs allowing high resolution analysis [77]. Although DNA hybridisation arrays may offer reduced DNA input requirements, simpler sample preparation protocols and data processing compared to sequencing techniques as well as access to discrete CpG sites and high-throughput sample recovery [104], however possible limitations related to DNA hybridisation specificity and probe selection specific to the DNA target still need to be considered.

Nonetheless, next-generation sequencing technologies have shown great promise in providing more cost-effective approaches of genome-wide analysis, therefore the potential of parallelising sequencing and array technologies for targeting and screening DNA methylation sites respectively could reduce the trade-offs of both methods while enhancing the information gathered by the under investigation targets. Table 2.3 provides an overview of the commonly used DNA methylation detection assays with advantages and limitations reported for each method.

2.5 DNA methylation ratio in DNA methylation computational analysis

DNA methylation has also offered a fertile ground for statistical analysis of methylated regions at a both locus-specific and genome-wide level. Computational tools for high-throughput epigenetic analysis have experienced a rapid progress, especially given the current initiatives for mapping of the human epigenome. Reference data sets and global epigenome maps are now being developed such as the *Blueprint* by the International Human Epigenome Consortium (IHEC) [105] and the US National Institutes of Health (NIH)

Table 2.3: Comparison of commonly used DNA methylation analysis techniques

Method	Type	Principle	Advantages	Disadvantages
MSP [97]	Qualitative	Amplification of methylated/ unmethylated sequences, single CpG analysis	Sensitive, rapid, no need for enzymes low amount of DNA required	Primer design optimisation, bisulfite conversion variations, prone to false positives
Bisulfite [101] **pyrosequencing**	Semi-quantitative	Single base resolution, multiple CpG analysis	Highly specific, high-throughput, control of bisulfite products	Costly, technically demanding
MethyLight [100]	Quantitative	MSP using real-time PCR technology, multiple CpG analysis	High-throughput, rapid, separate analysis of sequences, low amount of DNA required	Bisulfite conversion variations, recognition only when site is fully methylated
COBRA [98]	Semi-quantitative	Bisulfite restriction analysis, single CpG analysis	Restriction enzymes used to control bisulfite products	Dependence on restriction sites, not suitable for multiple CpG sites
MS-SNuPE [99]	Quantitative	Bisulfite restriction analysis, radioactive incorporation, single CpG analysis	Rapid, low amount of DNA required	Handling of radioisotopes, PCR bias, labor intensive
RLGS [84]	Qualitative	Methylation sensitive restriction digestion, genome-wide methylation analysis	Sensitive in differential methylation detection	Technically complex, large amounts of DNA required
MeDIP [89]	Qualitative	Methylation sensitive affinity enrichment analysis using microarrays or sequencing at a genome-wide level	Fast, simple low amount of DNA required	Costly, dependence on antibodies, copy number bias, low specificity
CHARM [86]	Quantitative	Genome-wide methylation sensitive restriction digestion analysis using high-density arrays	Cost-effective, computational algorithm for correction of biases after digestion	Limited number of CpG sites for investigation due to dependence on restriction sites, not applied in regions of low CpG content

Abbreviations with sequence of appearance: MSP, Methylation-Specific PCR; COBRA, Combined Bisulfite Recognition Analysis; MS-SNuPE, Methylation-Sensitive Single Nucleotide Primer Extension; RLGS, Restriction Landmark Genomic Scanning; MeDIP, Methyl-DNA immunoprecipitation; CHARM, Comprehensive High-throughput Arrays for Relative Methylation.

Roadmap Epigenomics Mapping Consortium [106], with the ultimate goal to decode the epigenetic signature of the human epigenome and to provide accessible resources of epigenetic maps and profiles of stem cells and somatic tissue types for a better understanding of their function and the correlation of epigenetic aberrancies with certain disease profiles. This may expose the effect of DNA methylation to certain CpG sites or promoter regions which may lead to the suppression of gene activity, an event related to early cancer development.

It is therefore apparent that there is a great demand for high-throughput screening approaches and high-resolution techniques for deep and in parallel analysis of DNA methylation patterns. Given the use of large scale microarrays and sequencing based methods for detection and analysis of DNA methylation of several CpG regions in parallel, the need for techniques to assess the signals derived from DNA methylation measurements as results of deep DNA methylation analysis of one or more genetic locations is highly important, given the requirements for a single base pair resolution of the methylation sequential information. The development of bioinformatic tools and analytical software to satisfy this need is under rapid development. For most platforms, DNA methylation measurements represent absolute values for a given sample, with the resulting measurements to be expressed in the form of a *ratio* fraction, a marker that has been used to assess the percentage of methylation [31]. The ratio is used as a way to express the signal derived from methylated sites against the sum of the signals from methylated and unmethylated sites as:

$$\%Meth = \frac{M}{M+U} \times 100\% \tag{2.1}$$

The resulting measurement is fitted on a scale from 0 to 1 or from 0 to 100%, with 0 indicating that no methylated cytosines were identified in the genetic location (CpG locus) under investigation and 1 or 100% indicating that all cytosines identified were methylated [31]. This is also mentioned as a β distribution. Examples of the use of the ratio of the methylated signal intensity have been reported by Bibikova et al. [103] and Hu et al. [107] to signify the percentage of methylation generated by a high-throughput array analysis of DNA methylation patterns while distinguishing normal cells from cancer cells and to measure the methylation percentage level in a sample using the method of Surface-Enhanced Raman spectroscopy (SERS) respectively.

Moreover, the DNA methylation ratio has been used as a biomarker for prenatal diagnosis of genetic abnormalities. Research conducted by Papageorgiou et al. [108] proposed the use of the ratio of methylation to investigate the DNA methylation pattern of differ-

entially methylated regions on chromosome 21, abnormalities in which can be related to genetic disorders such as the Down's syndrome. The DNA methylation ratio was used as a biomarker for detection of abnormal genetic traits of the fetus allowing for quantification of the amount of fetal DNA in free fetal maternal circulating DNA. The ratio was calculated based on the differences of the methylated regions of chromosome 21 between the mother and the fetus through the use of the methods MeDIP and quantitative PCR.

In addition to the use of the DNA methylation ratio for DNA methylation analysis of signals derived from given DNA samples, the use of $log(M/U)$ to quantify DNA methylation using the ratio of methylated and unmethylated molecules of a given CpG region has also gained acceptance, especially when used in conjunction with microarray based methylation analysis methods [86, 109]. The use of $log(M/U)$ may create however constraints given that M and U are not entirely inversely correlated within CpG regions. Also the use of M/U may create distortions in the processing analysis when multiple CpG regions are to be processed, given its ability to assess only independent CpG loci [31]. In this thesis, we will show how to use integrated circuits to perform computation of the ratio in real-time using semiconductor based pH sensors.

2.5.1 Other approaches for DNA methylation detection

Additionally to the well-established methods for DNA methylation detection that have been described above, further attempts have been made on performing DNA methylation analysis using other detection techniques both optical and electrical, labelled and label-free, with variable sensitivities and detection limits.

Several label-free optical biosensors for DNA methylation detection have been developed promising a label-free approach for amplification and analysis of methylated sequences. Previously reported work by Suter et al. [110] proposed the use of Opto-Fluidic Ring Resonators (OFRR) for quantitative DNA methylation analysis, combined with the use of methyl-binding proteins or antibodies to capture methylated sequences in real-time. Although the proposed method performed a good discrimination between methylation changes in DNA samples, the method depends on the limitations that affinity based methods are challenged by as has been mentioned in Section 2.4.2. Also the fact that methyl-binding proteins show higher specificity to double-stranded DNA opposed to antibodies which tend to bind more effectively to single-stranded DNA, makes the standardisation of the method a necessary requirement. Following on from this, Shin et al. [111] proposed the use of arrays of label-

free silicon microring resonators to detect and quantify DNA methylation in bladder cancer biomarkers while avoiding the use of methyl-binding proteins. DNA methylation probes were immobilised on the microrings and methylated or unmethylated genetic targets hybridised to the probes only when complementary matching was to be achieved. The signal derived from hybridisation was detected as a wavelength shift of the resonators which was varying based on the gene methylation density. However, the specificity of both [110, 111] can be highly dependent on the length of the DNA probe therefore affecting the wavelength shift and thus the signal of detection. Additionally, possible mismatches during hybridisation may be difficult to be detected with a direct effect to the methods detection sensitivity. Moreover, Feng et al. [55] suggested the use of a label-free system for optical analysis of the methylation status of specific CpG sites, offering a fluorescence based detection while avoiding the use of dye-labeled DNA probes.

In addition to the previously mentioned methods and the use of optical approaches and/or magnetic beads [116] or the use of nanoparticles [117] in DNA methylation based methods of detection, which may increase the levels of complexity when the need for large scale technologies stays paramount, new detection techniques have been proposed, offering electrical discrimination of methylated from unmethylated molecules, fewer false positives and good accuracy of detection. Zhang et al. [112] reported the use of an arrayed droplet-in-oil microfluidic platform deposited on a silicon substrate, combined with Methylation-Specific PCR (MSP) for methylation-specific DNA amplification and detection, allowing infusion of minute amounts of DNA sample for array based DNA methylation analysis. The proposed method performs high-density methylation-specific amplification reactions in parallel, using micro MSP assays which benefit from the use of microfluidic open chambers hosting the reaction mixtures after a series of injections, arranged in a circular array set-up, with the detection results to be analysed using fluorescent dyes.

Moreover, Maki et al. [113] first presented the use of nanowire field effect transistor based biosensor technology for label-free electrical DNA methylation detection on-chip, avoiding the use of bisulfite treatment of a DNA sample or of any extra step of DNA amplification. Magnetic beads are used to capture the methylated DNA targets which are then released and introduced on the sensing surface of the nanowire based transistor. Changes in the inherent negative DNA charge due to the captured DNA targets, already recognised by monoclonal antibodies immobilised on the sensing surface, induce a change in the electrical properties of the nanowire based transistor, generating an electronic signal as a result of DNA methylation detection. The method reported good sensitivity of detection and no false

Table 2.4: Comparison of main optically and electrically based DNA methylation techniques

Method	Type	Principle	Limitation	Label-free
Opto-Fluidic Ring Resonators (OFRR) [110]	Quantitative	Affinity based optical detection using ring resonators	Dependence on antibodies or methyl-binding proteins, difficult to standardise	Yes
Silicon microring resonators [111]	Quantitative	MSP combined with array of microrings, DNA hybridisation	Dependence on DNA probe invariabilities	Yes
Droplet-in-oil PCR array [112]	Quantitative	MSP in circular arrays on silicon substrate	Technical demands, dependence on dyes	No
Nanowire Field-Effect Transistor [113]	Quantitative	Affinity based methylation-specific detection combined with DNA hybridisation and nanowire based electrical sensing	Dependence on antibodies, magnetic beads, nanowire fabrication	Yes
Solid-state nanopores [114, 115]	Quantitative	Electrical detection using nanopores	Electrical signals depend on structure and stability of nanopores, dependence on methyl-binding proteins in case of [115]	No

positives. However, the use of antibodies as well as of tags for detecting targeted sequences increases the complexity of the method with a secondary limitation of the post-processing steps added during nanowire fabrication which may affect dramatically the behaviour of the nanopore as well as the signal to noise ratio, together with the incompatibility of such patterns with large scale integration using CMOS.

Finally, synthetic solid-state nanopores have also been proposed by Misraidov et al. [114] to test the electromechanical properties of methylated DNA due to the interruption these molecules may create to the ionic flow through the pore. The methylation level of DNA molecules was correlated to changes in the threshold voltage of the nanopore observed during the permeation of methylated DNA through the pore. Only one DNA molecule could permeate each pore at a time due to the small size of the nanopore, forced by the use of an electric field strong enough to avoid any pore blockage during permeation. The permeability of the pore was expressed with respect to the voltage applied across its membrane with the efficiency of detection of methylated molecules to be claimed as comparable as to the one of methyl-binding proteins. One more example of using solid-state nanopores for detection and quantification of DNA methylation was presented by Shin et al. [115], showing the capability of electrical discrimination between methylated and unmethylated DNA using methyl-binding proteins at a single methylated CpG site resolution. The number of methylation sites was determined based on the number of methyl-binding proteins with the thickness of the nanopore to be defined such that multiple bound proteins could contribute to the current measured, increasing however the chance for non-specific products. Also, the electronic signals generated for a given voltage set across the pore were dependent on the reproducible structural stability of the nanopores. Variations in the shape of nanopores may also contribute in the ionic noise induced in the detectable signal during the recordings and thus in low yield per assay.

Hence, after reviewing the most frequently used methods for DNA methylation detection together with possible limitations that they may be accompanied with, as seen in Table 2.4, it becomes apparent that what is required to accommodate the needs for a sensitive and specific approach for such application is first, a technology that would overcome the limitations of the current methods for DNA methylation detection and further enhance the applicability through large scale integration. Such method should be easily accessible to blood based biomarkers and should be capable of giving a clear sign on the status and aggressiveness of cancer, avoiding the inherent complexity that such disease has by nature, by reducing the amount of false positives/negatives. Thus, there is an urgent need for the development

of DNA methylation detection assays using technologies capable to offer large scale integration and standardised procedures of fabrication, while meeting the current demands of healthcare which are simplicity, portability, low cost, accuracy, rapid time to result and intelligence. This will potentially remove the existing and justified scepticism around the reliability and sensitivity of a lab based test for cancer screening or of a commonly applied therapy scheme, which will pave the way for future technology in cancer management, acting as a powerful tool towards the closed-loop detection and guided therapy of cancer. We believe that there is great potential for this task to be realised using well-established CMOS technology, due to its inherent capability for large scale integration of microelectronic based sensing platforms.

2.6 Summary

Epigenetic modifications cause significant dysregulation on the transcriptional activity of tumour suppressor genes or the pathways responsible for gene expression, being considered as a central driving force in the molecular pathology of various cancer types, influencing the stages of tumour initiation and progression through gene inactivation. DNA methylation, in particular, has been one of the key epigenetic factors as well as an attractive biomarker involved in human development but also in a number of diseases, especially cancer. The role of DNA methylation in cancer development is well characterised by aberrancies in methylation patterns of tumour suppressor genes, located in the CpG regions of the promoter regions of genes, contributing in gene silencing, an event frequently seen and studied in cancer.

The analysis of DNA methylation based biomarkers is a rapidly advancing area of research, being actively studied in all stages of cancer progression in multiple cancer types, with the possibility of the methylation profile of genes to distinguish tumour types and perhaps the response to therapeutic regimes. Already, DNA methylation patterns in cancer related genes have been identified in blood (i.e. plasma, serum) of cancer patients as well as in body fluids, apart from tumour biopsies, letting DNA methylation be described as a very promising biomarker for tumour detection and validation of tumour types as well as for prediction of the risk of tumour recurrence. Therefore, the need for detection of DNA methylation patterns appears to be of paramount importance, especially for early screening of cancer when the disease may not have expressed its signs yet.

Several well-established methods have been developed for DNA methylation detection and analysis, providing information at a CpG locus or at a sequence level, with various sensitivities, resolution and signal densities. Novel methods have also been developed based on optical or electrical principles of detection, with varying complexities, post-processing requirements, implementation challenges and cost needs. Nonetheless, the need for accurate and well-targeted DNA methylation detection strategies is still existent with the requirements for large scale analysis of large numbers of samples to continuously increase. Hence, there is an urgent need for the development of detection assays, using well-established technologies that would meet these demands, in addition to satisfying some of the current needs of healthcare technology such as simplicity, portability, sensitivity, low cost, scalability, rapid time to result and intelligence, ultimately leading to the realisation of a well-targeted strategy towards cancer screening.

References

[1] M. Esteller, "Epigenetics in cancer," *New England Journal of Medicine*, vol. 358, no. 11, pp. 1148–1159, 2008.

[2] R. Weinberg, *The biology of cancer*. Garland Science New York, 2007.

[3] B. Vogelstein and K. Kinzler, "Cancer genes and the pathways they control," *Nature Medicine*, vol. 10, no. 8, pp. 789–799, 2004.

[4] D. Hanahan and R. Weinberg, "Hallmarks of cancer: the next generation," *Cell*, vol. 144, no. 5, pp. 646–674, 2011.

[5] P. Jones and S. Baylin, "The epigenomics of cancer," *Cell*, vol. 128, no. 4, pp. 683–692, 2007.

[6] M. Esteller, "Cancer epigenomics: DNA methylomes and histone-modification maps," *Nature Reviews Genetics*, vol. 8, no. 4, pp. 286–298, 2007.

[7] Z. Herceg, "Epigenetics and cancer: towards an evaluation of the impact of environmental and dietary factors," *Mutagenesis*, vol. 22, no. 2, pp. 91–103, 2007.

[8] S. Baylin and P. Jones, "A decade of exploring the cancer epigenome-biological and translational implications," *Nature Reviews Cancer*, vol. 11, no. 10, pp. 726–734, 2011.

[9] M. Lambert and Z. Herceg, "Epigenetics and cancer, 2nd IARC meeting, Lyon, France, 6 and 7 December 2007.," *Molecular Oncology*, vol. 2, no. 1, p. 33, 2008.

[10] J. Qiu, "Epigenetics: unfinished symphony," *Nature*, vol. 441, no. 7090, pp. 143–145, 2006.

[11] M. Widschwendter and U. Menon, "Circulating methylated DNA: a new generation of tumor markers," *Clinical Cancer Research*, vol. 12, no. 24, pp. 7205–7208, 2006.

[12] A. Feinberg and B. Tycko, "The history of cancer epigenetics," *Nature Reviews Cancer*, vol. 4, no. 2, pp. 143–153, 2004.

[13] P. Jones and S. Baylin, "The fundamental role of epigenetic events in cancer," *Nature Reviews Genetics*, vol. 3, no. 6, pp. 415–428, 2002.

[14] P. Laird, "The power and the promise of DNA methylation markers," *Nature Reviews Cancer*, vol. 3, no. 4, pp. 253–266, 2003.

[15] M. Dawson and T. Kouzarides, "Cancer epigenetics: from mechanism to therapy," *Cell*, vol. 150, no. 1, pp. 12–27, 2012.

[16] S. Baylin and J. Herman, "DNA hypermethylation in tumorigenesis: epigenetics joins genetics," *Trends in Genetics*, vol. 16, no. 4, pp. 168–174, 2000.

[17] P. Das and R. Singal, "DNA methylation and cancer," *Journal of Clinical Oncology*, vol. 22, no. 22, pp. 4632–4642, 2004.

[18] M. Esteller, "CpG island hypermethylation and tumor suppressor genes: a booming present, a brighter future.," *Oncogene*, vol. 21, no. 35, p. 5427, 2002.

[19] J. Herman and S. Baylin, "Gene silencing in cancer in association with promoter hypermethylation," *New England Journal of Medicine*, vol. 349, no. 21, pp. 2042–2054, 2003.

[20] C. Waddington, "An introduction to modern genetics.," *An Introduction to Modern Genetics.*, 1939.

[21] C. Waddington, "The epigenotype," *Endeavor*, vol. 1, pp. 18–20, 1942.

[22] J. Slack, "Conrad Hal Waddington: the last renaissance biologist?," *Nature Reviews Genetics*, vol. 3, no. 11, pp. 889–895, 2002.

[23] A. Portela and M. Esteller, "Epigenetic modifications and human disease," *Nature biotechnology*, vol. 28, no. 10, pp. 1057–1068, 2010.

[24] S. Sharma, T. Kelly, and P. Jones, "Epigenetics in cancer," *Carcinogenesis*, vol. 31, no. 1, pp. 27–36, 2010.

[25] A. Meissner, "Epigenetic modifications in pluripotent and differentiated cells," *Nature Biotechnology*, vol. 28, no. 10, pp. 1079–1088, 2010.

[26] J. Sandoval and M. Esteller, "Cancer epigenomics: beyond genomics," *Current opinion in genetics & development*, vol. 22, no. 1, pp. 50–55, 2012.

[27] J. You and P. Jones, "Cancer genetics and epigenetics: two sides of the same coin?," *Cancer Cell*, vol. 22, no. 1, pp. 9–20, 2012.

[28] P. Jones, "Overview of cancer epigenetics," *Seminars in Hematology*, vol. 42, pp. S3–S8, 2005.

[29] M. Łuczak and P. Jagodzinski, "The role of DNA methylation in cancer development," *Folia Histochem Cytobiol*, vol. 44, pp. 143–154, 2006.

[30] B. Sadikovic, K. Al-Romaih, J. Squire, and M. Zielenska, "Cause and consequences of genetic and epigenetic alterations in human cancer," *Current Genomics*, vol. 9, no. 6, p. 394, 2008.

[31] P. Laird, "Principles and challenges of genome-wide DNA methylation analysis," *Nature Reviews Genetics*, vol. 11, no. 3, pp. 191–203, 2010.

[32] H.-C. Tsai, H. Li, L. Van Neste, Y. Cai, C. Robert, F. Rassool, J. Shin, K. Harbom, R. Beaty, *et al.*, "Transient low doses of DNA-demethylating agents exert durable antitumor effects on hematological and epithelial tumor cells," *Cancer Cell*, vol. 21, no. 3, pp. 430–446, 2012.

[33] K. Robertson *et al.*, "DNA methylation and chromatin-unraveling the tangled web," *Oncogene*, vol. 21, no. 35, pp. 5361–5379, 2002.

[34] Y. Kanai and S. Hirohashi, "Alterations of DNA methylation associated with abnormalities of DNA methyltransferases in human cancers during transition from a precancerous to a malignant state," *Carcinogenesis*, vol. 28, no. 12, pp. 2434–2442, 2007.

[35] S. Cross and A. Bird, "CpG islands and genes," *Current Opinion in Genetics & Development*, vol. 5, no. 3, pp. 309–314, 1995.

[36] A. Bird, "DNA methylation patterns and epigenetic memory," *Genes & Development*, vol. 16, no. 1, pp. 6–21, 2002.

[37] D. Takai and P. Jones, "Comprehensive analysis of CpG islands in human chromosomes 21 and 22," *Proceedings of the National Academy of Sciences*, vol. 99, no. 6, pp. 3740–3745, 2002.

[38] M. Esteller, P. Corn, S. Baylin, and J. Herman, "A gene hypermethylation profile of human cancer," *Cancer Research*, vol. 61, no. 8, pp. 3225–3229, 2001.

[39] H. Heyn and M. Esteller, "DNA methylation profiling in the clinic: applications and challenges," *Nature Reviews Genetics*, vol. 13, no. 10, pp. 679–692, 2012.

[40] Z. Zhao and L. Han, "CpG islands: algorithms and applications in methylation studies," *Biochemical and Biophysical Research Communications*, vol. 382, no. 4, pp. 643–645, 2009.

[41] Y. Wang and F. Leung, "An evaluation of new criteria for CpG islands in the human genome as gene markers," *Bioinformatics*, vol. 20, no. 7, pp. 1170–1177, 2004.

[42] H. Cheung, T. Lee, O. Rennert, and W. Chan, "DNA methylation of cancer genome," *Birth Defects Research Part C: Embryo Today: Reviews*, vol. 87, no. 4, pp. 335–350, 2009.

[43] M. Ongenaert, L. Van Neste, T. De Meyer, G. Menschaert, S. Bekaert, and W. Van Criekinge, "PubMeth: a cancer methylation database combining text-mining and expert annotation," *Nucleic Acids Research*, vol. 36, no. suppl 1, pp. D842–D846, 2008.

[44] T. Murphy, A. Perry, and M. Lawler, "The emergence of DNA methylation as a key modulator of aberrant cell death in prostate cancer," *Endocrine-related cancer*, vol. 15, no. 1, pp. 11–25, 2008.

[45] M. Esteller, M. Sanchez-Cespedes, R. Rosell, D. Sidransky, S. Baylin, and J. Herman, "Detection of aberrant promoter hypermethylation of tumor suppressor genes in serum DNA from non-small cell lung cancer patients," *Cancer Research*, vol. 59, no. 1, p. 67, 1999.

[46] I. Wong, Y. Lo, J. Zhang, C.-T. Liew, M. Ng, N. Wong, P. Lai, W. Lau, N. Hjelm, and P. Johnson, "Detection of aberrant p16 methylation in the plasma and serum of liver cancer patients," *Cancer Research*, vol. 59, no. 1, pp. 71–73, 1999.

[47] R. Board, L. Knight, A. Greystoke, F. Blackhall, A. Hughes, C. Dive, and M. Ranson, "DNA methylation in circulating tumour DNA as a biomarker for cancer," *Biomarker Insights*, vol. 2, p. 307, 2007.

[48] D. Hodgson, R. Wellings, M. Orr, R. McCormack, M. Malone, R. Board, and M. Cantarini, "Circulating tumour-derived predictive biomarkers in oncology," *Drug Discovery Today*, vol. 15, no. 3-4, pp. 98–101, 2010.

[49] S. Leon, B. Shapiro, D. Sklaroff, and M. Yaros, "Free DNA in the serum of cancer patients and the effect of therapy," *Cancer Research*, vol. 37, no. 3, pp. 646–650, 1977.

[50] R. Tetzner, F. Model, G. Weiss, M. Schuster, J. Distler, K. Steiger, R. Grützmann, C. Pilarsky, J. Habermann, P. Fleshner, *et al.*, "Circulating methylated SEPT9 DNA in plasma is a biomarker for colorectal cancer," *Clinical Chemistry*, vol. 55, no. 7, pp. 1337–1346, 2009.

[51] S. Shukla, S. Mirza, G. Sharma, R. Parshad, S. Gupta, and R. Ralhan, "Detection of RASSF1A and RARβ hypermethylation in serum DNA from breast cancer patients.," *Epigenetics: official journal of the DNA Methylation Society*, vol. 1, no. 2, p. 88, 2006.

[52] C. Goessl, H. Krause, M. Muller, R. Heicappell, M. Schrader, J. Sachsinger, and K. Miller, "Fluorescent methylation-specific polymerase chain reaction for DNA-based detection of prostate cancer in bodily fluids," *Cancer Research*, vol. 60, no. 21, p. 5941, 2000.

[53] S. Tan, H. Ida, Q. Lau, B. Goh, W. Chieng, M. Loh, and Y. Ito, "Detection of promoter hypermethylation in serum samples of cancer patients by methylation-specific polymerase chain reaction for tumour suppressor genes including RUNX3," *Oncology Reports*, vol. 18, no. 5, pp. 1225–1230, 2007.

[54] I. Wong, Y. Dennis Lo, W. Yeo, W. Lau, and P. Johnson, "Frequent p15 promoter methylation in tumour and peripheral blood from hepatocellular carcinoma patients," *Clinical Cancer Research*, vol. 6, no. 9, p. 3516, 2000.

[55] F. Feng, H. Wang, L. Han, and S. Wang, "Fluorescent conjugated polyelectrolyte as an indicator for convenient detection of DNA methylation," *Journal of the American Chemical Society*, vol. 130, no. 34, pp. 11338–11343, 2008.

[56] G. Heller, C. Zielinski, and S. Zöchbauer-Müller, "Lung cancer: from single-gene methylation to methylome profiling," *Cancer and Metastasis Reviews*, vol. 29, no. 1, pp. 95–107, 2010.

[57] W. Niklinska, W. Naumnik, A. Sulewska, M. Kozłowski, W. Pankiewicz, and R. Milewski, "Prognostic significance of DAPK and RASSF1A promoter hypermethylation in non-small cell lung cancer (NSCLC)," *Folia Histochemica et Cytobiologica*, vol. 47, no. 2, pp. 275–280, 2009.

[58] T. Vaissière, R. Hung, D. Zaridze, A. Moukeria, C. Cuenin, V. Fasolo, G. Ferro, A. Paliwal, P. Hainaut, P. Brennan, *et al.*, "Quantitative analysis of DNA methylation profiles in lung cancer identifies aberrant DNA methylation of specific genes and its association with gender and cancer risk factors," *Cancer Research*, vol. 69, no. 1, pp. 243–252, 2009.

[59] G. Pfeifer and T. Rauch, "DNA methylation patterns in lung carcinomas," in *Seminars in Cancer Biology*, vol. 19, pp. 181–187, Elsevier, 2009.

[60] P. Anglim, T. Alonzo, and I. Laird-Offringa, "DNA methylation-based biomarkers for early detection of non-small cell lung cancer: an update," *Molecular Cancer*, vol. 7, no. 1, p. 81, 2008.

[61] S. Belinsky, D. Klinge, J. Dekker, M. Smith, T. Bocklage, F. Gilliland, R. Crowell, D. Karp, C. Stidley, and M. Picchi, "Gene promoter methylation in plasma and sputum increases with lung cancer risk," *Clinical Cancer Research*, vol. 11, no. 18, pp. 6505–6511, 2005.

[62] M. Brock, C. Hooker, E. Ota-Machida, Y. Han, M. Guo, S. Ames, S. Glöckner, S. Piantadosi, E. Gabrielson, G. Pridham, *et al.*, "DNA methylation markers and early recurrence in stage I lung cancer," *New England Journal of Medicine*, vol. 358, no. 11, pp. 1118–1128, 2008.

[63] L. Van Neste, J. Herman, G. Otto, J. Bigley, J. Epstein, and W. Van Criekinge, "The epigenetic promise for prostate cancer diagnosis," *The Prostate*, vol. 72, no. 11, pp. 1248–1261, 2012.

[64] T. Debniak, B. Gorski, T. Huzarski, T. Byrski, C. Cybulski, A. Mackiewicz, S. Gozdecka-Grodecka, J. Gronwald, E. Kowalska, O. Haus, *et al.*, "A common variant of CDKN2A (p16) predisposes to breast cancer," *Journal of Medical Genetics*, vol. 42, no. 10, pp. 763–765, 2005.

[65] A. Dworkin, T.-M. Huang, and A. Toland, "Epigenetic alterations in the breast: Implications for breast cancer detection, prognosis and treatment," in *Seminars in Cancer Biology*, vol. 19, pp. 165–171, Elsevier, 2009.

[66] E. Dulaimi, J. Hillinck, I. de Caceres, T. Al-Saleem, and P. Cairns, "Tumor suppressor gene promoter hypermethylation in serum of breast cancer patients," *Clinical Cancer Research*, vol. 10, no. 18, pp. 6189–6193, 2004.

[67] M. Hoque, Q. Feng, P. Toure, A. Dem, C. Critchlow, S. Hawes, T. Wood, C. Jeronimo, E. Rosenbaum, J. Stern, *et al.*, "Detection of aberrant methylation of four genes in plasma DNA for the detection of breast cancer," *Journal of Clinical Oncology*, vol. 24, no. 26, pp. 4262–4269, 2006.

[68] J. Brooks, P. Cairns, and A. Zeleniuch-Jacquotte, "Promoter methylation and the detection of breast cancer," *Cancer Causes & Control*, vol. 20, no. 9, pp. 1539–1550, 2009.

[69] H. Müller, A. Widschwendter, H. Fiegl, L. Ivarsson, G. Goebel, E. Perkmann, C. Marth, and M. Widschwendter, "DNA methylation in serum of breast cancer patients an independent prognostic marker," *Cancer Research*, vol. 63, no. 22, pp. 7641–7645, 2003.

[70] J. Graff, E. Gabrielson, H. Fujii, S. Baylin, and J. Herman, "Methylation patterns of the E-cadherin 5' CpG island are unstable and reflect the dynamic, heterogeneous loss of E-cadherin expression during metastatic progression," *Journal of Biological Chemistry*, vol. 275, no. 4, pp. 2727–2732, 2000.

[71] H. Kawasaki, E. Igawa, R. Kohosozawa, M. Kobayashi, R. Nishiko, and H. Abe, "Detection of aberrant methylation of tumor suppressor genes in plasma from cancer patients," *Personalized Medicine Universe*, 2013.

[72] E. Braggio, A. Maiolino, M. Gouveia, R. Magalhães, J. Souto Filho, M. Garnica, M. Nucci, and I. Renault, "Methylation status of nine tumor suppressor genes in multiple myeloma," *International Journal of Hematology*, vol. 91, no. 1, pp. 87–96, 2010.

[73] M. Kim, J. Lee, and D. Sidransky, "DNA methylation markers in colorectal cancer," *Cancer and Metastasis Reviews*, vol. 29, no. 1, pp. 181–206, 2010.

[74] B.-L. Liu, J.-X. Cheng, W. Zhang, X. Zhang, R. Wang, H. Lin, J.-L. Huo, and H. Cheng, "Quantitative detection of multiple gene promoter hypermethylation in tumor tissue, serum and cerebrospinal fluid predicts prognosis of malignant gliomas," *Neuro-oncology*, vol. 12, no. 6, pp. 540–548, 2010.

[75] L. Kristensen and L. Hansen, "PCR-based methods for detecting single-locus DNA methylation biomarkers in cancer diagnostics, prognostics, and response to treatment," *Clinical Chemistry*, vol. 55, no. 8, pp. 1471–1483, 2009.

[76] A. Harrison and A. Parle-Mcdermott, "DNA methylation: a timeline of methods and applications," *Frontiers in Genetics*, vol. 2, no. 74, pp. 1–13, 2011.

[77] J. Sandoval, H. Heyn, S. Moran, J. Serra-Musach, M. Pujana, M. Bibikova, and M. Esteller, "Validation of a DNA methylation microarray for 450,000 CpG sites in the human genome," *Epigenetics*, vol. 6, no. 6, pp. 692–702, 2011.

[78] M. Bibikova, B. Barnes, C. Tsan, V. Ho, B. Klotzle, J. Le, D. Delano, L. Zhang, G. Schroth, K. Gunderson, *et al.*, "High density DNA methylation array with single CpG site resolution," *Genomics*, vol. 98, no. 4, pp. 288–295, 2011.

[79] I. Hatada, A. Kato, S. Morita, Y. Obata, K. Nagaoka, A. Sakurada, M. Sato, A. Horii, A. Tsujimoto, and K. Matsubara, "A microarray-based method for detecting methylated loci," *Journal of human genetics*, vol. 47, no. 8, pp. 448–451, 2002.

[80] R. Harris, T. Wang, C. Coarfa, R. Nagarajan, C. Hong, S. Downey, B. Johnson, S. Fouse, A. Delaney, Y. Zhao, *et al.*, "Comparison of sequencing-based methods to profile DNA methylation and identification of monoallelic epigenetic modifications," *Nature biotechnology*, vol. 28, no. 10, pp. 1097–1105, 2010.

[81] R. Lister and J. Ecker, "Finding the fifth base: genome-wide sequencing of cytosine methylation," *Genome Research*, vol. 19, no. 6, pp. 959–966, 2009.

[82] C. Waalwijk and R. Flavell, "DNA methylation at a CCGG sequence in the large intron of the rabbit β-globin gene: tissue-specific variations," *Nucleic acids research*, vol. 5, no. 12, pp. 4631–4642, 1978.

[83] A. Nygren, N. Ameziane, H. Duarte, R. Vijzelaar, Q. Waisfisz, C. Hess, J. Schouten, and A. Errami, "Methylation-specific MLPA (MS-MLPA): simultaneous detection of cpg methylation and copy number changes of up to 40 sequences," *Nucleic Acids Research*, vol. 33, no. 14, pp. e128–e128, 2005.

[84] T. Akama, Y. Okazaki, M. Ito, H. Okuizumi, H. Konno, M. Muramatsu, C. Plass, W. Held, and Y. Hayashizaki, "Restriction landmark genomic scanning (RLGS-M)-based genome-wide scanning of mouse liver tumors for alterations in DNA methylation status," *Cancer Research*, vol. 57, no. 15, pp. 3294–3299, 1997.

[85] T.-M. Huang, M. Perry, and D. Laux, "Methylation profiling of CpG islands in human breast cancer cells," *Human Molecular Genetics*, vol. 8, no. 3, pp. 459–470, 1999.

[86] R. Irizarry, C. Ladd-Acosta, B. Carvalho, H. Wu, S. Brandenburg, J. Jeddeloh, B. Wen, and A. Feinberg, "Comprehensive high-throughput arrays for relative methylation (CHARM)," *Genome Research*, vol. 18, no. 5, pp. 780–790, 2008.

[87] B. Khulan, R. Thompson, K. Ye, M. Fazzari, M. Suzuki, E. Stasiek, M. Figueroa, J. Glass, Q. Chen, C. Montagna, *et al.*, "Comparative isoschizomer profiling of cytosine methylation: the HELP assay," *Genome Research*, vol. 16, no. 8, pp. 1046–1055, 2006.

[88] M. Oda, J. Glass, R. Thompson, Y. Mo, E. Olivier, M. Figueroa, R. Selzer, T. Richmond, X. Zhang, L. Dannenberg, *et al.*, "High-resolution genome-wide cytosine methylation profiling with simultaneous copy number analysis and optimization for limited cell numbers," *Nucleic Acids Research*, vol. 37, no. 12, pp. 3829–3839, 2009.

[89] J. Weber, M.and Davies, D. Wittig, E. Oakeley, W. Haase, M.and Lam, and D. Schuebeler, "Chromosome-wide and promoter-specific analyses identify sites of differential DNA methylation in normal and transformed human cells," *Nature Genetics*, vol. 37, no. 8, pp. 853–862, 2005.

[90] T. Down, V. Rakyan, D. Turner, P. Flicek, H. Li, E. Kulesha, S. Graef, N. Johnson, J. Herrero, E. Tomazou, *et al.*, "A Bayesian deconvolution strategy for immunoprecipitation-based DNA methylome analysis," *Nature Biotechnology*, vol. 26, no. 7, pp. 779–785, 2008.

[91] D. Serre, B. Lee, and A. Ting, "MBD-isolated Genome Sequencing provides a high-throughput and comprehensive survey of DNA methylation in the human genome," *Nucleic Acids Research*, vol. 38, no. 2, pp. 391–399, 2010.

[92] M. Ball, J. Li, Y. Gao, J.-H. Lee, E. LeProust, I.-H. Park, B. Xie, G. Daley, and G. Church, "Targeted and genome-scale strategies reveal gene-body methylation signatures in human cells," *Nature Biotechnology*, vol. 27, no. 4, pp. 361–368, 2009.

[93] M. Frommer, L. McDonald, D. Millar, C. Collis, F. Watt, G. Grigg, P. Molloy, and C. Paul, "A genomic sequencing protocol that yields a positive display of 5-methylcytosine residues in individual DNA strands," *Proceedings of the National Academy of Sciences of the United States of America*, vol. 89, no. 5, pp. 1827–1831, 1992.

[94] S. CIark, J. Harrison, C. Paul, and M. Frommer, "High sensitivity mapping of methylated cytosines," *Nucleic Acids Research*, vol. 22, no. 15, pp. 2990–2997, 1994.

[95] O. Sadik, A. Aluoch, and A. Zhou, "Status of biomolecular recognition using electrochemical techniques," *Biosensors and Bioelectronics*, vol. 24, no. 9, pp. 2749–2765, 2009.

[96] O. Ammerpohl, J. Martín-Subero, J. Richter, I. Vater, and R. Siebert, "Hunting for the 5th base: Techniques for analyzing DNA methylation," *Biochimica et Biophysica Acta (BBA)-General Subjects*, vol. 1790, no. 9, pp. 847–862, 2009.

[97] J. Herman, J. Graff, S. Myöhänen, B. Nelkin, and S. Baylin, "Methylation-specific PCR: a novel PCR assay for methylation status of CpG islands," *Proceedings of the National Academy of Sciences*, vol. 93, no. 18, pp. 9821–9826, 1996.

[98] Z. Xiong and P. Laird, "COBRA: a sensitive and quantitative DNA methylation assay," *Nucleic Acids Research*, vol. 25, no. 12, pp. 2532–2534, 1997.

[99] M. Gonzalgo and P. Jones, "Rapid quantitation of methylation differences at specific sites using methylation-sensitive single nucleotide primer extension (Ms-SNuPE)," *Nucleic Acids Research*, vol. 25, no. 12, pp. 2529–2531, 1997.

[100] C. Eads, K. Danenberg, K. Kawakami, L. Saltz, C. Blake, D. Shibata, P. Danenberg, and P. Laird, "MethyLight: a high-throughput assay to measure DNA methylation," *Nucleic Acids Research*, vol. 28, no. 8, pp. e32i–e32viii, 2000.

[101] K. Uhlmann, A. Brinckmann, M. Toliat, H. Ritter, and P. Nürnberg, "Evaluation of a potential epigenetic biomarker by quantitative methyl-single nucleotide polymorphism analysis," *Electrophoresis*, vol. 23, no. 24, pp. 4072–4079, 2002.

[102] M. Ronaghi, S. Karamohamed, B. Pettersson, M. Uhlén, P. Nyrén, *et al.*, "Real-time DNA sequencing using detection of pyrophosphate release," *Analytical biochemistry*, vol. 242, no. 1, pp. 84–89, 1996.

[103] M. Bibikova, Z. Lin, L. Zhou, E. Chudin, E. Garcia, B. Wu, D. Doucet, N. Thomas, Y. Wang, E. Vollmer, *et al.*, "High-throughput DNA methylation profiling using universal bead arrays," *Genome Research*, vol. 16, no. 3, pp. 383–393, 2006.

[104] M. Bibikova, J. Le, B. Barnes, S. Saedinia-Melnyk, L. Zhou, R. Shen, and K. Gunderson, "Genome-wide DNA methylation profiling using Infinium assay," *Epigenomics*, vol. 1, no. 1, pp. 177–200, 2009.

[105] D. Adams, L. Altucci, S. Antonarakis, J. Ballesteros, A. B. C. Beck, S.and Bird, *et al.*, "BLUEPRINT to decode the epigenetic signature written in blood," *Nature biotechnology*, vol. 30, no. 3, pp. 224–226, 2012.

[106] B. Bernstein, J. Stamatoyannopoulos, J. Costello, A. Ren, B.and Milosavljevic, A. Meissner, M. Kellis, M. Marra, A. Beaudet, J. Ecker, *et al.*, "The NIH roadmap epigenomics mapping consortium," *Nature biotechnology*, vol. 28, no. 10, pp. 1045–1048, 2010.

[107] J. Hu and C.-Y. Zhang, "Single base extension reaction-based surface enhanced Raman spectroscopy for DNA methylation assay," *Biosensors and Bioelectronics*, vol. 31, no. 1, pp. 451–457, 2012.

[108] E. Papageorgiou, A. Karagrigoriou, E. Tsaliki, V. Velissariou, N. Carter, and P. Patsalis, "Fetal-specific DNA methylation ratio permits noninvasive prenatal diagnosis of trisomy 21," *Nature medicine*, vol. 17, no. 4, pp. 510–513, 2011.

[109] F. Model, P. Adorjan, A. Olek, and C. Piepenbrock, "Feature selection for DNA methylation based cancer classification," *Bioinformatics*, vol. 17, no. suppl 1, pp. S157–S164, 2001.

[110] G. Yang, I. White, and X. Fan, "An opto-fluidic ring resonator biosensor for the detection of organophosphorus pesticides," *Sensors and Actuators B: Chemical*, vol. 133, no. 1, pp. 105–112, 2008.

[111] Y. Shin, A. Perera, J. Kee, J. Song, Q. Fang, G.-Q. Lo, and M. Park, "Label-free methylation specific sensor based on silicon microring resonators for detection and quantification of DNA methylation biomarkers in bladder cancer," *Sensors and Actuators B: Chemical*, 2012.

[112] Y. Zhang, V. Bailey, H. Easwaran, J. Griffiths, E.and Herman, C. Puleo, S. Baylin, and T.-H. Wang, "DNA methylation analysis on a droplet-in-oil PCR array," *Lab on a Chip*, vol. 9, no. 8, pp. 1059–1064, 2009.

[113] W. Maki, N. Mishra, E. Cameron, B. Filanoski, S. Rastogi, and G. Maki, "Nanowire-transistor based ultra-sensitive DNA methylation detection," *Biosensors and Bioelectronics*, vol. 23, no. 6, pp. 780–787, 2008.

[114] U. Mirsaidov, W. Timp, X. Zou, V. Dimitrov, K. Schulten, A. Feinberg, and G. Timp, "Nanoelectromechanics of methylated DNA in a synthetic nanopore," *Biophysical Journal*, vol. 96, no. 4, pp. L32–L34, 2009.

[115] J. Shim, G. Humphreys, B. Venkatesan, J. Munz, X. Zou, C. Sathe, K. Schulten, F. Kosari, A. Nardulli, G. Vasmatzis, *et al.*, "Detection and quantification of methylation in DNA using solid-state nanopores," *Scientific Reports*, vol. 3, pp. 1–8, 2013.

[116] M. Li, W. Chen, N. Papadopoulos, S. Goodman, N. Bjerregaard, S. Laurberg, B. Levin, H. Juhl, N. Arber, *et al.*, "Sensitive digital quantification of DNA methylation in clinical samples," *Nature Biotechnology*, vol. 27, no. 9, pp. 858–863, 2009.

[117] J. Hu and C. Zhang, "Single base extension reaction-based surface enhanced Raman spectroscopy for DNA methylation assay," *Biosensors and Bioelectronics*, vol. 31, no. 1, pp. 451–457, 2012.

Chapter 3

The Ion-Sensitive Field-Effect Transistor

3.1 Introduction

There has been a tremendous convergence in the last decade seeing CMOS based microtechnology play a crucial role in chemical sensing applications. This has been enabled using solid-state sensors which can be implemented in planar form and fabricated using CMOS technology, monolithically integrated on a single chip. This now provides opportunity for chemical sensing platforms to leverage on semiconductor technology which may offer advantages such as scalability, miniaturisation, batch fabrication and integration with intelligent instrumentation.

This chapter begins with a brief review of the field of solid-state chemical sensing, focusing on the electrochemical sensing technologies namely voltammetry, conductimetry and potentiometry, with special mention given to the latter and especially to the Ion-Sensitive Field-Effect Transistor (ISFET) which will be used for DNA methylation detection in this thesis. The ISFET as a pH sensor is discussed, followed by some background theory on its properties, the operational characteristics, the model used to describe its behaviour and one of its key sensing properties, the sensitivity to pH. Some more information is given on ISFETs fabricated in unmodified CMOS, emphasising on the advantages of pH sensing using the native passivation layer used in the CMOS process, avoiding the need for extra processing steps or for deposition of additional materials to define its sensing capability. Key works using CMOS ISFETs for biomedical applications are also given, highlighting their applicability in areas such as DNA detection. The chapter concludes with the principles of weak inversion operation along with the model used for simulation of CMOS ISFETs in such region and the device characteristics and non-idealities which exist.

3.2 Solid-state chemical sensing

Several solid-state chemical sensor technologies have been developed based on optical, magnetic, piezoelectric, mass-sensitive, thermal, coulometric and frequency based detection of chemical species among which electrochemical biosensors have been the ones with the most widespread utility [1, 2]. Electrochemical sensors are based on ion or electron transfer at an interface created between a sample and a solid-state substrate due to a binding event at the sensor's surface, resulting in a direct transduction of the concentration of the sensed analyte in a detectable signal which is dependent on the type of measurement method chosen. Also, the dependence of the magnitude of the signal on the equilibrium concentration of the

analyte instead of the number of absorbing species, combined with additional advantages such as the minimal complexity due to CMOS implementation, which avoids the need for fluorescent labels and lenses that optical sensors require, make such sensors ideal for use in applications that focus on real-time detection and portability [3]. Solid-state electrochemical sensors can perform detection using well-known chemical sensing techniques such as voltammetry, conductimetry and potentiometry, as have been reviewed by [1, 3] and will now be discussed.

Voltammetry requires the presence of a three-electrode system consisting of a working, a counter and a reference electrode to detect a species of interest by imposing a time-varying potential to the reference electrode, measuring the current flowing through the working electrode which is proportional to the concentration of the analyte to be detected. The method of detection is called *amperometry* when the potential applied to the reference electrode is fixed at an electrode/solution interface, whereby oxidation (the chemical species pass electrons to the electrode) or reduction (the chemical species obtain electrons from the electrode) is caused, leading to a potential gradient between the reference and the working electrode, a result of a redox reaction [4, 5]. The concentration of the species is then defined by the amount of measured current through the working electrode, while the counter electrode is used to prevent current flow through the reference electrode. Voltammetric sensors may exhibit lower limits of detection, they provide however more information on the detected analytes given the time-varying potential being applied. Planar microelectrodes (silver, platinum or gold) are examples that fall in the category of electrochemical detection using either non-CMOS based microfabrication or post-CMOS processing [3]. *Conductimetry* is based on measuring the conductance of a sample to determine the presence and thus the concentration of charge carriers. Chemiresistors and chemicapacitors are conductimetric sensors measuring the change of resistance or capacitance between electrodes selective to specific species, thus determining their concentration [1, 6].

Finally, *potentiometric* sensors are based on measuring the potential between an Ion-Selective Electrode (ISE) and a reference electrode, as can be seen in Fig. 3.1, caused by a potential difference in solution as a result of a difference in ionic concentration between the analyte and the reference solution, with a standard liquid junction silver/silver chloride (Ag/AgCl) electrode to be normally used as a reference. Potentiometric sensors are based on the measurement of the potential at an electrode under ionic equilibrium conditions, when no current is flowing during a measurement in presence of a stable, reproducible and reversible reference system also in contact with the solution [1]. The measured potential,

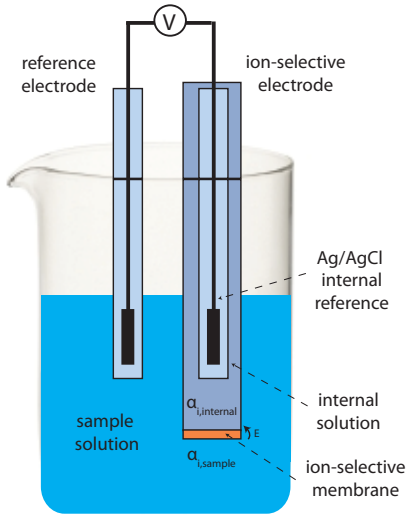


Figure 3.1: Potentiometric measurement set-up using an ISE

E_{men}, developed between the sensing and the reference electrode, defined as the one developed due to primary ion activity[1] on either sides of a selectively permeable membrane, is governed by the Nernst-equation [1, 8] for a constant activity of the reference solution as:

$$E_{mem} = \frac{RT}{n_i F} \ln \frac{\alpha_{i,sample}}{\alpha_{i,internal}} \tag{3.1}$$

where R is the universal gas constant, T is the absolute temperature in Kelvin, n_i is the charge of the measured primary ion, F is the Faraday constant, $\alpha_{i,sample}$ is the activity of the measured primary ion i in the sample solution and $\alpha_{i,internal}$ is the activity of the ion in the ISE's internal solution. For a known activity of the ion i in the internal solution ($\alpha_{i,internal}$), the measured potential can be expressed as:

$$E_{mem} = constant + 2.303 \frac{RT}{n_i F} \log \alpha_{i,sample} \tag{3.2}$$

which gives a sensitivity of $\frac{59}{n_i}$ (mV) for a unit change in pH or a decade variation in ion activity at T=298K. This derivation, extrapolated for a standard pH sensor, would result

[1]The activity of an ion in solution, α_i, represents its chemical effectiveness that is governed by the amount and type of other ions in solution. The activity is dependent on the ionic strength of the solution that takes into account the interaction between ions as represented in the equation $\alpha_i = \gamma_i \; c_i$ where γ_i is the activity coefficient and c_i the ionic concentration [7].

in 59mV change to be considered as the ideal sensitivity, in presence of a Ag/AgCl metal reference electrode being used in contact with an ionic solution so that a stable potential is provided.

Field-Effect Transistor (FET) based chemical sensors (ISFETs, Work function FETs, CHEMFETs or chemical-FETs, EnFETs or Enzyme-FETs) are examples of popular potentiometric based sensors with which different chemical compounds can be sensed by applying processing techniques on top of the CMOS substrate, such as deposition of ion-selective membranes on top of the insulating membranes (i.e. CHEMFETs, ISFETs) or by immobilisation of enzymes which react with the analyte of interest in solution, to produce or consume hydrogen ions (i.e. EnFETs) [2]. FET based chemical sensors belong into the category of sensors whereby the charge in solution exposed to a floating gate can be sensed by a stable reference electrode. Among these sensors, only ISFETs and CHEMFETs can be fully integrated in CMOS, with various implementations resulting in detection of numerous analytes, as has been summarised by [3]. Among these two, the ISFET has shown the ability to sense chemical changes that result in changes in the pH of a solution due to the release of hydrogen ions or protons, H^+, even without the need for any additional deposition of an ion-sensitive layer through post-processing modifications for defining the ionic selectivity of the sensor when fabricated in standard CMOS [9].

What is desirable for solid-state chemical sensing is the minimisation of post-processing steps which would reduce cost requirements for fabrication and manufacturing complexity. Post-processing is required for defining or enhancing the ionic selectivity of the sensors through the deposition of electrodes on dies or of additional sensing layers. Specifically in the field of DNA detection, where the requirements for sensor density, large scale integration and in parallel detection are emerging, in for example sensor arrays for DNA analysis at a genome or sequential level and label-free semiconductor based sequencing using ISFETs for monitoring changes in pH resulting from DNA chain extension reactions [10–12]. In the following section, a brief comparison of the use of solid-state technologies in CMOS applied for DNA detection is to be shown based on the already mentioned detection principles.

3.3 Label-free DNA detection in CMOS

For applications related to DNA detection in CMOS, various methods have been developed, examples of which are shown in Table 3.1 and categorised based on the principle of detection.

Table 3.1: Solid-state electrochemical sensing methods for DNA detection in CMOS

Method	Principle	Post Proc.	Label-free	Scaling	Ref.
Amperometric	Redox-cycling	Yes	No	Electrode dependent	[15]
Potentiometric	pH	No	Yes	Moore's law	[12]
Conductimetric	Capacitance	Yes	Yes	Electrode dependent	[16]

Most of them mainly focus on the use of DNA microarray chips for parallel analysis of a large number of DNA sites, with or without the additional requirement of post-processing implementation on the silicon substrate. Traditionally, optical detection techniques have been used for array based DNA detection, requiring the use of fluorescent markers attached on DNA target molecules [13, 14]. Known sequences of single-stranded DNA, also referred to as "DNA probes", complementary to the DNA targets, are immobilised on the surface of a DNA microarray chip on defined locations. The principle of detection of DNA microarrays is based on the event of DNA hybridisation taking place when complementary matching happens between the DNA probes and the target strands and thus fluorescence where light is shone.

Moreover, electrochemical techniques based on the principle of redox-cycling have also been used for CMOS based DNA detection [15, 17] through the use of gold electrodes of pre-defined size on the sensing site of a DNA microarray. A post-processing step of depositing a chemical substrate on the surface of the array for DNA probe immobilisation is required for the event of DNA hybridisation to take place between the DNA probe and the in-solution DNA target. The detectable signal would be the result of a conducted current when a DNA match is observed.

CMOS based label-free electrochemical techniques have also been proposed, offering low-cost solutions by avoiding the use of pre-processing steps such as DNA tagging using fluorescent labels combined with the need for laboratory equipment for optical signal detection [12].

Label-free methods following the principle of capacitance based DNA detection have been proposed by [16, 18–20]. Gold electrodes are used to sense the chemical binding of DNA strands immobilised on the surface of a silicon chip, with capacitance decrease being observed in the sensing electrode-electrolyte interface, induced by the event of DNA hybridisation, due to the low dielectric constant that DNA strands are inherently exhibiting.

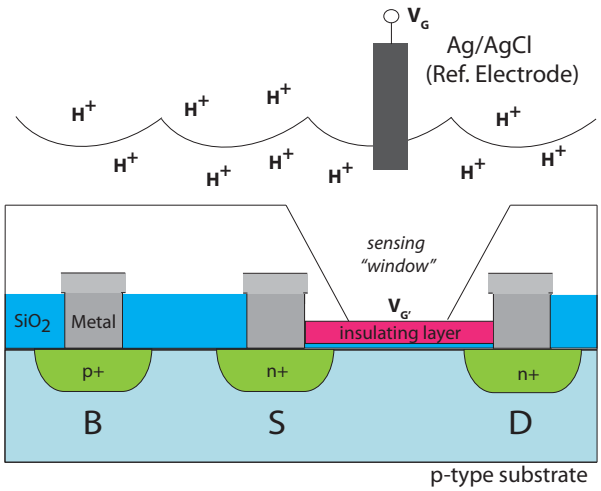


Figure 3.2: The Ion-Sensitive Field-Effect Transistor (ISFET)

Finally, CMOS ISFET arrays have been used for electrochemical DNA detection [12, 21], integrating sensors and microfluidics on a single platform, bypassing the need for pre-processing or post-processing steps, taking advantage of the capability of ISFET sensors to be fabricated in standard CMOS, whereby the Si_3N_4 native CMOS passivation layer can be used as an sensing membrane.

The principle of DNA detection using the ISFET was first introduced by [10], showing that when there is a match between a DNA target and a DNA probe, hydrogen ions or protons, H^+, are released, changing the pH of the solution. The ISFET being selective to H^+, can detect resulting changes in pH derived from DNA detection events based on the principle of DNA chain extension, and therefore can be utilised for applications such as DNA methylation detection, the analysis of which is to be explained in Chapter 4, enabling integration with circuit techniques, as described in Chapter 5 and Chapter 6, to provide more intelligent and robust DNA methylation detecting systems. The mechanism behind the operation of the ISFET as a pH sensor and its characteristics are to be explored in the following sections.

3.4 The Ion-Sensitive Field-Effect Transistor (ISFET)

The Ion-Sensitive Field-Effect Transistor (ISFET) was first introduced in the 1970s by Piet Bergveld [9]. It was originally used for electrophysiological measurements due to its small

size and fast response time. Since the discovery of its chemical sensing capabilities, it has been one of the most popular potentiometric sensors, being involved in several applications from *in vivo* continuous measurement of blood pH as mentioned in [22], to label-free DNA detection [12] and genome sequencing [11], forming CMOS based Lab-on-Chip (LoC) systems comprising of ISFET arrays.

The ISFET was originally implemented using a standard metal oxide semiconductor field-effect transistor (MOSFET), by omitting the gate metal, replacing it with a remote gate (standard liquid junction Ag/AgCl reference electrode, V_G) to set a stable potential or gate bias to the solution, as the principles of potentiometric sensors require, exposing a chemically sensitive insulating membrane to the electrolyte, as can be seen in Fig. 3.2. Initially, silicon dioxide (SiO_2) was used as the sensing membrane exposed to an electrolyte solution [23]. However, silicon dioxide has been shown to be quite an unstable insulating layer due to hydration effects causing cracks in the membrane's surface through the gate. For this to be overcome, the single layer of SiO_2 is replaced by a double layer of it or of a single layer of other insulating membranes such as silicon nitride (Si_3N_4), aluminium oxide (Al_2O_3) and tantalum oxide (Ta_2O_5) deposited on top of the silicon dioxide layer when enhancements in hydrogen ions sensitivity and sensor's stability are desired [22].

The insulating membrane is used to trap protons on its surface. The activity of protons is related to the ions in the solution and so is representing the pH of the analyte based on the definition of the natural logarithm of the hydrogen ion concentration:

$$pH = -log([H^+]) \tag{3.3}$$

which shows how acidic (minimum pH=1) or alkaline (maximum pH=14) a solution is. Changes in ionic concentration can result in changes in the charge distribution in the ISFET's channel which can be identified as changes in the threshold voltage of the device. A description of the properties of the ISFET as a pH sensing device along with the physical and operational characteristics shall now be explained.

3.4.1 ISFET operation

Originally the ISFET was described based on a close comparison to the MOSFET equivalent model, whereby the MOSFET's insulating membrane (SiO_2) is covered by a polysilicon gate to create a contact to a top metal, so that the device could be biased with a gate potential.

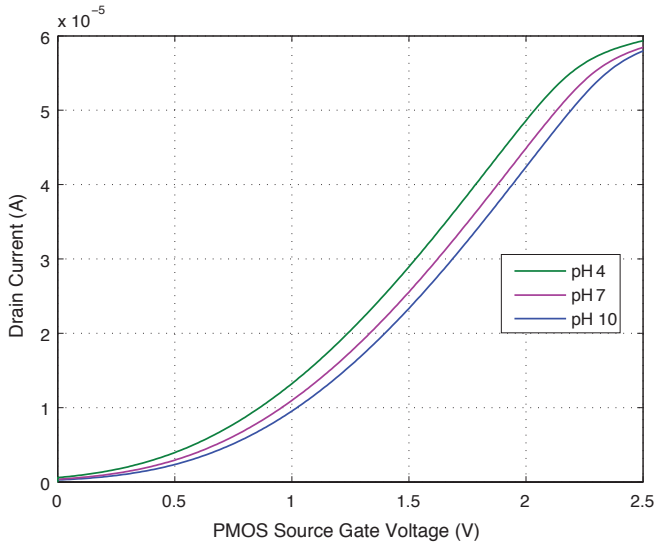


Figure 3.3: Shift in the I_D-V_{GS} characteristic for variable pH

The definition of the ISFET as a pH sensing device without a metal gate, in contact with an electrolyte and a reference electrode, can be expanded to an ion-sensitive gate whose threshold voltage can be modulated by changes in the ionic concentration or the pH of the solution. The threshold voltage of the ISFET exhibits a dependence on the pH variations in solution, as can be shown in Fig. 3.3, which can be mathematically derived based on the threshold voltage of a MOSFET, $V_{th(MOSFET)}$, described by Eq. 3.4, as analysed by [22].

$$V_{th(MOSFET)} = \frac{\phi_m - \phi_{Si}}{q} - \frac{Q_{ox} + Q_{SS} + Q_B}{C_{OX}} + 2\phi_f \tag{3.4}$$

The first term ϕ_m - ϕ_{Si} expresses the difference in work function between the gate metal, ϕ_m and the silicon surface, ϕ_{Si} and q is the electronic charge. The second term is consisted of the charge accumulated in the oxide, Q_{ox}, the oxide-silicon interface, Q_{SS}, and the depletion charge in silicon, Q_B. ϕ_f stands for the Fermi potential of the semiconductor and C_{OX} for the insulator capacitance per unit area. The expression of the threshold voltage in the case of an ISFET, as shown in Eq. 3.5, will differ from Eq. 3.4 in that the work function of the metal, ϕ_m, will be replaced by the terms E_{ref} and x_{sol} which express the potential of the reference electrode and the potential due to the presence of dipole molecules in the solution respectively:

$$V_{th(ISFET)} = E_{ref} - \psi_o + x_{sol} - \frac{\phi_m}{q} + V_{th(MOSFET)} \tag{3.5}$$

ψ_o is a pH dependent chemical potential [24] also referred to as the surface dipole potential [22], whose dependence on pH is given by:

$$\psi_o = 2.3\frac{kT}{q}\alpha(pH_{pzc} - pH) \tag{3.6}$$

where pH_{pzc} is the pH at the point of zero charge derived in [24] and α is the deviation from the Nernstian response, which shall be defined later in this chapter.

As proposed by [2], the chemical potentials E_{ref}, ψ_o, x_{sol} and $\frac{\phi_m}{q}$ can be grouped in the potential V_{chem} expressed by:

$$V_{chem} = E_{ref} + x_{sol} - \psi_o - \frac{\phi_m}{q} \tag{3.7}$$

The pH-sensing capabilities of the ISFET through the use of Eq. 3.7 shall now be described.

3.4.2 pH sensitivity

The pH sensitivity of the ISFET or the dependence of the electrolyte-insulator potential ψ_o on pH can be explained based on the site-binding theory [25] and the Gouy-Chapman-Stern capacitive double layer model [26, 27]. When the surface of the insulating membrane of the ISFET comes in contact with an electrolyte of a fixed ionic concentration, the ions of the solution interact with the membrane, creating accumulation of charge on the surface of the insulator.

A change in pH in the solution results in a change in the SiO_2 potential on the surface of the gate oxide that is in contact with the solution. The insulating membrane therefore traps hydrogen ions whose activity is related to the ionic activity of the electrolyte. Given that the surface of any metal oxide contains hydroxyl groups acting as "binding locations", specifically for the case of SiO_2, $SiOH$ exist on the surface [22]. These can be protonised (OH_2^+) thus positively charged, acting as proton acceptors, deprotonised (O^-) thus negatively charged, acting as proton donors or they can be neutral (OH), dependent on the pH

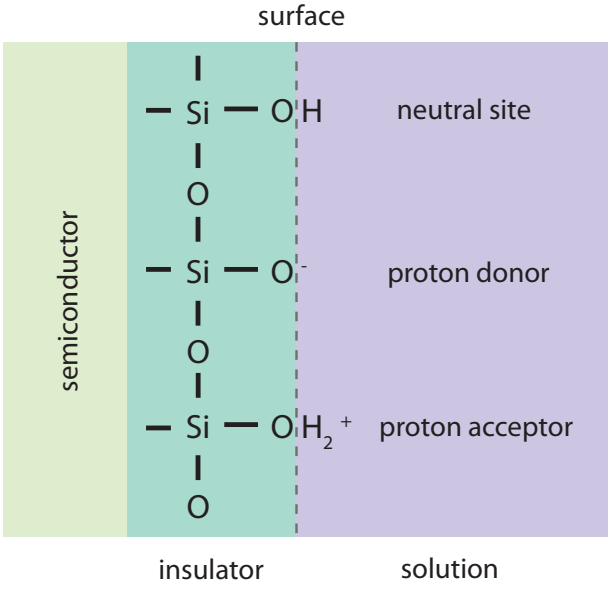


Figure 3.4: Site-binding model at a SiO_2-solution interface. Figure adapted from [22].

of the solution [23, 24]. Fig. 3.4 is an illustration of the mechanism behind the side-binding theory at the interface between a SiO_2 insulating membrane and the solution, responsible for an equilibrium to be reached between protons in the solution and amphoteric $SiOH$ surface sites.

The charge accumulated on the insulator's surface, due to the presence of hydrogen ions, is dependent on the number of sites available which react with the hydrogen ions present, based on the reactions:

$$SiOH \rightleftharpoons SiO^- + H_S^+, \; with \; K_a = \frac{[SiO^-][H^+]_S}{[SiOH]} \tag{3.8}$$

$$SiOH + H_S^+ \rightleftharpoons SiOH_2^+, \; with \; K_b = \frac{[SiOH_2^+]}{[SiOH][H^+]_S} \tag{3.9}$$

where H_S^+ represents the concentration of hydrogen ions at the insulator's surface and K_a and K_b the equilibrium constants of the binding reaction, defining the concentration species on both sides of the reaction when it is in equilibrium. From Eq. 3.8 and Eq. 3.9 it is clear that a surface that is originally neutral in charge ($SiOH$) can become positively charged ($SIOH_2^+$) after accepting a proton from the solution as well as negatively charged

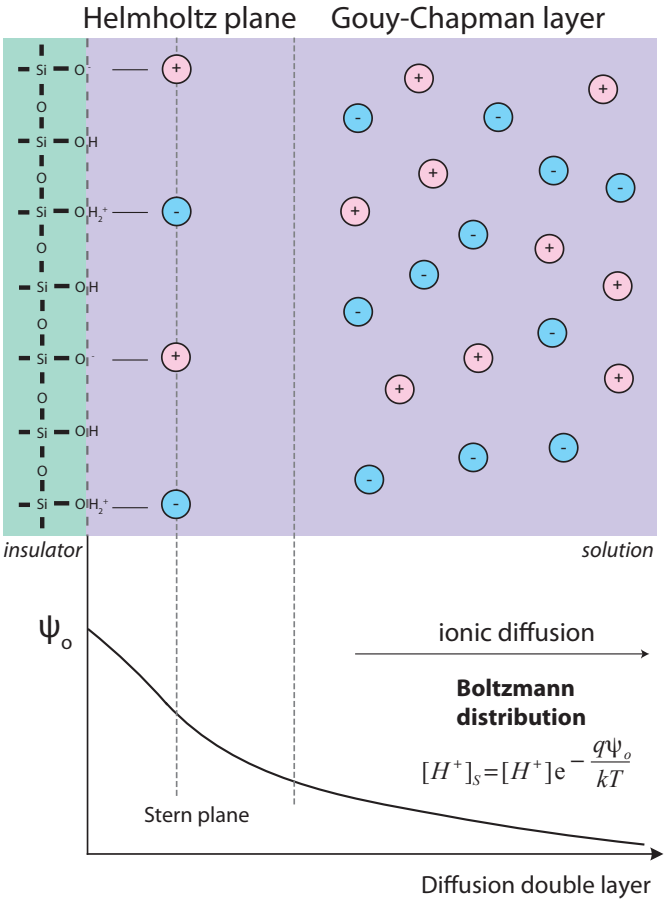


Figure 3.5: Charge and potential distribution of electrolyte-insulator (SiO_2) interface. The ionic distribution on the surface of the ISFET together with the formation of the Helmholtz plane and the Gouy-Chapman layer is illustrated.

(SiO^-) after donating a proton to the solution, which explains the term "amphoteric" used to describe the binding sites of the insulator [22].

The result of a charge build-up at the electrolyte-insulator interface is an equal and opposite charge, spreading across the double layer, resulting in the $Helmholtz$ plane which is defined as the charge distribution attracted to the surface sites of the insulator, as well as the charge that follows a Boltzmann distribution described as the $Gouy - Chapman$ layer, before it diffuses evenly in the bulk of the solution [3, 26]. The total distribution of charge can be illustrated in Fig. 3.5. The combination of these two layers result in an almost linear drop of the potential in the Helmholtz plane followed by an exponential drop through the Gouy-Chapman layer as the charge diffuses into the electrolyte bulk. The distribution of

charge in both layers can be modelled using the capacitances C_{Helm} and C_{Gouy} in series given by:

$$\frac{1}{C_{diff}} = \frac{1}{C_{Gouy}} + \frac{1}{C_{Helm}} \tag{3.10}$$

where C_{diff} is the total capacitance in the double layer, dependent on the pH of the solution as defined by [27].

Following the hypothesis that the ionic concentration equals to the ionic activity (dilute sample), the concentration of hydrogen ions bound to the surface of the insulator, $[H^+]_S$, is related to the concentration of hydrogen ions in the bulk of the solution, $[H^+]$, following the Boltzmann distribution:

$$[H^+]_S = [H^+]e^{-q\psi_o/kT} \tag{3.11}$$

where ψ_o is the electrolyte-insulator interface potential and can be used to derive the pH dependence according to Eq. 3.6, k is the Boltzmann constant and T is the absolute temperature. Following on to that, the pH sensitivity for a Nernstian response, S_N, is given by:

$$S_N = \frac{dE_{mem}}{dpH} = \frac{d\psi_o}{dpH} = \frac{2.303RT}{nF} = \frac{2.303KT}{q} \quad = 2.303U_t = 59mV \tag{3.12}$$

given that $\frac{RT}{nF}$=$\frac{kT}{q}$ based on the Einstein's equation.

This results in the definition of pH sensitivity for ISFETs, S_{ISFET}, as:

$$S_{ISFET} = \frac{2.303\alpha KT}{q} \tag{3.13}$$

$$\alpha = \frac{S_{ISFET}}{S_N} = \left(\frac{2.3kTC_{diff}}{q^2\beta_{int}} + 1\right)^{-1} \tag{3.14}$$

where α is a dimensionless sensitivity parameter, defined in Eq. 3.14 [28], stating the deviation from the Nernstian response and is in the range of 0 to 1, with 1 representing a Nernstian sensitivity of 59.2mV/pH at 298K, depending on the intrinsic buffer capacity of

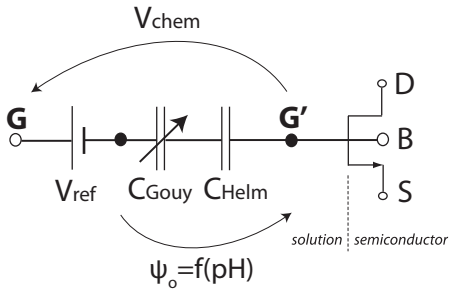


Figure 3.6: ISFET behavioural macromodel [29]

the oxide surface β_{int}[2] and the equivalent capacitance C_{diff} of the double layer, as defined in Eq. 3.10.

Substituting Eq. 3.13 into Eq. 3.7 results in a more simplistic and widely used form of V_{chem} originally presented by [30]:

$$V_{chem} = \gamma + \frac{2.303\alpha kT}{q} pH \ = \gamma + 2.303\alpha U_t pH \tag{3.15}$$

where γ is a grouping of pH independent chemical potentials and U_t is the temperature dependent thermal voltage of the ISFET, also expressed as kT/q.

The derivations of the expressions stated above for the ISFET operation can be illustrated using the behavioural macromodel of the MOSFET adapted for the ISFET, as can be seen in Fig. 3.6, originally shown by Martinoia et al. [29]. It includes the standard MOSFET but adds the double layer capacitance C_{Gouy}-C_{Helm} and the reference electrode potential.

3.5 ISFETs fabricated in CMOS

Following on from the discovery of the ISFET as a pH sensor, attempts have been made for ISFETs to be fabricated in CMOS. Wong et al. and Bousse et al. [31, 32] were the first to propose processes of CMOS fabrication, including custom steps to etch away the passivation and polysilicon gate so that an insulating membrane is added on top of a silicon dioxide

[2]The intrinsic buffer capacity is defined as $\beta_{int}=\frac{d([SiO^-]+[SiOH_2^+])}{dpH_S}$, which is the capability for changes in the number of surface sites available for a given change in pH [28]. It is described as *intrinsic* because small changes can only be buffered in the surface pH and not in the bulk of the solution, under normal conditions.

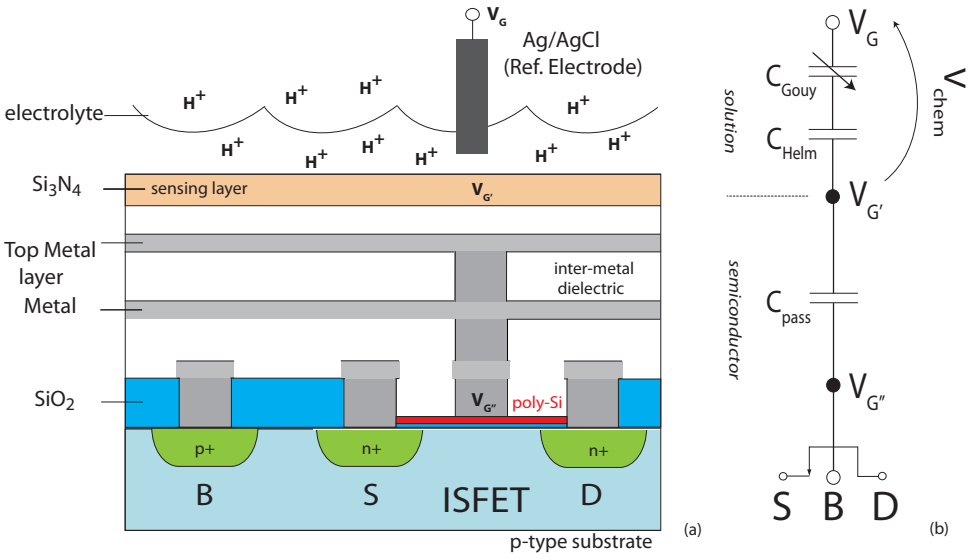


Figure 3.7: (a) CMOS ISFET structure, (b) behavioural macromodel.

layer on the substrate. Later, Cane et al. showed that unmodified CMOS implementation was possible [33], with advances on the process proposed by Bausells et al. [34] using the 'extended gate' approach, as can be seen in Fig. 3.7a, by utilising the native top passivation layer, which tends to be silicon nitride or silicon oxynitride (added by plasma enhanced chemical vapour deposition (PECVD)) as the sensing membrane, also playing the role of the insulating membrane for the ISFET. Through this, the polysilicon gate is extended to the passivation layer using multiple metal layers, all floating, with charge bound to the surface of the passivation, coupled to the polysilicon gate layers of metal. A comparison with the original ISFET design of Fig. 3.2 shows the inclusion of the passivation capacitance, C_{pass}, which is due to the insulator in contact with the top metal.

From this progress in the field onwards, several CMOS based systems have been developed, creating the basis for a new area of systems where integrated circuits and ISFET sensors could co-exist on a single chip. This allows for advantages such as wafer scale processing, scalability, which is a great merit for array based systems, miniaturisation of sensor size, low-cost mass fabrication, integration with well-known circuit techniques, intelligent sensor processing as well as ease of sample handling through the use of microfluidics to be realised. ISFETs in CMOS have been largely integrated, creating arrays for several applications most importantly of biomedical nature, from cell culturing, to electrolyte imaging to DNA detection. Table 3.2 summarises key works over the last decade in several tech-

Table 3.2: Comparison of CMOS ISFET arrays over the last decade

Year	Tech.	Array Size	Pixel Size	Application	Ref.
2001	$1.2\mu m$	6 (6 × 1)	-	blood gas	[35]
2004	$0.35\mu m$	4 (2 × 2)	$2.9 \times 6.2\mu m$	cell culturing	[36]
2005	$0.35\mu m$	256 (16 × 16)	$12.8 \times 12.8\mu m$	extracellular imaging	[37]
2006	$0.18\mu m$	50 (5 × 10)	$50 \times 50\mu m$	DNA detection	[38]
2008	$0.35\mu m$	33 (3 × 11)	$57.5 \times 57.5\mu m$	electrolyte imaging	[39]
2008	$0.35\mu m$	256 (16 × 16)	$11.6 \times 11.6\mu m$	extracellular imaging	[40]
2008	$0.35\mu m$	4 (2 × 2)	$11.6 \times 11.6\mu m$	electrolyte imaging	[41]
2009	$0.18\mu m$	64 (8 × 8)	$20 \times 2\mu m$	handheld inst.	[42]
2009	$1.2\mu m$	256 (16 × 16)	$105.3 \times 81.4\mu m$	DNA detection	[43]
2010	$0.35\mu m$	40 (40 × 1)	-	DNA detection	[21]
2010	$0.35\mu m$	64 (8 × 8)	$50 \times 50\mu m$	Opto-chemical imaging	[44]
2010	$0.35\mu m$	8 (8 × 1)	$30 \times 100\mu m$	-	[45]
2011	$0.35\mu m$	1.5M	$5.1 \times 5.1\mu m$	DNA detection	[11]
2012	$0.18\mu m$	9 (3 × 3)	$10 \times 10\mu m$	DNA detection	[46]
2012	$0.35\mu m$	256 (16 × 16)	$14 \times 14\mu m$	electrolyte imaging	[47]
2012	$0.35\mu m$	4096 (64 × 64)	$10.2 \times 10.2\mu m$	electrolyte imaging	[48]
2013	$0.35\mu m$	40 (40 × 1)	$104 \times 34\mu m$	DNA amplification	[12]

nologies, showing that this field has been emerging and fast growing, especially for DNA detection.

3.5.1 Device characteristics in weak inversion

In applications where low power is required in addition to low currents and energy efficient processing, weak inversion is a suitable region of operation. Specifically in the current-mode domain, weak inversion enables the use of translinear circuit techniques which can be used to perform low power processing of ISFET signals on-chip. Weak inversion has been utilised in this thesis for the realisation of novel circuits such as the ratiometric approach for detecting DNA methylation using the "Methylation Cell" and the ISFET based Chemical

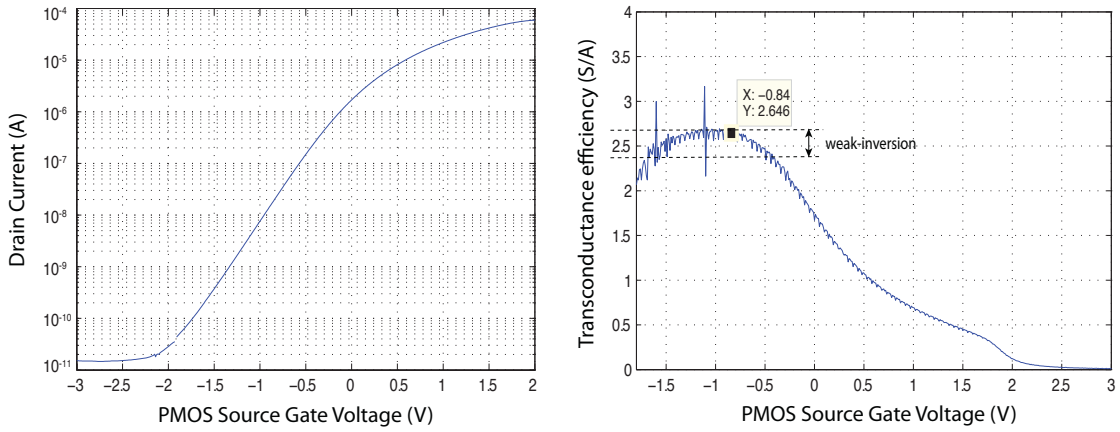


Figure 3.8: ISFET $I_D V_{GS}$ characteristics (left) and transconductance (right) at pH 7, with the operational range of weak inversion to be highlighted.

Gilbert Cell, as will be further presented in this thesis.

In order to understand the device operating characteristics and simulate ISFETs in CMOS operating in weak inversion, an elaborated macromodel is used, as proposed by [49], based on the initially defined behavioural macromodel as shown in Fig. 3.6.

Fig. 3.9 illustrates this, which includes the capacitance C_{pass} to describe the passivation layer of the CMOS ISFET, located between the top metal and the solution, scaling down the effective gate voltage measured on the surface of the insulating membrane from $V_{G'}$ to $V_{G''}$, which indicates the voltage seen by the MOSFET beneath the passivation layer. C_{pass} is several orders of magnitude smaller than that of the Helmholtz capacitance, C_{helm}, and of Gouy-Chapman capacitance, C_{Gouy}, causing minimum attenuation of any biasing potential applied [49].

The voltage $V_{G'}$ has also been expressed with respect to the voltage applied to the reference electrode, V_G, the chemically dependent potential, V_{chem} (3.15), and the input trapped charge potential, V_{tc}, which models the measured trapped charge in the passivation layer, as has been described by [49]:

$$V_{G'} = V_G - V_{tc} - V_{chem} \tag{3.16}$$

Operation in the weak inversion or sub-threshold region requires low voltage values between the gate and the source of the device below its threshold voltage, $V_{GS} < V_{th}$, with

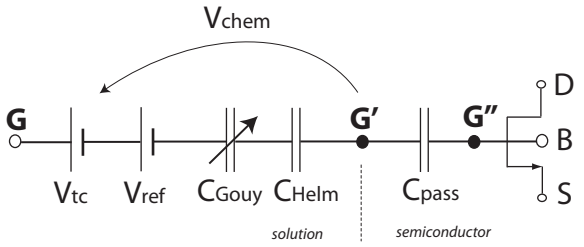


Figure 3.9: CMOS ISFET behavioural macromodel [49]

the current being exponentially related to the gate-source voltage. As the gate voltage increases, charge is initially driven away from the channel, forming a 'depletion layer', depleted of electrons or holes. A slight further increase in the gate voltage results in electrons beginning to diffuse from the source to the drain into the channel, forming an electron-rich (for the case of an NMOS) 'inversion layer'. Thus, the channel created between the drain and the source of the device is governed solely by the diffusion of charge carriers, as described by the Boltzmann distribution, rather than by drift [50]. This drain current in weak inversion is thus described by the expression:

$$I_D = I_o \exp \frac{V_{G''S}}{nU_t}(1 - \exp \frac{-V_{DS}}{U_t}) \tag{3.17}$$

which shows that the drain current of the ISFET is exponentially related to the gate-source voltage, with I_o to stand for a positive constant current resulting from grouping constants, n the sub-threshold slope coefficient, $V_{G''}$ the effective voltage on the gate of the transistor, which is an attenuated version of the voltage defined by Eq. 3.16 as a result of the capacitive division due to C_{pass}, oxide and depletion capacitancies of the MOS transistor [2] and V_{DS} the drain-source potential. Fig. 3.8(left) depicts a typical $I_D - V_{GS}$ ISFET characteristic of a typical 0.35μm CMOS process, with the weak inversion region of operation to be represented by drain currents typically in the order of nanoamps. The weak inversion transconductance is given by the expression:

$$g_m = \frac{I_D}{nUt} \tag{3.18}$$

or

$$\frac{g_m}{I_D} = \frac{1}{nUt} \tag{3.19}$$

with the latter expression to show the transconductance efficiency, Fig. 3.8(right), which for the weak inversion region is constant, given that n is constant in that region. The peak of the curve is given by $1/nU_t$, determined by the weak inversion slope factor n. Operating in weak inversion provides maximum values of transconductance to current ratio, g_m/I_D, which as shown in Fig. 3.8(right) can reach the top 90% of the curve, as illustrated by the two dotted lines, a region that would satisfy the operation of an ISFET in weak inversion providing with the maximum intrinsic voltage gain [49].

In addition to this, the ISFET's sensing capability for pH changes of the solution as a result of binding of hydrogen ions in the CMOS passivation layer (silicon nitride) can be interpreted as changes in the ISFET's drain current, I_D, in weak inversion, described by the equation [49]:

$$I_D = I_o e^{\frac{V_{GS}-\gamma-\alpha S_N pH}{nU_t}} \tag{3.20}$$

which can also be described with respect to the hydrogen ion concentration ($[H+]$) by:

$$I_D = I_o e^{\frac{V_{GS}}{nU_t}} K_{chem}[H+]^{\frac{\alpha}{n}} \tag{3.21}$$

where K_{chem}=$e^{-\gamma/nU_t}$ stands for a grouping of constant chemical potentials. This leads to the observation that the drain current of the ISFET biased in weak inversion is exponentially related to the pH of the solution, which in turn is log-related to the hydrogen ion concentration sensed by the ISFET sensor.

3.5.2 Non-ideal effects

Trapped charge

ISFETs normally suffer from variation in threshold voltage, shown as the DC offset, V_{tc} in Eq. 3.16. This is the result of trapped charge left by fabrication which can exist in the passivation layer on the floating gate. Since the ISFET is effectively a floating gate MOSFET device, any charge left on the floating gate will have no path to discharge to ground. As a result it remains trapped inducing an offset. UV radiation has been proposed as a suitable mechanism to remove this charge [41].

Drift

Drift is an issue which is very common in most chemical sensors. It normally appears as a slowly increasing signal at a slower rate than the reaction. In ISFETs, the drift is caused by the slow conversion of the silicon based insulating surface to a hydrated silicon oxide or oxynitride layer during contact with the solution [51]. The growth of this surface layer affects the overall capacitance of the passivation, C_{pass}, Fig. 3.7, and thus can appear to be a change in the threshold voltage. Typically differential measurements can be used to significantly reduce the effects of drift [21] or if the reaction amplitude is larger and at a faster rate its effects can be negligible.

3.6 Summary

In this chapter, the ISFET as a potentiometric chemical sensor has been briefly reviewed based on the principles that solid state chemical sensors follow for applications related to label-free DNA detection. The mechanisms behind ISFET's operation and its inherent pH sensitivity compared to the ideal Nernstian have been explained along with the capability for integration in standard CMOS. This allows the development of systems and large scale fully integrated platforms consisting of ISFET sensors in the form of arrays with great benefits especially in biomedical applications, such as DNA detection.

The weak inversion region of operation of the ISFET is shown, emphasising the advantages of low power pH sensing, providing great opportunity for CMOS ISFETs to include analog computation of signals implemented using novel circuits, as will be described later in this thesis. We now proceed with describing the use of the ISFET for DNA methylation detection and proving its utility in CMOS.

References

[1] A. Hierlemann and H. Baltes, "CMOS-based chemical microsensors," *Analyst*, vol. 128, no. 1, pp. 15–28, 2003.

[2] P. Georgiou, *Chemical Bionics - A novel design approach using Ion Sensitive Field Effect Transistors*. PhD thesis, Imperial College London, London, 2008.

[3] L. Shepherd, *Low-power computational interfacing with CMOS ISFETs*. PhD thesis, Imperial College London, London, 2008.

[4] M. Lambrechts and W. Sansen, *Biosensors: Microelectrochemical Devices*. Institute of Physics Publishing, 1992.

[5] J. Janata and R. Huber, *Solid State Chemical Sensors*. Academic Press, 1985.

[6] A. Kummer and A. Hierlemann, "Configurable electrodes for capacitive-type sensors and chemical sensors," *IEEE Sensors*, vol. 6, no. 1, pp. 3–10, 2006.

[7] R. Compton and G. Sanders, *Electrode potentials*. Oxford University Press Oxford, 1996.

[8] A. Bard and L. Faulkner, *Electrochemical methods: fundamentals and applications*, vol. 2. Wiley New York, 1980.

[9] P. Bergveld, "Thirty years of ISFETOLOGY - what happened in the past 30 years and what may happen in the next 30 years," *Sensors and Actuators B: Chemical*, vol. 88, no. 1, pp. 1–20, 2003.

[10] S. Purushothaman, C. Toumazou, and C. Ou, "Protons and single nucleotide polymorphism detection: a simple use for the Ion Sensitive Field Effect Transistor," *Sensors and Actuators B: Chemical*, vol. 114, no. 2, pp. 964–968, 2006.

[11] J. Rothberg, W. Hinz, T. Rearick, J. Schultz, W. Mileski, M. Davey, J. Leamon, K. Johnson, M. Milgrew, M. Edwards, *et al.*, "An integrated semiconductor device enabling non-optical genome sequencing," *Nature*, vol. 475, no. 7356, pp. 348–352, 2011.

[12] C. Toumazou, L. Shepherd, S. Reed, G. Chen, A. Patel, D. Garner, C.-J. Wang, C.-P. Ou, K. Amin-Desai, *et al.*, "Simultaneous DNA amplification and detection using a pH-sensing semiconductor system," *Nature Methods*, vol. 10, no. 7, pp. 641–646, 2013.

[13] M. Schena, *DNA microarrays: a practical approach*. No. 205, Oxford University Press, 1999.

[14] M. Schena *et al.*, *Microarray biochip technology*. Eaton Pub., 2000.

[15] M. Schienle, C. Paulus, A. Frey, F. Hofmann, B. Holzapfl, P. Schindler-Bauer, and R. Thewes, "A fully electronic DNA sensor with 128 positions and in-pixel A/D conversion," *IEEE Journal of Solid-State Circuits*, vol. 39, no. 12, pp. 2438–2445, 2004.

[16] C. Stagni, C. Guiducci, L. Benini, B. Riccò, S. Carrara, C. Paulus, M. Schienle, and R. Thewes, "A fully electronic label-free DNA sensor chip," *IEEE Sensors*, vol. 7, no. 4, pp. 577–585, 2007.

[17] M. Augustyniak, C. Paulus, R. Brederlow, N. Persike, G. Hartwich, D. Schmitt-Landsiedel, and R. Thewes, "A 24x16 CMOS-based chronocoulometric DNA microarray," in *IEEE Conference on Solid-State Circuits (ISSCC)*, pp. 59–68, IEEE, 2006.

[18] C. Guiducci, C. Stagni, G. Zuccheri, A. Bogliolo, L. Benini, B. Samorı, and B. Ricco, "DNA detection by integrable electronics," *Biosensors and Bioelectronics*, vol. 19, no. 8, pp. 781–787, 2004.

[19] C. Stagni, C. Guiducci, L. Benini, B. Riccò, S. Carrara, B. Samorí, C. Paulus, M. Schienle, M. Augustyniak, and R. Thewes, "CMOS DNA sensor array with integrated A/D conversion based on label-free capacitance measurement," *IEEE Journal of Solid-State Circuits*, vol. 41, no. 12, pp. 2956–2964, 2006.

[20] C. Stagni, D. Esposti, C. Guiducci, C. Paulus, M. Schienle, M. Augustyniak, G. Zuccheri, B. Samori, L. Benini, B. Ricco, *et al.*, "Fully electronic CMOS DNA detection array based on capacitance measurement with on-chip analog-to-digital conversion," *IEEE Conference on Solid-State Circuits (ISSCC)*, pp. 69–78, 2006.

[21] D. Garner, H. Bai, P. Georgiou, T. Constandinou, S. Reed, L. Shepherd, W. Wong, K. Lim, and C. Toumazou, "A multichannel DNA SoC for rapid point-of-care gene detection," *IEEE Conference on Solid-State Circuits (ISSCC)*, pp. 492–493, 2010.

[22] P. Bergveld, "ISFET, theory and practice," *IEEE Sensor Conference*, vol. 10, pp. 1–26, 2003.

[23] P. Bergveld, "Development of an ion-sensitive solid-state device for neurophysiological measurements," *IEEE Transactions on Biomedical Engineering*, no. 1, pp. 70–71, 1970.

[24] L. Bousse, N. De Rooij, and P. Bergveld, "Operation of chemically sensitive field-effect sensors as a function of the insulator-electrolyte interface," *IEEE Transactions on Electron Devices*, vol. 30, no. 10, pp. 1263–1270, 1983.

[25] D. Chan, T. Healy, and L. White, "Electrical double layer interactions under regulation by surface ionization equilibria-dissimilar amphoteric surfaces," *Journal of the Chemical Society, Faraday Transactions I*, vol. 72, pp. 2844–2865, 1976.

[26] A. Bard and L. Faulkner, *Electrochemical Methods: Fundamentals and Applications*. John Wiley and Sons, 2001.

[27] R. Van Hal, J. Eijkel, and P. Bergveld, "A general model to describe the electrostatic potential at electrolyte oxide interfaces," *Advances in colloid and interface science*, vol. 69, no. 1, pp. 31–62, 1996.

[28] R. Van Hal, J. Eijkel, and P. Bergveld, "A novel description of ISFET sensitivity with the buffer capacity and double-layer capacitance as key parameters," *Sensors and Actuators B: Chemical*, vol. 24, no. 1, pp. 201–205, 1995.

[29] S. Martinoia and G. Massobrio, "A behavioral macromodel of the ISFET in SPICE," *Sensors and Actuators B: Chemical*, vol. 62, no. 3, pp. 182–189, 2000.

[30] L. Shepherd and C. Toumazou, "A biochemical translinear principle with weak inversion ISFETs," *IEEE Transactions on Circuits and Systems I: Regular Papers*, vol. 52, no. 12, pp. 2614–2619, 2005.

[31] H.-S. Wong and M. White, "A self-contained CMOS integrated pH sensor," in *International Electron Devices Meeting, Technical Digest (IEDM)*, pp. 658–661, IEEE, 1988.

[32] L. Bousse, J. Shott, and J. Meindl, "A process for the combined fabrication of ion sensors and CMOS circuits," *IEEE Electron Device Letters*, vol. 9, no. 1, pp. 44–46, 1988.

[33] C. Cane, A. Götz, A. Merlos, I. Gracia, A. Errachid, P. Losantos, and E. Lora-Tamayo, "Multilayer ISFET membranes for microsystems applications," *Sensors and Actuators B: Chemical*, vol. 35, no. 1, pp. 136–140, 1996.

[34] J. Bausells, J. Carrabina, A. Errachid, and A. Merlos, "Ion-sensitive field-effect transistors fabricated in a commercial CMOS technology," *Sensors and Actuators B: Chemical*, vol. 57, no. 1-3, pp. 56–62, 1999.

[35] E. Lauwers, J. Suls, W. Gumbrecht, D. Maes, G. Gielen, and W. Sansen, "A CMOS multiparameter biochemical microsensor with temperature control and signal interfacing," *IEEE Journal of Solid-State Circuits*, vol. 36, no. 12, pp. 2030–2038, 2001.

[36] M. Milgrew, P. Hammond, and D. Cumming, "The development of scalable sensor arrays using standard CMOS technology," *Sensors and Actuators B: Chemical*, vol. 103, no. 1, pp. 37–42, 2004.

[37] M. Milgrew, M. Riehle, and D. Cumming, "A large transistor-based sensor array chip for direct extracellular imaging," *Sensors and Actuators B: Chemical*, vol. 111, pp. 347–353, 2005.

[38] A. Hassibi and T. Lee, "A programmable 0.18-μm CMOS electrochemical sensor microarray for biomolecular detection," *IEEE Sensors*, vol. 6, no. 6, pp. 1380–1388, 2006.

[39] P. Georgiou and C. Toumazou, "An adaptive ISFET chemical imager chip," in *IEEE International Symposium on Circuits and Systems (ISCAS)*, pp. 2078–2081, IEEE, 2008.

[40] M. Milgrew, M. Riehle, and D. Cumming, "A 16Ã16 CMOS proton camera array for direct extracellular imaging of hydrogen-ion activity," pp. 590–638, 2008.

[41] M. Milgrew and D. Cumming, "Matching the transconductance characteristics of CMOS ISFET arrays by removing trapped charge," *IEEE Transactions on Electron Devices*, vol. 55, no. 4, pp. 1074–1079, 2008.

[42] W. Chan, B. Premanode, and C. Toumazou, "64 pH-ISFET averaging array employing global negative current feedback," *Electronics Letters*, vol. 45, no. 11, pp. 536–537, 2009.

[43] K. Nakazato, "An integrated ISFET sensor array," *Sensors*, vol. 9, no. 11, pp. 8831–8851, 2009.

[44] C. Z. Goh, P. Georgiou, T. Constandinou, T. Prodromakis, and C. Toumazou, "A CMOS-based ISFET chemical imager with auto-calibration capability," *IEEE Sensors*, vol. 11, no. 12, pp. 3253–3260, 2011.

[45] Y. Liu and C. Toumazou, "An ISFET based sensing array with sensor offset compensation and pH sensitivity enhancement," in *IEEE International Symposium on Circuits and Systems (ISCAS)*, pp. 2283–2286, IEEE, 2010.

[46] K. Wang, Y. Liu, C. Toumazou, and P. Georgiou, "A TDC based ISFET readout for large-scale chemical sensing systems," in *IEEE Biomedical Circuits and Systems Conference (BioCAS)*, pp. 176–179, IEEE, 2012.

[47] P. Shields, B. Nemeth, R. Green, M. Riehle, and D. Cumming, "High-speed imaging of 2-D ionic diffusion using a 16x16-pixel CMOS ISFET array on the microfluidic scale," *IEEE Sensors*, vol. 12, no. 9, pp. 2744–2749, 2012.

[48] B. Nemeth, M. Piechocinski, and D. Cumming, "High-resolution real-time ion-camera system using a CMOS-based chemical sensor array for proton imaging," *Sensors and Actuators B: Chemical*, vol. 171, pp. 747–752, 2012.

[49] P. Georgiou and C. Toumazou, "ISFET characteristics in CMOS and their application to weak inversion operation," *Sensors and Actuators B: Chemical*, vol. 143, no. 1, pp. 211–217, 2009.

[50] E. Vittoz and J. Fellrath, "CMOS analog integrated circuits based on weak inversion operations," *IEEE Journal of Solid-State Circuits*, vol. 12, no. 3, pp. 224–231, 1977.

[51] P. Hammond and D. Cumming, "Encapsulation of a liquid-sensing microchip using SU-8 photoresist," *Microelectronic engineering*, vol. 73, pp. 893–897, 2004.

Chapter 4

DNA methylation detection using ISFETs

4.1 Introduction

Increasing knowledge on the role of epigenetic markers, such as DNA methylation in cancer, has provided an exceptional opportunity for the evaluation of such epigenetic modifications as potential cancer biomarkers, highlighting their great future in cancer diagnostics and disease monitoring schemes as described in Chapter 2. Therefore, the need for detection of DNA methylation in the promoter region of tumour suppressor genes appears to play a very important role in early detection of cancer.

Methods for DNA methylation pattern analysis of candidate genes, reported in Chapter 2, have been developed to assess the levels of DNA methylation in cancer cells compared to normal cells in a gene-specific or genome-wide manner. Each one of them is associated with several advantages but also possible limitations related to matters of accuracy of detection or complexity through the addition of post-processing steps, especially when the use of fluorescent labels or affinity based enrichment techniques are involved. Also, matters such as the need for computational power, the cost of bioinformatic processing and the lack of the potential for large scale integration can create certain constraints when a method is to be widely used for genome-wide based applications for DNA methylation detection.

In the last decade, semiconductor technology has impacted healthcare making the use of integrated circuits provide novel solutions for early detection, diagnosis and therapy of disease. CMOS technology used for the manufacturing of personal computers and mobile

phones has been exploited for applications such as genetics, bringing the inherent advantages of CMOS into practice [1, 2]. The basic element of these CMOS based fully integrated systems, providing with the sensing capability and electrical detection, lies behind a CMOS based ion sensor, the ISFET (Ion-Sensitive Field-Effect Transistor), the principles of operation of which have been analysed in Chapter 3. At that point, aiming to apply the benefits of using the technology of ISFETs in an epigenetically driven application and specifically in detecting the methylation status of a DNA template towards the early screening of cancer, the very first proof-of-concept for determining and validating the methylation status of a DNA template (pUC19 plasmid DNA) is shown, followed by DNA methylation detection as a result of a DNA chain extension reaction taking place in the presence of a methylated DNA template. The DNA template was amplified under thermocycling conditions based on the method of pH-PCR [1], according to which the change in pH observed after the completion of the DNA chain extension reaction was detected using the commercially available pH sensitive ISFET technology (ISFET sensor by Sentron Europe B.V.). This is the first proof-of-concept for ISFET based DNA methylation detection.

Further to the development of the method of using the ISFET as a sensor for detecting DNA methylation in given genetic areas, the idea of using ISFETs integrated in standard CMOS technology is further developed into practice, using the multichannel DNA SoC platform (Appendix D), first described by [1, 3], applied in two different genes ($DAPK1$, $CDKN2A/p16\text{-}INK4$ ($p16$)) with different ratios of DNA methylation under isothermal conditions of DNA amplification using the method of pH-LAMP [1]. The SoC platform, is an ion-sensitive semiconductor based platform, bringing simultaneous amplification and detection of nucleic acids together on a single chip, by performing real-time monitoring of the pH of a DNA extension reaction using ISFETs as pH sensors, thus sensing the hydrogen ions (H^+) generated as a result of an amplification taking place. In this research, real-time detection of DNA methylation in CMOS using the SoC platform was achieved, generating a strong differential signal, therefore distinguishing methylated from unmethylated DNA in each gene case, proving that DNA methylation can be detected on-chip. This will allow us to create integrated systems such as the "Methylation Cell" and the ISFET based Chemical Gilbert Cell as described in Chapter 5 and Chapter 6 respectively.

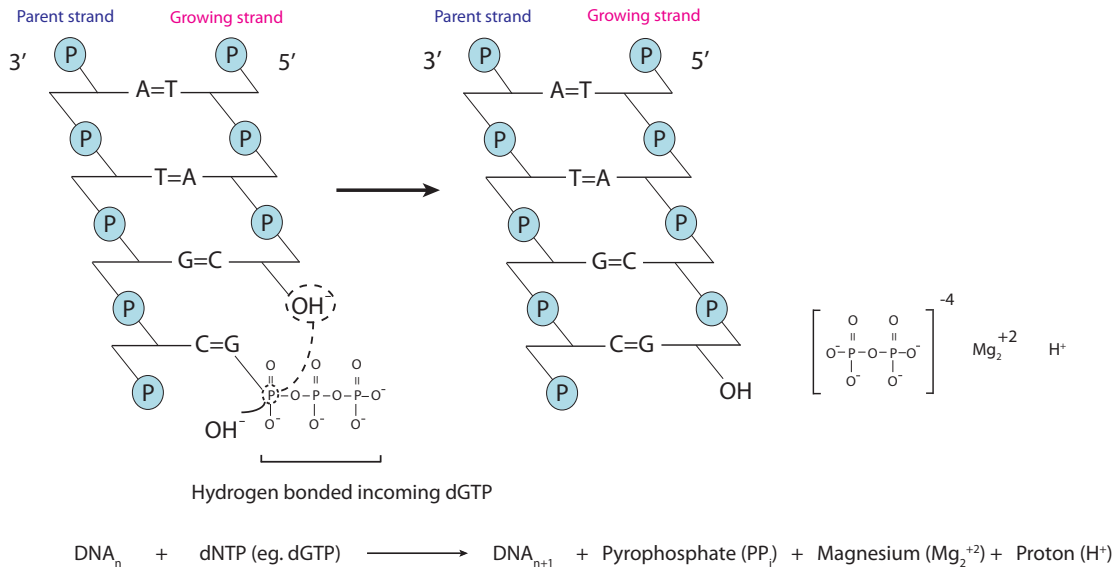


Figure 4.1: Biochemical mechanism for H^+ release following nucleotide incorporation. Figure obtained and adapted from [6].

4.2 DNA base pair incorporation detection

The biochemical information needed for DNA methylation to be detected by the ISFETs is obtained as a result of DNA amplification of the methylated region of the DNA sample taking place (either under thermocycling or isothermal conditions). This would be based on a DNA chain extension or elongation reaction, the biochemistry of which was first proposed by [4] who described the use of an ISFET to monitor the time course of a chain elongation reaction, during which the incorporation of dNTPs (deoxynucleotide triphosphates or nucleotide bases acting as the essential blocks of a DNA sequence, consisting of four nucleotides dATP, dTTP, dCTP, dGTP [5]) into a DNA strand results in the production of hydrogen ions or protons (H^+) leading to a growing DNA strand and the production of pyrophosphate (PP_i), resulting in a change in pH, monitored by the ISFET. Later on, work published by [6] reported a method for detecting DNA and more specifically SNPs, by monitoring the change in pH during nucleotide incorporation occurring in a DNA chain extension reaction.

As reported by [6] and shown in Fig. 4.1, while the double-stranded structure of the "parent" DNA opens, each single strand acts as a template to which the dNTPs (e.g. dGTP used in Fig. 4.1) are added, following the rules of complementary matching (A pairs

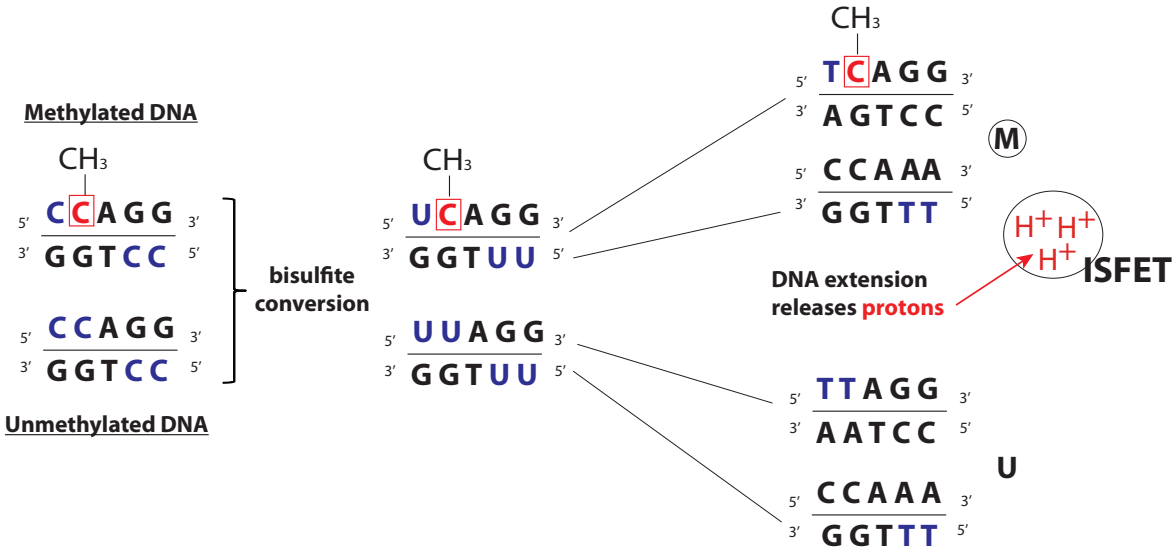


Figure 4.2: ISFETs can be used as pH sensors to detect methylated DNA (M) and distinguish it from unmethylated DNA (U) due to the presence of hydrogen ions (H^+) resulting from an extension reaction taking place in the presence of methylated DNA. For this to happen, the process of *bisulfite conversion* (method explained in Section 2.4, Chapter 2) is applied, which differentiates M from U. DNA strands are treated with sodium bisulfite so that methylated cytosines remain preserved through a DNA chain extension reaction whereas unmethylated cytosines are converted to uracils. This is a methylation dependent pre-amplification modification that is applied to the targeted genetic areas so that DNA methylation information is kept unaltered throughout the process.

with T, C pairs with G), under the essential presence of the DNA polymerase enzyme which is immobilised on the ISFET's surface and the addition of monovalent and divalent ions, primarily Magnesium (Mg^{+2}) which tends to enhance the activity of DNA polymerase [7]. The dNTPs are incorporated into the growing single-stranded DNA, Fig. 4.1, as the hydroxyl group from the 3' terminal of the growing DNA strand performs a nucleophilic "attack" to the α-phosphate group of the nucleotide base added [8], provided that the phosphate groups involved in the reaction are fully ionised given the starting pH profile of the reaction [6]. As a result, the incorporation of one nucleotide leads to the production of pyrophosphate and most importantly to the release of a hydrogen ion from the hydroxyl group of the 3' terminal of the growing strand, leading to a change in the pH of the reaction due to the increase of the solution's acidity. The pH would then be an indication of a single nucleotide incorporation taking place leading to a DNA extension reaction of a targeted gene site, monitored by the ISFET.

Additionally, for a given DNA template (double-stranded) to be amplified and thus a DNA chain extension reaction to happen, a sequence-specific pair of primers (one for each strand) or single-stranded oligonucleotides often described as DNA probes, need to be designed as the starting point of DNA amplification of the target sequence, defining the start and stop of the DNA strand that is to be copied. Primers can hybridise under specific temperature conditions, dependent on the nature of the amplification process (in this case we are referring to thermocycling or isothermal conditions) to their complementary target sequence, as the starting point of the DNA chain extension followed by the addition of dNTPs with the aid of the DNA polymerase enzyme, resulting in multiple copies of the DNA target being produced, leading to its amplification.

For the purpose of this research, single-stranded DNA probes were designed specifically to identify the region of a methylated DNA target with the sequence of which designed as the product of sodium bisulfite treatment, a chemical method which as explained in Section 2.4, Chapter 2, contributes in the enhancement of the signal derived from amplified methylated sequences, while altering the unmethylated bases, preserving DNA methylation during amplification. The under amplification methylated DNA target will therefore be equal to the product of the DNA target after chemical conversion of bisulfite treatment. The primers would hybridise only to the complementary DNA target sequence where DNA methylation is existent, aiming for a methylation-specific amplification, the result of which is to be detected by the ISFET, as can be graphically illustrated in Fig. 4.2.

For the proof-of-concept approach, two DNA amplification techniques were used resulting in DNA extension products: (a) Polymerase Chain Reaction (PCR) [9, 10] whereby DNA is amplified through a thermocycler leading to exponential amplification of products and (b) Loop-Mediated Isothermal Amplification (LAMP) [11] whereby DNA is amplified through isothermal conditions, at a stable temperature, without the need for a thermocycler. Both methods were combined with the use of the pH signal recorded by the ISFET before and after the event of amplification, as an indication of the presence of a reaction determined by the magnitude of the pH drop [12, 13]. The monitoring of the pH before and after a PCR and LAMP amplification in the presence of the methylated DNA target is reflected during the use of the term pH-mediated or pH-sensitive PCR (pH-PCR) and pH-mediated or pH-sensitive LAMP (pH-LAMP) [1], with the analysis of the methods and the discussion of the results to be shown in the following sections.

4.3 DNA methylation detection using pH-PCR

Several molecular biology methods were followed to carry out a structural way of producing naturally methylated/unmethylated DNA, validating the presence of methylation and finally developing a proof-of-concept method for detecting methylated DNA using the pH-sensitive method pH-PCR in conduction with the ISFET as the pH sensor.

For the realisation of the proof-of-concept method for DNA methylation detection at first, a gene target (i.e. pUC19 double-stranded plasmid DNA [14]) was selected as the sample "basis". The methylation levels of that gene were naturally modelled through the method of $transformation$ [15] by introducing the target gene in two host bacterial laboratory strains (competent cells) which were "competent" or ready to host the plasmid that needed to be inserted in the strain. As a result, through the process of *cloning* [15], multiple copies of two bacterial strains were produced resulting in producing the DNA target pUC19 in two forms: a methylated (dcm^+) and an unmethylated (dcm^-) form. This was achieved by using two host bacteria: one that was carrying a DNA cytosine methylase or *dcm methylase*, encoded by the *dcm* gene of E.coli [16], therefore modifying the internal cytosines at the 2nd C^5-position (C in bold) on both strands within the sequence ($5...C\mathbf{C}(A/T)GG...3$) leading to methylated plasmids (dcm^+), or by using methyltransferase deficient chemically competent E.coli cells, therefore growing plasmids free of *dcm* methylation (dcm^-).

As soon as the methylated/unmethylated DNA was produced and then purified, restriction enzymes were used to validate the result followed by the quantification of the DNA extracted from the bacterial strains. This was followed by the process of pH-PCR amplification of the resulting genetic targets, whereby a methylated gene target would be amplified specifically with the aid of pre-designed primers (primers designed according to the information and requirements reported by [5, 7]) that would anneal selectively to it and thus distinguish it from the unmethylated one. The signal generated from the amplification of the methylated gene would then be sensed by the ISFET pH sensor, to show that a methylation-specific pH change as a result of a DNA extension reaction taking place in presence of methylated DNA can be used as a marker for DNA methylation detection. Consequently, for a proof-of-concept approach for DNA methylation detection using the ISFET, two reactions are needed, one resulting to a PCR product and the other resulting to no PCR product. The materials and methods used for the experimental needs together with the results of pH detection of amplified methylated DNA are presented in the following

section.

4.3.1 Materials and Methods

Chemicals, Biolochemicals and Oligonucleotides

Oligonucleotides as primers for PCR/pH-PCR, dNTPs and $Truestart^{TM}$ Taq DNA polymerase enzyme were supplied by Thermo Fisher Scientific. Other reagents parts of the PCR buffer such as $MgCl_2$, KCl were supplied by Sigma-Aldrich. Oligonucleotides were dissolved in Sigma water at desired concentrations upon the first use and stored at -20^{o}C. Water was supplied by Sigma-Aldrich, otherwise, distilled water was manually sterilised by filtration using Sterile $Acrodisc$® Syringe Filters through a 0.2μm $Supor$® membrane.

Bacterial Strains

To naturally create two different DNA targets, one with DNA methylation being present and the other with DNA methylation being absent, two different E.coli strains were used. One $Shot$® $Mach1^{TM}$-$T1$® chemically competent E.coli cells (Life Technologies) [17] were used to allow the growth of pUC19 plasmid DNA with a native percentage of dcm^+ methylation present and dcm^- competent E.coli cells (New England BioLabs) [18] were used to allow the growth of pUC19 plasmid DNA free of dcm methylation. The "parent" strain of $Mach1^{TM}$-$T1$® E.coli cells was the non-K12 wild-type W strain (ATCC #9637, S.A. Waksman) whereas the "parent" strain of dcm^- E.coli was K12 [18], a cultivated strain in a laboratory environment.

DNA target

Plasmid DNA pUC19 (GenBank Accession #: L09137) (New England BioLabs), as shown in Fig. 4.3, is a double-stranded circular molecule of 2686 base pairs length, isolated from the bacterial strain E.coli (dam^+/dcm^+), being a commonly used plasmid vector in E.coli [14]. It is known for its small size and the fewer number of genes compared to genomic DNA, being used as the DNA target in these series of experiments. pUC19 contains several restriction sites, Fig. 4.3, areas on its "body" that are recognised by restriction enzymes (enzymes that can selectively cut recognisable DNA sequences). Moreover, as all plasmids, pUC19 as well, carries antibiotic resistance genes that can enable it to survive in an environment

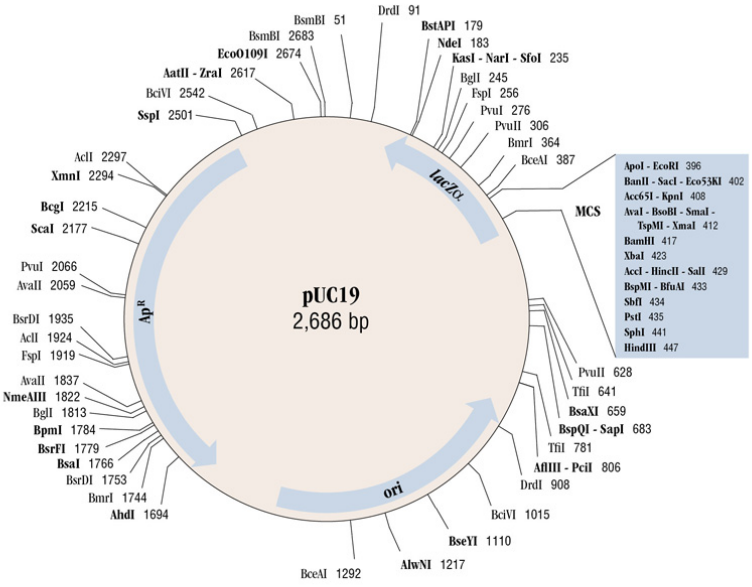


Figure 4.3: Map of pUC19. Visible are the areas of antibiotic resistance (Ap^R, where Ap stands for the antibiotic Ampicillin), the origin of plasmid replication (*ori*) and the multiple cloning sites including the actual coding sequence (*lac*) [14, 21]. Restriction sites are also shown in bold and regular font.

or medium that contains an antibiotic (usually Ampicillin). pUC19 contains a gene that makes it resistant to the antibiotic Ampicillin (Ap^R in Fig. 4.3) [14], which means that it passes this resistance to the bacterial strain that will be hosting the plasmid, which is of vital importance given that Ampicillin would let only the bacteria having acquired the plasmid survive.

For the purpose of this research, pUC19 was introduced in two bacterial E.coli strains, in order for the internal cytosines of the plasmid DNA to be either methylated by the *dcm methylase*, encoded by the *dcm* gene, contained in $Mach1^{TM}$-$T1$® E.coli cells, transfering a methyl group at the C^5 position of the internal cytosine (in bold) in the sequences $C\mathbf{C}AGG$ and $C\mathbf{C}TGG$ [19, 20], or unmethylated by methyltransferase deficient chemically competent E.coli cells, suitable for growing plasmids that lack of *dcm* methylation.

Stock solutions and bacterial growth media

Antiobiotic *Ampicillin* was prepared as 100mg/ml stock solution. It was sterilised by filtration through a 0.2μm *Supor*® membrane and kept in aliquots at -20^{o}C. Also, Luria-

Bertani (LB) bacterial growth medium, a medium commonly used in bacterial cultures, consisted of 1% (w/v) tryptone, 0.5% (w/v) yeast extract and 1% (w/v) NaCl. Similarly, Luria-Bertani Agar (LBA) medium was produced by LB solidified with 1.5% (w/v) agar. Both media were sterilised by autoclaving. 100μg/ml antibiotic *Ampicillin* was obtained from stock and then added to LBA medium so that the colonies selected would only be positive.

Molecular biology methods

Transformation of plasmid DNA into competent cells

Frozen competent cells (*One Shot*® *Mach*1™-*T*1® E.coli cells and dam-/ dcm- competent E.coli cells) were thawed on ice for each transformation. 1μl of DNA (pUC19) was added into each of the vials of the competent cells followed by a gentle mix and then kept on ice for 30min. For the negative controls, 1μl of distilled water, already filtered through a 0.2μm *Supor*® membrane, was added to 30μl of each of the competent cells and left on ice for 30min as well. The cells were then heat-shocked for 30sec at 42^{o}C without shaking and the tubes were placed on ice for 2min. Following that stage, 250μl of LB medium was added to each vial. The vials, tightly capped, were then inserted in a shaking incubator at 37^{o}C for 1 hour at 225rpm. After that, 50μl of the transformation mixes were spread on the LBA plates (where 100μg/ml Ampicillin was already added) using sterilised spreaders. The plates were left inverted in the incubator at 37^{o}C for 16 hours.

Preparation of plasmid DNA - DNA Purification - DNA Quantification

A single colony was selected from each plate of the overnight-grown colonies and then inoculated in solution of 10ml containing LB medium, 5ml and Ampicillin (100μg/ml), 5ml. The cell culture was left to grow overnight at 37^{o}C for 16 hours at 220rpm in a shaking incubator. Bacterial cells were harvested by centrifugation at >8,000rpm in a conventional, table-top microcentrifuge for 3min at room temperature. The plasmid DNA was then prepared and purified using QIAprep Miniprep kit by Qiagen. Pelleted bacterial cells were resuspended in 250μl suspended buffer, provided by the kit, and transferred to a microcentrifuge Eppendorf tube. Another 250μl of alkaline buffer was added and the tube was gently inverted 4-6 times. This was followed by the addition of 350μl buffer and then was mixed thoroughly before being centrifuged for 10min at 13,000 rpm in a table-top

microcentrifuge. The supernatants were applied to a QIAprep spin column provided with the Miniprep kit and then centrifuged for 30-60sec. The flow-through was discarded and so the column was washed with 750μl of ethanol buffer followed by a second centrifuge for 30-60sec. The flow-through was discarded again and the column was centrifuged for an additional 1min. The obtained plasmid DNA was eluted from the column by 50μl of sterilised water (which is the final volume of the plasmid DNA) and finally centrifuged for an additional 1min. For a long-term storage of the plasmid DNA after the transformation, 30% of the cell culture (150μl) was mixed well with 70% of glycerol (350μl) in a 1.5ml Eppendorf tube, kept frozen at -80^{o}C. Glycerol was used due to its ability to provide both intracellular and extracellular protection to the sample against long-time freezing.

Purified DNA was then tested and quantified using the NanoDrop ND-1000 Spectrophotometer v3.7, at 260μm and 280μm, brought by Thermo Fisher Scientific. 1μl sample was used for each measurement. In case of a more concentrated quantified DNA (eg. >1μg) after the NanoDrop quantification, aliquots of 50ng/μl were prepared. The purpose of aliquoting was also to reduce the continuation of a sample being thawed and frozen consecutively, therefore preserving the DNA sample from degradation [22].

Restriction enzyme cleavage

Restriction enzymes recognise specific sequences of DNA in areas specified as *restriction sites* and then cut them into DNA fragments, called *restriction fragments* [15]. For the purpose of this work, restriction enzymes were used for the validation of the methylation status of pUC19, after being prepared through the process of transformation. In general, DNA isolated from E.coli does not have the same extent of DNA methylation present and more importantly, methylation added by a *dcm methylase* inhibits the possibility of the DNA target to be digested by certain restriction enzymes. In particular, *dcm methylases*, in prokaryotes (plasmid DNA) are elements whose role is to protect the host DNA from cleavage by the corresponding restriction enzymes. DNA methylation can block, slow the rate of cleavage or leave the cleavage of the recognition sites unaffected. Cleavage may depend on the under study sites as well as on the reaction conditions, as it may lead to a partial or incomplete digestion products when applied in multiple sites.

After conducting some research on the commercially available restriction enzymes that were either sensitive or insensitive in the existence of methylated DNA, two restriction enzymes $EcoRII$, $MvaI$ (Thermo Fisher Scientific) were finally isolated and an investigation

Table 4.1: Restriction digestion protocol set-up for validation of methylated and unmethylated pUC19 plasmid DNA using *EcoRII* and *MvaI* restriction enzymes.

Restriction digestion protocol - Components	Amounts
Restriction Enzyme *EcoRII*/*MvaI*	1μl (10 units sufficient)
DNA dcm^+,dcm^-	2μl (from 50ng/μl stock purified DNA prepared in Section 4.3.1)[2]
10X Buffer O/R[3]	1μl
Nuclease-free water	6μl
Total reaction volume	10μl
Incubation time	1 hour
Incubation temperature	37^{o}C

was undergone on whether they could recognise and so cleave the methylated recognition sites (dcm^+) while distinguishing them from the unmethylated ones (dcm^-), as a preliminary and indirect way of validating the presence of DNA methylation in pUC19.

More specifically, in the experiments conducted, *EcoRII* restriction enzyme was selected based on its ability to protect methylated cytosines from being digested by completely overlapping the methylated sites. The methylated pUC19 (dcm^+) would therefore be resistant against cleavage by *EcoRII*, given that *EcoRII* has the ability to block the areas of *dcm* methylation, by only digesting the unmethylated (dcm^-) cytosines respectively as shown by the recognition sequence 5'.../$C\mathbf{C}(A\ or\ T)GG$...3' [1] [19, 20]. The activity of *EcoRII* was then compared with the cleavage effect of a second restriction enzyme, *MvaI*, which was able to digest both methylated and unmethylated cytosines (5'...$C\mathbf{C}$/$(AorT)GG$...3') since its activity is not blocked by *dcm* methylation.

Both the purified DNA templates (dcm^+ and dcm^-) and the enzymes were kept on ice prior to the experiment when not in the freezer. The components, as displayed on Table 4.1, were mixed prior to the addition of the enzyme, by pipetting up and down the reaction mixture for a few seconds. As soon as the enzyme was added, the reaction mixture was

[1] The symbol / indicates the point of cleavage following the 5' - 3' direction of the DNA sequence, with the internal cytosine (in bold) to be methylated.

[2] Initial trials have shown that 1μl of DNA template added to the total reaction volume was not sufficient enough for a complete digestion of the DNA sample. Thus, the volume of the DNA sample was increased to 2μl of the same concentration (50ng/μl).

[3] Buffers O and R were supplied for use with the enzymes *EcoRII* and *MvaI* respectively.

centrifuged and then left in the incubator at 37^oC for 1hour. The reaction mixtures were divided into two groups: the first group included the unmethylated (dcm^-) DNA template chosen to be digested separately by the restriction enzymes $EcoRII$ and $MvaI$, using each time the relevant buffer solution for the specific enzyme and nuclease-free water. Undigested DNA was used as a positive control mixture, also included in the first group of reactions, containing the dcm^- template and water, scaling the reaction mixture up to 10μl. Similarly, the second group was composed of the methylated (dcm^+) DNA template to be validated for its methylation status by the enzymes $EcoRII$ and $MvaI$, together with the positive control, containing the dcm^+ template and water. The mixtures additionally contained the relevant buffers and nuclease-free water. In total, 6 reaction mixtures were produced and then loaded to agarose gels for electrophoresis, as explained in Appendix E.

Polymerase Chain Reaction (PCR)

PCR is a well-established sequence-specific DNA amplification method first introduced by Mullis in the early 1980s [9, 10, 23, 24] and has been widely used in the field of molecular diagnostics and clinical research, combining detection and analysis of DNA amplification products of an under investigation DNA source. Since its discovery, it has rapidly progressed in applications such as genetic/epigenetic expression, sequencing, infectious disease identification (viral, bacterial analysis), forensics and biotechnology.

It is a standard method for exponentially amplifying small copies of DNA molecules using the law of complementary matching of nucleotide bases in the double-helix DNA structure. DNA is initially *denatured* as a result of temperature increase of a DNA sample in an aqueous solution, resulting in the separation of the two DNA strands and the formation of two single strands [5, 7]. After lowering the temperature of the solution, DNA fragments (primers) specifically designed in pairs with the aid of a primer design software ($Vector\ NTI^{®}\ Software$ by Life Technologies was used for the scope of this research [25]) are used to frame the terminal points of amplification based on specifications reported by [7, 15, 26]. Primers *hybridise* or *anneal* to both the sense strand ($forward\ primer$: it has the same sequence as the top or sense strand) and the complementary anti-sense strand ($reverse\ primer$: it has the same sequence as the bottom or antisense strand), following a complementary alignment between primer and DNA target [5, 27, 28], as can be seen in Fig. 4.4. The figure illustrates the specific example of methylation-specific primer design to achieve amplification of methylated pUC19 DNA producing a DNA fragment of 322 base

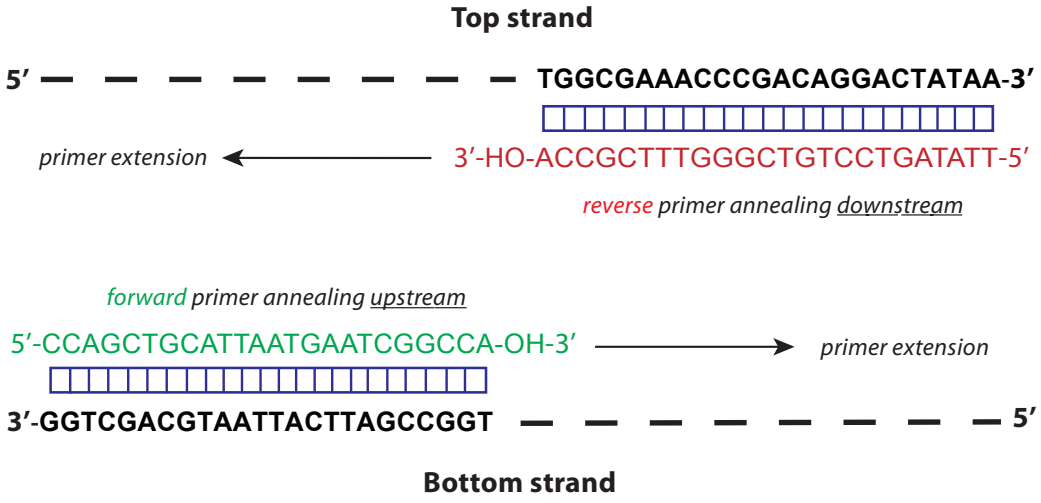


Figure 4.4: Forward and reverse primers designed to amplify the target DNA fragment of methylated pUC19 plasmid DNA using PCR and pH-PCR.

Table 4.2: Primers designed for methylated pUC19

Primer	Sequence
Forward: $p19.F6$ (5'-3')	CCAGCTGCATTAATGAATCGGCCA
Reverse: $p19.R6$ (5'-3')	TTATAGTCCTGTCGGGTTTCGCCA

pairs (bp) long, with primers shown in Table 4.2 corresponding to the methylated DNA target sequence, specific to the region of the methylation site of pUC19.

The temperature then increases for the *elongation* or *extension* step to proceed, which produces two identical DNA strands (often referred to as the *amplicon*) under the presence of PCR reagents: thermostable $Truestart^{TM}$ Taq DNA polymerase enzyme [29], dNTPs, PCR buffer consisting of $MgCl_2$ and KCl. This leads to the end of the 1st cycle of DNA replication and the beginning of the exponential amplification of the DNA target accumulated in billions of copies [5, 7, 15] after a given number of cycles (in this research 40 cycles were completed). A very elaborated example of the theory of PCR based on the methylated selected site of pUC19 together with the annealing effect of the designed primers, Table 4.2, is shown in Fig. 4.5 and continues in Fig. 4.6 illustrating the result of PCR amplification during the first 3 cycles. It is interesting to note that after the 1st cycle, 4 strands have been produced, the initial 2 used as the DNA template for amplification and 2

Table 4.3: Thermal cycling program for a 55-66^{o}C temperature annealing investigation

Temperature	Duration	Function
95^{o}C	1min	DNA denaturation
Repeat for 40 cycles the following:		
95^{o}C 55-66^{o}C	15sec 10sec	primer annealing - DNA extension

Table 4.4: Primers designed for positive control for the temperature gradient PCR investigation

Primer	Sequence
Forward: $p19.F4$ (5'-3')	CACAATTCCACACAACATACGAGCCG
Reverse: $p19.R4$ (5'-3')	GAGCCTATGGAAAAACGCCAGCAAC

more as a result of primer extension. The extension starts from a framed position (beginning of primer) but continues given that the DNA polymerase enzyme keeps adding nucleotides as far as it can go, covering the distance of a few thousands of bases. Consequently, DNA fragments of different lengths are produced and only at the 3rd cycle, where 8 DNA strands are created, does the desired DNA fragment (322-bp) become visible (black box in Fig. 4.6).

The primers ($p19.F6/p19.R6$) used in this research to amplify the methylated DNA sequences of pUC19 were initially tested for the optimal annealing temperature to be chosen[4]. A temperature gradient of 6 temperature values was performed between 55^{o}C and 66^{o}C for the set of primers designed for methylation-specific amplification of pUC19 DNA. The thermal cycling program performed for the temperature annealing investigation using a PCR machine (*Applied Biosystems*®, Life Technologies) is also summarised on Table 4.3 for 0.1μl of the pUC19 DNA template, equivalent to 10^6 copies in the reaction volume.

The PCR reaction was performed in 35μl reaction volume with 1.5Units/μl of $Truestart^{TM}$ *Taq* DNA polymerase, 800μM dNTPs, 0.5μM of each primer in the reaction buffer freshly

[4]The annealing temperature is the temperature chosen for the primer strands to anneal to the complementary strand of the "parent" template. It is possibly the most critical part for optimising the specificity of a single PCR reaction per primer set. The higher the annealing temperature, the more exact the match would be, but the more stringent the conditions for the primers to hybridise on the template [26, 28].

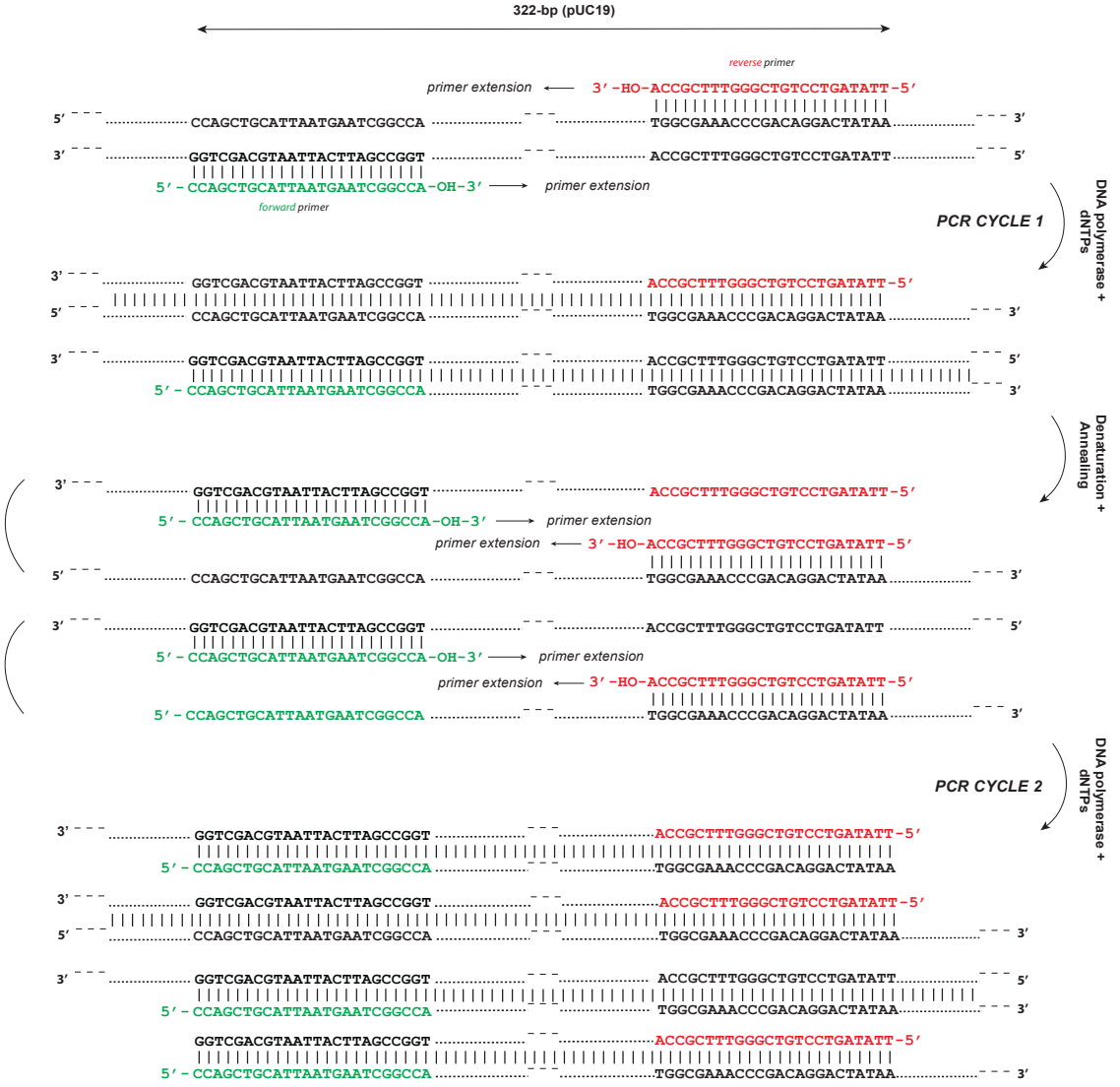


Figure 4.5: Synthesis of a 322-bp fragment of pUC19 DNA used for the demonstration of the initial steps of a PCR reaction which includes *denaturation* of the DNA template, *hybridisation* of the primers on the DNA template, also referred to as the *annealing* step, followed by *elongation* of the DNA template with the aid of the DNA polymerase enzyme and of dNTPs, a step also called *DNA extension* or *DNA replication*. The figure shows the sequence of events during 2 PCR cycles which is continued in Fig. 4.6 for the completion of 3 cycles.

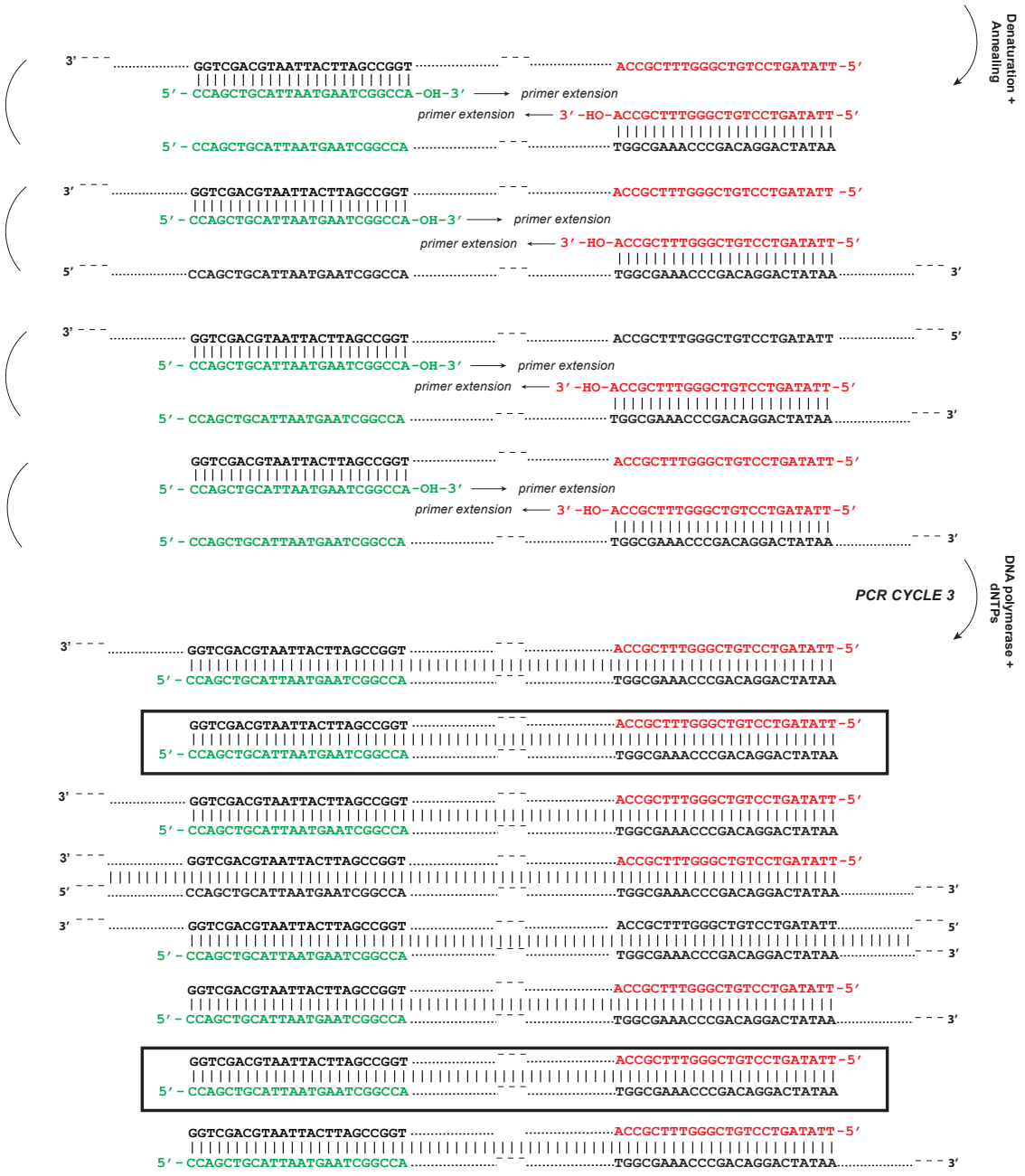


Figure 4.6: Continuation of Fig. 4.5 resulting in the accumulation of the resulting 322-bp DNA template, while the PCR amplification exponentially continues.

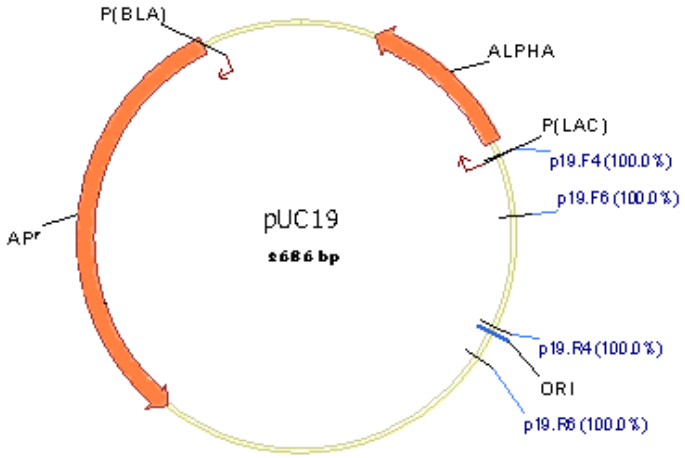


Figure 4.7: Map of pUC19. The location of amplification by the methylation-specific primer pair $p19.F6/p19.R6$, Table 4.2, which performs a 100% match with the target pUC19 template is displayed together with the location for the primer pair $p19.F4/p19.R4$, Table 4.4, used for positive control, performing 100% match with the "parent" template as well.

prepared, containing 3mM $MgCl_2$ and 50mM KCl and Sigma water to reach the total volume of 35μl. For the positive control mixture, the previously mentioned quantities were repeated in a new reaction mixture, differing from the previous one only in the use of a different set of primers $p19.F4/p19.R4$, Table 4.4, of the same quantity as in the main reaction mixture prepared for methylation-specific amplification, aiming to hybridise with the "parent" template of pUC19 at a location away from the methylation sites, producing a DNA fragment 379-bp long. The amplified product was resolved in a 1.75% agarose gel in 1xTBE buffer and the DNA band of the correct size was then confirmed using the method of agarose gel electrophoresis as explained in Appendix E, Section E.

pH-PCR

The method of pH-PCR and the principal protocol that describes the procedure followed was established by Toumazou et al. [1, 12, 13], applied for single base detection in applications such as Single Nucleotide Polymorphism (SNP) detection [3, 6] and DNA sequencing [30]. Using this as the core basis, the principal method for DNA methylation detection based on pH-mediated amplification and detection using the ISFET as the pH sensor was herein developed. The pH-PCR method includes the monitoring of the pH in PCR tubes before and

Table 4.5: pH-PCR thermal cycling program

Temperature	Duration	Function
95^oC	1min	DNA denaturation
Repeat for 40 cycles the following:		
95^oC 66^oC	15sec 10sec	primer annealing - DNA extension

after PCR amplification of a reaction where methylated DNA (pUC19, dcm^+) is present compared to a reaction where unmethylated DNA (pUC19, dcm^-) is present, including pH adjustments using 10M NaOH and 1M HCl (Sigma-Aldrich) in order for the start pH of the under amplification DNA reaction mixture to be as close as possible to the pH of the dNTPs [6]. The pH was monitored in sample volumes of 35μl using a commercially available Al_2O_3 ISFET sensor containing a Ag/AgCl reference electrode (Sentron Europe B.V.). The measurements were taken after having checked that the pH probes calibration slope was within the acceptable values, according to the manufacturer's guidelines, for a pH measurement to be valid. The terms of use, preparation and calibration steps of the Sentron ISFET pH probe combined with an Argus pH-meter (Sentron Europe B.V.) are included in Appendix C.

Before the start of the PCR amplification, the pH of the DNA reactions was adjusted to around pH 8.00 at room temperature using 10mM HCl (1M HCl stock solution) or 10mM NaOH (10M stock solution), dependent on the baseline of the pH measurements. Once the optimal annealing temperature (66^oC) of the primers was established through PCR (experimental validation on Section 4.3.2), the reaction mixtures (35μl in total) were then prepared for PCR following the protocol: 1.0 Units/μl of $Truestart^{TM}$ Taq DNA polymerase, 800μM dNTPs, 0.5μM of the primer set $p19.F6/p19.R6$ as displayed on Table 4.2, designed to amplify only the methylated pUC19 dcm^+ DNA template at a concentration of 0.02ng/μl in the PCR reaction or 1ng of 10μg/μl aliquoted pUC19. 3mM $MgCl_2$ and 50mM KCl were further weakly buffered in the 35μl reaction volume to help stabilise the fluctuation of pH, thus contributing in the kinetics of the reaction. The rest of the pH buffer was filled with Sigma water. A negative control reaction with no pUC19 DNA template also known as Non-Template Control (NTC) was setup in parallel as a reference baseline. The reactions were run in triplicates to evaluate the credibility of the result.

The PCR reaction was paused initially at the 5th cycle of the PCR program (beginning of PCR) and then at the 40th cycle (end of PCR) for pH measurements to be taken by the ISFET sensor. 5 cycles (instead of 0) were selected as a starting reliable point of conducting the pH measurements, as the pH of the samples measured at 0 cycles compared to 5 cycles during initial trials was quite high, possibly because of the CO_2 trapped in the reaction tubes. Consequently, the environmental parameters under which the pH measurements were taken were affecting less the measurements taken after 5 cycles and were thus closer to the conditions of those taken at 40 cycles.

The ISFET will then be able to sense the expected drop in pH, as a result of the amplification of methylated DNA, leading to a pH change produced by the incorporation of dNTPs in the reaction, as explained in Section 4.2. Hence, the DNA solution post-PCR would be enriched with hydrogen ions, the presence of which would perform the immobilisation of the chemically sensitive ISFET surface of the pH probe leading to an observed pH drop. The amplified products were quantified using Qubit Fluorometer (Qubit Quant-iT HS kit, Life Technologies) and then resolved in a 1.75% agarose gel in 1xTBE buffer. The DNA fragments of the correct size were then confirmed with agarose gel electrophoresis following the procedure as explained in Appendix E.

4.3.2 Results

Restriction Enzyme Cleavage

Restriction enzymes $MvaI$, $EcoRII$ were chosen to validate the presence or absence of DNA methylation in a methylated (dcm^+) and unmethylated (dcm^-) state of pUC19 plasmid DNA. The results of the restriction enzyme cleavage based on the protocols reported in Section 4.3.1, Table 4.1 can be seen in Fig. 4.8.

The number of digested fragments expected to be seen through gel electrophoresis were 5 in total, of sizes 13, 121, 191, 288 and 2073 bps, which was validated with the use of the software *Restriction Mapper* [31]. This may vary though based on the activity of the enzymes in presence of DNA methylation. In specific, the restriction enzyme $MvaI$ showed the capability of digesting both the unmethylated (dcm^-) and methylated (dcm^+) DNA targets, with the correct fragment sizes of 121, 191 and 288 clearly seen in Fig. 4.8, the location of which was assessed by using the DNA ladders of two different sizes. Compared to the activity of $MvaI$, the restriction enzyme $EcoRII$ did not cleave the areas where

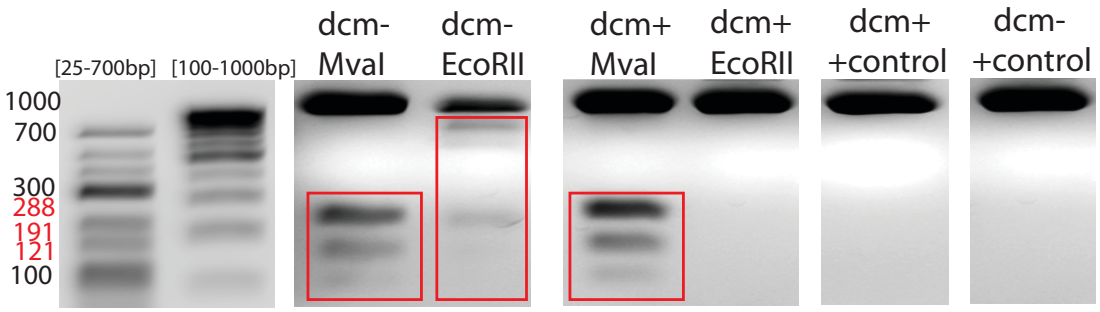


Figure 4.8: DNA cleavage using the restriction enzymes $MvaI$ and $EcoRII$ on dcm^+/dcm^- pUC19.

methylated DNA was present, but digested as was expected the unmethylated ones. Very small (13-bp) fragments were unable to be seen because of the sizes of the DNA ladders used during the electrophoresis. Very large (2073-bp) fragments should sit on the top of the gel, based on their high molecular weight. Two big fragments that appeared on the top of the gel, in the case of dcm^-, digested by $EcoRII$, may have been derived from the fragmented ends (5' or 3') of the circular plasmids strands. Also, positive control for both dcm^+ and dcm^- was used, including either of the templates (dcm^+ or dcm^-) and water. Evidently, the use of the specific pair of enzymes, as described above, was proved to work successfully as a preliminary method of distinguishing as well as characterising methylated from unmethylated sequences of pUC19.

PCR: primer annealing temperature

In parallel with the process of validation of pUC19 plasmid DNA via restriction digestion analysis, a first attempt was made to design gene specific primers that would have the ability to anneal to targeted methylated sequences and can further be used to detect DNA methylation through PCR amplification, by amplifying the methylated gene regions selectively and further on through pH-PCR, via detecting the pH changes of the reaction volume before and after PCR using a commercially available ISFET pH sensor.

A first step was to run a gradient temperature PCR amplification on pUC19, Table 4.3, in order for the optimal annealing temperature of the designed methylation-specific primers to be determined, a critical step for the optimisation of amplification using the primer pair shown on Table 4.2. What was observed was a very good annealing of the primer set $p19.F6/p19.R6$ for dcm^+ pUC19, which was justified by the fact that there was obtained

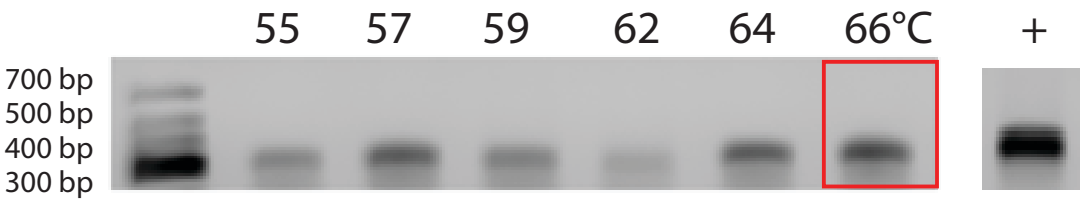


Figure 4.9: Gradient PCR using the primer set $p19.F6/p19.R6$ for 6 different temperature values using pUC19 as a DNA template. The primer set $p19.F4/p19.R4$ was used as positive control.

100% alignment match with the parent template pUC19, observation that was apparent from the gel images and the clear bands of Fig. 4.9. The best annealing temperature of the primer set was found at 66°C with a resulting amplified product of 322-bp long, as defined by the DNA ladder loaded in the gel. The primer set $p19.F4/p19.R4$ was used as the positive control, with an amplified product of 379-bp.

pH-PCR

After having adjusted the pH of the pre-amplification reaction volume in the range of pH 8.00 in order for an amplification to be observed after the completion of the thermocycling program, displayed in Table 4.5, as explained in Section 4.3.1, pH measurements were taken after 5 cycles of the initiation of the PCR program and then compared to the ones taken after the completion of 40 cycles. The results of the pH drop of the reaction mixtures are shown in Fig. 4.10a.

There is observed a higher pH drop between 5 and 40 cycles for the methylated DNA (pUC19 dcm^+) extension reaction mixture (M1-M3) compared to the unmethylated DNA (pUC19 dcm^-) reaction mixture (U1-U3) that showed no amplification due to the selectivity of the primers to anneal only to the methylated DNA template. More specifically, it can be seen that the pH values obtained, post PCR, from the methylation-specific DNA extension reaction, started from an average value of pH=7.62 at 5 cycles and then experienced a drop of 0.44 reaching an average of pH=7.18 after 40 cycles.

On the other hand, for the after pH-PCR reaction mixture containing the unmethylated DNA template, the measured pH values of 5 cycles reached on average a pH=7.69 and then dropped after 40 cycles to a pH=7.41, with a lower drop of 0.28 pH values being observed due to the absence of methylated DNA, therefore distinguishing whether the ISFET sensor

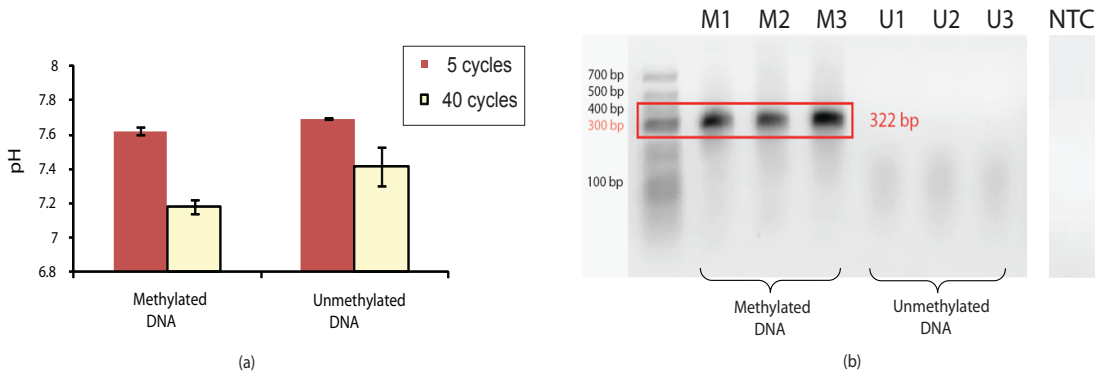


Figure 4.10: Methylation-specific pH-PCR in-tube: (a) average pH drop from 3 trials of triplicates in the cases of methylated/unmethylated pUC19. Error bars are also adapted in both charts based on the standard deviation of the pH recordings, (b) results of DNA extension reaction in triplicates for methylated pUC19 DNA (M1, M2, M3) compared to no extension reactions taking place for unmethylated pUC19 DNA (U1, U2, U3). Non-Template Control (NTC) was also clear showing no contamination of the reaction.

Table 4.6: pH average values between 5 and 40 cycles of pH-PCR (3 trials) for methylated pUC19 DNA (M) vs unmethylated pUC19 DNA (U) together with resulting ΔpH and standard deviation values for both reaction mixtures.

Cycle no.	pH-M (avg)	pH-U (avg)	std-M	std-U	ΔpH-M	ΔpH-U
5	7.62	7.69	0.02	0.01	0.44	0.28
40	7.18	7.41	0.04	0.11		

could detect or not a DNA extension reaction due to the presence of methylated DNA. A comparison between the pH signals obtained from the result of amplification of methylated DNA (pUC19 dcm^+) versus the non-amplification product due to the presence of unmethylated DNA (pUC19 dcm^-) together with calculated standard deviation values from 3 trials are displayed on Table 4.6.

Finally, after completing the pH measurements, the amplified products were then resolved in a 1.75% agarose gel in 1xTBE buffer, where the bands of the correct DNA fragment size were confirmed through agarose gel electrophoresis for methylated/unmethylated DNA. The agarose gel was left running for 15min with a constant voltage of 220V. The results are shown in Fig. 4.10b, illustrating that the methylated DNA template (pUC19 dcm^+) was amplified and so the gene-specific primers designed specifically for the methylated DNA

target did anneal, producing the correct size of a DNA fragment (322-bp) as appears in the gel image. Also quantification of the amplified products after the end of the PCR program was performed, reaching a 10^4 fold of amplification.

It is therefore clear that the ISFET as a pH sensor can be used for DNA methylation detection, structuring an initial proof-of-concept approach through the use of pH-PCR, showing the ability of successfully distinguishing the relatively bigger pH drop derived from a DNA extension reaction of a methylation-specific DNA template, after being annealed by a set of gene-specific primers, compared to an unmethylated DNA template, hence providing a robust tool for differentiating and distinguishing DNA methylation in two DNA samples.

4.4 DNA methylation detection using pH-LAMP

Following to the development of a proof-of-concept multiple-staged method for determining, validating and detecting methylated DNA using the method of pH-PCR as has been explained in detail in Section 4.3.1, a DNA methylation assay was also developed, with an enhanced sensitivity of detection, compared to the assay developed in Section 4.3.1, using the method of pH-LAMP [1] for the promoters of two genes ($DAPK1$, $CDKN2A/p16$-$INK4$ ($p16$)), as shown in [32]. The purpose of this was to prove that DNA methylation can be detected under isothermal conditions as well, with the signal of amplification to be sensed by both a commercial ISFET sensor (Sentron Europe B.V.) and ISFET sensors integrated in CMOS in real-time using the label-free System-on-Chip (SoC) platform, as described by [1, 3]. The SoC platform is an ion-sensitive semiconductor based platform, bringing simultaneous amplification and detection of nucleic acids together on a single chip, by performing real-time monitoring of the pH of the amplification reaction thus sensing the hydrogen ions generated. In this research, the chemical front end of the SoC platform was developed especially for the need of DNA methylation detection to achieve optimal conditions for gene-specific isothermal amplification, demonstrating a robust and highly sensitive method while highlighting the potential for a large multiple gene on-chip methylation analysis, taking advantage of CMOS technology.

The sequence of the two gene promoters was cloned in the plasmid vector $pUC57$ by GeneScript in both a methylated and unmethylated state after bisulfite treatment and methylated-specific primers were used to amplify only the methylated regions in each gene case, as reported by [33]. The methylated state of the genes ($DAPK1_M$ and $p16_M$) was

defined as all methylated cytosines remaining unaltered after bisulfite treatment while unmethylated cytosines being converted to uracils. The unmethylated state of the genes ($DAPK1_U$ and $p16_U$) was defined as all cytosines being converted into uracils after bisulfite treatment. Non-Template Control (NTC) was used as a negative control (chemical reference) for the in-tube tests and on the SoC platform (Chamber 2, Fig. 4.12).

4.4.1 Materials and Methods

Chemicals, Biochemicals and Oligonucleotides

Plasmids for pH-LAMP were synthetically generated by GeneScript and oligonucleotides, as primers for pH-LAMP, were synthesised by Integrated DNA Technology (IDT). Other agents parts of the LAMP buffer such as KCl, $NaOH$, NH_4Cl, $MgSO_4$, Betaine, Triton-X 100, BSA, dNTPs and water were supplied by Sigma-Aldrich. *Bst* polymerase was supplied by New England BioLabs. Oligonucleotides were dissolved in Sigma water at desired concentrations upon the first use and stored at -20^{o}C.

DNA targets

Purified synthesised plasmid DNA (pUC57) was used as the DNA target, incorporating the target sequences of two gene promoters of the genes $DAPK1$ or *Death Associated Protein Kinase* 1 [34] and $CDKN2A$ or $Cyclin-Dependent\ Kinase\ Inhibitor\ 2A$ also known as $p16$-$INK4$ ($p16$) [35], in a methylated and unmethylated state, emulating the two scenarios of a gene promoter after bisulfite treatment. These two genes were selected in specific due to the fact that their disrupted DNA methylation profile has been reported to play a significant role in influencing several antitumour pathways when hypermethylation in the CpG islands of their promoters occurs. In more detail, $DAPK1$ is related to the stage of apoptosis or programmed cell death [36] also recognised as a tumour suppressor gene related to metastatic tumour stages, one of the first being found to be methylated in cancer [37], with the CpG hypermethylation occurring in the promoter regions of the gene playing a significant role in cancer development of different organs [38–40]. Additionally, $p16$ gene takes part in regulatory mechanisms of cell cycle and is a well-characterised tumour suppressor gene, the promoter methylation of which is considered as a major mechanism of the gene's inactivation and loss of transcription in numerous primary tumours when hypermethylation of normally unmethylated CpG islands in the promoter region of the

gene occurs [41, 42].

The principle of the LAMP method

The method of Loop-Mediated Isothermal Amplification (LAMP) was first introduced by Notomi et al. [11], providing fast DNA amplification with high efficiency and specificity for the target sequence, under isothermal conditions. Due to its design, it is considered as highly selective for the target sequence given that four different primers (FIP, BIP, F3, B3) are used to recognise six genetic regions of the targeted gene, bringing the accuracy level relatively high even when few copies of DNA are available for analysis. The amplification occurs in loops with the aid of two additional loop primers (LF and LB). Unlike PCR, LAMP does not require the step of denaturation of the DNA template [43] given the ability of a DNA polymerase enzyme (*Bst* polymerase from *Bacillus stearothermophilus* DNA polymerase I [44]) to perform auto-cycling strand displacement DNA synthesis. This is initiated by the inner primers (FIP and BIP), Fig. 4.11, with sequences of the sense and antisense strand of the DNA target followed by the outer primers (F3, B3) which displace the annealed strand with the aid of *Bst* polymerase, releasing a single DNA strand, forming a "dumbbell" shape, which promotes the cycling amplification process at a constant temperature [11, 45]. The result of LAMP amplification is consisted of fragments of double-stranded DNA of variable length, with the initial few copies of DNA been amplified in less than an hour, in high specificity [11]. We proceed by validating DNA methylation detection using the method of LAMP using first commercial ISFET pH sensors (Sentron) in PCR tubes (in-tube tests) and then ISFETs in CMOS using the SoC platform.

Method: pH-LAMP in-tube

pH-LAMP was performed initially for both gene assays ($DAPK1_M/DAPK1_U$ and $p16_M/p16_U$), whereby a commercially available Al_2O_3 ISFET sensor with an Ag/AgCl reference electrode was used (Sentron Europe B.V.). The ISFET as a pH sensor was used to show that a methylation-specific LAMP reaction could be monitored given the release of hydrogen ions as a result of successful incorporation of nucleotides. pH-LAMP was carried out for both gene assays in triplicates in a total 35μl reaction mixture consisted of 50mM KCl, 2.5mM NH_4Cl, 6mM $MgSO_4$, 1M Betaine, 1mM $NaOH$, 0.1% Triton-X 100, 1mg/ml BSA, 2.8mM dNTPs, 30U of *Bst* DNA polymerase, 1.6μM each FIP and BIP, 0.2μM each F3 and B3, 0.8μM each LoopF and LoopB and 1pg/μl (equivalent of 10^5 copies after a

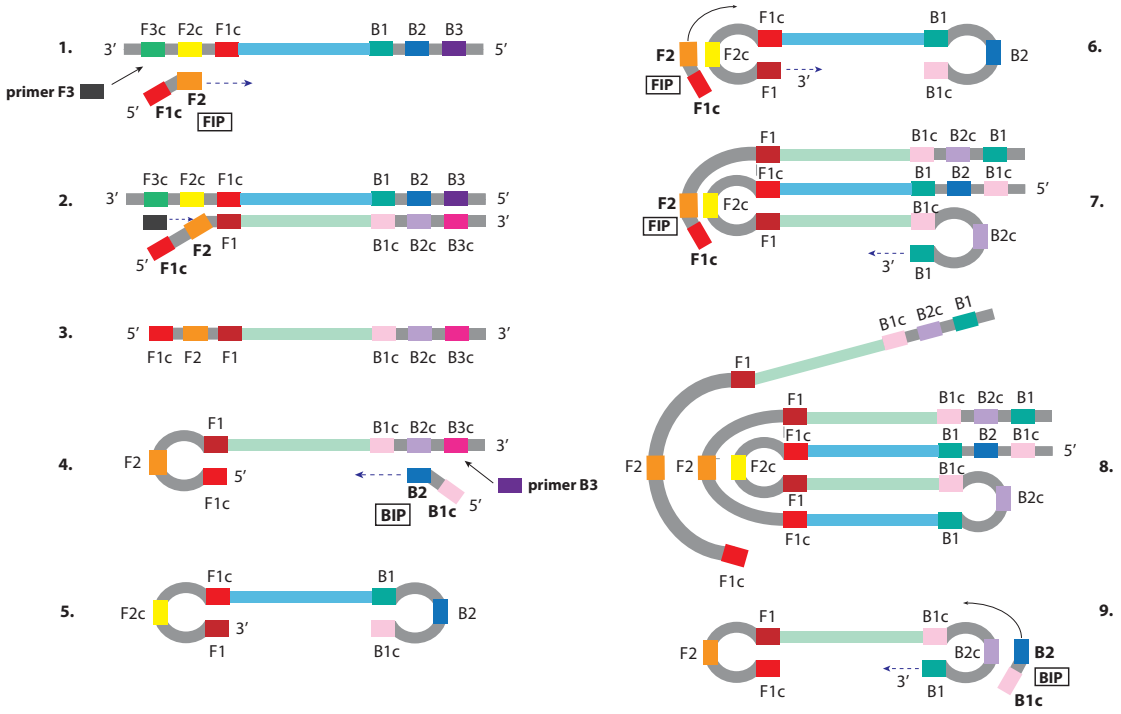


Figure 4.11: Principle of LAMP method adapted from [11]. Steps 1-8 represent the starting points of LAMP amplification, with DNA synthesis starting with the primer FIP (F2+F1c) (step 1) whereby the region F2 anneals to the complementary F2c on the DNA target, initiating DNA extension, with the process to continue with the primer BIP (B2+B1c) (step 4). Primer F3 anneals to the complementary F3c targeted region, initiating strand displacement and DNA synthesis (steps 2, 3), while the 5'-3' single strand is being released (step 3), forming the first loop structure, creating a "dumbbell" shape (step 5). The cycling amplification step then starts with the structure of step 5 being used as the template for DNA synthesis, to continue with primer FIP annealing to a single strand from the 3' end of the F1 region to the F2c region (step 6, 7), creating a loop structure. Through step 8, this leads to step 9 where one more "dumbbell" shape is produced, complementary to the one of step 5 [11].

3-fold serial dilution from 10^8) of each methylated/unmethylated DNA, forming the lowest limit of detection of this assay. The pH of the reaction mixture was adjusted between 8.15 and 8.8 as a pre-amplification pH range based on the DNA methylation assay's kinetics.

The program was performed with the aid of a PCR machine (Applied Biosystems, Life Technologies). To increase the buffer capacity of the reaction mixtures and to stabilise the amplification process, additives including monovalent and divalent ions were contained. The temperature of the isothermal program was set at 63°C after having been optimised

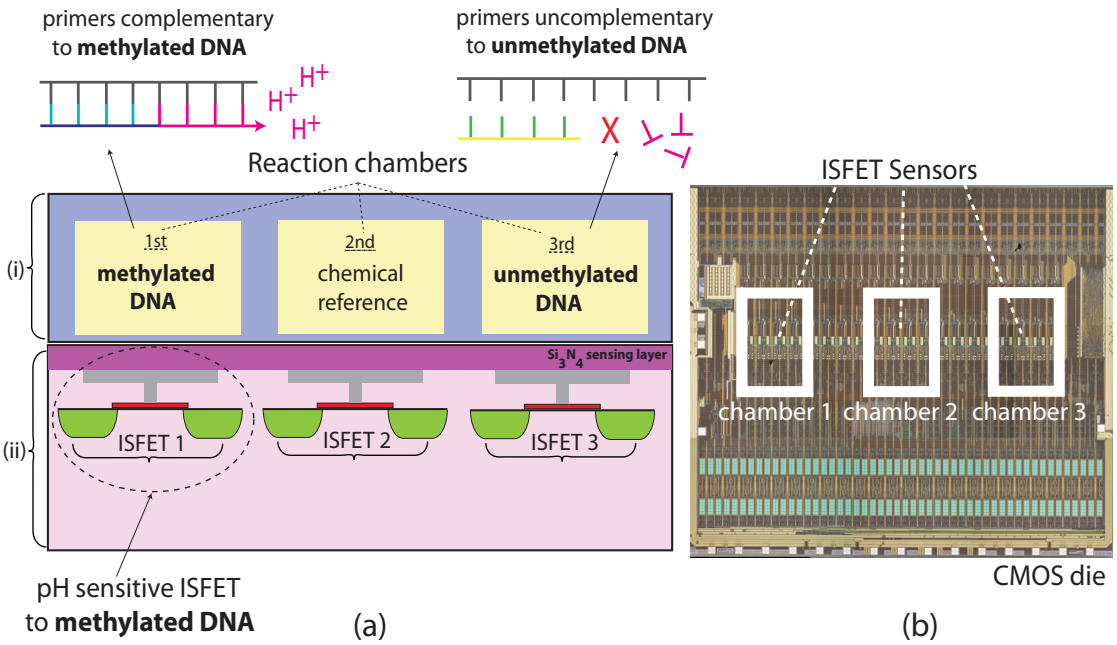


Figure 4.12: ISFETs in CMOS for real-time detection of methylated DNA versus unmethylated DNA using pH-LAMP in the 3-chamber SoC with (a,i) indicating the integration of a microfluidic assembly in chambers interfacing with CMOS ISFETs and (a,ii) showing the area where CMOS ISFETs, temperature sensors, digital IO and ADCs are embedded. Image of the fabricated CMOS die in 0.35μm process on (b) indicates the 3 reaction chambers and location of ISFET sensors.

for methylation-specific primer annealing for both gene assays and was maintained stable throughout the amplification for a duration period of 2100s (35min). The reactions were interrupted once at 180s (3min) from the starting point of pH measurements. The reaction was left running for real-time monitoring of the pH signal. After the completion of the program, the reaction mixtures were cooled down to room temperature and then the final pH was measured for both methylated and unmethylated reactions of both genes. Finally, the amplification yield was quantified using the fluorescent based Qubit Fluorometer (Qubit & Quant-iT HS kit, Life Technologies). Agarose gel electrophoresis was run to confirm the result of methylation-specific amplification.

Method: Real-time pH-LAMP on semiconductor integrated CMOS chip

Both assays ($DAPK1_M/DAPK1_U$ and $p16_M/p16_U$) were applied on the CMOS chip to achieve real-time detection of methylation-specific areas using pH-LAMP. After mixing the

Table 4.7: pH average values at 180s and 2100s of pH-LAMP in-tube (10 trials) for $DAPK1_M$ vs $DAPK1_U$ together with resulting ΔpH and standard deviation values for both reaction mixtures.

Time	pH-M (avg)	pH-U (avg)	std-M	std-U	ΔpH-M	ΔpH-U
180s	8.24	8.18	0.08	0.06	1.91	0.07
2100s	6.33	8.11	0.05	0.08		

Table 4.8: pH average values at 180s and 2100s of pH-LAMP in-tube (10 trials) for $p16_M$ vs $p16_U$ together with resulting ΔpH and standard deviation values for both reaction mixtures.

Time	pH-M (avg)	pH-U (avg)	std-M	std-U	ΔpH-M	ΔpH-U
180s	8.29	8.27	0.07	0.05	1.58	0.06
2100s	6.71	8.21	0.05	0.06		

reagents including the assay-specific primers, a small fraction was loaded in the chambers of the IC as seen in Fig. 4.12. For each assay in particular, Chamber 1 contained the methylated "version" of each gene ($DAPK1_M$ or $p16_M$), Chamber 2 a chemical reference control mixture lacking a dNTP (in this case dCTP) and Chamber 3 the unmethylated "version" of each gene ($DAPK1_U$ or $p16_U$). A common temperature of 63^oC was set through the heating elements of the IC to allow for isothermal conditions of amplification on the chip. The pH of the reaction mixture was adjusted between 8.15 and 8.8 as a pre-amplification pH range based on the DNA methylation assay's kinetics. After the completion of the program, the reaction mixture was removed from the chip and fluorescent based quantification of the amplification yield was performed using the Qubit Fluorometer (Qubit & Quant-iT HS kit, Life Technologies). Agarose gel electrophoresis was finally conducted to confirm the amplification observed real-time from the IC's interface.

4.4.2 Results

pH-LAMP in-tube

To prove the concept of methylation-specific pH-LAMP using ISFETs, initial tests in-tube were performed (10 trials in total) following the process explained in Section 4.4.1. The pH

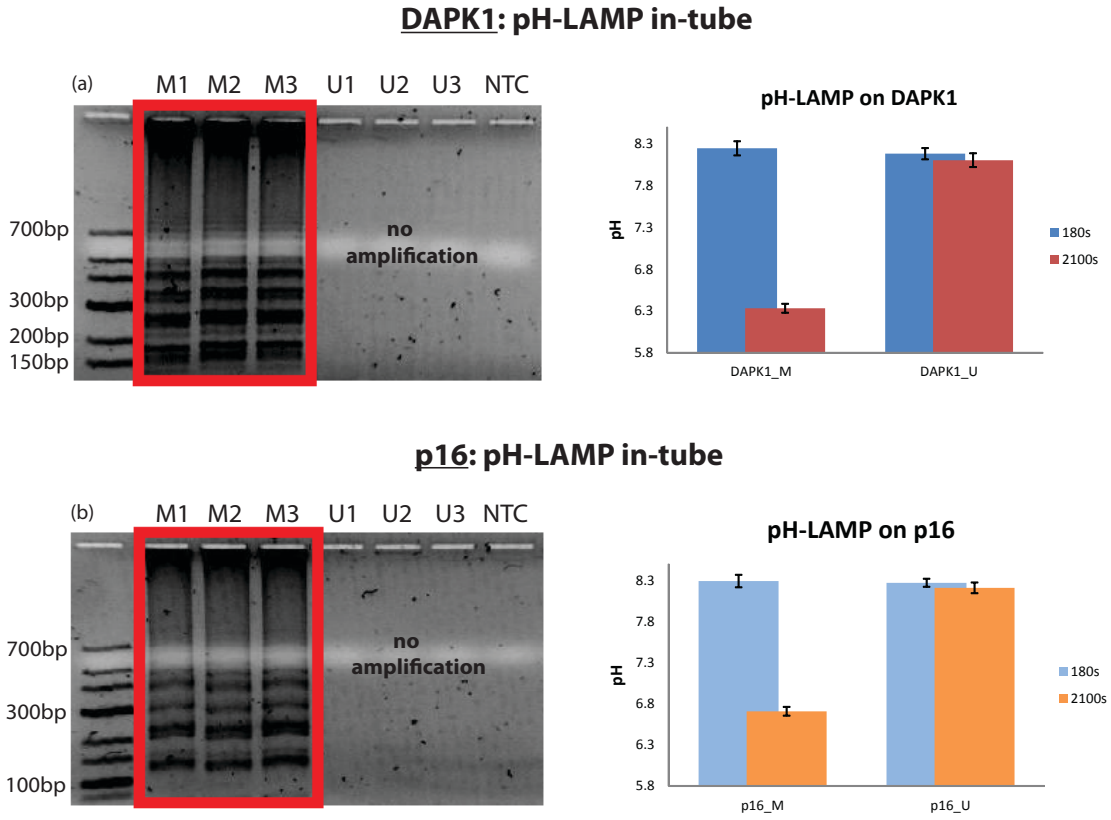


Figure 4.13: Methylation-specific pH-LAMP in-tube: triplicates of pH-LAMP for isothermal assays designed to detect $DAPK1_M$ (a) and $p16_M$ (b). Results of DNA chain extension reactions are shown in both (a) and (b) due to the presence of methylated DNA (M1, M2, M3). No extension reactions take place due to the presence of unmethylated DNA (U1, U2, U3). Non-template control also came clear showing no contamination or any nonspecific amplification in the reaction. A bar chart on the right hand side reveals the average pH drop from 10 trials of triplicates, in the cases of methylated DNA ($DAPK1_M$, $p16_M$) as a result of amplification happening in both DAPK1 and p16 assays. No significant pH change was detected in cases of unmethylated DNA ($DAPK1_U$, $p16_U$). Error bars are also adapted in both charts based on the standard deviation measured values of the pH recordings.

sensitivity of the assays was tested based on the occurrence of a DNA chain extension reaction happening in the presence of target sequences of methylated DNA. Results as shown in Fig. 4.13 illustrate that a methylation-specific reaction took place in both gene assays, using primer sets specifically designed for each methylation-specific gene assay, amplifying the genetic areas complementary to $DAPK1_M$ in Fig. 4.13a and $p16_M$ in Fig. 4.13b accordingly, showing a repeatable signal of detection, with the final pH values of the amplified reactions to be in the range of 6.3-6.8 pH.

In parallel to the previous results, reaction mixtures including the unmethylated genes ($DAPK1_U$ or $p16_U$) in both assays did not produce a signal as a result of the absence of extension reaction due to the inability of dNTPs to be incorporated since primers were uncomplementary to the unmethylated areas. The results of pH measurements of 10 trials for both methylation-specific pH-LAMP assays are also shown in Fig. 4.13a,b with the average pH change between 180s (3min) and 2100s (35min) seen in the presence of $DAPK1_M$ reaching the value of 1.91 as seen in Table 4.7, compared to 0.07 seen in presence of $DAPK1_U$. In parallel to this, the average pH change for the same time duration in presence of $p16_M$ reached the value of 1.58 compared to 0.06 in presence of $p16_U$, Table 4.8. It is therefore clear that the ISFET as a pH sensor can be used for DNA methylation detection using pH-LAMP, showing the ability to successfully and repeatedly distinguish the significantly big pH drop derived from the extension reactions of two methylation-specific genetic areas annealed by methylation-specific primers, together with an in-parallel amplification quantification. The results of quantification of the 10 trials of the amplified methylated products showed a good fold of amplification reaching 10^5 times the initial copy number of the starting amplicon for $DAPK1$ and $p16$ assays.

Real-time pH-LAMP on semiconductor integrated CMOS chip

Furthermore, both gene assays were applied on-chip, as per description in Section 4.4.1, using the 3-chamber SoC platform as illustrated in Fig. 4.12. 7 chips were run for each assay. Results from the isothermal pH-LAMP assay appear in Fig. 4.14a for the $DAPK1$ assay and in Fig. 4.14b for the $p16$ assay. Results of multiple chip runs are shown with the real-time traces derived from Chip 1 appearing on the left hand side of both figures. The reactions exhibited a good amplification response in the time period of 50min, with the final plateau of amplification of $DAPK1_M$ to take place at 2000s and at 2500s for $p16_M$.

In the $DAPK1$ assay, DNA extension reaction took place due to the presence of primer sets complementary to $DAPK1_M$, amplifying the targeted methylated region as seen in Fig. 4.14a, exhibiting a maximum real-time differential signal change of 37mV detected by the ISFET sensors of Chamber 1 (shown in pink and yellow), being a strong indicator of $DAPK1_M$ detection. Consequently, primers showed an uncomplementary behaviour towards the target sequence of $DAPK1_U$ as shown by the traces derived from the ISFET sensors output of Chamber 3 (shown in green and orange). Chamber 2 showed a stable signal at 0mV as it was used as a chemical reference to indicate the validity of the result in

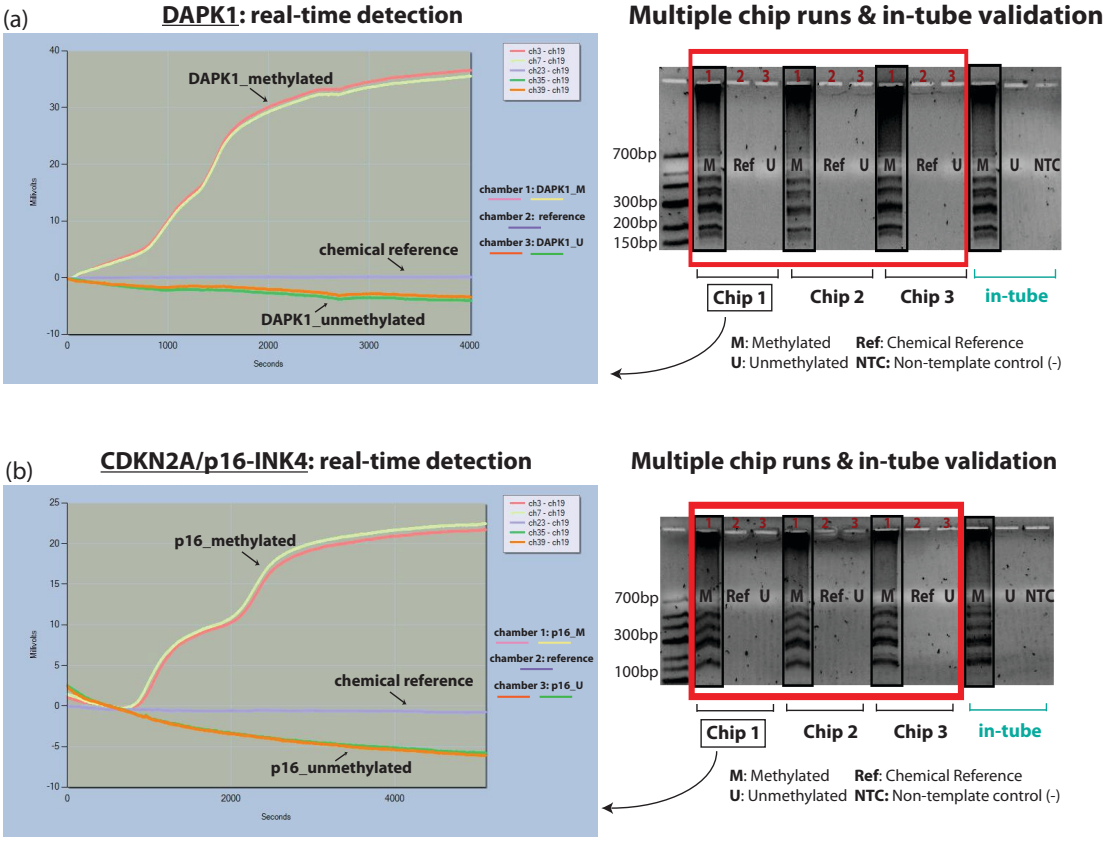


Figure 4.14: Real-time methylation-specific pH-LAMP on-chip together with gel electrophoresis validation for (a) DAPK1 gene and (b) p16 gene

terms of purity of product.

Similarly, for the $p16$ assay, primer sets were used complementary to $p16_M$, Fig. 4.14b, amplifying the targeted region, reaching a maximum real-time differential signal change of 23mV detected by the ISFET sensors of Chamber 1 (shown in pink and yellow), indicating the detection of $p16_M$. Primers were uncomplementary to $p16_U$ as shown by the traces derived from the ISFET sensors output of Chamber 3 (shown in green and orange) therefore no DNA extension reaction products were found. Chamber 2 gave a stable signal at 0mV as should provide a chemical reference.

In both assays, pH-LAMP in-tube tests were performed in parallel from the same reaction cocktail that was dispensed on the chip, as can be seen in Fig. 4.14 for both genes. The purpose of this was to validate the result of the on-chip amplification products of $DAPK1_M$ and $p16_M$, confirming accurate real-time DNA methylation amplification and

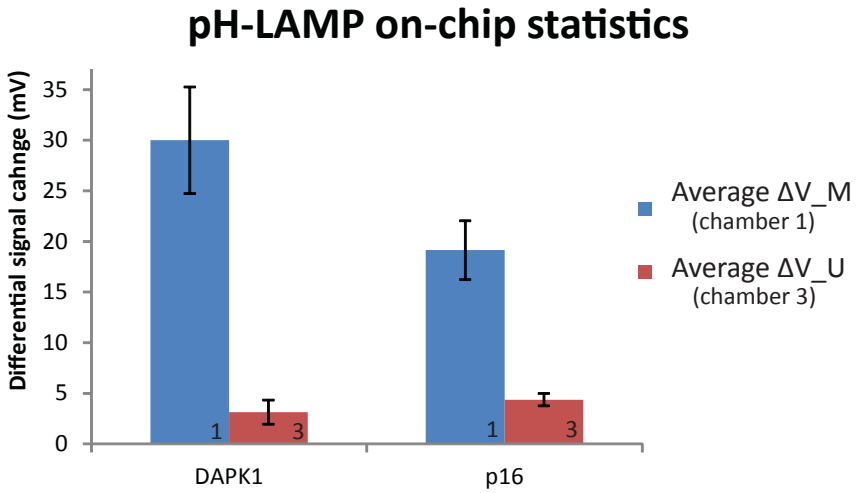


Figure 4.15: Chip statistics from real-time pH-LAMP results for both assays as has been shown in Fig. 4.14 for $DAPK1$ (a) and $p16$ (b) genes. Chip statistics indicate the average differential voltage change for $DAPK1_M$ and $p16_M$ (blue) versus $DAPK1_U$ and $p16_U$ (red) respectively. Results from 7 chips are displayed for $DAPK1$ and $p16$ assays. Methylated products are inserted in Chamber 1 and unmethylated products in Chamber 3 of the SoC. Chamber 2 was used as a negative control chemical reference.

detection using pH-LAMP. Products from Chambers 1, 2 and 3 were removed from the chip after the end of the pH based monitoring process and a gel electrophoresis was run to confirm amplification followed by quantification of the products, with the results from the real-time on-chip pH-LAMP overlapping with the results obtained from the pH-LAMP in-tube.

Chip statistics were finally performed from the real-time on-chip trials. For both assays, chips in groups of 7 were running giving us the differential voltage response as shown in Fig. 4.14. The average values of the differential signals obtained are shown in Fig. 4.15 for both $DAPK1_M/DAPK1_U$ and $p16_M/p16_U$ targeting a mean of $30mV \pm 5.25$ for $DAPK1_M$, $3.13mV \pm 1.18$ for $DAPK1_U$, $19.14mV \pm 2.91$ for $p16_M$ and $4.37mV \pm 0.6$ for $p16_U$ as stated in Table 4.9 and Table 4.10. It is clearly seen that the signal sensed by the ISFET sensors in the presence of methylated DNA is more than 5 times bigger than the signal generated by the unmethylated DNA in both cases.

Table 4.9: Average values of differential signal change, ΔV (mV), during pH-LAMP on the SoC platform (7 trials) for $DAPK1_M$ vs $DAPK1_U$ together with standard deviation values for both reaction mixtures.

Time Duration (avg)	ΔV-M	ΔV-U	std-M	std-U
4000s	30	3.13	5.25	1.18

Sensitivity of the SoC platform has been estimated to be 25mV/pH

Table 4.10: Average values of differential signal change, ΔV (mV), during pH-LAMP on the SoC platform (7 trials) for $p16_M$ vs $p16_U$ together with standard deviation values for both reaction mixtures.

Time Duration (avg)	ΔV-M	ΔV-U	std-M	std-U
4500s	19.14	4.37	2.91	0.6

Sensitivity of the SoC platform has been estimated to be 25mV/pH

4.5 Summary

This chapter presents work demonstrating that the ISFET as a pH-sensing device can be ideally used for DNA methylation detection through methylated specific pH-mediated DNA amplification under both thermocycling and isothermal conditions. To achieve this, a series of biochemical protocols were followed to naturally produce methylated/unmethylated DNA (transformation of plasmid, DNA purification, DNA quantitation) as well as to determine the presence of DNA methylation in a DNA target (pUC19) which was validated through the process of restriction enzyme cleavage. This was followed by DNA extension reactions through the method of PCR to determine the optimal temperature for primer annealing in targeted methylated areas. The final stage of DNA methylation detection was performed by using the method of pH-sensitive amplification pH-PCR, specifically optimised for the methylated state of pUC19 (dcm^+). The methylation-specific amplification, occurring as a result of a DNA extension reaction, was governed by a drop in pH, twice as much as the pH resulting from no amplification and thus no DNA extension reaction taking place in presence of unmethylated DNA, with the pH being measured by a commercially available ISFET sensor (Sentron Europe B.V.). This led to the development of the proof-of-concept approach of using commercially available ion-sensitive semiconductor technology for DNA methylation detection using the method of pH-PCR in-tube.

Moreover, the first semiconductor based label-free electrochemical approach for DNA methylation detection using CMOS based technology for two well-known tumour suppressor genes ($DAPK1$ and $p16$) was demonstrated using the method of pH-LAMP isothermal amplification. For each gene, an optimised methylation-specific biochemical platform was developed leading to pH-sensitive amplification standardised initially in-tube and then tested real-time on-chip using the fully integrated SoC platform using ISFET sensors in CMOS [1, 3]. The ability for DNA methylation detection was demonstrated, combined with sensing of the signal of DNA amplification in pH by the ISFET, generating a strong differential output signal, therefore distinguishing methylated from unmethylated DNA in each gene case.

The pH sensitivity of the assays was tested based on the occurrence of a DNA chain extension reaction happening in the presence of target sequences of methylated DNA. Initial results of pH measurements from in-tube tests were shown for 10 trials of pH-LAMP assays of both genes, exhibiting an average pH signal change of 1.91 for $DAPK1_M$ and of 1.58 for $p16_M$ achieving a very good discrimination between methylated and unmethylated DNA. The amplified methylated products of 10 pH-LAMP trials were quantified showing a good fold of amplification reaching 10^5 times the initial copy number of the starting amplicon for both assays. Following on to this proof-of-concept of methylation-specific pH-LAMP using the ISFET, results of real-time pH-LAMP on-chip from the SoC platform revealed a good differential voltage change for methylated DNA, reaching 37mV for $DAPK1$ assay and 23mV for $p16$ assay compared to no considerable differential voltage change been generated for unmethylated DNA in both assays. Finally, CMOS chip statistics for 7 dies validated the sensitivity of the real-time methylation-specific pH-LAMP on-chip, exhibiting average values of differential voltage signals for methylated DNA more than 5 times bigger than the signals coming from unmethylated DNA.

The use of the SoC platform brings real-time amplification and detection of DNA methylation into a perspective of highly multiplexed integration of multiple gene methylation-specific analysis on a single disposable silicon microchip, with the full integration of ISFET sensor arrays in CMOS combined with sophisticated microfluidics on a single platform, highlighting the potential for simultaneous DNA methylation reaction monitoring in presence of hypermethylated tumour suppressor genes directly correlated to specific tumour types. This proof-of-concept will now allow us the realisation of novel integrated systems in CMOS for DNA methylation detection.

References

[1] C. Toumazou, L. Shepherd, S. Reed, G. Chen, A. Patel, D. Garner, C.-J. Wang, C.-P. Ou, K. Amin-Desai, *et al.*, "Simultaneous DNA amplification and detection using a pH-sensing semiconductor system," *Nature Methods*, vol. 10, no. 7, pp. 641–646, 2013.

[2] C. Toumazou and P. Georgiou, "Bio-inspired semiconductors for early detection and therapy," *IEEE Asian Solid-State Circuits Conference (ASSCC)*, pp. 129–132, 2011.

[3] D. Garner, H. Bai, P. Georgiou, T. Constandinou, S. Reed, L. Shepherd, W. Wong, K. Lim, and C. Toumazou, "A multichannel DNA SoC for rapid point-of-care gene detection," *IEEE Conference on Solid-State Circuits (ISSCC)*, pp. 492–493, 2010.

[4] T. Sakurai and Y. Husimi, "Real-time monitoring of DNA polymerase reactions by a micro ISFET pH sensor," *Analytical chemistry*, vol. 64, no. 17, pp. 1996–1997, 1992.

[5] E. van Pelt-Verkuil, A. Van Belkum, and J. Hays, *Principles and technical aspects of PCR amplification*. Springer, 2008.

[6] S. Purushothaman, C. Toumazou, and C. Ou, "Protons and single nucleotide polymorphism detection: a simple use for the Ion Sensitive Field Effect Transistor," *Sensors and Actuators B: Chemical*, vol. 114, no. 2, pp. 964–968, 2006.

[7] G. Viljoen, L. Nel, and J. Crowther, *Molecular diagnostic PCR handbook*. International Atomic Energy Agency, 2005.

[8] C. Mathews, K. Van Holde, and K. Ahern, *Biochemistry 3rd ed.* Pearson Benjamin Cummings, 2000.

[9] R. Saiki, S. Scharf, F. Faloona, K. Mullis, G. Horn, H. Erlich, and N. Arnheim, "Enzymatic amplification of beta-globin genomic sequences and restriction site analysis for diagnosis of sickle cell anemia," *Science*, vol. 230, no. 4732, pp. 1350–4, 1985.

[10] K. Mullis and F. Faloona, "Specific synthesis of DNA in vitro via a polymerase-catalyzed chain reaction," *Methods in Enzymology*, vol. 155, pp. 335–350, 1987.

[11] T. Notomi, H. Okayama, H. Masubuchi, T. Yonekawa, K. Watanabe, N. Amino, and T. Hase, "Loop-mediated isothermal amplification of DNA," *Nucleic Acids Research*, vol. 28, no. 12, pp. E63–E69, 2000.

[12] C. Toumazou, S. Purushothaman, *et al.*, "Sensing apparatus and method." US Patent No. US 2010/0151479 A1, 2010.

[13] C. Toumazou, S. Purushothaman, *et al.*, "qPCR using solid-state sensing," 2011.

[14] "New England BioLabs: puC19 map." [Online]. Available: http://www.neb.com, May 2013.

[15] M. Green, J. Sambrook, and J. Sambrook, *Molecular cloning: a laboratory manual (4th ed.)*. Cold Spring Harbor Laboratory Press, 2012.

[16] "New England BioLabs: *dcm* methylases of E.coli." [Online]. Available: http://www.neb.com, May 2013.

[17] "Life Technologies: One *Shot*® *Mach*1™-*T*1®." [Online]. Available: http://products.invitrogen.com, May 2013.

[18] "New England BioLabs: dam^-/dcm^- competent E.coli." [Online]. Available: http://www.neb.com, May 2013.

[19] M. Marinus and N. Morris, "Isolation of deoxyribonucleic acid methylase mutants of Escherichia coli K-12," *Journal of Bacteriology*, vol. 114, no. 3, pp. 1143–1150, 1973.

[20] M. May and S. Hattman, "Analysis of bacteriophage deoxyribonucleic acid sequences methylated by host-and R-factor-controlled enzymes.," *Journal of Bacteriology*, vol. 123, no. 2, pp. 768–770, 1975.

[21] T. Brown, *Gene cloning and DNA analysis: an introduction*. Wiley-Blackwell, 2010.

[22] M. Altshuler, *PCR Troubleshooting: The Essential Guide*. Caister Academic Press, 2006.

[23] R. Saiki, D. Gelfand, S. Stoffel, S. Scharf, R. Higuchi, G. Horn, K. B. Mullis, and H. Erlich, "Primer-directed enzymatic amplification of DNA with a thermostable DNA polymerase," *Science*, vol. 239, no. 4839, pp. 487–491, 1988.

[24] K. Mullis *et al.*, "The unusual origin of the polymerase chain reaction," *Scientific American*, vol. 262, no. 4, pp. 56–61, 1990.

[25] "Life Technologies: $Vector\ NTI^{®}\ Software$." [Online]. http://www.invitrogen.com, June 2013.

[26] M. Innis, D. Gelfand, J. Sninsky, T. White, *et al.*, *PCR protocols: a guide to methods and applications*. Academic press, 1990.

[27] K. Jain *et al.*, "Current trends in molecular diagnostics.," *Medical device technology*, vol. 13, no. 9, p. 14, 2002.

[28] G. Lisby, "Application of nucleic acid amplification in clinical microbiology," *Molecular Biotechnology*, vol. 12, no. 1, pp. 75–99, 1999.

[29] A. Chien, D. Edgar, and J. Trela, "Deoxyribonucleic acid polymerase from the extreme thermophile Thermus aquaticus," *Journal of Bacteriology*, vol. 127, no. 3, pp. 1550–1557, 1976.

[30] S. Purushothaman, C. Toumazou, and J. Georgiou, "Towards fast solid state DNA sequencing," vol. 4, pp. 169–172, IEEE, 2002.

[31] "Restriction Mapper." [Online]. Available: http://www.restrictionmapper.org, June 2013.

[32] M. Kalofonou and C. Toumazou, "Semiconductor technology for early detection of DNA methylation for cancer: From concept to practice," *Sensors and Actuators B: Chemical*, vol. 178, pp. 572–580, 2013.

[33] F. Zerilli, C. Bonanno, E. Shehi, G. Amicarelli, D. Adlerstein, and G. Makrigiorgos, "Methylation-specific loop-mediated isothermal amplification for detecting hypermethylated DNA in simplex and multiplex formats," *Clinical Chemistry*, vol. 56, no. 8, pp. 1287–1296, 2010.

[34] "National center for biotechnology information (NCBI): $DAPK1$." [Online]. Available: http://www.ncbi.nlm.nih.gov/gene/69635, June 2013.

[35] "National center for biotechnology information (NCBI): $CDKN2A/p16\text{-}INK4\ (p16)$." [Online]. Available: http://www.ncbi.nlm.nih.gov/gene/1029, June 2013.

[36] S. Bialik and A. Kimchi, "The death-associated protein kinases: structure, function, and beyond," *The Annual Review of Biochemistry*, vol. 75, pp. 189–210, 2006.

[37] P. Cairns, "Gene methylation and early detection of genitourinary cancer: the road ahead," *Nature Reviews Cancer*, vol. 7, no. 7, pp. 531–543, 2007.

[38] M. Esteller, P. Corn, S. Baylin, and J. Herman, "A gene hypermethylation profile of human cancer," *Cancer Research*, vol. 61, no. 8, pp. 3225–3229, 2001.

[39] M. Esteller, "Epigenetics in cancer," *New England Journal of Medicine*, vol. 358, no. 11, pp. 1148–1159, 2008.

[40] P. Laird, "The power and the promise of DNA methylation markers," *Nature Reviews Cancer*, vol. 3, no. 4, pp. 253–266, 2003.

[41] J. Rocco and D. Sidransky, "p16 (MTS-1/CDKN2/INK4a) in cancer progression," *Experimental Cell Research*, vol. 264, no. 1, pp. 42–55, 2001.

[42] M. Esteller, M. Sanchez-Cespedes, R. Rosell, D. Sidransky, S. Baylin, and J. Herman, "Detection of aberrant promoter hypermethylation of tumor suppressor genes in serum DNA from non-small cell lung cancer patients," *Cancer Research*, vol. 59, no. 1, p. 67, 1999.

[43] K. Nagamine, K. Watanabe, K. Ohtsuka, T. Hase, and T. Notomi, "Loop-mediated isothermal amplification reaction using a Nondenatured template," *Clinical Chemistry*, vol. 47, no. 9, pp. 1742–1743, 2001.

[44] "New England BioLabs: *Bst* DNA Polymerase." [Online]. Available: http://www.neb.com, June 2013.

[45] N. Tomita, Y. Mori, H. Kanda, and T. Notomi, "Loop-mediated isothermal amplification (LAMP) of gene sequences and simple visual detection of products," *Nature Protocols*, vol. 3, no. 5, pp. 877–882, 2008.

Chapter 5

An analogue ratiometric method for DNA methylation detection

5.1 Introduction

The need for detection of aberrancies of DNA methylation in tumour suppressor genes, genes whose partial or complete inactivation leads to an increased likelihood of cancer development, appears to be one of the most important assays in early cancer diagnosis and so the demand for prognostic and predictive markers has been strongly desired [1, 2].

Many array based methods for DNA methylation analysis have been developed in the past at a genome-wide scale or a single-gene level, consisting of methods for chemical processing of DNA samples, identification of targeted regions followed by statistical processing algorithms, aiming to profile DNA methylation patterns as well as process DNA methylation measurements. A common sequence of events is essentially adopted to achieve that, consisting of methods that involve the collection of samples in the form of remote media i.e blood, sputum or urine followed by a sample preparation step including the purification of samples and DNA extraction. These are then followed by chemical modifications of the targeted DNA regions, with the most widely used technique, the *bisulfite conversion*, to be applied so that DNA is modified in a methylation-dependent way using primers, specific to the converted sequences. Such methylated sites can be distinguished from unmethylated ones, with methylated sites to be considered as those with more than 50% methylation existent compared to unmethylated sites as those with less than 50% methylation existent, as reported by [3]. This allows DNA methylation information to be preserved during the

sample processing steps, which is distinguishable from the rest of the highly concentrated genetic information carried in the genes and then amplified to provide a detectable signal, ready to be analysed in detail.

Several methods have been adopted for DNA methylation analysis as has been reported in Chapter 2. One of these which has been proven most important for performing a quantitative analysis on DNA methylation is the computation of ratio fractions or percentages of DNA methylation levels [4]. This can be described as:

$$\%Meth = \frac{M}{M+U} \times 100\% \tag{5.1}$$

where M stands for the signal from methylated sites and U for the signal from unmethylated sites[1]. Using this ratio we can formulate a process for detecting the level of aberrancy of DNA methylation existent in genes of interest, specifically in areas responsible for the expression of tumour suppressor genes, enabling us to determine the differences between a pathogenic gene and a healthy gene, whose under investigation genetic areas are unmethylated. This would allow the development of an early detection tool to identify early warning signs of cancer.

When implementing such a tool for a Point-of-Care (PoC) system, there is a need for an efficient low power system to detect this ratio. Conceptually, the system will be as shown in Fig. 5.1. It will include two sensors to measure methylated/unmethylated DNA and then compute the ratio between the two. If the ratio exceeds a certain percentage, it will give a YES/NO result, indicating if the under investigation genetic region is aberrantly methylated (YES) or normally unmethylated (NO). The purpose would be the detection of the methylation status of genetic sites of interest using a ratiometric approach that would be able to calculate the ratio between the methylated DNA of a gene site possibly correlated to pathogenesis and the unmethylated version of the same gene site, showing no aberrancies, therefore corresponding to the normal status of it. The detection of the level of methylation is possible with two ISFETs, one to detect methylated DNA and the other unmethylated DNA respectively.

As demonstrated in Chapter 4, the methylated and unmethylated DNA based information needed for the computation of the ratio can be obtained from the amplification of the

[1]Resulting measurements vary from 0 to 1 or 100%, where 0 indicates that no methylated sites have been identified while 1 or 100% indicates that all identified sites are methylated.

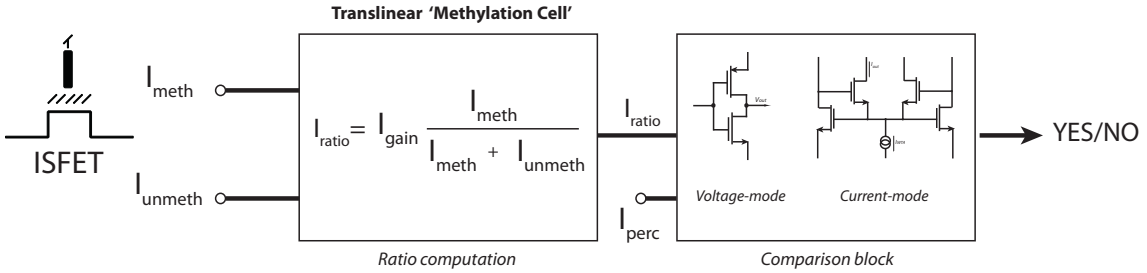


Figure 5.1: System level block diagram of the ratiometric computation method towards the detection of DNA methylation

methylated/unmethylated region of the DNA sample through a hydrolysis reaction, detecting the production of hydrogen ions, which will cause a change in pH as described by the reaction:

$$dNTP + DNA_n \rightarrow PP_i + DNA_{n+1} + Mg_2 + H^+ \tag{5.2}$$

releasing pyrophosphate and hydrogen ions in the presence of a DNA polymerase enzyme, as described in Section 4.2, Chapter 4. For the purpose of DNA methylation detection, a single-stranded methylation-specific DNA probe can be designed to identify a methylated site of the DNA target and distinguish it from the equivalent unmethylated one. Hydrogen ions will therefore be released in solution, resulting to a pH drop as a result of DNA amplification taking place when the targeted genetic region containing methylated DNA is detected, using the methylation-specific primers annealing only the complementary methylated regions in the under investigation gene. This could then allow the implementation of the ratio using an electronic circuit.

What is required for a Point-of-Care system is circuits capable of continuous calculation of the methylated/unmethylated DNA ratio, giving a discrete output signal when methylation reaches and exceeds a certain predefined percentage. Additionally, the percentage threshold should be tunable to the given reaction, operating in low power. A circuit technique that could allow this by performing division and multiplication of current signals needed for the ratiometric computation is the "translinear principle".

This chapter presents a hardware efficient system that can compute the ratio of DNA methylation. Termed the "Methylation Cell", it utilises the translinear principle to implement the system shown in Fig. 5.1. It is able to measure the signal from a DNA extension

reaction taking place due to the presence of methylated DNA sensed by a CMOS based ISFET sensor ($ISFET_{X1}$), compared to a no reaction signal sensed or measured by an ISFET in a separate reaction chamber ($ISFET_{X2}$). This is followed by a comparison block that would provide two alternative ways (voltage-mode or current-mode) to get a binary answer (YES/NO) based on an applied threshold given the result of the reaction or the value of the ratio calculated from the "Methylation Cell". The contents of each block and the cell's ability to compute the ratio and to distinguish methylated from unmethylated DNA sites using the translinear principle shall now be described.

5.2 The translinear principle

In electronics, a very convenient way of conducting multiplication or division of current signals derived from transistors in saturation is by using circuits that exploit the exponential current-voltage characteristic of the devices through a process which is known as the "translinear principle" [5–8].

The term *translinear* was originally suggested by Barrie Gilbert in 1975 for bipolar transistors (BJT), based on the fact that their transconductance is linearly proportional to the collector current of a BJT so as to aim for "fundamentally exact, temperature-insensitive algebraic transformations" [5]. Not until the early 1990s, did Gilbert distinguish the use of translinear circuits for general application purposes based on the original definition, from circuits whereby both inputs and outputs are in the current domain, enclosing one or more closed translinear loops, therefore offering an effective way for building current-mode circuits and systems with small voltage variations [6].

The translinear circuit principle was extended for implementation by MOS transistors operating in strong inversion in 1991 by [7] followed by [8] to weakly inverted MOS transistors, exploiting the exponential relationship between current and voltage in this region. The principle of operation can be described by considering diodes connected in a loop, Fig. 5.2, whereby each diode represents the V_{GS} of a MOS transistor in weak inversion. These can form single or multiple loops whereby the number of transistors arranged clockwise equals to the number of transistors arranged counterclockwise, with the loop containing an even number of devices [5, 7]. Applying Kirchhoff's voltage law, the gate-source voltages of the MOS transistors around the loop now follow the expression [7]:

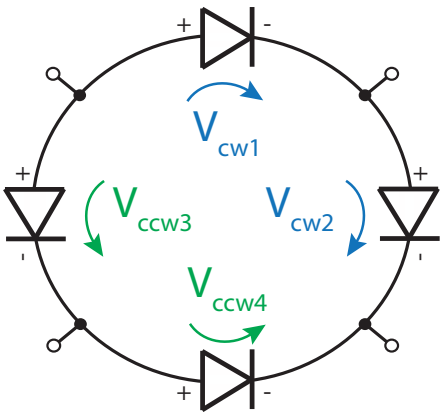


Figure 5.2: Translinear loop consisted of four diodes

$$\sum_{CW} V_{GS} = \sum_{CCW} V_{GS} \tag{5.3}$$

where CW and CCW stand for clockwise and counterclockwise connected MOS transistors respectively. This is more clearly illustrated in Fig. 5.2 whereby the V_{GS} drop of the MOS transistors is represented by the voltage across a forward biased diode which also follows an exponential relationship. A closed loop is then formed where the summation of the V_{GS} of the devices connected clockwise equals to the summation of the V_{GS} of the devices connected counterclockwise:

$$V_{CW1} + V_{CW2} = V_{CCW3} + V_{CCW4} \tag{5.4}$$

Given that V_{GS} expressed as:

$$V_{GS} = nU_t log\frac{I_{DS}}{I_o} \tag{5.5}$$

is logarithmically related to the devices drain-source current, I_{DS}, the addition of V_{GS} leads to products of currents through the addition of logarithms, which leads to a relationship between the current densities (current/area) in the clockwise direction, being also equal to the current densities in the counterclockwise direction [5, 8]:

$$\prod_{CW} current\ density = \prod_{CCW} current\ density \tag{5.6}$$

If we now replace the diode connected voltages or the gate-source voltages of the weakly inverted MOS transistors with their respective drain currents, I_D, which are expressed by [9]:

$$I_D = I_o S e^{\frac{V_{GS}}{nU_t}} e^{\frac{(n-1)V_{BS}}{nU_t}} \tag{5.7}$$

where I_o is a characteristic current, $S = W/L$ is the size of the transistors, V_{GS} is the voltage between the gate and the source, n is the subthreshold slope coefficient, V_{BS} is the voltage between the bulk and the source and U_t is the thermal voltage, then the summation of voltages of Eq. 5.4 will be transformed into a summation of natural logs of currents:

$$ln\frac{I_{D_{CW1}}}{I_o} + ln\frac{I_{D_{CW2}}}{I_o} = ln\frac{I_{D_{CCW3}}}{I_o} + ln\frac{I_{D_{CCW4}}}{I_o} \tag{5.8}$$

where each current represents the drain current of the MOS transistor in the translinear loop. The addition of natural logs will then be expressed as the multiplication of currents:

$$I_{D_{CW1}} I_{D_{CW2}} = I_{D_{CCW3}} I_{D_{CCW4}} \tag{5.9}$$

which may represent the inputs and outputs of the translinear circuit.

Research has shown that the translinear principle can be applied with ISFETs in weak inversion, thus having a direct application in the field of biomedical engineering [10, 11], facilitating its use in calculating ratios from biochemical input signals using low power current-mode methods. The investigation of using the translinear principle in designing relevant circuits to detect biochemical signals from DNA methylation related reactions follows in the next section.

5.2.1 The translinear "Methylation Cell"

The translinear "Methylation Cell" shown in Fig. 5.3, as has been first introduced by [12], is an ISFET based translinear cell, capable of computing the ratio between the output

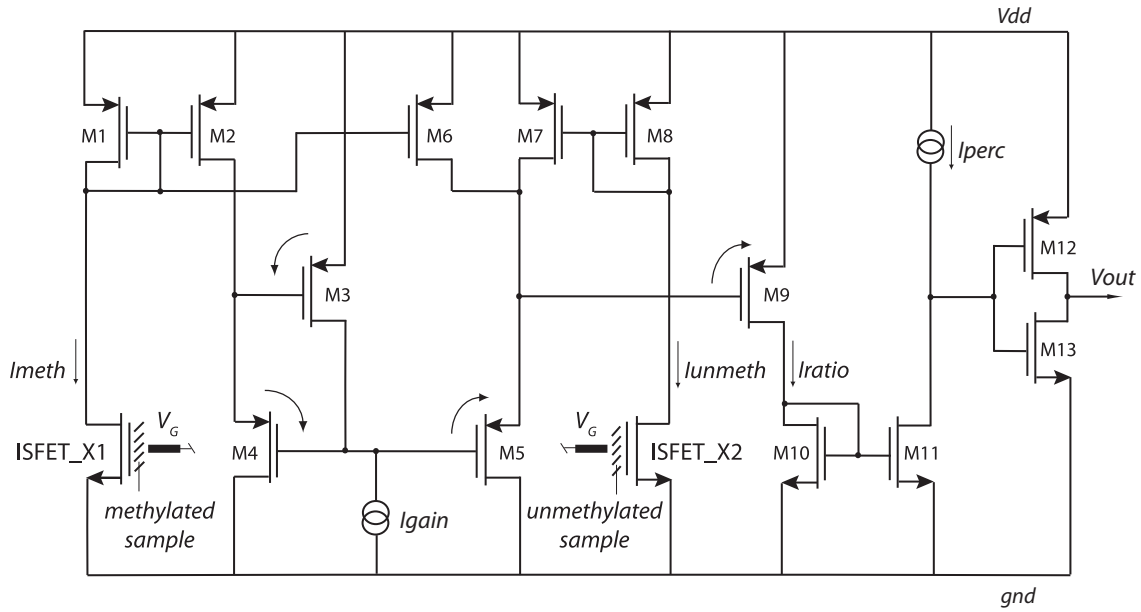


Figure 5.3: ISFET based translinear current divider using voltage-mode switching

currents of two ISFET sensors, X1 and X2, implementing the function of the system shown in Fig. 5.1.

Signals obtained due to the presence of aberrantly methylated tumour suppressor genes are sensed by the first ISFET sensor, $X1$ and signals representing the unmethylated version of the same gene derived from a healthy control are sensed by the second ISFET sensor, $X2$. The signal from $X1$ is then compared to the one from $X2$ and a ratio is computed, expressed as an output current, I_{ratio}, formulating a process of using the ISFET to sense and indicate the level of aberrancy of methylation existent in tumour suppressor genes, directly correlated with early stages of tumour development. Moreover, a reference current, I_{perc}, is used to set a threshold with which I_{ratio} will be compared to, to give a binary answer when methylation exceeds a predetermined percentage. This is implemented using a current comparator consisting of a current mirror, a reference current source and a CMOS inverter, as can be seen in Fig. 5.3.

The theory behind the operation of the translinear "Methylation Cell" is primarily based on the principles of the ISFET's operation, as has been described in Chapter 3. In principle, the ISFET transduces a chemical signal to electrical to give a drain current dependent on the ionic concentration of the under test solution, while offering an exponential relationship to pH. The generalised drain current, I_D, of the ISFET sensors is expressed by:

$$I_D = I_o e^{\frac{V_{GS}}{nU_t}} K_{chem}[H+]^{\frac{a}{n}} \tag{5.10}$$

whereby I_o stands for the intrinsic current in the device, V_{GS} is the voltage between the gate and the source, n is the subthreshold slope coefficient and U_t is the thermal voltage, kT/q, with k the Boltzmann constant, T the absolute temperature and q the electronic charge. Finally, K_{chem} is a grouping of constant chemical potentials, a is the sensitivity parameter for the sensed ions, both of which are temperature independent and $[H+]$ is the concentration of hydrogen ions in solution.

For the case of methylated and unmethylated DNA, the drain currents, I_D, of the ISFET devices generated in the presence of methylated DNA (X1=meth) and unmethylated DNA (X2=unmeth) are defined as I_{meth} and I_{unmeth} respectively:

$$I_{meth(X1)} = I_o e^{\frac{V_{GS}}{nU_t}} K_{meth}[meth]^{\frac{a_{meth}}{n}} \tag{5.11}$$

and

$$I_{unmeth(X2)} = I_o e^{\frac{V_{GS}}{nU_t}} K_{unmeth}[unmeth]^{\frac{a_{unmeth}}{n}} \tag{5.12}$$

The rest of the system is composed of an ISFET based translinear cell (M3, M4, M5, M9) capable of computing the division between the drain currents, I_{meth} and I_{unmeth}. Current mirrors (M1-M2-M6, M7-M8) are used to input sensor currents I_{meth} and I_{meth}+I_{unmeth} into the translinear loop in a way such that the ratio can be calculated.

We can see how the ratio is calculated by performing a KVL on the loop indicated by the arrows of Fig. 5.3 on devices M3, M4, M5, M9:

$$V_{GS3} + V_{GS4} = V_{GS5} + V_{GS9} \tag{5.13}$$

and after substituting for the weak inversion drain current and dividing by nU_t we have:

$$ln\frac{I_{gain}}{I_o} + ln\frac{I_{meth}}{I_o} = ln\frac{I_{meth} + I_{unmeth}}{I_o} + ln\frac{I_{ratio}}{I_o} \tag{5.14}$$

By using the basic relation of adding natural logs we get the final expression for the computation of the ratio between methylated and unmethylated DNA represented by I_{ratio}:

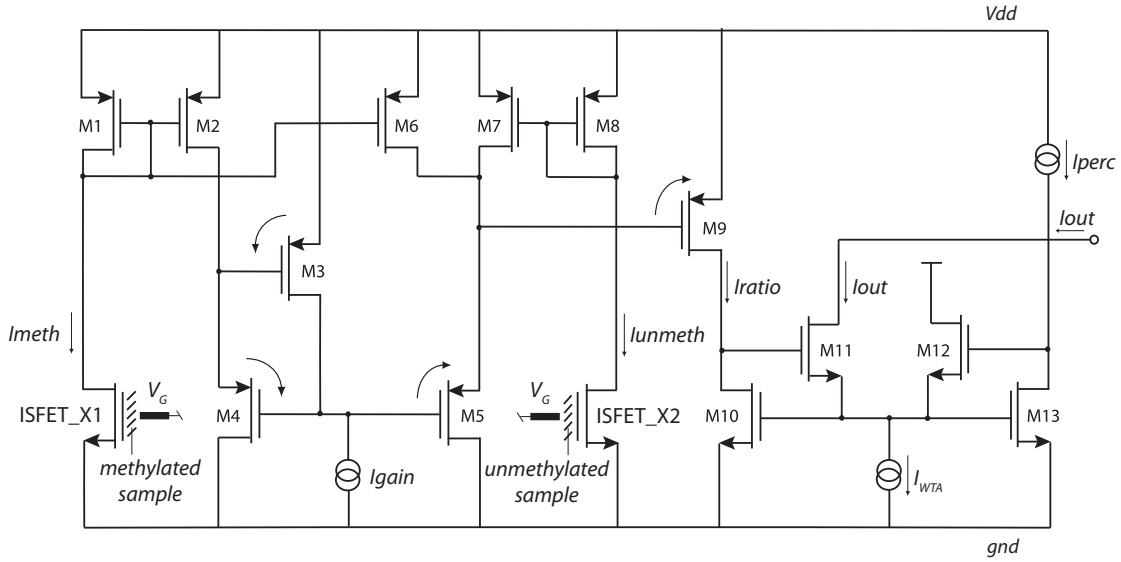


Figure 5.4: ISFET based translinear current divider using current-mode switching

$$I_{ratio} = I_{gain} \frac{I_{meth}}{I_{meth} + I_{unmeth}} \tag{5.15}$$

whereby I_{gain} is a pre-defined gain term for the ratio computation and I_{ratio} is the output ratio current. With this calculation, the ratio derived from the "Methylation Cell" can now be compared to a threshold value set by I_{perc} showing if it has passed a preset tunable value.

To implement the comparison block which would allow us to compare I_{ratio} with a defined percentage value, I_{perc}, we consider two approaches. These consist (a) of a voltage-mode switching configuration, as shown in Fig. 5.3, which uses a CMOS inverter (M12, M13) leading to a voltage output V_{out}, whereby a logic decision (YES/NO) is based on a voltage output signal and (b) of a current-mode switching configuration, as shown in Fig. 5.4, using a winner-take-all (WTA) circuit for a current comparator (M10, M11, M12, M13), providing a current output I_{out} and so a logic decision (YES/NO) based on a current output signal. In voltage-mode switching, the CMOS inverter is switched at a cut-off point according to the relationship shown in Table 5.1, giving V_{out}=3.3V when I_{ratio} exceeds I_{perc}, whereas in current-mode switching, the WTA comparator causes switching of the output current giving I_{out}=1μA when I_{ratio} exceeds I_{perc}.

Table 5.1: Cut-off point of the CMOS inverter and voltage/current output of the translinear cell

$I_{ratio} : I_{perc}$	$Logic$	V_{out}	I_{out}
≥ 1	1	3.3V	1μA
< 1	0	0	0

- *Voltage-out operation*:

  In the case of the voltage-mode switching, an increase in $[H]^+$ percentage will lead to an increase in I_{meth} and thus in I_{ratio}, resulting in a discharge of the parasitic capacitance on the input node of the CMOS inverter when the current exceeds the current I_{perc} used to set the threshold. This will in turn cause the voltage output, V_{out}, to go high giving a discrete indication of a YES/NO answer.

- *Current-out operation*:

  Similarly, for the current-mode switching, when an increase in I_{ratio} exceeds a value of a preset current, I_{perc}, the output current of the comparator, I_{out}, is activated by the winner-take-all (WTA) regulator to give a discrete logic decision (YES/NO) based on current determined by I_{wta}.

The current comparison offered by the 'comparison block' can now be used to distinguish the critical ratio values from the normal ones, for given genetic regions of investigation. Consequently, this implementation of the ratio of methylation derived from Eq. 5.15 would be an indication of the level of aberrancy of methylation existent in tumour suppressor genes of interest, therefore defining an epidemiological factor based on the disruption of normality of the function of such genes correlated with the level of methylation accordingly.

5.3 Simulation results

The translinear "Methylation Cell" was designed in a typical 0.35μm 2P4M CMOS technology using Cadence Spectre (5.1.41isr2) simulator. The design specifications were, a supply voltage of 3.3V and device sizes optimised at (W/L) 10μm/10μm for all transistors so that matching errors were minimised and 1/f noise was reduced in weak inversion.

The translinear "Methylation Cell" characteristics using the voltage-mode switching comparator were initially tested by applying current values to the current inputs based on the expected ISFET drain current range for the given device operating dimensions in weak inversion [13]. The ratio computation was tested by applying a current ramp starting from 1nA as the methylated DNA input, I_{meth}, and a current source of 10nA, used to simulate the unmethylated DNA input, I_{unmeth}. This selection was made to emulate the scenario of a reaction taking place due to the presence of methylated DNA, monitored as a change in I_{meth}, while a steady signal is monitored by I_{unmeth} due to the absence of methylated DNA or presence of unmethylated DNA.

For the computation of I_{ratio}, the fixed gain term I_{gain} was set at 10nA in order for a range of 0-100% to be mapped to I_{ratio}=0-10nA, whereby no methylation present would indicate 0% $\approx$ 0nA or methylation at full coverage of the gene site would indicate 100%, 10nA. Also, I_{perc} was set at 5nA so that the limit of detection was fixed at 50% based on the definition of methylated sites given in Section 5.1. The results of the simulated computation of I_{ratio} are shown in Fig. 5.5 with the voltage-mode current comparator to be switched through the use of the CMOS inverter. For a value of I_{ratio} being above a desired threshold, set by I_{perc}, the discrete voltage output V_{out} of the inverter is interpreted as a logic YES/NO decision, which in this case means that the voltage output V_{out} of the comparator will switch from 0V to 3.3V, when the level of methylation exceeds 50%, as shown in Fig. 5.5 when I_{ratio}=5nA.

Furthermore, the "Methylation Cell" was simulated for varying incremental percentage changes in the reference current, I_{perc}, to demonstrate the effect of tunability on I_{ratio} and the voltage-mode switching of V_{out} for different percentages of methylation. Starting from 0%, the threshold levels increased to 20, 40, 60 and 80% respectively in order for the transient response of the "Methylation Cell" to be monitored towards the maximum I_{ratio} that the cell could achieve. The results of the transient response of the "Methylation Cell" are shown in Fig. 5.6, illustrating the capability of the comparator of the translinear circuit to compare I_{ratio} to I_{perc} and thus to switch at a current level as has been set by the percentage increase.

Additional simulations of the translinear "Methylation Cell" using the current-mode switching comparator, Fig. 5.4, were conducted, as shown in Fig. 5.7. A current ramp of 1nA to 100nA was applied as the methylated DNA input, I_{meth} while I_{unmeth} remained fixed at a value defined by a current source of 20nA. I_{gain} and I_{perc} were set at 20nA and

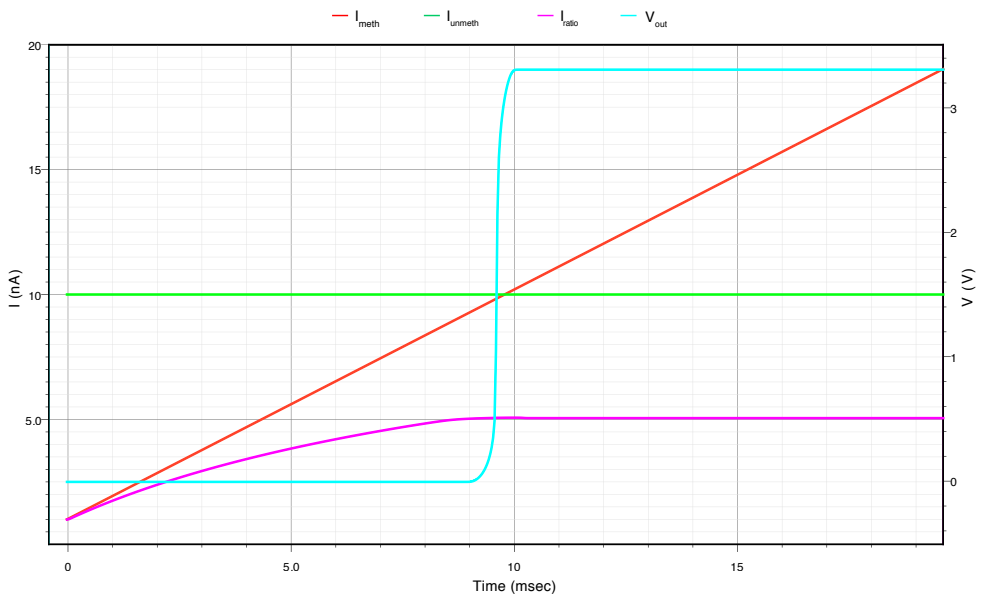


Figure 5.5: Transient response of the translinear "Methylation Cell" with voltage-mode switching

15nA respectively. As I_{meth} is increasing, I_{ratio} is being computed and once a threshold is reached, defined by I_{perc}, I_{out} switches from 0-I_{wta} indicating a YES/NO answer.

5.4 Fabricated system

The "Methylation Cell" was fabricated, as seen in Fig. 5.8 (bottom), with each ISFET sensor designed[2] with a sensing area of 34μm×100μm and an electrical area of 200μm×1μm, as shown in Fig. 5.9. The area covered by circuit was 7725μm^2 (309μm×25μm).

The fabricated system was encapsulated using a standard epoxy encapsulation procedure, described in Appendix F, with the experimental set-up used for the electrical characterisation of the ISFETs and the common pH buffer solution tests shown in Fig. C.1 and Fig. C.2, Appendix C. In parallel, a microfluidic assembly in a Lab-on-Chip set-up involving two isolated chambers, as seen in Fig. 5.10, was used, adapted on the ISFET based CMOS microchip, with the set-up for electrical characterisation of ISFETs using such configuration as shown in Fig. C.3, Appendix C.

[2]ISFET sensors were designed based on measured devices fabricated within the Centre for Bio-Inspired Technology [14].

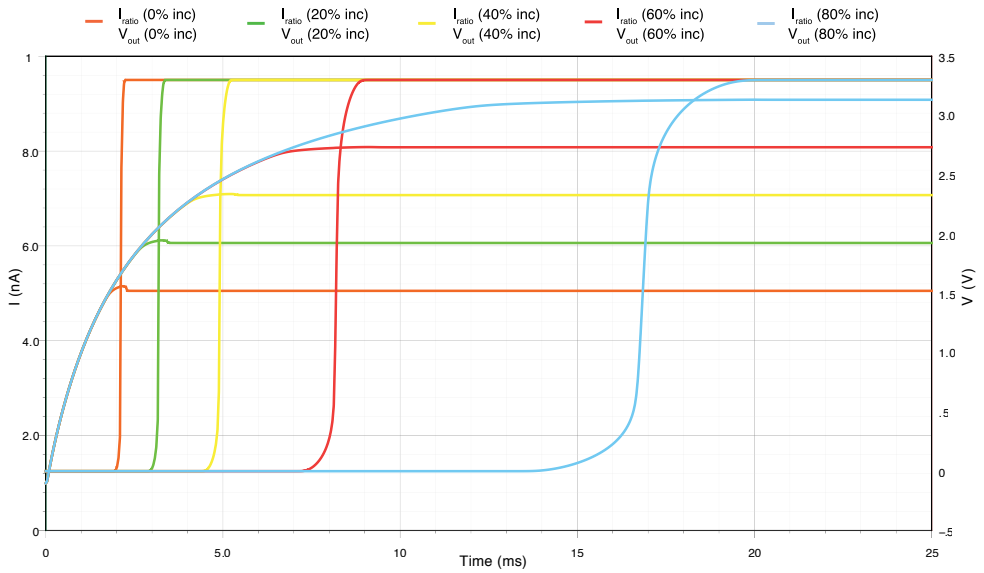


Figure 5.6: Translinear circuit voltage-mode switching at different incremental percentages of I_{perc}

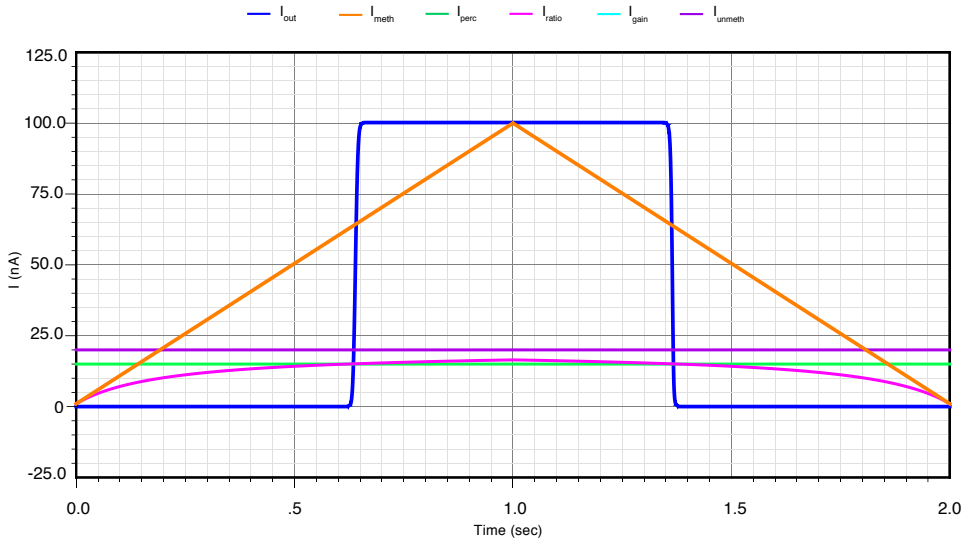


Figure 5.7: Transient response of the translinear "Methylation Cell" with current-mode switching

The latter set-up was used to expose the ISFET sensors to separate solutions for real-time monitoring of reactions occurring in isolated chambers. This intends to facilitate the isolation of a signal monitored from a reaction taking place in one chamber due to the presence of methylated DNA, compared to no reaction occurring in the twin chamber, due to

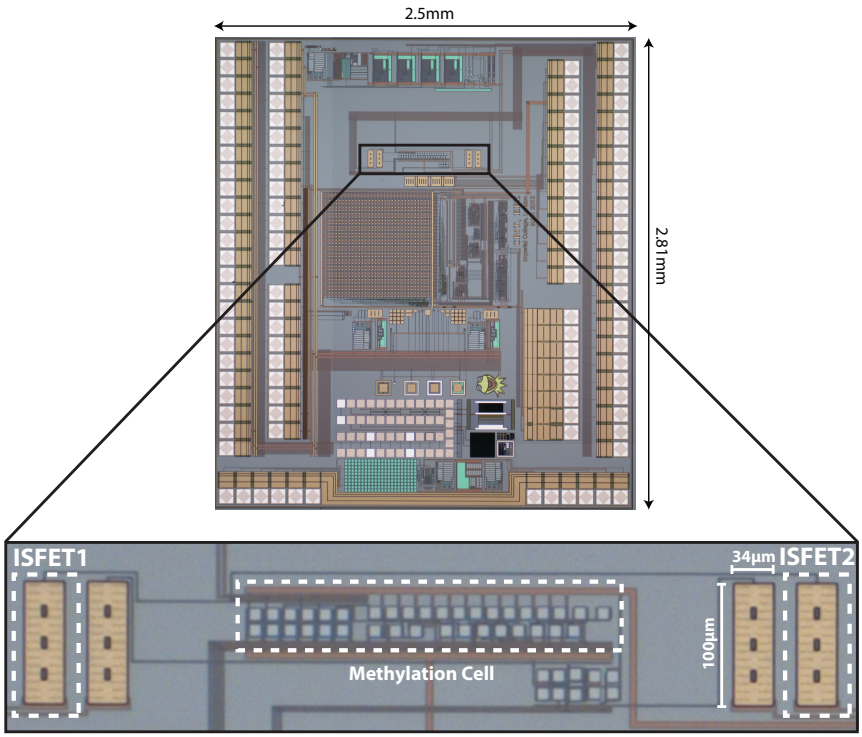


Figure 5.8: Top: Microphotograph of the floorplan of the fabricated die, highlighting in black the relevant circuit area. Bottom: Magnification of the "Methylation Cell" and of the two ISFETs connected to it.

the absence of methylated DNA. The platform was also used to prevent cross contamination of fluid through the chambers, offering a more accurate signal derived from the "Methylation Cell".

Both ISFETs were spaced at 500μm from each other to allow ease of integration with a microfluidic device mounted on top of the silicon microchip, Fig. 5.10a, consisting of two microchambers, 400μm in diameter, both of a size of 1mm$\times$0.4mm$\times$0.4mm. The sensing area exposing the ISFETs was defined by the maximum volume of fluid inserted in both micro-chambers, which was reaching 0.3μl. To define the potential of the electrolyte solution inserted in the micro-chambers, an Ag/AgCl reference electrode was inserted, passing through both chambers, Fig. 5.10b, biasing the ISFETs, shown in chambers on Fig. 5.10c, in the weak inversion region of operation.

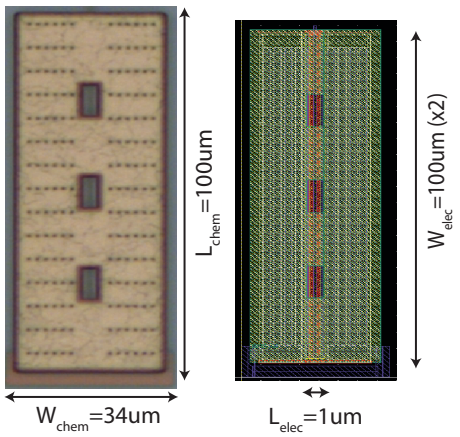


Figure 5.9: Single ISFET sensor with pixel dimensions. Left: Chemical sensing area of the ISFET. Right: Electrical dimensions of the gate.

5.5 Measured results

Measured results were obtained using (a) an epoxy encapsulation set-up and (b) a microfluidic manifold Lab-on-Chip set-up. Epoxy encapsulation was initially used to test the functionality of the electronics and the ISFET sensors in the bucket solutions followed by the development of a microfluidic manifold to allow in parallel pH sensing using two chambers with separable pH.

The Lab-on-Chip was experimentally tested using a semiconductor parameter analyser (Keithley 4200SCS). During all experiments the system was biased at 3.3V and ISFET currents were biased at a current optimised for weak inversion operation. The ability of the translinear "Methylation Cell" to perform the computation of ratio in buffer solutions of pH 5-9 was tested as well as during a pH jump between 8.8 and 6.8, indicating the maximum pH difference that a DNA reaction can produce when DNA methylation is present, shown by the biochemical reactions produced in Section 4.4, Chapter 4.

pH buffer solutions 5, 6, 7, 8 and 9 were prepared using 100mM Tricine and 1M KCl, adjusting the pH using 10M NaOH and 1M HCl. All four solutions were provided by Sigma-Aldrich. A commercially available Al_2O_3 ISFET sensor with an Ag/AgCl reference electrode was also used as a pH probe (Sentron Europe B.V.) for conducting the pH measurements after having completed a calibration process as described in Appendix C. The pH solutions were titrated in the microfluidic chambers using 20μl Eppendorf micropipette tips.

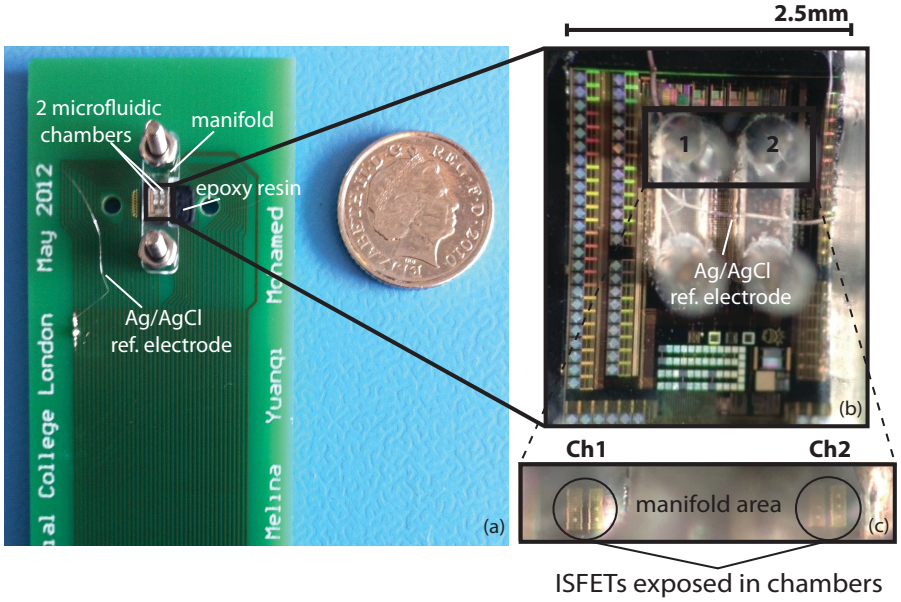


Figure 5.10: (a) ISFET based CMOS microchip mounted and encapsulated on pcb with microfluidic assembly adapted on top. (b) Magnification of the manifold and the two microfluidic chambers. An Ag/AgCl reference electrode is passing through the chambers, creating a stable potential to the solution added in chambers. (c) ISFETs visible in both chambers integrated in the manifold area. The two chambers were spaced at 300μm from each other.

Experimental results are presented in this section and demonstrate the electrical functionality of the ISFETs in weak inversion as well as their sensitivity under different pH solutions. The capability of the "Methylation Cell" using a common pH buffer solution is also proven through a detailed experimental analysis on the computation of I_{ratio} and the comparator's switching mechanism through various pH steps.

5.5.1 Measured results using epoxy encapsulation

The initial experimental set-up to test the response of the "Methylation Cell", involved the ISFET based CMOS chip covered with epoxy, mounted on pcb with ISFETs exposed in a common pH buffer solution. The experimental setup is shown in more detail in Fig. C.1 and Fig. C.2, Appendix C. A fixed potential to the solution was set through the use of a glass Ag/AgCl reference electrode (Sentron Europe B.V.), which was also used to set the operating point of the ISFET, by applying a suitable bias for the individual devices.

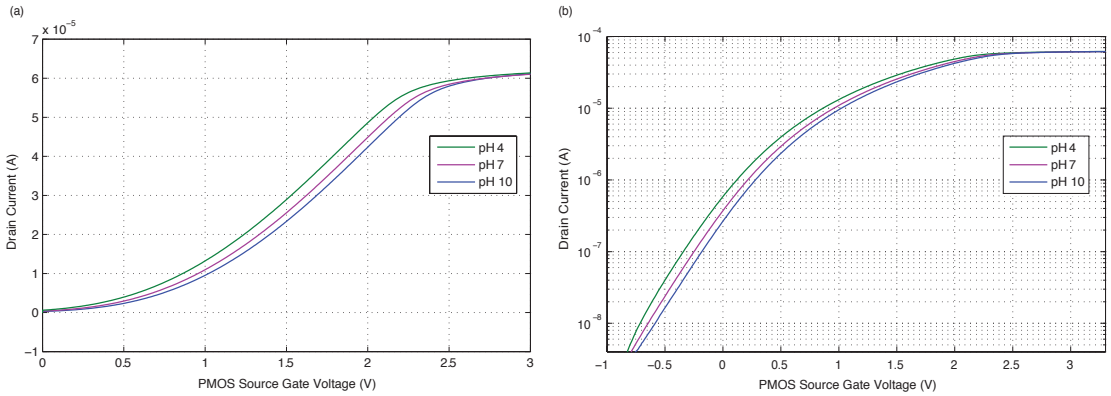


Figure 5.11: Measured I_D-V_{GS} sweep of a pMOS ISFET for pH buffer solutions of 4, 7 and 10 showing the relationship between the drain current, the source gate voltage and the shift in the threshold voltage for strong inversion (left) and weak inversion (right).

- *pH sensitivity*:

  The DC characteristics of the ISFETs were observed through the I_D-V_{GS} measurements, as displayed in Fig. 5.11, which were conducted at three different pH values (pH 4, 7 and 10) and at room temperature. The ISFET sources were biased externally and independently at 3.3V and the reference electrode's voltage was swept from 0V to 3V. The y-axis shows the drain current of the ISFET and the x-axis the gate voltage subtracted from the source voltage (V_{GS}) of the ISFETs. I_D-V_{GS} characteristics were generated for both strong inversion, Fig. 5.11 (left) and weak inversion Fig. 5.11 (right), whereby the weak inversion linear region of the drain current can be observed, for a source gate voltage spreading for approximately 500mV for all pH values. Moreover, a shift in the characteristic of 90mV due to a change in the threshold voltage is observed as the pH buffer becomes less acidic, which by relative calculations shows a sensitivity of 30mV/pH, which is in line with ISFETs fabricated in unmodified CMOS [14]:

$$S_{ISFET} = \frac{\Delta V_{GS}}{\Delta pH} = \frac{0.09}{3} V/pH = 30mV/pH \tag{5.16}$$

- *Computation of ratio*:

  After confirming the pH sensitivity of the ISFET and its ability to show a good linearity in weak inversion, the ability of the translinear "Methylation Cell" and specifically of the translinear circuit to compute the ratio, Eq. 5.15, was tested.

- I_{ratio} *vs* I_{meth} for fixed I_{gain} and I_{unmeth}:
  The ratiometric computation of the translinear cell was tested initially in a buffer solution of pH 7. The ISFETs source voltages were set at 2V and the voltage of the Ag/AgCl reference electrode was set at 1.8V, establishing a V_{GS}=200mV. The output current of the translinear circuit, I_{ratio}, was measured by initially applying electrically incremental and decremental steps in I_{meth} by changing V_{GS}, while leaving I_{unmeth} constant for a fixed I_{gain} of 50nA, as seen in Fig. 5.12a, with the absolute values of the output ratio current I_{ratio} changing as the ratio is computed, shown in Fig. 5.12c. The steps resulting in increasing or decreasing the currents were applied by inducing a 50mV change to the ISFET sources related to I_{meth} and I_{unmeth}.
- I_{ratio} *vs* I_{unmeth} for fixed I_{gain} and I_{meth}:
  Alternatively, the same procedure was followed by applying changes to I_{unmeth} while leaving I_{meth} constant for the same value of I_{gain} as used previously, shown in Fig. 5.12b, resulting in absolute changes in I_{ratio} accordingly, shown in Fig. 5.12d.

For the experiments illustrated in Fig. 5.12a and Fig. 5.12b, it can be observed that I_{meth} in Fig. 5.12a was drifting less than I_{unmeth} in Fig. 5.12a, something that can be portrayed in the respective current output changes of Fig. 5.12c and Fig. 5.12d. However, what can be seen from both is that the output of the cell computing the ratio of the input currents of the ISFETs, I_{meth} and I_{unmeth}, given a fixed I_{gain} of 50nA was experimentally validated.

Fig. 5.13 shows more clearly how I_{ratio} was following the changes in I_{meth} and I_{unmeth} during the increasing and decreasing values of the respective ISFET currents in a buffer solution of pH 7. Fig. 5.13a shows the relationship between I_{ratio} and I_{meth} and Fig. 5.13b shows the relationship between I_{ratio} and I_{unmeth}. The values of I_{ratio} for different I_{meth} points during six incremental steps for a constant I_{unmeth} are shown in Table 5.2. Similarly, the values of I_{ratio} for different I_{unmeth} points during four decremental steps are shown in Table 5.3, taking into account that the constant values of I_{meth} and I_{unmeth} respectively followed different drift trends as shown in Fig. 5.12.

- I_{ratio} *vs* I_{gain} for fixed I_{meth} and I_{unmeth}:
  The dependence of I_{ratio} to I_{gain} was also tested for a constant value of I_{meth} and I_{unmeth} set at 100nA, as can be seen in Fig. 5.14, in a buffer solution of pH 7. I_{gain}

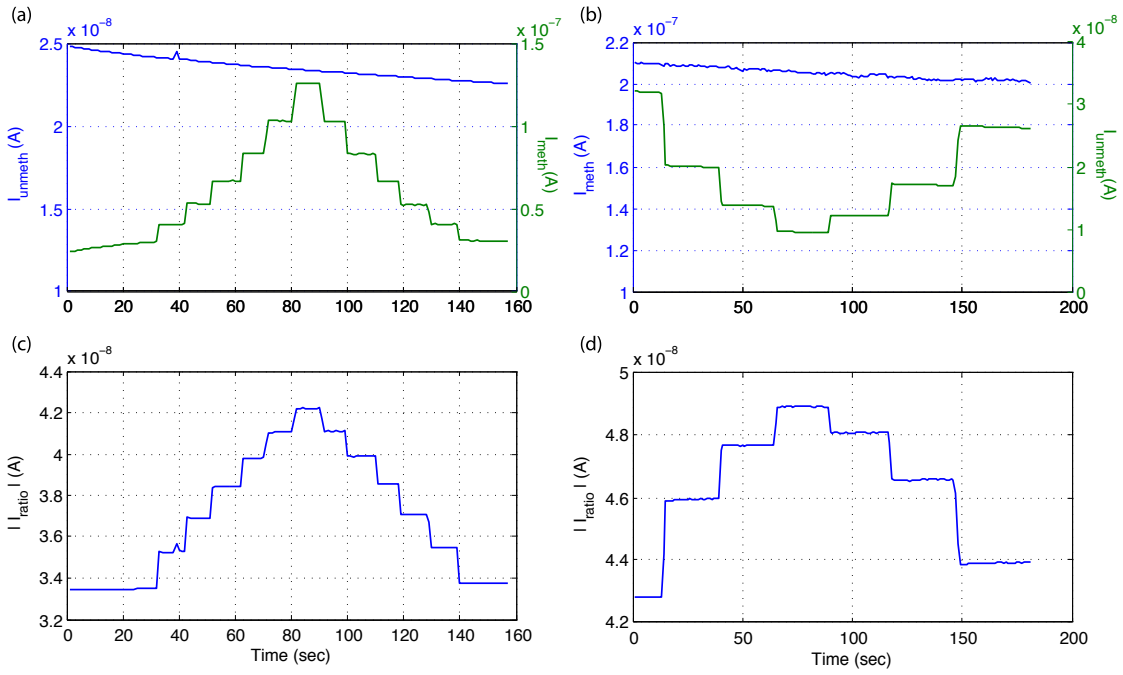


Figure 5.12: Measured transient response of the "Methylation Cell": shown are (a) variations in I_{meth} for constant I_{unmeth} resulting in I_{ratio} in (c) and (b) variations in I_{unmeth} for constant I_{meth} resulting in I_{ratio} in (d).

Table 5.2: I_{ratio} for different I_{meth} values and I_{unmeth}=23.59±0.63(nA)

I_{meth}(nA)	28.8	40.62	52.85	67.06	84.08	103.6
I_{ratio}(nA)	33.47	35.28	36.90	38.43	39.8	41.07

Table 5.3: I_{ratio} for different I_{unmeth} values and Imeth=18.14±2.75(nA)

I_{unmeth}(nA)	31.91	19.98	13.76	9.54
I_{ratio}(nA)	42.82	45.95	47.67	48.94

values varied from 20nA to 200nA. I_{meth} and I_{unmeth} were chosen at such value given the information obtained from the I_D-V_{GS} characteristics for both ISFETs in weak inversion, as seen in Fig. 5.11. It can be seen that there is a linear relationship between I_{ratio} and I_{gain}, as expected from Eq. 5.15 of I_{ratio}, which is determined by the

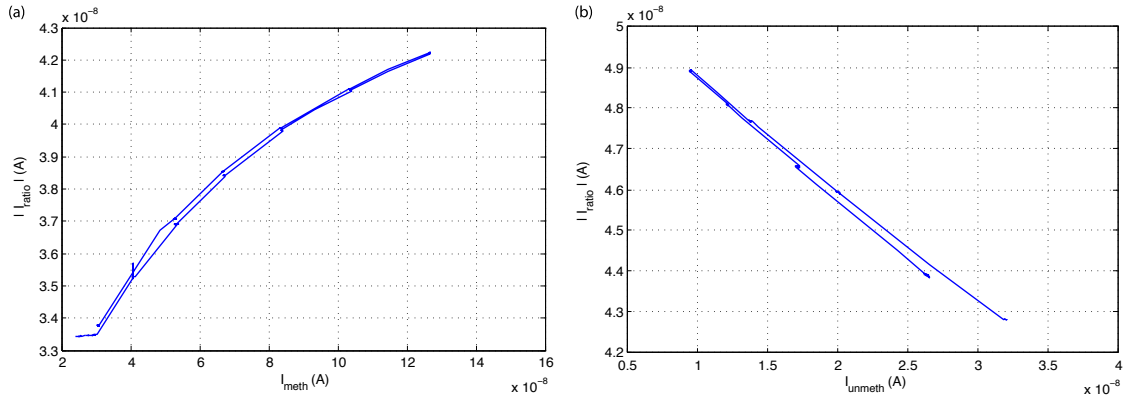


Figure 5.13: Transient response of the "Methylation Cell" illustrating the current loops between I_{ratio} and I_{meth} in (a) and between I_{ratio} and I_{unmeth} in (b) during increasing and decreasing values of I_{meth} and I_{unmeth} as shown in Fig. 5.12.

translinear principle. The value of 100nA was chosen as a DC bias for both ISFETs, which achieves the most linear operation of the translinear circuit and contributes in producing the most noticeable and closest to the theoretical value current of I_{ratio} for a given I_{gain} of 100nA for one pH step, demonstrating the best operation of the "Methylation Cell" with a minimum offset of recordings. Shown in Fig. 5.14 is a result of 50% (50nA) when all currents are equal.

The ability of the current comparator to compare I_{ratio} with a current threshold set by I_{perc} was tested, by emulating a 1 pH change scenario by applying a change of 50mV in the V_{GS} of the ISFETs. For the voltage-mode switching circuit, Fig. 5.3, the experimental analysis on the switching effect of the CMOS inverter included in Section G.2.1, Appendix G, showed that certain limitations may have arisen such as delays in the discharge time of the inverter's node producing a less accurate response. For this reason, the current-mode switching of the circuit of Fig. 5.4 was used for a more detailed analysis on the response of the comparator.

To investigate the performance of the current-mode comparator, an initial experiment was conducted to see how the output of the comparator, I_{out}, can change as I_{ratio} increases. The voltage bias for measuring I_{out} and I_{ratio} was set at 2V to allow the output devices to be in saturation and the current bias for I_{wta} was set at 1μA for good output drive strength. The reference electrode voltage was set to 1.8V. What can be seen in Fig. 5.15 is that I_{out} switches from 0μA to 1μA when the reaction of I_{ratio} increases above 50nA, with I_{perc} set

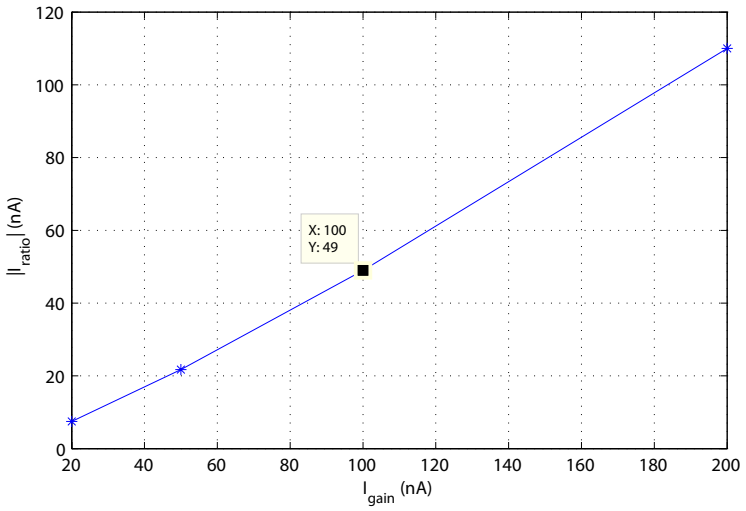


Figure 5.14: Measured response of I_{ratio} for varying values of I_{gain} while both I_{meth} and I_{unmeth} are set at 100nA.

at 50nA and I_{gain}=50nA. Specifically for the case of I_{meth} and I_{unmeth}, with drain currents of both ISFETs set at 100nA and I_{gain}=100nA, we can see in Fig. 5.16 that an incremental change of 1 pH causes I_{ratio} to change from 49nA to 59nA. From this, we deduce that to best demonstrate the functionality of the circuit for 1 pH change, we can set I_{perc}=56nA which will cause I_{out} to switch.

The information collected from the experimental performance of the "Methylation Cell" when epoxy encapsulation was selected was taken into account so that the best performance characteristics of the translinear circuit were to be used under the Lab-on-Chip set-up.

5.5.2 Measured results on Lab-on-Chip set-up

Based on the Lab-on-Chip set-up, Fig. 5.10 (assembly detailed in Section 5.4), the response of the "Methylation Cell" was tested using retrospective data from the biochemical experiments analysed in Chapter 4. This means that a methylation reaction is to be represented by a change in pH from 8.8 to 6.8.

Initially, the computation of the current output, I_{ratio}, of the translinear circuit was experimentally measured in real-time through the microfluidic assembly shown in Fig. 5.10 to confirm functionality. This was achieved by changing the pH of the solution of Ch 1 within a range of fixed pH values, while keeping the pH of the solution of Ch 2 steady at

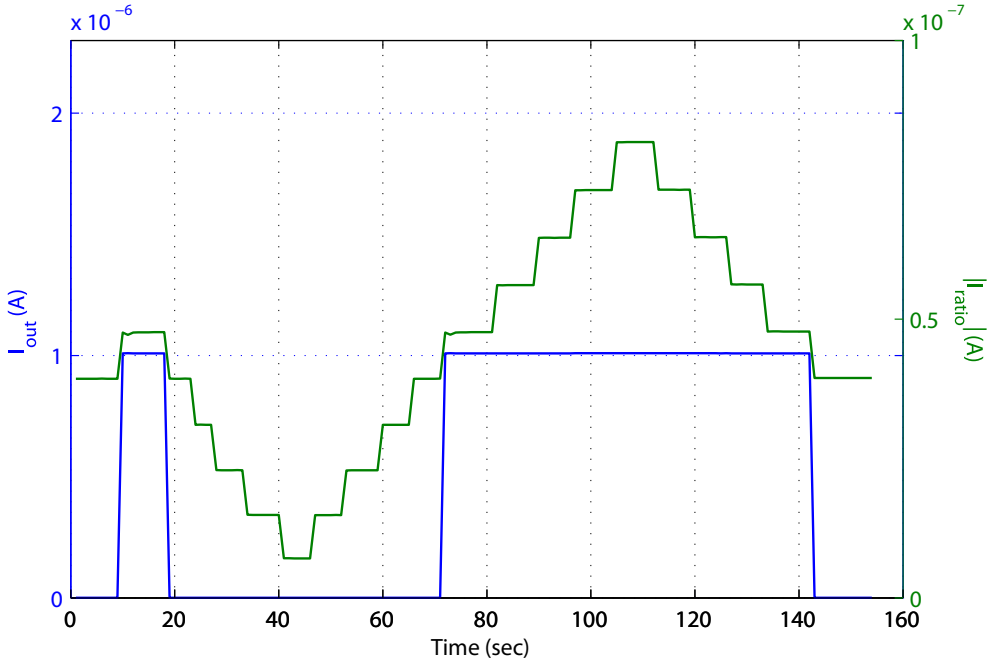


Figure 5.15: I_{out} vs I_{ratio} during 1 pH change for I_{perc}=50nA and I_{gain}=50nA

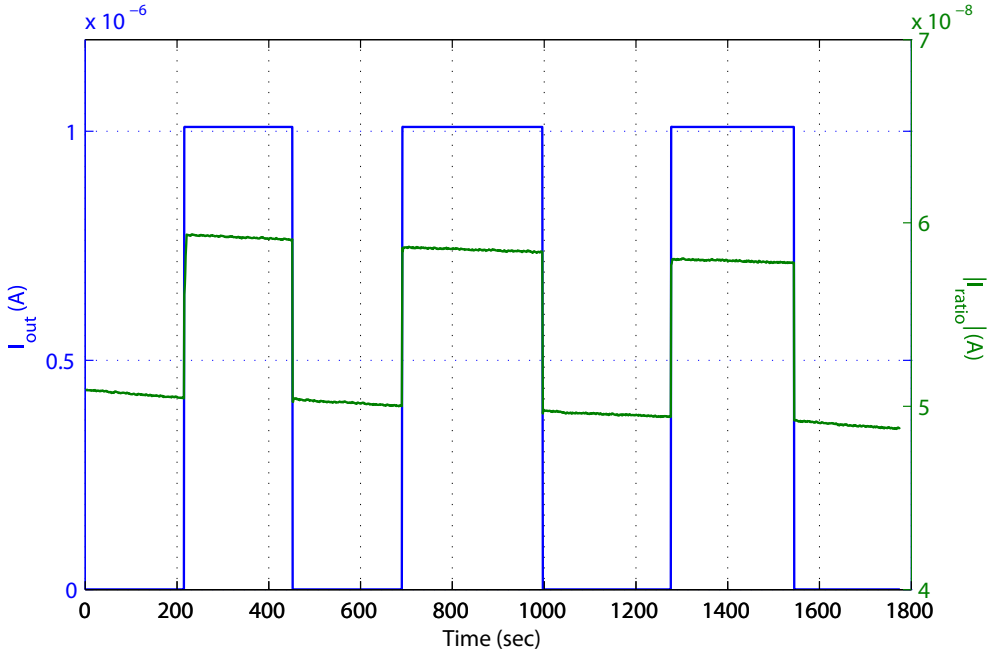


Figure 5.16: I_{out} vs I_{ratio} during 1 pH change for I_{perc}=56nA and I_{gain}=100nA

pH 7, emulating the scenario of a chemical reaction taking place in Ch 1, where the ISFET sensors producing the current I_{meth} lie underneath the chamber. The solutions selected to test the response of the circuit were varied from pH 5 to pH 9. Experiments were conducted separately for the range pH 7 to pH 9 and pH 5 to pH 7 with ascending and descending steps of ΔpH of 1. Both ISFET sources were biased at 1V due to shifting of the ISFET operating point by induced trapped charge as a result of assembling using the manifold. The reference electrode was kept steady at 1.5V based on the ISFET DC characteristics as shown in Fig. 5.11 to give V_{GS}=500mV, I_{DS}=100nA, focusing on the weak inversion region of operation, and I_{gain} was tuned at 100nA.

Results are shown in Fig. 5.17 for the range pH 7 to pH 9 and pH 5 to pH 7 with sequence of display, whereby the response of I_{meth} and I_{ratio} is observed during ascending and descending pH values, with I_{unmeth} kept constant at 100nA. Specifically, Fig. 5.17a,b illustrate the current response of I_{meth} and of the absolute values of I_{ratio} during the pH 7-9 steps whereas Fig. 5.17c,d illustrate I_{meth} and the absolute values of I_{ratio} during the pH 5-7 steps respectively. This analysis confirms that I_{ratio} is computed experimentally at a very good precision as expected from the translinear theory and from the theoretical values derived from Eq. 5.15, showing good response to changes in pH and good resolution, with a maximum error across all pH values to be found to be 2% from the ideal. Also, the average, absolute values of I_{ratio} for increasing and decreasing pH values, as shown in Fig. 5.17, are interpreted in Fig. 5.18 with respect to the range of pH values used (pH 5-9), separated in pH 7-9 in Fig. 5.18a and pH 5-7 in Fig. 5.18b, showing the cycle of currents during the rise and fall of pH, also highlighting the effect of drift during the rise and fall of pH while I_{ratio} is being monitored. The line in red which represents the average of I_{ratio} in both cases, is giving an indication of the average of the current values for the same pH steps in both ascending and descending cases. What can be seen is that the ratio is computed accurately but the drift can distort the result, which can be overcome using techniques such as differential measurements, as introduced in the next chapter, or letting the ISFETs burn in.

Additionally, a detailed summary of the average values of I_{meth}, I_{unmeth} and I_{ratio} together with the standard deviation points for the two repeats during the pH steps 7-9 and 5-7 are summarised in Table 5.4 and Table 5.5 accordingly. For the pH range of 7-9 shown in Table 5.4, the standard deviation values observed for the two repeats for a given pH are within the range of 0nA to 2.828nA with a mean of 0.801nA, given the time frame of 700sec and the minimum effect of drift.

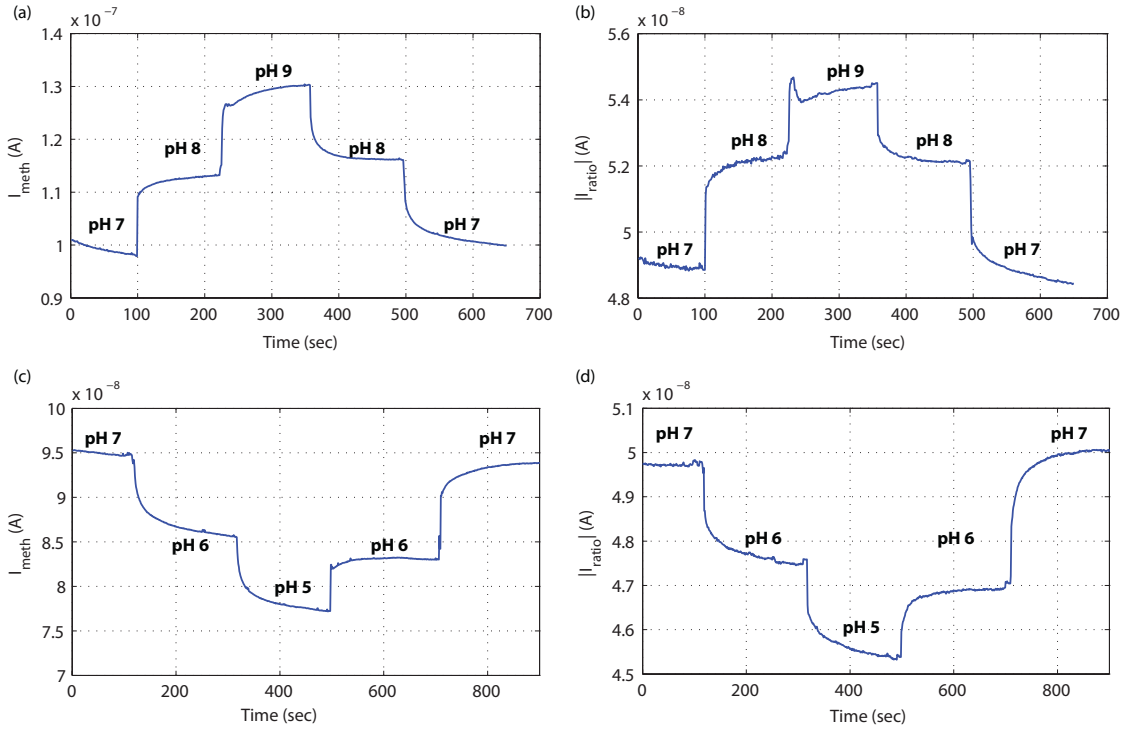


Figure 5.17: Transient response of I_{meth} and absolute I_{ratio} during decremental pH steps

Table 5.4: Average values with standard deviation results of I_{ratio} and I_{meth} for given I_{unmeth} values for two repeats during ascending and descending pH steps from pH 7 to pH 9 for I_{gain}=100nA.

	pH=7	pH=8	pH=9	pH=8	pH=7
I_{meth}(nA)	100	111.5±0.707	128.5±0.707	117±1.414	104±2.828
I_{unmeth}(nA)	100	101±1.414	103±1.414	103±1.414	103±1.414
I_{ratio}	49.6	51.5±0.707	54	52	49

A more detrimental effect of drift in the same experiment of two more repeats under different time frames can be seen in Table G.1 in Appendix G. For the pH range of 5-7 shown in Table 5.5, the standard deviation values are slightly larger achieving a mean of 0.942nA, although the values varied from 0nA to 2.828nA. The effect of drift in this case seems slightly less, an observation that can be correlated with the fact that the drift tends to decrease in acidic conditions [15].

Table 5.5: Average values with standard deviation results of I_{ratio} and I_{meth} for given I_{unmeth} values for two repeats during ascending and descending pH steps from pH 5 to pH 7 for I_{gain}=100nA.

	pH=7	pH=6	pH=5	pH=6	pH=7
I_{meth}(nA)	100	91±2.828	81.5±2.121	85.5±2.121	94.5±2.121
I_{unmeth}(nA)	100	98.5±2.121	94.5±2.121	96	95
I_{ratio}	49	47	45	46.5±0.707	50

Power Consumption

The "Methylation Cell" under test operated in the weak inversion region. The total power in the system may be calculated as:

$$P = V_{DD}(3I_{ISFET_{X1}} + 2I_{ISFET_{X2}} + I_{gain} + I_{ratio} + I_{perc} + I_{wta}) \tag{5.17}$$

The system achieves a power consumption of 2.3μW for a biasing current I_{DC}=100nA for both ISFETs and a gain current I_{gain}=100nA, operating at 3.3V supply, without the I_{wta} part which is determined by the drive strength of the circuit. The chip can be operated with biasing currents of below 10nA, as can be seen in Fig. 5.11, leading to further reductions in power.

5.5.3 Validation based on real methylated data

After proving the computation of I_{ratio} during a sequence of pH values of ΔpH of 1, the ability of the translinear circuit during a change in pH from 8.8 to 6.8 was tested. The selection of these pH values was decided according to the pH values obtained before and after a DNA reaction occurring when DNA methylation is present in given genetic areas under investigation, as has been explained in Section 4.4, Chapter 4, where ΔpH was shown to be able to reach a maximum difference of almost 2 pH.

But above all, in this occasion, the primary aim was to prove that the ratio of two signals obtained from two separate reactions could be successfully calculated on a Lab-on-Chip microfluidic environment. The results of such hypothesis are displayed in Fig. 5.19, with Fig. 5.19a representing the transient response of absolute I_{ratio} from two superimposed

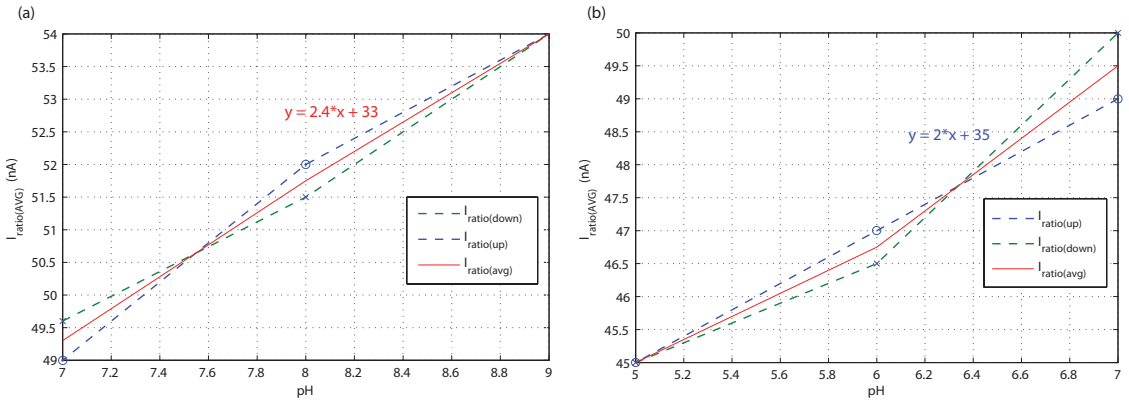


Figure 5.18: Average values of two repeats of I_{ratio} with respect to the range of pH values 7-9 and 5-7. The red line illustrates the average of $I_{ratio_{avg}}$ values collected from the data during decremental ascending and descending pH steps for pH 7-9 in (a) and pH 5-7 in (b) drawn as dashed lines. The best linear fit equations are displayed in both figures, with the one in (a) to overlap with the average of I_{ratio} of both ascending and descending pH values and the one in (b) to overlap with the blue line representing the response of the average values of I_{ratio} during incremental pH steps.

normalised trials where 8.8 is the pH of both chambers Ch 1 and Ch 2 (before DNA reaction) and 6.8 is the pH of Ch 1 (after DNA reaction) while the pH of Ch 2 stayed the same as in the beginning of the experiment. The same experiment was conducted with opposite starting pH in chambers, as shown in Fig. 5.19b, with pH 6.8 being induced in both chambers at the beginning of the experiment and pH 8.8 induced only in Ch 1 for no other reason other than to test the reproducibility of the computation of I_{ratio} during a pH step of the opposite direction. Both ISFET sources were biased initially at 100nA with V_S=1V and reference electrode voltage set at 1.5V, while I_{gain} was fixed at 100nA leading to starting point of around I_{ratio}=49nA, 1nA deviation from the theoretical calculation of I_{ratio}, based on Eq. 5.15.

What can be seen from Fig. 5.19 is that the transient change in I_{ratio} during both pH steps results in a ΔI_{ratio} change of about 7nA to 9nA, with both repeats following almost the same trend over time. Moreover, the aim of this experiment was also to provide with the essential information on the values at which I_{perc} should be set, based on the observed change on I_{ratio}, for the current comparator of the translinear circuit to be activated as soon as a new buffer of lower or higher pH is induced. The range of values of I_{perc} to be set for the pH step change from 8.8 to 6.8, based on the information obtained from Fig. 5.19a, would be around 49nA to 46nA and for a pH step change from 6.8 to 8.8 would be around

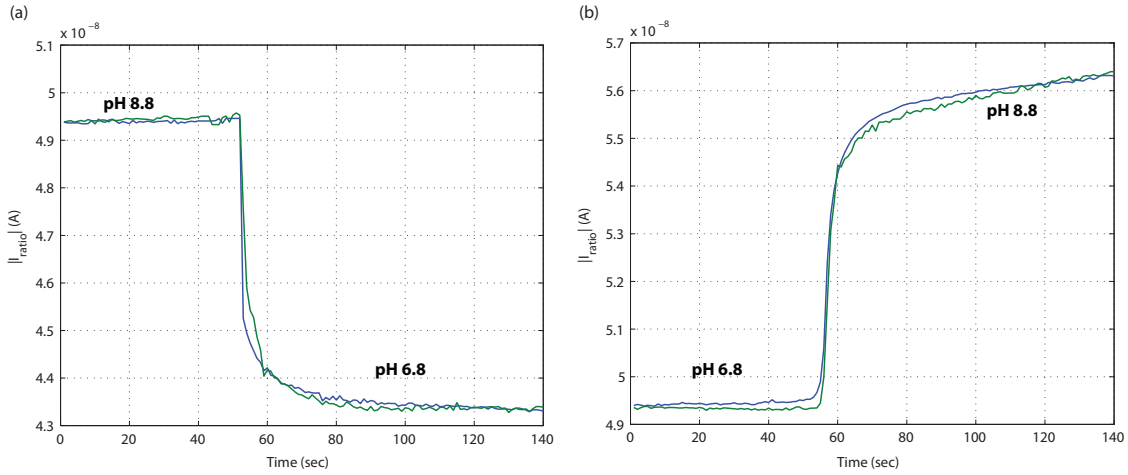


Figure 5.19: Transient response of absolute I_{ratio} of two repeats during (a) a pH step change from 8.8 to 6.8 and (b) a pH step change from 6.8 to 8.8.

49nA to 52nA, based on the information provided by Fig. 5.19b.

The ability of the current comparator to switch from 0μA to 1μA during a pH step change from 6.9 to 7.9 was tested for two repeats, one followed by the other, within a time frame of 400sec. The current bias for I_{wta} was set at 1μA as the maximum current observed when a pH step change occurs, giving a discrete indication of the pH change when I_{ratio} exceeds a preset current value set by I_{perc}. The results of the transient response of I_{out} through changes in absolute I_{ratio}, derived for the given pH step change, are shown in Fig. 5.20 for I_{perc}=52nA. It can be seen that the translinear circuit's capability of switching current state during a ΔpH of 1 has been successful, with the results being reproducible twice in two consecutive runs. The values of I_{ratio} started from 49nA when the pH in both chambers was the same and then jumped to 52nA when the change was induced in Ch 1. I_{ratio} was brought down to 49nA after 135sec, while I_{out} jumping down to 0nA, and the same experiment was repeated once again. The time duration of this experiment was as short as 400sec so that the risk of evaporation of the pH buffers in the 0.3μl chambers was reduced.

As the ability of the current comparator, I_{out}, to indicate discretely a change in pH based on a preset I_{perc} was proven to work for a ΔpH of 1, as seen in Fig. 5.20, and the computation of I_{ratio} was successfully achieved for a ΔpH of 2, as seen in Fig. 5.19, defining a range of currents for I_{perc} given the values of I_{ratio} during that pH step change, the combination of both features are finally left to be proven. Fig. 5.21 shows the results

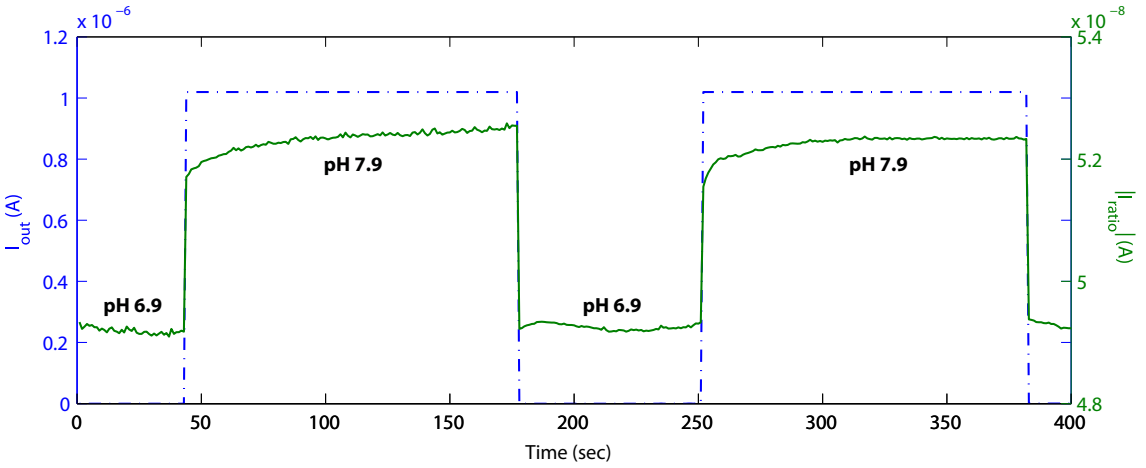


Figure 5.20: Transient response of the current comparator I_{out} and absolute I_{ratio} of two consecutive repeats during an incremental and decremental pH step change of 6.9 to 7.9.

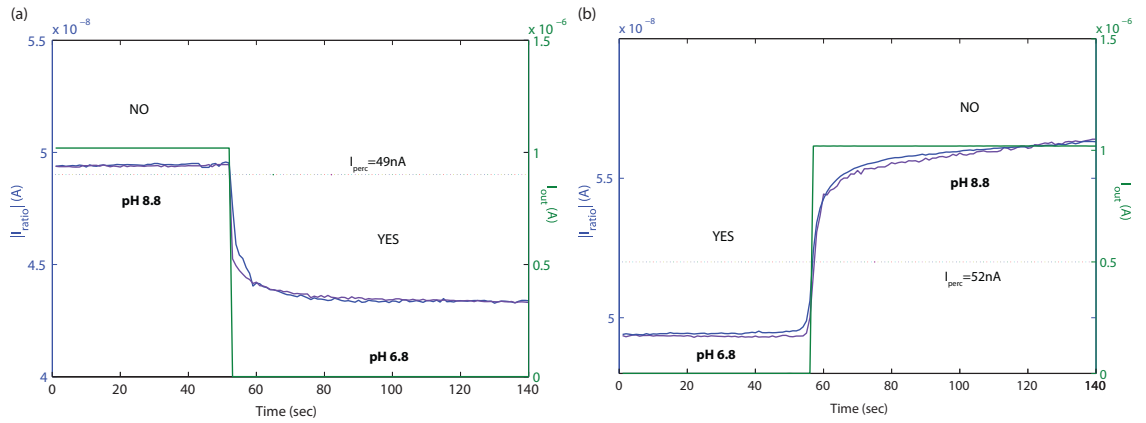


Figure 5.21: Absolute I_{ratio} and I_{out} of two repeats with respect to time, during a pH step change from 8.8 to 6.8 and a preset I_{perc} value during descending (a) and ascending (b) directions of the pH step change, followed by the values of I_{perc} for a reaction to take place (YES) or not (NO).

reported on Fig. 5.19, with the additional feature of using the current comparator set at a specific value based on the information gathered by Fig. 5.19.

More specifically, I_{perc} was set at 49nA during the descending pH step from 8.8 to 6.8 and at 52nA during the ascending pH step from 6.8 to 8.8. An indication of 'NO' was made when no reaction was happening, when the pH of the reaction chamber (Ch 1) was 8.8, which turned into a 'YES' when Ch 1 was induced with 6.8, confirming that the sample induced was methylated DNA. The comparator was tested for both pH directions to prove

Table 5.6: System properties and performance characteristics

Technology	AMS 0.35μm 2P4M CMOS
Die dimensions	2.5mm × 2.81mm
Passivation Si_3N_4/SiO_2	1030nm/1000nm (about 120fF)
ISFET pixel: W×L (electrical)	200μm × 1μm
ISFET pixel: W×L (chemical)	34μm × 100μm
Sensing area	3400μm^2
Transistor sizes (W×L)	10μm × 10μm
Transistors per pixel	37
Power supply	3.3V
Chamber size	1mm × 0.4mm × 0.4mm
Chamber diameter	400μm
Chamber volume	0.3μl
pH sensitivity	30mV/pH
ISFET drain current	100nA
I_{gain} @ (I_{DC}=100nA)	100nA
Power consumption @ (I_{DC}=100nA, I_{gain}=100nA)	2.3μW

its functionality as well as to validate the selection of the values of I_{perc} accordingly.

5.6 Summary

In this chapter, the concept of a ratiometric approach using the translinear "Methylation Cell" towards DNA methylation detection was presented, simulated, fabricated and tested using (a) an epoxy encapsulation set-up to demonstrate the computational functionality of the circuit and (b) a microfluidic manifold Lab-on-Chip set-up to allow real-time sensing of pH signals derived from two separate and isolated from each other microfluidic chambers. The signals were originated from (i) DNA reactions taking place in presence of methylated DNA existent in genetic areas responsible for tumour suppression compared to (ii) no reactions taking place due to the absence of DNA methylation or the presence of unmethylated DNA in the same under investigation genetic regions. Some of the system's properties and performance characteristics are summarised in Table 5.6.

Based on this concept, a novel ISFET based readout has been proposed for the continuous computation of the ratio between methylated and unmethylated DNA in the form of current signals sensed by two ISFET sensors, by adopting the circuit technique known as

the "translinear principle". The readout is then followed by a comparison block (voltage-mode or current-mode) that would give a discrete output when methylation reaches and exceeds a predetermined, tunable percentage.

Simulation results demonstrated the capability of the translinear "Methylation Cell" to compute the ratio between two currents, also defined as the output current of the translinear circuit, I_{ratio}, which represents the ratio of methylation, amplified by a fixed gain term, I_{gain}. For a value of I_{ratio} above a threshold, set to define the limit of detection, a discrete boolean value was given as an output of the ISFET pair of the cell, utilising voltage-mode and current-mode switching techniques, able to indicate whether the level of methylation exceeds 50%. This can thus highlight that the corresponding genetic areas appear hypermethylated, implying that the tumour suppressor function of the regulatory region of the gene may be hindered, leading to the potential inactivation of the gene which can be associated with early stages of tumour development.

The capability of the translinear "Methylation Cell" for ratio computation was validated experimentally, focusing on the current-mode switching through the realisation of a fabricated system, while assessing experimentally the performance of the current comparator by emulating a scenario of 1 pH change and thus selecting the best performance characteristics for the translinear circuit (I_{meth}, I_{unmeth} and I_{gain} set at 100nA) to compute I_{ratio}. Additionally, a range of values for the threshold current, I_{perc}, were experimentally selected for further use and validation of the current switching by the Lab-on-Chip microfluidic set-up that was also developed. The Lab-on-Chip consisted of two microchambers, ideal for in parallel monitoring of chemical pH signals generated by the two ISFETs. The computation of I_{ratio} was validated experimentally firstly in various pH buffers and then during a pH jump of given values of pH obtained before and after a DNA reaction taking place when DNA methylation was present. Finally, the functionality of the current comparator was tested as well as its ability to indicate the event of a reaction taking place due to methylated DNA being present, concluding with the values that need to be used for I_{perc} so that the output of the current comparator, I_{out}, accurately switches from 0μA to 1μA with a minimum time delay.

The "Methylation Cell" successfully sets the basis for a system integrating ISFET sensors for detecting epidemiological ratios of DNA methylation in real-time, giving as an output a discrete indication of the level of normality of DNA methylation. It can also be efficiently scaled to address CMOS ISFET arrays for in parallel detection of DNA methyla-

tion in multiple tumour suppressor genes that appear as hypermethylated in genetic regions responsible for their control, associated with the early development as well as progression of cancer. This method would primarily contribute in forming a powerful tool as well as a novel approach in early diagnosis of cancer, ultimately in predicting the clinical outcome, reducing the data bandwidth requirements for an array based platform to just 1 bit per pixel pair due to the use of a discrete boolean value as an output and finally leveraging the needs for power due to the operation in the weak inversion region, a significant requirement for a Point-of-Care implementation.

References

[1] M. Esteller, "Cancer epigenomics: DNA methylomes and histone-modification maps," *Nature Reviews Genetics*, vol. 8, no. 4, pp. 286–298, 2007.

[2] P. Laird, "The power and the promise of DNA methylation markers," *Nature Reviews Cancer*, vol. 3, no. 4, pp. 253–266, 2003.

[3] H. Wang, M. Maurano, H. Qu, K. Varley, J. Gertz, F. Pauli, K. Lee, T. Canfield, M. Weaver, R. Sandstrom, *et al.*, "Widespread plasticity in CTCF occupancy linked to DNA methylation," *Genome Research*, vol. 22, no. 9, pp. 1680–1688, 2012.

[4] P. Laird, "Principles and challenges of genome-wide DNA methylation analysis," *Nature Reviews Genetics*, vol. 11, no. 3, pp. 191–203, 2010.

[5] B. Gilbert, "Translinear circuits: A proposed classification," *Electronics Letters*, vol. 11, no. 1, pp. 14–16, 1975.

[6] B. Gilbert, "Current-mode circuits from a translinear viewpoint: A tutorial," *In Chapter 2 of Toumazou, C., Lidgey, F.J. and Haigh, D.G. eds., Analogue IC Design: the current-mode approach*, pp. 11–91, 1990.

[7] E. Seevinck and R. Wiegerink, "Generalized translinear circuit principle," *IEEE Journal of Solid-State Circuits*, vol. 26, no. 8, pp. 1098–1102, 1991.

[8] A. Andreou and K. Boahen, "Translinear circuits in subthreshold MOS," *Analog Integrated Circuits and Signal Processing*, vol. 9, no. 2, pp. 141–166, 1996.

[9] E. Vittoz and J. Fellrath, "CMOS analog integrated circuits based on weak inversion operations," *IEEE Journal of Solid-State Circuits*, vol. 12, no. 3, pp. 224–231, 1977.

[10] L. Shepherd and C. Toumazou, "Weak inversion ISFETs for ultra-low power biochemical sensing and real-time analysis," *Sensors and Actuators B: Chemical*, vol. 107, no. 1, pp. 468–473, 2005.

[11] L. Shepherd and C. Toumazou, "A biochemical translinear principle with weak inversion ISFETs," *IEEE Transactions on Circuits and Systems I: Regular Papers*, vol. 52, no. 12, pp. 2614–2619, 2005.

[12] M. Kalofonou, P. Georgiou, C.-P. Ou, and C. Toumazou, "An ISFET based translinear sensor for DNA methylation detection," *Sensors and Actuators B: Chemical*, vol. 161, no. 1, pp. 156–162, 2012.

[13] P. Georgiou and C. Toumazou, "ISFET characteristics in CMOS and their application to weak inversion operation," *Sensors and Actuators B: Chemical*, vol. 143, no. 1, pp. 211–217, 2009.

[14] P. Georgiou, *Chemical Bionics - A novel design approach using Ion Sensitive Field Effect Transistors*. PhD thesis, Imperial College London, London, 2008.

[15] J.-C. Chou and C.-N. Hsiao, "Drift behavior of ISFETs with a-Si: H-SiO_2 gate insulator," *Materials Chemistry and Physics*, vol. 63, no. 3, pp. 270–273, 2000.

Chapter 6

A current-mode approach for differential DNA methylation detection

6.1 Introduction

Advances in semiconductor technology during the last decade have provided novel solutions in healthcare, especially in the fields of early detection, diagnosis and therapy of disease. Specifically CMOS technology has enabled next generation fully integrated Lab-on-Chip systems due to the inherent advantages of large scale integration, low cost of fabrication and intelligent processing on-chip [1]. When such systems are designed for applications such as DNA testing at the point of care, additional requirements of miniaturisation and low power consumption are needed to ensure that portability and maximum battery life of the medical device can be achieved [2]. In order for these systems to be realised, a basic sensing element, capable of being miniaturised in CMOS, integratable with standard circuits and scalable to multiple sensor arrays is needed. This is realised using a CMOS based ion sensor called the Ion-Sensitive Field-Effect Transistor (ISFET), introduced in Chapter 3.

The ISFET has gained significant popularity for use as a chemical, solid-state, pH sensing element since it has been adopted in various chemically driven applications [3–5], including auto-calibrated Lab-on-Chip platforms [6], but also in biomedically driven ones [7, 8], with a significant role in the field of genetics [9–12] as well as of epigenetics [13, 14], through the use of DNA methylation as a biomarker for cancer detection, as has been described in Chapter 4. They have therefore shown great capability for measuring ionic concentration

changes resulting from biochemical reactions, forming front-ends for applications that use a pH change as a marker to indicate the presence of a reaction. Such applications have highlighted the benefits of using ISFETs, letting us now exploit the simplicity given by well-known current-mode techniques, such as the translinear principle, with the possibility to fabricate fully integrated Lab-on-Chip systems for real-time monitoring of pH signals. This offers great potential for in parallel biochemical reaction detection and monitoring, ideal for the scope of this research which is focusing on approaches towards DNA methylation detection.

Although CMOS ISFETs have been widely used in fully integrated sensing systems, certain non-idealities limit their wide usage as pH sensors. These include drift, temperature instability and threshold voltage variation [15]. Given the challenges that these bring in sensing absolute pH concentration, applications which require monitoring of changes in reaction rather than absolute pH [10] are more suited.

Furthermore, the need for differential pH measurements instead of absolute pH values is required to guarantee steady and robust circuit operation independent of temperature and common-mode noise. This is especially important when DNA amplification methods are used such as thermocycling (PCR) or isothermal (LAMP) amplification, whereby controlling temperature conditions is a matter of great importance given that such types of reactions are very sensitive to temperature. This can be achieved through differential ISFET measurement [15] and topologies that could be used for monitoring differentially derived changes in pH from ISFET sensors using low power current-mode methods. One such topology is the "Gilbert Gain Cell" which is well suited for differential measurement and will be utilised for the scope of this research.

This chapter presents a low power, current-mode approach for DNA methylation detection in CMOS, the ISFET based Chemical Gilbert Cell, which combines a microfluidic assembly that achieves monitoring of differentially derived changes in pH, sensed using ISFET sensors, and suitable for applications that require differential monitoring in small volumes, such as DNA amplification as result of the presence or absence of DNA methylation. By adopting the Chemical Gilbert Cell, certain significant non-idealities that ISFETs have by nature, such as drift and temperature dependence are tackled and in parallel detection of separate pH signals is achieved. Furthermore, through the inclusion of a tunable gain on the monitored output, a method for amplification is realised. The system has been designed and fabricated, with simulation and experimental results reported and analysed,

confirming functionality and demonstrating the capabilities of the front-end at a microscopic level through integration in a Lab-on-Chip (LoC) set-up. The chapter then concludes with the summary of the results, highlighting the capabilities of such system which facilitates its use for large scale integration and applications that require robust, low power differential chemical measurement and monitoring.

6.2 Differential CMOS ISFET topologies

The ISFET sensor has been commonly used as part of microsystems (eg. Lab-on-Chip) for its ability to measure the pH of a solution where a reaction may take place. In various biomedical applications, some of the requirements of sensor based Lab-on-Chip systems have been (a) temperature stability and control due to the expectations of operation of such systems in different temperature conditions, [16], as well as (b) good common-mode rejection to reduce drift and common-mode noise through the use of differential topologies, such as the differential ISFET-REFET front-end proposed by [17]. Also given the need for minimum instrumentation, (c) integration of multiple sensors per chip is required to allow high density integration, therefore achieving low area and power, with a very recent example presented in [12].

For overcoming common non-idealities such as the threshold voltage variation as a result of the time dependent variation of the ISFET's sensed signal (drift) or the temperature dependence, various differential topologies have been proposed in the past, instead of single-ended ISFET read-out circuits. Such topologies have reported to offer compensation schemes with an effort to improve the signal stability of the ISFET sensor while reducing the effect of fluctuations of the experimental conditions. To date, current differential CMOS ISFET topologies tend to use ISFET pairs or ISFET/reference FET (REFET) configurations through interfacing to one or more operational amplifiers (OTAs), mainly operating in voltage-mode [18–25]. Current-mode implementations have on the other hand shown strong potential, replacing the use of OTAs, and provide novel interfaces for differential measurements [26, 27] with [17] achieving low transistor count and low power consumption when the weak inversion mode of operation is used. We now proceed in describing these.

6.2.1 Voltage-mode topologies

The concept of a differential measuring system using ISFETs was initially suggested by Bergveld in 1989. This consisted of an ISFET/REFET pair providing a differential voltage output, as result of changes in the pH of the analyte solution sensed by the ISFET, relative to an ion-insensitive FET (REFET) [18]. A platinum (Pt) electrode was used as an on-chip pseudo-reference electrode, implemented using an evaporated platinum layer on the substrate that the ISFET or REFET were fabricated on. Its role was to bias both ISFET and REFET in the differential measurement set-up, with any instability caused by the varying composition of the electrolyte translated into variations in V_{ref} to be rejected as common-mode noise through the differential configuration. Fig. 6.1 illustrates a schematic representation of the differential arrangement, with the ISFET and REFET sensors being the inputs of a differential amplifier, which provides the output of the system.

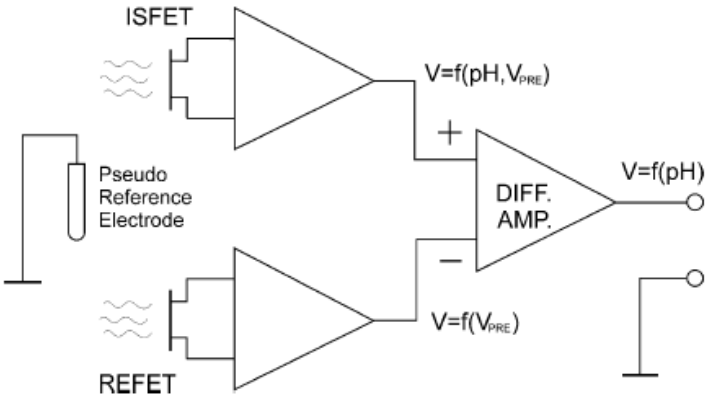


Figure 6.1: A differential ISFET/REFET measuring system [15]

Palan et al. [20] proposed a CMOS differential configuration with a sensor interface of two ISFETs, each covered with a different ion sensitive layer (ISFET1 with Si_3N_4 and ISFET2 with SiO_2), adopting the source-drain follower circuit configuration, using two OTAs per ISFET, as can be seen in Fig. 6.2, and Pt as the reference electrode. A similar arrangement proposed by Hammond et al. [23] is shown in Fig. 6.3, with an ISFET/REFET pair as part of the differential arrangement in unmodified CMOS in a System-on-Chip set-up. Si_3N_4 was used as the sensing membrane of the ISFET and a PVC polymer membrane was added in the case of the REFET, following a post-processing procedure, to create a non-sensitive layer by preventing hydrogen ions immobilising in the membrane's surface.

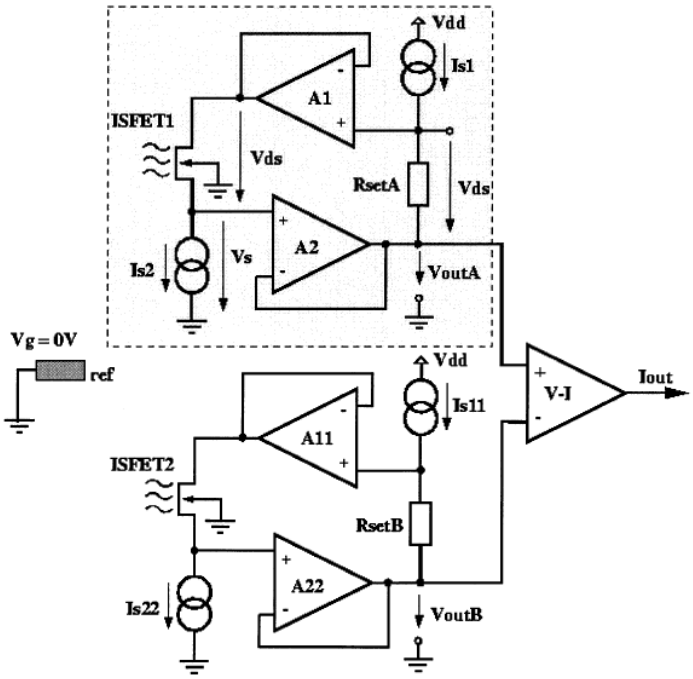


Figure 6.2: Differential ISFET interface for measurement of sensors [20]

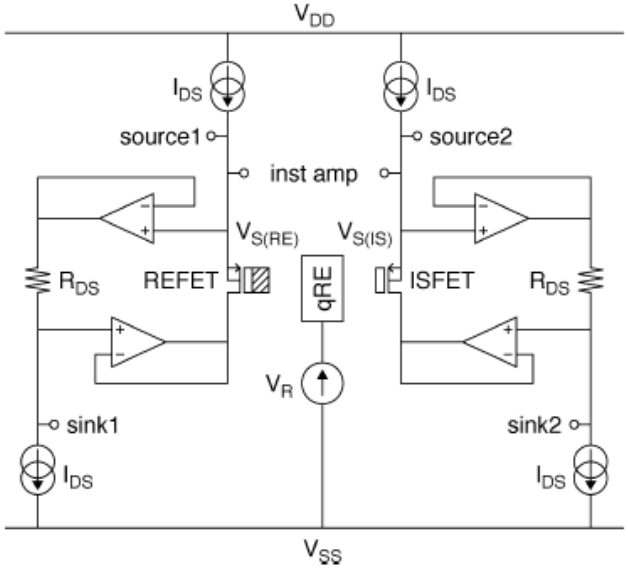


Figure 6.3: Differential circuit schematic [23]

A CMOS based approach for differential read-out of ISFET and REFET sensors was also proposed by Ravezzi et al. [21] with the schematic diagram appearing in Fig. 6.4. It consisted of a CMOS read-out circuit based on switched-capacitor techniques, providing a low-impedance analog output signal proportional to the differential input between the ISFET/REFET sensors, performed by the "differential stage". Si_3N_4 was used as the ISFET's sensing membrane and a buffered hydrogel layer was used to form the REFET's ion insensitive layer. A Pt reference electrode was also used to create the electrical contact to the solution. The proposed read-out's aim was to provide compensation strategies, to allow reduction of the sensor's dependence on temperature fluctuations and drift, achieving high resolution.

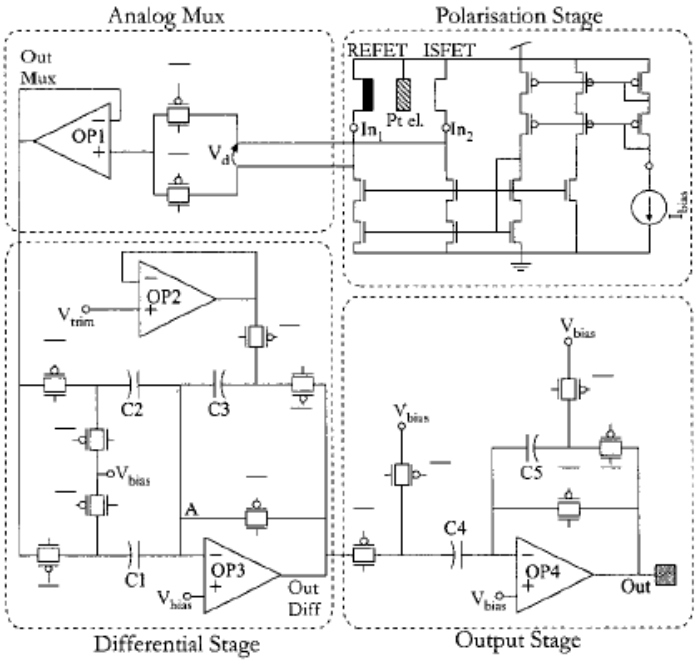


Figure 6.4: A differential ISFET/REFET read-out using switched capacitors [21]

Wei et al. [24] proposed a fully integrated interface circuit in CMOS for pH measurement using an ISFET/REFET differential pair and amplifiers in symmetry leading to a differential output voltage. The schematic of the ISFET amplifier can be seen in Fig. 6.5 with the drain-source voltage to be kept constant. A pseudo reference electrode was used to provide with biasing conditions independent to the sensor's input or to any variations in temperature conditions. For the ISFET/REFET pair, Ta_2O_5 and PVC were used respectively as inputs of the ISFET and REFET.

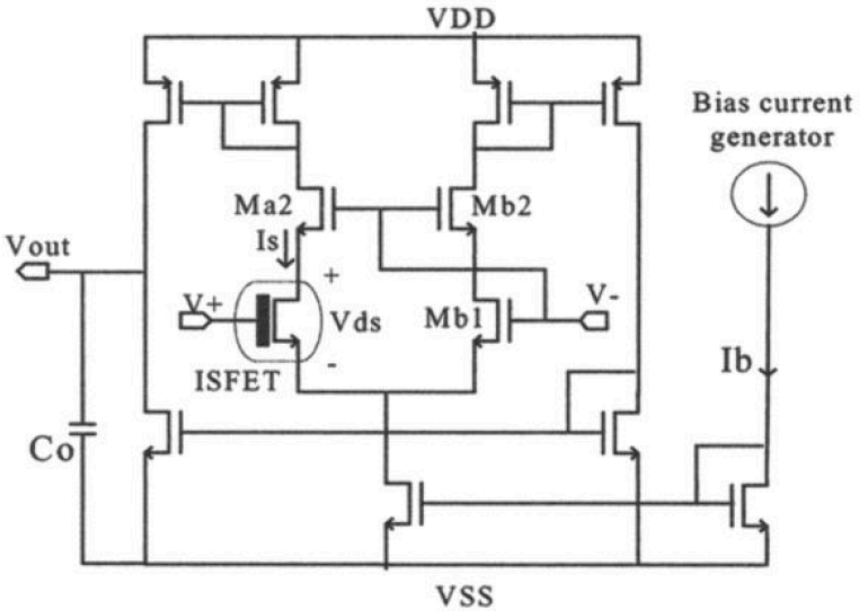


Figure 6.5: Schematic of the ISFET amplifier used in the differential read-out circuit [24]

Finally, Chodavarapu et al. [22] proposed a pseudo-differential read-out architecture consisting of two ISFETs in the forms of OTAs integrated as the input stage (ISFET OTAs or IOTAs), as illustrated in Fig. 6.6, by applying indirect feedback to the floating gates which were shared by more than one devices. The ISFETs of the IOTAs are reported to be identical [25], with the sensitivity of each ISFET to vary based on the size of the PMOS load, instead of using two ISFETs with different pH sensitivities, therefore avoiding any post-processing steps. It therefore achieves different pH sensitivities on the same chip by only adjusting the dimensions of the PMOS loads in the two IOTAs. Si_3N4 was used as the sensing layer of the ISFETs and a gold wire was adopted as the pseudo reference electrode to bias the solution. Such a differential read-out proposes an architecture that achieves constant bias operational conditions with the ability to track changes in the ISFET threshold voltage and therefore in pH.

To summarise on the voltage-mode topologies, from the very fundamental architecture of differential measurement system suggested by Bergveld in 1989 to the latest CMOS-integrated ISFET interfaces for differential read-outs, they all share the use of power hungry operational amplifiers to achieve constant bias conditions and read-out, for following potential changes in ionic concentration of the solution. There are however several restric-

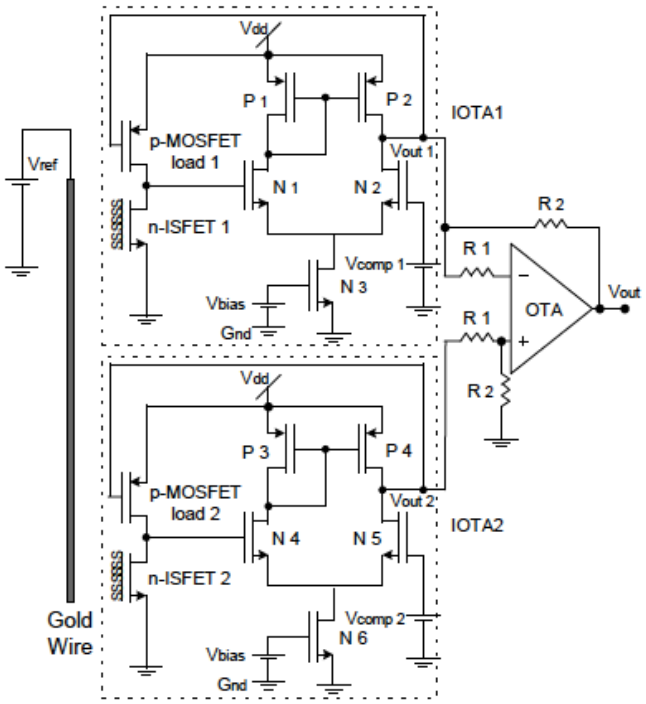


Figure 6.6: CMOS ISFET differential read-out system architecture [22]

tions in the proposed interfaces regarding the operating range, the power consumption, as well as the transistor count. The current-mode topologies reviewed in the next section are presenting alternative CMOS ISFET interfaces able to achieve differential measurement, allowing for low power consumption by avoiding the use of operational amplifiers providing with the ability to perform computation using simple techniques such as the translinear principle.

6.2.2 Current-mode topologies

In current-mode topologies, a differential read-out has been reported in 2004 by Ghallab et al. [26, 27] proposing the use of current conveyors instead of operational amplifiers. By using two operational floating current conveyors (OFCCs) per ISFET and REFET respectively, the input currents were conveyed through the ISFET and REFET to the output, providing with a differential current output, linearly proportional to any changes in pH sensed by the ISFET. The current-mode differential measurement read-out circuit was preferred as a method to reduce the impact of common-mode instabilities generated by the reference

electrode or the temperature dependency of the ISFET. Such topology is reported to have the potential for use in Lab-on-Chip and biomedical applications.

A current-mode topology offering differential measurements has also been proposed by Shepherd et al. [17] using a CMOS integrated differential ISFET/REFET front-end biased by a quasi-reference electrode (Pt), avoiding the use of OTAs, as seen in Fig. 6.7, providing with a low power method for a differential implementation. The reported method provides capability for voltage regulation by clamping the drain voltage of the ISFET therefore achieving a fixed bias point applied in a pseudo-differential arrangement through subtraction of currents from the ISFET/REFET pair. It shows great potential for implementation in large scale ISFET arrays, achieving low power consumption when operated in weak inversion, with the capability to apply further on-chip processing steps and gain stages, making it suitable for biomedical implementations. Finally, Pookaiyaudom et al. [28] presented the concept of a chemical current conveyor with the ability to perform differentiation of pH signals derived from ISFETs.

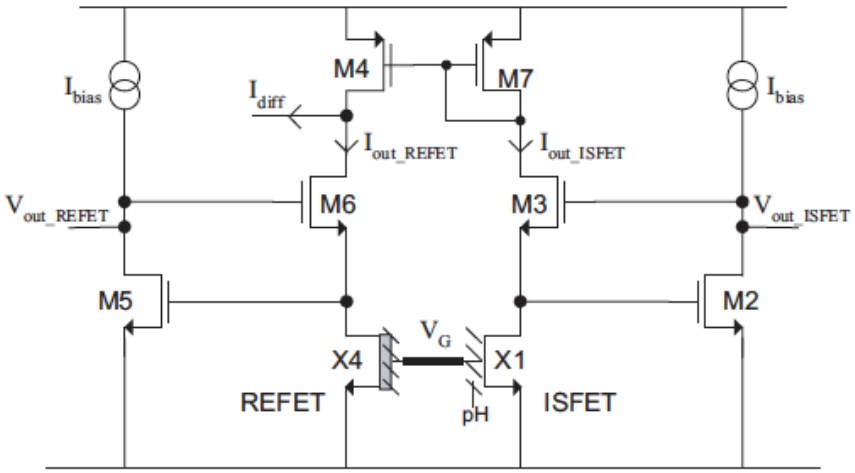


Figure 6.7: CMOS based differential ISFET/REFET read-out [17]

These current-mode topologies proposed differential arrangements highlighting the need for additional gain stages to amplify the sensed read-out signal in order to achieve a good resolution. In this research, a CMOS integrated interface for differential pH measurement is proposed using the ISFET based Chemical Gilbert Gain Cell, integrating an adjustable gain by using single tuning current, providing a scalable differential output measurement between two ISFETs. The topology proposed is fundamentally based on the "Gilbert Gain

Cell", a current-mode circuit, the analysis of which follows in the next section.

6.3 Gilbert Gain Cell

The "Gilbert Gain Cell" shown in Fig. 6.8, first introduced in 1968 by Barrie Gilbert [29], is a current-mode circuit with the ability to differentially measure currents with a tunable gain in a compact way of using only four transistors. As has been explained by Gilbert in 1990 [30], a differential input current signal, I_{in}, is sensed by the two transistors M3 and M4, as can be seen in Fig. 6.8, and is added in phase with the outputs coming from M1 and M2. Such configuration can provide the advantage of broadband amplification without affecting the differential input, by cascading a series of "Gain Cells", with the output stage of one cell adding up as the input of the next, providing the driving current for operation, thus contributing to the total output signal. An additional advantage is that the gain is linearly dependent on any of the input currents of the cell, achieving a minimum net gain of 1 given an inner stage gain of less than 1, which increases the speed of the output response of the circuit [29, 30].

The expressions of the input current, I_{in}, and the output current, I_{out}, as defined by [30], are given by:

$$I_{in} = (1+x)I_x - (1-x)I_x = 2xI_x \tag{6.1}$$

and

$$\begin{aligned} I_{out} &= I^+ - I^- = (1+x)(I_x + I_y) - (1-x)(I_x + I_y) \\ &= 2x(I_x + I_y) \end{aligned} \tag{6.2}$$

leading to the definition of the modulation index x as:

$$x = \frac{I_{in}}{2I_x} \tag{6.3}$$

where x represents the normalised differential input signal amplified by a gain, dependent on a DC bias, I_x, and I^+, I^- are the two output currents as shown in Fig. 6.8. I_y is an entity proportional to the gain current, I_{gain}, according to the expression:

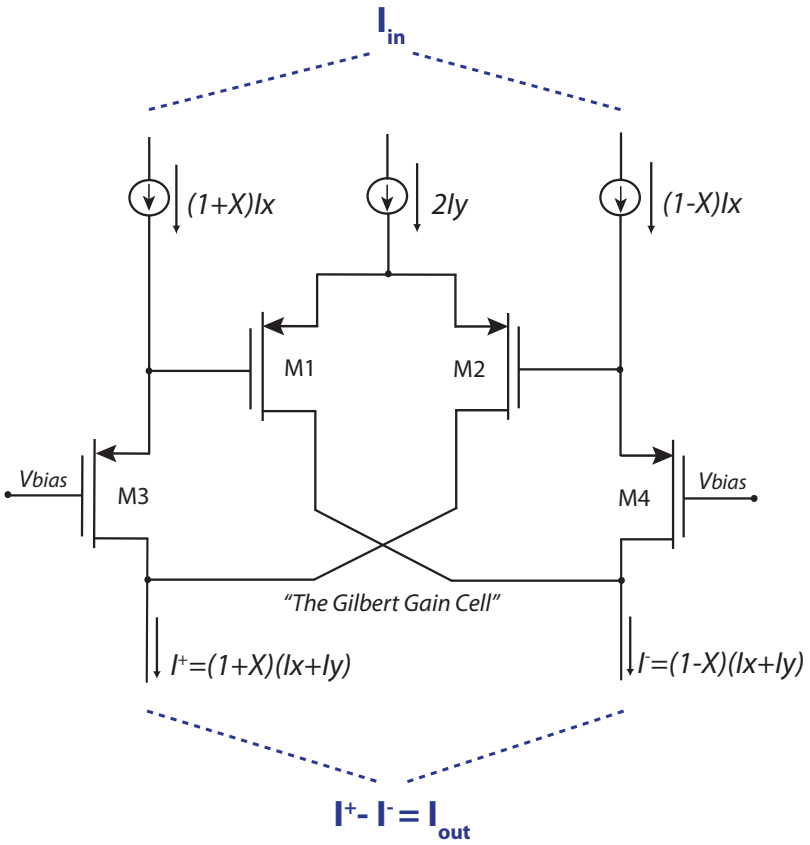


Figure 6.8: The Gilbert Gain Cell

$$I_{gain} = 2I_y \tag{6.4}$$

Therefore, by tuning I_y, adjustments to the gain term can be facilitated, achieving a continuous control on the gain of the cell. The description of the "Gilbert Gain Cell" as a differential cascode with gain can be therefore justified since it provides a differential output current, I_{out}, through a gain stage defined by I_{gain}.

The "Gilbert Gain Cell" is one example of applying the translinear principle to MOS circuits to multiply/divide currents derived from transistors operating in the weak inversion region. The term *translinear* and the benefits of using translinear circuits has been analysed in detail in Section 5.2, Chapter 5. The use of ISFETs as ion sensors in the subthreshold region in combination with the inherent benefits of the "Gilbert Gain Cell" is presented in the following sections.

6.4 Chemical Gilbert Cell

Further to the development of the "Gilbert Gain Cell", an ISFET based Chemical Gilbert Cell is presented herein and shown in Fig. 6.9 [31], fundamentally based on the use of the "Gilbert Gain Cell" as mentioned in Section 6.3. This consists of two ISFET sensors acting as probes, capable of principally detecting pH signals from separate reaction chambers. Chemical changes are detected and transduced to the drain currents, I_D, of the ISFET due to the presence of hydrogen ions in solution, as described in Eq. 3.21, Section 3.5.1 in Chapter 3.

The use of the Chemical Gilbert Cell provides advantages such as differential measurements, offering drift reduction and temperature stability as well as a linearly tunable current gain as has been firstly shown in [32]. The theory behind the operation of the Chemical Gilbert Cell is derived by the translinear loop of PMOS transistors (M1-M2 and M3-M4) operating in weak inversion, with the input currents of M3 and M4 been added in phase with the output currents of M1 and M2. The ISFETs are biased by applying a suitable bias at the reference electrode (indicated as stable potential V_G) for weak inversion operation. The gain, A, of the Chemical Gilbert Gain Cell is represented by the equation:

$$A = \frac{I_x + I_y}{I_x} \tag{6.5}$$

where I_x is the input DC biasing current signal and I_y is the gain term. Considering its operation for differential pH measurement whereby one ISFET sensor (ISFET1, Fig. 6.9) is used to detect the pH change generated from a reaction taking place in chamber 1 (Ch 1) generating an I_{pH1} or I_{ISFET1} and the other ISFET sensor (ISFET2, Fig. 6.9) is used to detect the pH of the buffer solution in chamber 2 (Ch 2) generating an I_{pH2} or I_{ISFET2}, the current expressions can be defined as:

$$I_{pH1} = I_{ISFET1} = I_{DC} + I_{drift} + I_{\Delta pH}\Big\} \qquad \textit{reaction chamber (Ch 1)} \tag{6.6}$$

and

$$I_{pH2} = I_{ISFET2} = I_{DC} + I_{drift}\Big\} \qquad \textit{buffer chamber (Ch 2)} \tag{6.7}$$

so that:

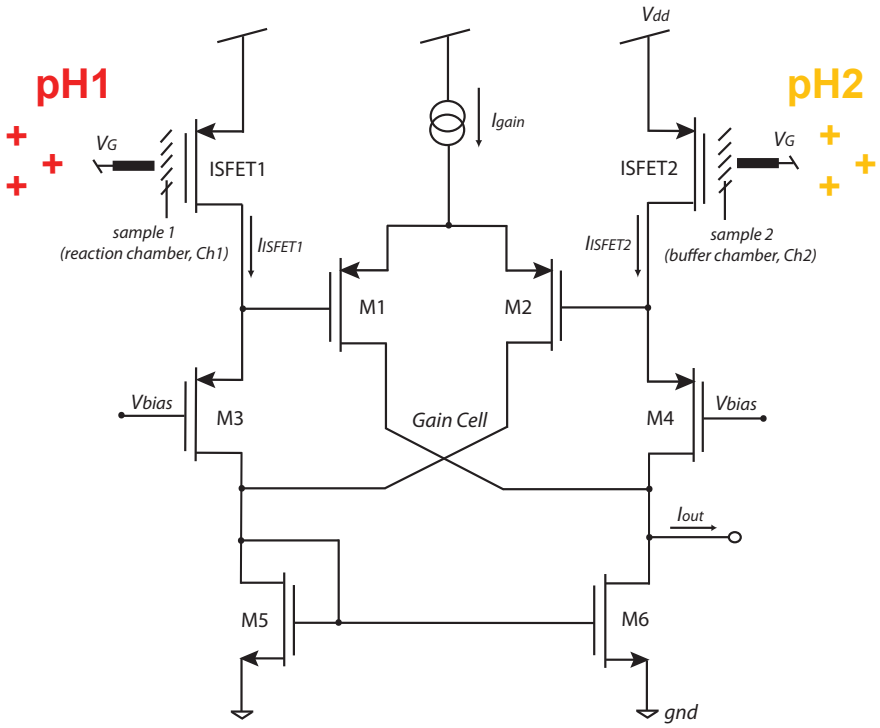


Figure 6.9: The ISFET based Chemical Gilbert Gain Cell. $ISFET1$ is sensing $pH1$ generated from the reaction chamber (Ch 1) and $ISFET2$ is sensing $pH2$ generated from the buffer chamber (Ch 2).

$$\begin{aligned} I_{ISFET1} - I_{ISFET2} &= I_{pH1} - I_{pH2} \\ &= I_{\Delta pH} \end{aligned} \tag{6.8}$$

where $I_{\Delta pH}$ is a real-time change in pH sensed by the drain currents of the ISFETs, differentially monitored by Ch 1 and Ch 2.

In parallel to these, the expressions of the input, I_{in}, and output, I_{out}, currents of the Chemical Gilbert Cell, based on the fundamental definition given by the "Gilbert Gain Cell", will be represented by:

$$\begin{aligned} I_{in} &= I_{ISFET1} - I_{ISFET2} \\ &= 2xI_x \end{aligned} \tag{6.9}$$

leading to the definition of x for the Chemical Gilbert Cell as:

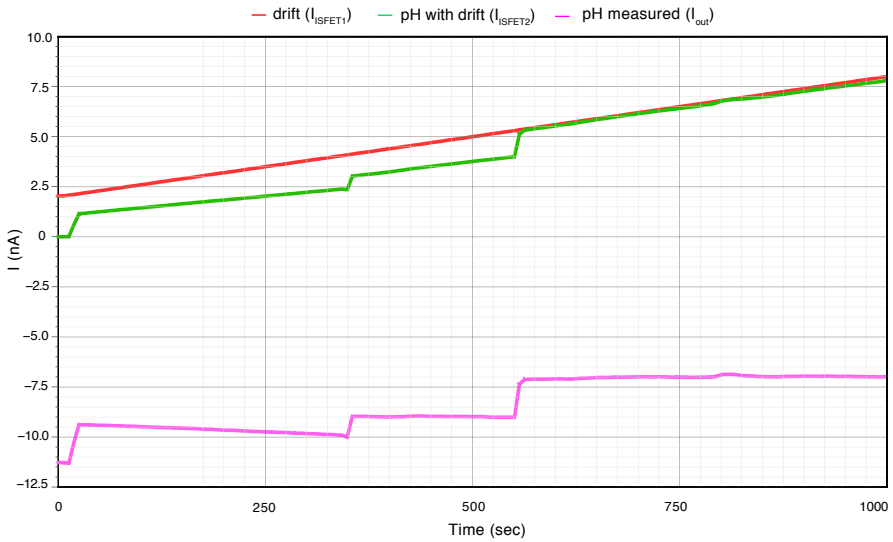


Figure 6.10: Transient response of the Chemical Gilbert Cell

$$x = \frac{I_{in}}{2I_x} = \frac{I_{\Delta pH}}{2I_x} \tag{6.10}$$

Thus the differential output current I_{out} of the Chemical Gilbert Cell will be following the principles proposed by Eq. 6.10 and Eq. 6.2 and will be expressed as:

$$I_{out} = \frac{I_x + I_y}{I_x} I_{in} = AI_{in} = AI_{\Delta pH} \tag{6.11}$$

where I_{out} varies linearly with the current change, $I_{\Delta pH}$, generated due to the pH difference created between the two ISFET sensors, and this is multiplied by a discrete gain value A.

6.4.1 Simulation results

The circuit was designed and simulated in a typical 0.35μm 2P4M CMOS technology using Cadence Spectre (5.1.41isr2) simulator. The design specifications for the Chemical Gilbert Cell were, a supply voltage of 3.3V and device sizes optimised at (W/L) 10μm/10μm for all transistors so that matching errors were minimised and 1/f noise was reduced. ISFET sensors were used with an electrical size of 200μm x 1μm.

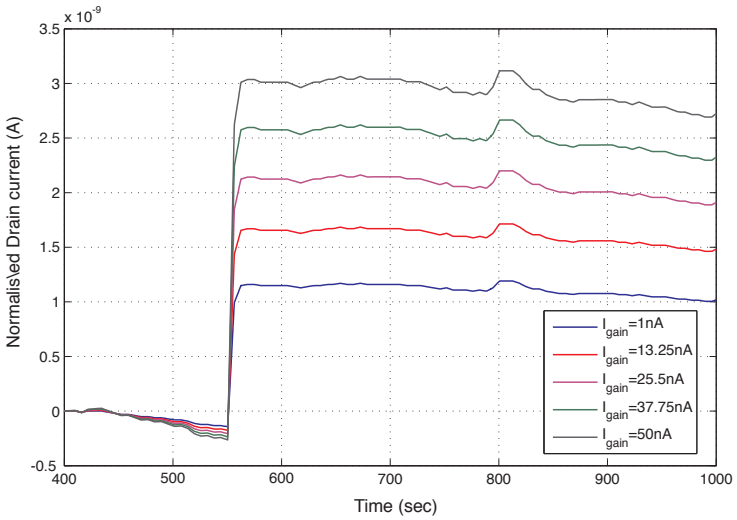


Figure 6.11: Parametric analysis on I_{gain} at 5 steps, from 1nA to 50nA

In order to test the Chemical Gilbert Cell, we used real ISFET data measured from an experiment in which pH was varied from 7.7 to 8.3 in steps of 0.3 pH. For this we used I_x=10nA, I_y=5nA and I_{gain}=10nA. Transient simulation results are shown in Fig. 6.10, using normalised values of simulated drift as well as the real extracted data from a pH dependent reaction, applied as inputs to sensors $ISFET1$ and $ISFET2$ respectively. The outputs of two ISFETs are subtracted, producing a current change due to the change in pH stated as $I_{\Delta pH}$, and then multiplied by a gain value set by the parameter A, as shown in Eq. 6.11, providing with a differential output current. Furthermore, what we can see in Fig. 6.10 is that the differential measurement simulation results show a drift reduction from 0.36nA/min for the single ISFET to just 3fA/min for the differential output.

A parametric analysis was also conducted on the gain current, I_{gain}, as is defined through Eq. 6.5. This was varied from 1nA to 50nA in a time window of less than 500s, as is seen in Fig. 6.11. What we can see is that the gain can be tuned within a range of required current steps for a given pH change. As can be seen by Eq. 6.5, the gain can be dependent on both the I_{gain} and the bias current of the ISFET, which for an I_x of 1nA can be as much as 40dB for this configuration.

The temperature stability of the system is shown in Fig. 6.12 for varying temperature conditions from 0^oC by up to 100^oC. For the clarity of the temperature variation effect, we display only 4 temperature changes. It can be observed that the response remains consistent within the temperature range applied, with the maximum absolute temperature percentage

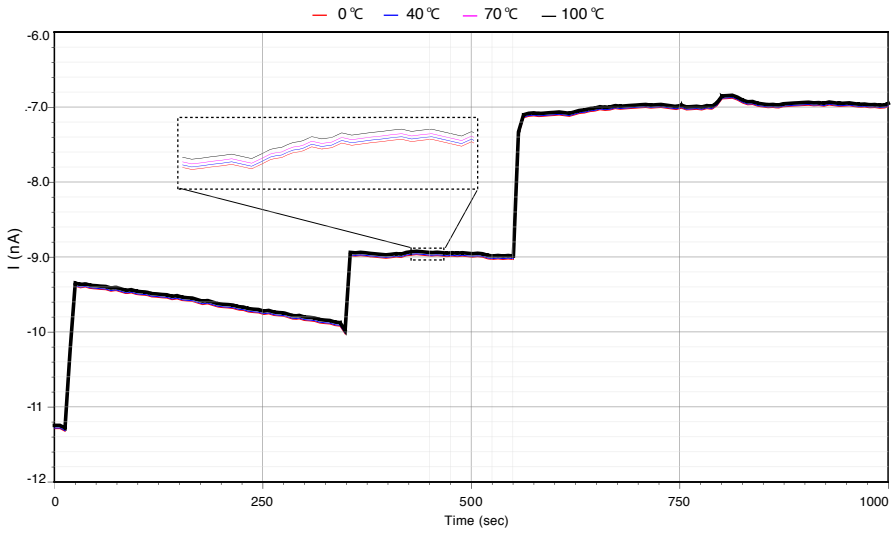


Figure 6.12: Temperature variation at 11 steps, from 0 °C to 100 °C

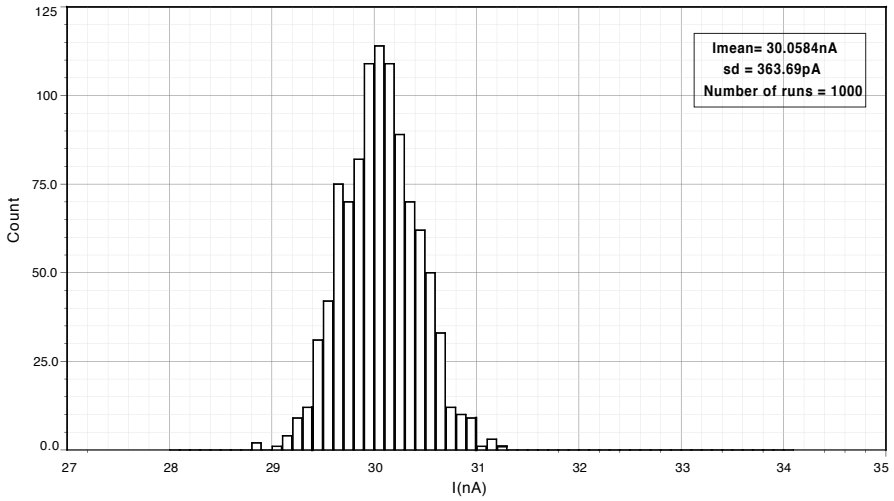


Figure 6.13: Monte Carlo analysis

change to be around 0.7% from the mean output current at room temperature conditions.

Finally, a Monte Carlo analysis of the circuit was conducted in order to test the variations of the devices in terms of process and mismatch parameters, after applying a DC current of 10nA as a differential input. The results of 1000 runs for the values of the cell's differential output current I_{out} are illustrated in Fig. 6.13, producing a resulting I_{mean} of 30.1nA with a standard deviation of 363.7pA, showing that the ISFET based Chemical Gilbert Cell is

rather robust to process and mismatch variation.

6.5 Fabricated system

The Chemical Gilbert Cell was fabricated in a typical 0.35μm 2P4M CMOS process, as seen in Fig. 6.14 (bottom), with each ISFET sensor designed[1] with a sensing area of 34μm×100μm and an electrical area of 200μm×1μm, as shown in Fig. 6.15. All sizes of PMOS devices used were optimised at (W/L) 10μm/10μm so that matching errors were minimised and 1/f noise was reduced. The area covered by circuit was 1960μm^2 (70μm×28μm).

The microfluidic assembly adapted on the ISFET based CMOS microchip in the form of a Lab-on-Chip as introduced in Section 5.4, Chapter 5, was used to achieve exposure of the ISFET sensors in buffers of different pH for the differential reaction monitoring. The same platform was used as in Fig. 5.10 to prevent cross contamination of fluid through the chambers, offering a more accurate signal derived from the Chemical Gilbert Cell. Both ISFETs were biased in the weak inversion mode of operation.

6.6 Measured results

The Lab-on-Chip was experimentally tested using a semiconductor parameter analyser (Keithley 4200SCS). During all experiments the CMOS chip was biased at 3.3V and ISFETs were biased at a static drain current of 20nA, optimised for weak inversion operation. pH solutions 8.15 and 6.83 were obtained from DNA reactions, as detailed in Section 4.4, Chapter 4, with 8.15 indicating the resulting pH of a DNA reaction not occurring when DNA methylation is absent in given genetic areas and 6.83 to indicate the pH of a DNA reaction taking place when DNA methylation is present in the given genetic areas. The ΔpH of 1.32 indicates the minimum change in pH that was observed in the experimental section, Section 4.4, Chapter 4, used as a limit of detection for the experimental validation of the Chemical Gilbert Cell.

pH buffer solutions 5, 6, 7, 8 and 9 were prepared using 100mM Tricine and 1M KCl, adjusting the pH using 10M NaOH and 1M HCl. All four solutions were provided by Sigma-Aldrich. A commercially available Al_2O_3 ISFET sensor with an Ag/AgCl reference electrode

[1]ISFET sensors were designed based on measured devices fabricated within the Centre for Bio-Inspired Technology [33].

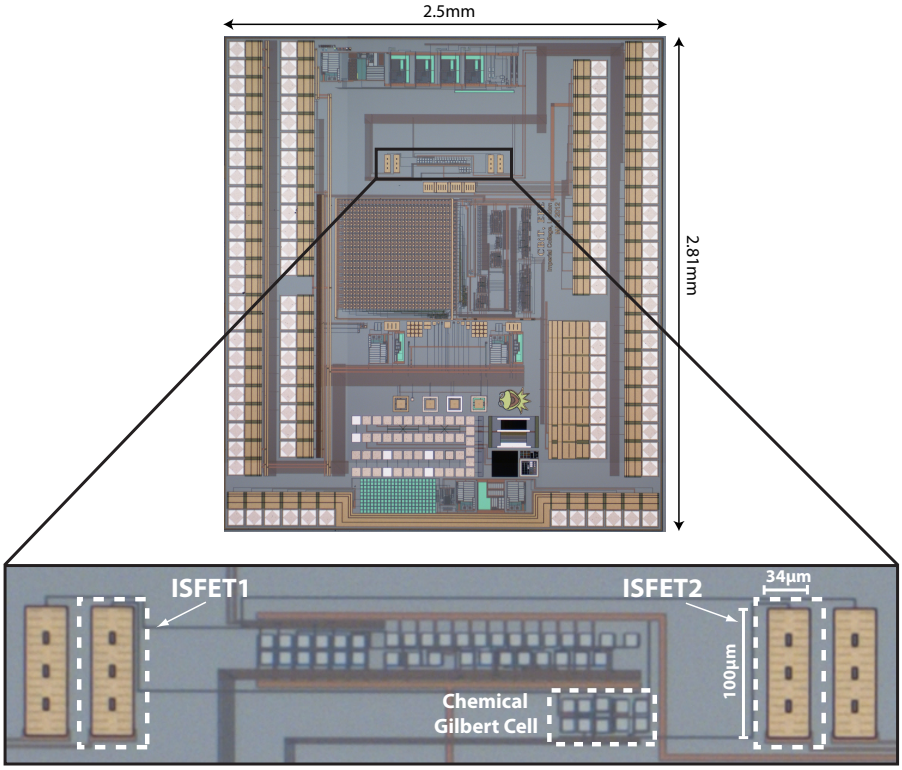


Figure 6.14: Top: Microphotograph of the floorplan of the fabricated die, highlighting in black the relevant circuit area. Bottom: Magnification of the ISFET based Chemical Gilbert Cell and of the two ISFETs connected to it.

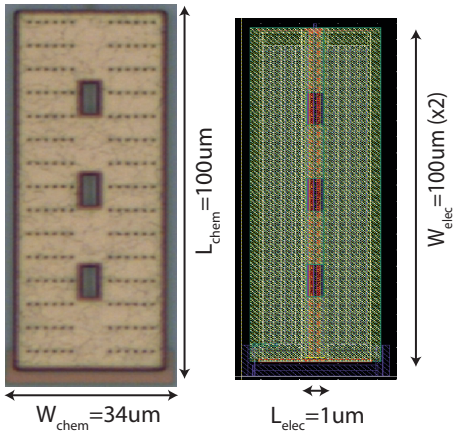


Figure 6.15: Single ISFET sensor with pixel dimensions. Left: Chemical sensing area of the ISFET. Right: Electrical dimensions of the gate.

was also used as a pH probe (Sentron Europe B.V.) for conducting the pH measurements after having completed a calibration process as described in Appendix C. The pH solutions were titrated in the microfluidic chambers using 20μl Eppendorf micropipette tips.

The output current I_{out} was measured after applying a voltage bias of 1V to the output to allow the current mirror of M5 and M6 (Fig. 6.9) to work in saturation. Both ISFETs in chambers were externally and independently biased with I_x=20nA in a buffer environment of pH 7. I_x=20nA was chosen based on the linear weak inversion operating region. After each pH change was induced by inserting a pH buffer (5-9) in Ch 1, both chambers were flushed with pH 7 and ISFETs were biased at I_x=20nA so that (a) the conditions for each recording remain the same before every pH change being induced and (b) the chamber is refilled with buffer solution in case of evaporation of fluid during the previous recording, providing both ISFETs with a maximum volume of exposure in fluid.

Experimental results are presented in this section, demonstrating the electrical functionality of the ISFETs in weak inversion as well as their sensitivity under different pH solutions in each chamber. The capability of the Chemical Gilbert Cell under the Lab-on-Chip set-up is also demonstrated by producing a differential output current read-out during one pH step change (induction of different pH buffer in Ch 1, see Fig. 5.10b) for a constant gain at first. Also, the pH sensitivity of the cell is shown during four pH step changes, followed by the results of a gain experimental analysis on the cell's differential output current I_{out} for one pH step change, followed by the gain tunability characteristics for four pH step changes. Finally, the drift minimisation of the cell is shown, pointing out a 100 times reduction of drift when a differential current output is computed in comparison to the drift observed at a single ISFET's current output signal.

6.6.1 DC characteristics

Initially, the I_D-V_{GS} characteristics for both ISFETs were conducted, as seen in Fig. 6.16, at a buffer solution of pH 7 at room temperature, to confirm the behaviour of ISFETs in weak inversion. The sources of both ISFETs were biased independently at 3.3V and the voltage applied on the reference electrode, V_G, was swept from 0V to 5V.

The y-axis shows the drain current and the x-axis the gate voltage subtracted from the source voltage of the ISFETs. It can be seen that the linearity of the exponential drain current characteristic is for currents from 0.1nA to 200nA for a range of source gate voltage

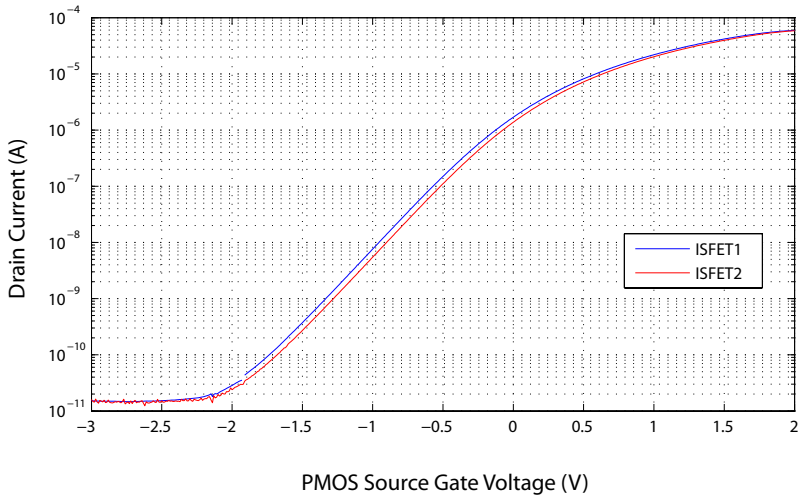


Figure 6.16: Measured I_D-V_{GS} sweep of the two pMOS ISFETs for pH buffer solution of 7, showing the relationship between the drain current and the applied source gate voltage.

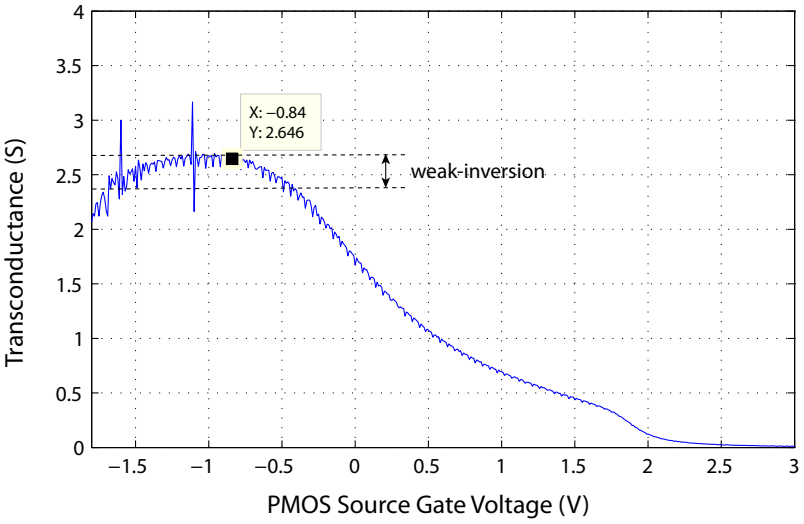


Figure 6.17: Transconductance with respect to source gate voltage for pH buffer solution of 7. The operational area of linear weak inversion range is highlighted.

of -1.7V to -0.5V. This means that weak inversion operation can be safely guaranteed for measured currents below 200nA. The validity of this assumption was confirmed in Fig. 6.17, showing the transconductance efficiency for pH 7. It is clearly shown that weak inversion can be reliably achieved in the area defined by the dotted lines, which is approximately covering an area of up to 10% reduction in the maximum peak of the linear transconductance

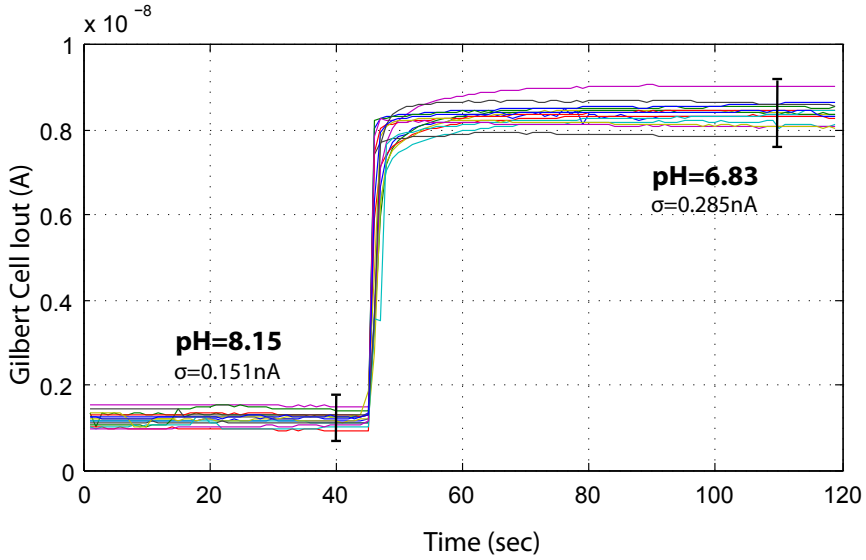


Figure 6.18: Transient response of 15 repeats over the course of two days of the Chemical Gilbert Cell's differential output I_{out} during a pH step change from 8.15 to 6.83 for I_{gain} at 10nA. Standard deviation bars of the pH recordings are also displayed for all repeats, seconds before the pH jump and towards the end of the recording.

efficiency range. This corresponds to source gate voltage of -0.84V to achieve optimal conditions of operation at an ISFET drain current of 20nA, which is our chosen ISFET DC current (I_x) for all experiments.

6.6.2 pH change

To test the response of the Chemical Gilbert Cell to pH changes, an experiment was conducted using pH values chosen as such according to the minimum range of values to discriminate the event of amplification, before and after a DNA chain extension reaction [14]. At first pH 8.15 was added in both chambers, depicted in Fig. 5.10b. Both ISFET sources were biased to give an I_x of 20nA, which corresponds to source gate voltage of -0.84V based on the DC characteristics extracted from Fig. 6.16.

The reference electrode voltage was kept steady at 3V and I_{gain} was tuned at 10nA. An injection of pH 6.83 was then applied to Ch 1 where $ISFET1$ was located, leading to a ΔpH of 1.3 between chambers. The experiment was repeated 15 times within the period of 48 hours and the transient measured response of the Chemical Gilbert Cell's differential output current, I_{out}, was monitored as shown in Fig. 6.18.

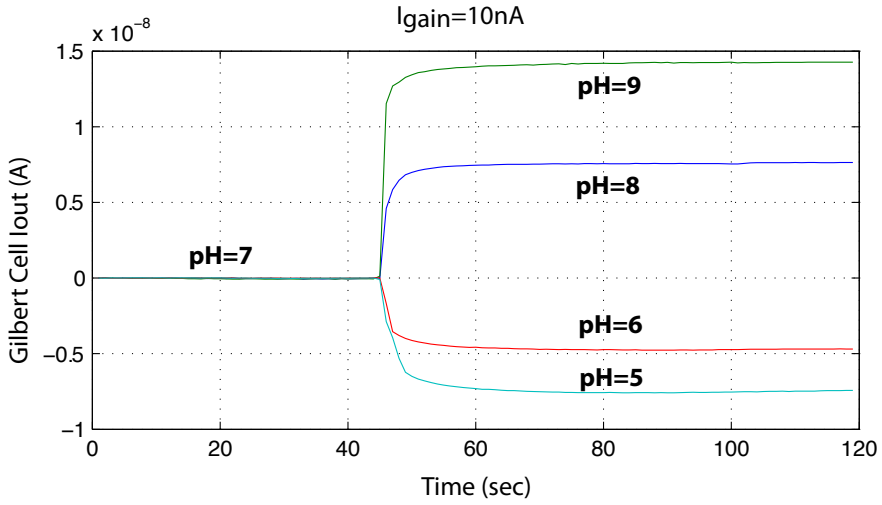


Figure 6.19: pH sensitivity of the Chemical Gilbert Cell showing the transient response of the differential output I_{out} for I_{gain}=10nA during four steps of pH change.

Table 6.1: ΔI_{out} for I_{gain}=10nA during four pH step changes

pH	5	6	7	8	9
ΔI_{out}(nA)	-7.564	-4.754	0	7.566	14.25

It is shown that the differential current I_{out} undergoes a positive change from around 1.2nA at pH 8.15 to 8.3nA at pH 6.83, creating a ΔI_{out} of 7nA for a ΔpH of 1.32. The standard deviation values before and after the pH jump, as can be seen in Fig. 6.18, were obtained from the data values at 40sec (just before the pH jump) for pH 8.15 and at 110s for pH 6.83 (after the pH jump towards the end of the pH recording). Their values satisfy the variation tolerance of the data obtained since they apply a less than 10% variation in the data values. As for the pH sensitivity of the ISFETs during this pH step, the average value of the ISFET source currents calculated during the 15 repeats was found to be 14.25nA which corresponds to -0.84V from the DC characteristics seen in Fig 6.16.

Following on from the single pH step change, four steps of pH changes were performed to confirm the system's sensitivity to all pHs, using a starting pH of 7 in both chambers, followed by injecting pH 5, 6, 8 and 9 in Ch 1. The results are shown in Fig. 6.19 and the values of ΔI_{out} with respect to the pH changes are summarised in Table 6.1. In between

Table 6.2: Average values of three repeats of ΔI_{out} for different I_{gain} values as seen in Fig. 6.20 with standard deviation results

I_{gain}(nA)	10	20	50	100	200
ΔI_{out}(nA)	6.89±0.46	7.96±0.49	13.24±0.40	18.74±0.08	30.2±0.52

the injections of different buffers, the volume of Ch 1 was flushed with pH 7 while Ch 2 was filled up with the same pH buffer during the process of the sensitivity experiment. Flushing Ch 2 with pH 7 before any recording was managed continuously during this experiment to eliminate evaporation of the buffer as realistically as possible leading to better diffusion of ions in the sensing surface of the ISFET. ISFET currents were also biased at 20nA before a new pH was inserted in Ch 1. After the currents were stabilised at a post pH change phase, the sources of both ISFETs were reduced to achieve 20nA independently, through an external biasing configuration, so that the experimental conditions were kept as similar as possible before flushing Ch 1 with a new buffer.

What can mainly be derived from Fig. 6.19 is that the output current I_{out}, for a given gain value (I_{gain}=10nA), responds to pH step changes derived from the chemical response of $ISFET1$, achieving a pH sensitivity of 45mV/pH, which is in agreement with ISFETs in unmodified CMOS [5]. Additionally to that, the current change observed for the pH step changes of pH 7 to 8 and 7 to 9 is relatively higher than the equivalent step changes of 7 to 6 and 7 to 5, which can be explained from the exponential characteristic of the ISFETs operating in weak inversion.

6.6.3 Tunable gain

An experimental analysis was also conducted on the gain current I_{gain} to demonstrate the gain tunability of the system. Gain current values varying from 10nA to 200nA were used, for a pH step change of 8.15 to 6.83. Each step was repeated three times resulting in collecting recordings within the time frame of 48 hours. The time window of each recording was 120s. For each gain value, ISFETs were initially biased with currents of 20nA and then I_{out} was monitored over time for the given pH step for all I_{gain} values. The values of I_{out} were normalised for purposes of clarity of differentiation of the output currents for the different gain values under the given pH change.

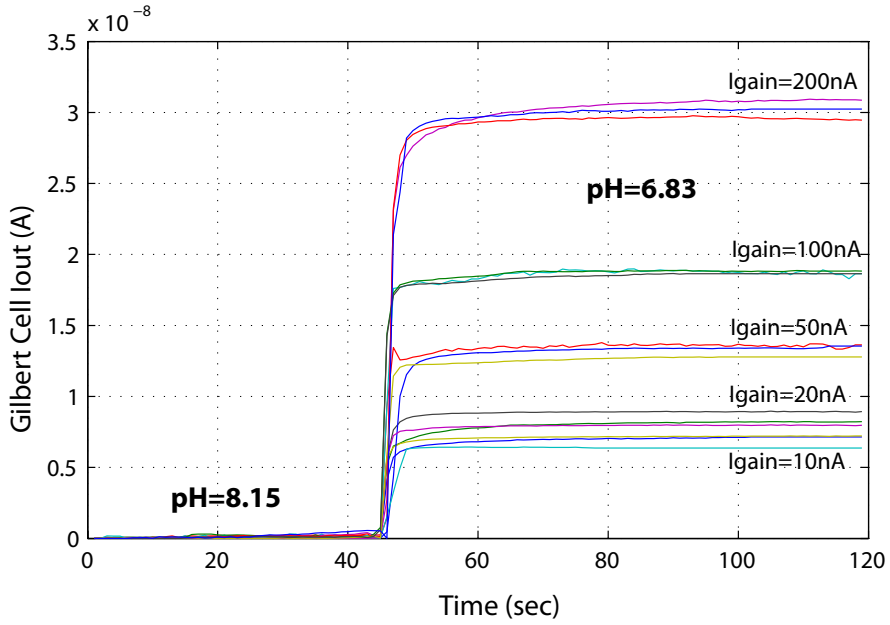


Figure 6.20: Experimental analysis on I_{gain} from 10nA to 200nA during a transient response of the Chemical Gilbert Cell's differential output I_{out} for a pH step change from 8.15 to 6.83. 3 repeats were performed per pH change.

Results are shown in Fig. 6.20 and values for I_{gain} from 10nA to 100nA are summarised in Table 6.2. The average values of all three repeats, as shown in Fig. 6.20, are collected at t=100s. Standard deviation values are also calculated for all repeats for each I_{gain} value for the given pH change. The results of the analysis show that for a minimum gain current of I_{gain}=10nA and I_x=20nA, a minimum ΔI_{out}=6.89nA is achieved. Similarly, for a maximum gain current of I_{gain}=200nA a maximum ΔI_{out}=30.2nA is achieved. This analysis confirms that the gain can be tuned for a given pH change, which in turn proves experimentally that the gain of the Chemical Gilbert Cell, as defined in Eq. 6.5, is dependent on the input biasing current, I_x, and the gain current I_{gain}, Eq. 6.4.

Moreover, further gain tunability experiments were conducted, covering four pH step changes, as described in Section 6.6.2, but instead of applying a fixed gain term, the gain values were varied from 10nA to 200nA. Initially, pH 7 was inserted in both chambers (Ch 1, Ch 2) followed by biasing both ISFETs, exposed in both chambers, at 20nA. Each pH buffer from the range 5, 6, 7 and 9 was then induced in Ch 1, creating a ΔpH and thus a ΔI_{out}. Fig. 6.21 illustrates the experimental results of the transient response of the cell's differential output I_{out} for five gain values. Two repeats are shown with the average value

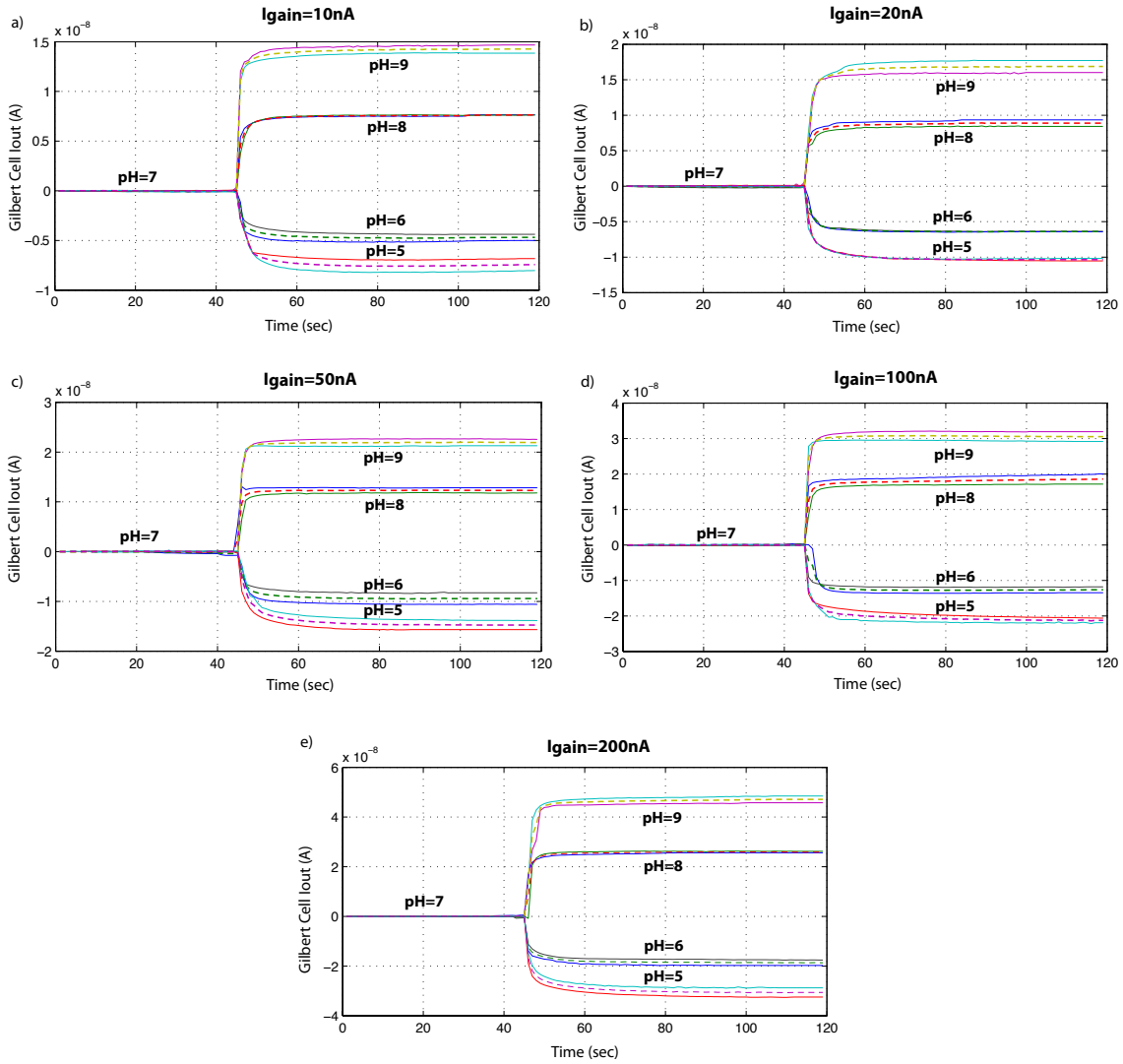


Figure 6.21: Transient response of the Chemical Gilbert Cell's differential output I_{out} for different values of I_{gain} following 4 pH step changes. In both chambers a buffer of pH 7 was initially induced giving a differential output current of 0nA, followed by a step change of pH when pH buffers of 5, 6, 8 and 9 were induced. The experimental results shown are confirmed after two repeats. The average value is also displayed as a dotted line.

of which been displayed as a dotted line in each subfigure.

The results of Fig. 6.23 can be summarised in Fig. 6.22 which illustrates more clearly the experimental analysis conducted on gain tunability. This was conducted for the purposes of depicting a better correlation between I_{out} and pH for varying values of I_{gain}, leading to the observation that the differential current produced during the pH change of 5 to 7

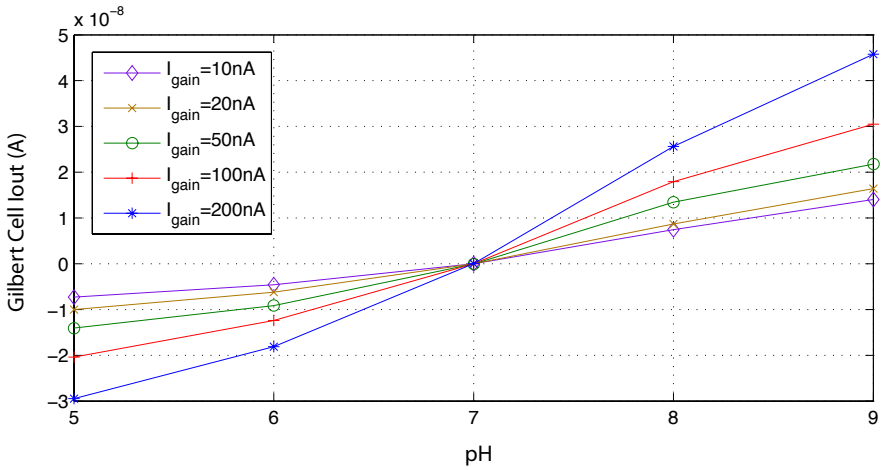


Figure 6.22: Experimental analysis on the differential output I_{out} in the range of four pH values.

Table 6.3: Average values of two repeats of ΔI_{out} in nA for different I_{gain} values as seen in Fig. 6.22 for each pH step

I_{gain}(nA)	pH=5	pH=6	pH=7	pH=8	pH=9
10	-7.282	-4.592	0	7.441	14.05
20	-9.999	-6.219	0	8.678	16.42
50	-14.04	-9.16	0	13.44	21.77
100	-20.39	-12.39	0	17.92	30.5
200	-29.45	-18.1	0	25.62	45.78

was smaller than that during the pH change of 7 to 9, which can be understood from the exponential relationship between current and $[H+]$, as described in Eq. 3.21, Section 3.5.1 in Chapter 3.

Finally, a different view on the results of Fig. 6.22 is shown in Fig. 6.23 whereby the differential output I_{out} is summarised in each subfigure focusing on one pH change per figure while varying I_{gain} from 10nA to 200nA. Two repeats are displayed for each gain value in every pH step change conducted, with the average of two shown in each case. It can be seen that the gain value that provided the minimum deviation in between repeats occurred for I_{gain}=10nA for all pH step changes. The same value was chosen for monitoring the transient measured response of the Chemical Gilbert Cell's differential output current I_{out},

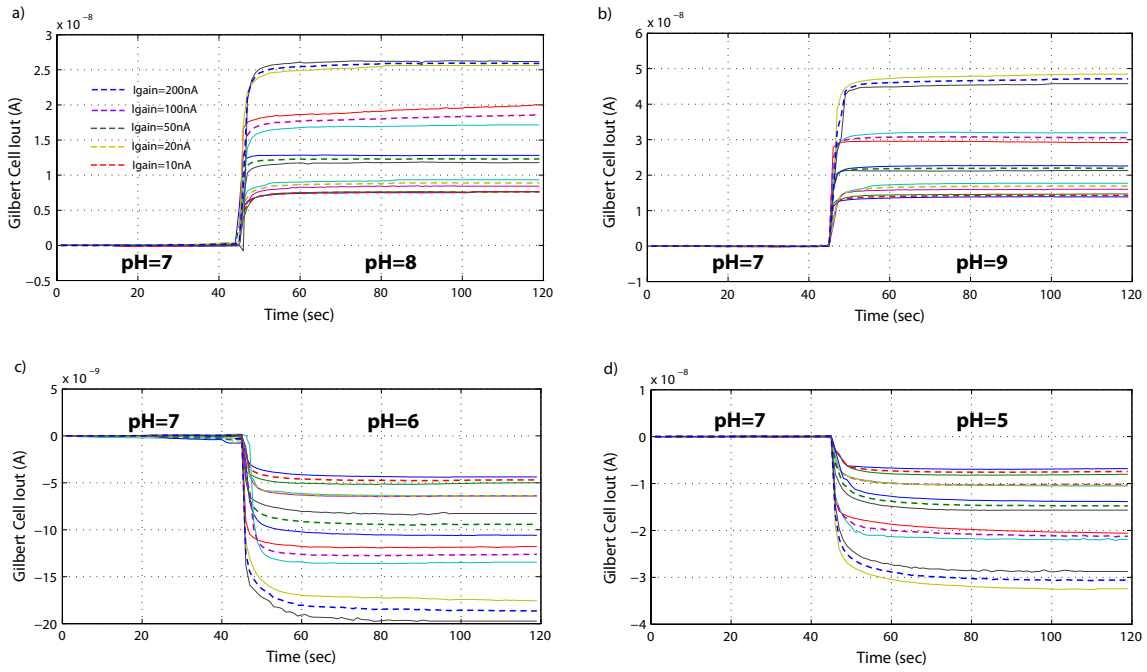


Figure 6.23: Gain variability for four pH steps change in the range of incremental current gains. The average value of two repeats is also displayed as a dotted line.

as seen in Fig. 6.18 and for testing the cell's pH sensitivity for different pH steps, as seen in Fig. 6.19. The biggest deviation on the other hand can be seen for I_{gain} valued 100nA or 200nA regardless the pH of the solution before and after the change.

Shown in Table 6.3 are the results of a differential pH change from 5 to 9 relative to pH 7, with both chambers starting with pH 7. What can be seen is that as I_{gain} increases from 10nA to 200nA, the differential output current I_{out} follows such increase relative to a rise in gain of as much as 15.56dB for a drain current I_x=20nA. This gain however could be made larger by reducing our DC operating current as defined by equation Eq. 6.5. Nevertheless, this still demonstrates efficient gain tunability and sensing capability over a large range of four pH values for very low current consumption.

6.6.4 Drift

Experiments were also conducted in an attempt to monitor the single-ended drift of I_{ISFET}, in comparison to the differential drift, I_{out}, as a result of the Chemical Gilbert Cell's function and thus to investigate the capability of the cell to minimise drift. Since drift varies between ISFETs, given that the threshold voltage of each device is not identical, we ensured the experimental conditions (biasing, temperature, light, pH) constant for both ISFETs during drift monitoring. A buffer solution of pH 7 was inserted in both microfluidic chambers for the scope of the drift monitoring experiment with both ISFETs left to drift for a period of 1000s, with the resuIts of the drift test illustrated in Fig. 6.24.

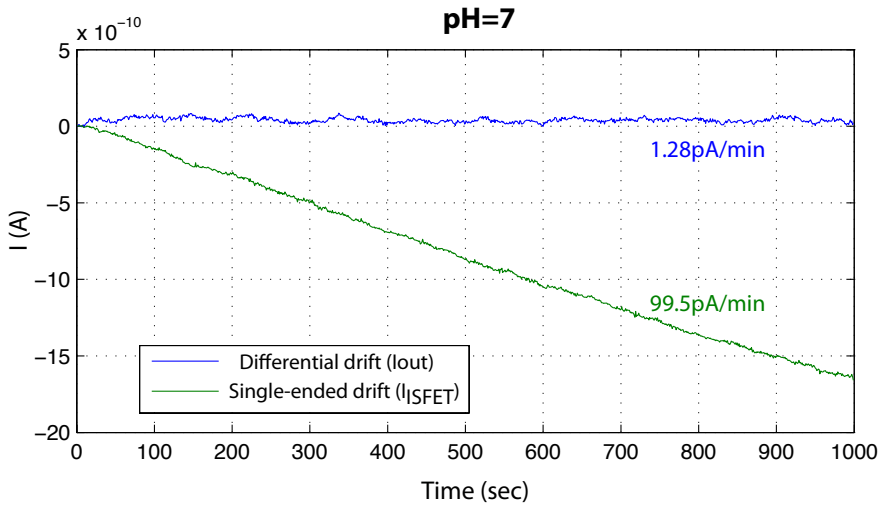


Figure 6.24: Single-ended drift I_{ISFET} in comparison to differential drift I_{out} for pH 7. Drift values are indicated for both current outputs.

To indicate the reduction of drift between the drift value at the beginning of the recording (t=0s) and the same at the end (t=1000s), the term $\Delta I/min$ is introduced to show the transient change of current throughout the course of the experiment, used in this instance to characterise drift. As can be seen from Fig. 6.24, the drift derived from a single ISFET reached the value of 99.5pA/min compared to the drift derived from the differential read out of the Chemical Gilbert Cell, which reached the value of 1.28pA/min for the given pH (pH=7) inserted in both chambers. The currents of both ISFETs were normalised so that the observation of the differential drift over the single-ended was more clear. It can be observed that the differential current output, I_{out}, resulted in almost 100 times reduction of drift in comparison to the drift derived from a single ISFET's current output.

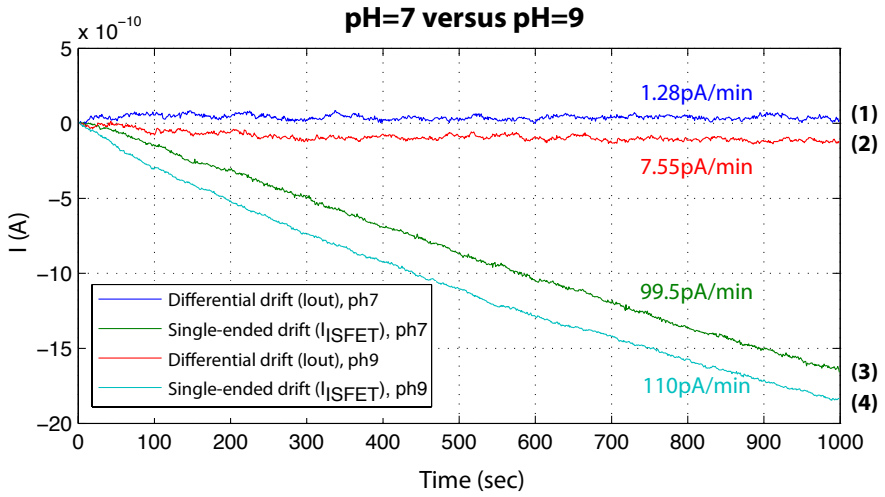


Figure 6.25: Single-ended drift I_{ISFET} in comparison to differential drift I_{out} for pH 7 corresponding to figure indicators (1) and (3) and pH 9 corresponding to figure indicators (2) and (4). Drift values are indicated for both current outputs.

Additionally, a closer comparison on single-ended and differential drift values was made for a buffer solution of pH 9, commonly inserted in both microfluidic chambers. The drift experiment conducted for pH 9 followed the same preparation and set-up as used for pH 7, with both microfluidic chambers starting at the same pH and with the transient response of currents having the same duration of 1000s. The results for pH 9 are superimposed with the results for pH 7 as presented in Fig. 6.25. Drift values, $\Delta I/min$, appear as well for pH 9 for both single-ended and differential output currents. Also, it may be useful to mention that the drift experiment for pH 9 was conducted 5 hours after the one for pH 7, allowing significant time for the ISFETs to 'burn in'.

The results of drift minimisation for pH 9, were comparable to those for pH 7 with the single-ended drift reaching a value of 110pA/min, slightly higher than the value obtained for pH 7. Also, the differential drift obtained for pH 9 reached the value of 7.55pA/min, around 7 times higher than the differential drift measured for pH 7. The results on drift for pH 7 and pH 9, as seen in Fig. 6.25, represent the average values of two repeats of recordings within the course of a day.

An additional observation on these results could be that there seems to be a slightly small pH dependence of the initial drift (single-ended/differential), recorded during the first few minutes of the experiment, on the pH of the solution. This may be explained based

on theory behind changes of the ionic diffusion on an insulator's surface correlated to the pH of the solution that the insulator is exposed to [34]. This may explain the observation of the slightly higher drift in the presence of an alkaline solution. The challenges of the microfluidic set-up including the incredibly small chamber volume (0.3μl) and the oxidation of the Ag/AgCl wire over time didn't allow a further investigation of such observation on the pH dependence of drift. Also, the comparison of drift (single-ended/differential) for pH 7 and pH 9 may not be as fair given that the buffer solution was not re-flushed in chambers to allow replenishment due to evaporation. However, what can be deduced from both Fig. 6.24 and Fig. 6.25 is that there is a clear comparison between the single-ended drift obtained as an output of a single ISFET and the differential drift obtained as an output of the Chemical Gilbert Cell for both pH solutions, demonstrating an additional capability, amongst the previously mentioned, which is drift minimisation.

6.6.5 Power consumption

The system under test operated in the weak inversion region. The total power in the system may be calculated as:

$$P = V_{DD}(I_{ISFET1} + I_{ISFET2} + I_{gain}) \tag{6.12}$$

The system achieves a very low power consumption of 165nW for a biasing current I_x=20nA for both ISFETs and a gain current I_{gain}=10nA, operating at a 3.3V supply. The chip can be operating with biasing currents of as low as 1nA as can be seen in Fig. 6.16 leading to further reductions in power. Nevertheless, with a power consumption of 165nW, this is the lowest reported power consumption for an integrated front-end with ISFET differential monitoring and a tunable gain.

6.6.6 Temperature stability

In this section, the temperature stability of the Chemical Gilbert Cell was attempted to be assessed experimentally without the use of the microfluidic device since the microfluidic chambers' maximum volume capability was 0.3μl and thus the solution available to be heated would not be in excess for a fair comparison with respect to temperature stability between a single ISFET's output and a differential output of the Chemical Gilbert Cell. As a result, the experimental set-up involved the ISFET based CMOS chip covered with epoxy

resin, mounted on pcb, with both ISFETs exposed in the buffer solution used (pH 7). A detailed view on the experimental set-up can be found in Fig. C.4, Appendix C. A fixed potential to the solution was set through the use of a glass Ag/AgCl reference electrode at 3V, to set the operating point of the chip, setting the bias points of the individual ISFETs by applying a suitable bias for weak inversion operation. The sources of the ISFETs were set at 10nA and the gain current of the Chemical Gilbert Cell, I_{gain}, was tuned at 1nA for comparison with the simulation results.

The experimental set-up consisted of a hot plate (RCT basic IKA®-VERKE) used as a heating element of a glass beaker filled with the buffer solution. The hot plate was essential to initially create a stable room temperature condition for the solution in which the chip was dipped in and also to set two temperature points needed to conduct the stability test. The temperature was controlled manually and was monitored using a mercury laboratory thermometer inserted in the solution. A magnetic stirring flea was also used to stir the solution so that the temperature generated by the hot plate was evenly distributed throughout the surface of exposure.

The initial temperature was manually set at 32^oC followed by an increase reaching 42^oC, achieving a ΔT=10^oC units followed by a similar decrease of the same amount of units. The results of the temperature stability experiment are shown in Fig. 6.26 whereby it can be seen that there is a reduced temperature dependence on the differential signal compared to the single-ended one, with a change in the differential output current to be around 7 times less than for the single ISFET as given by:

$$\left.\frac{I_{ISFET_{T1}} - I_{ISFET_{T2}}}{T1 - T2} = 570pA/^{\circ}\text{C}\right\} \qquad \textit{Single-ended} \tag{6.13}$$

$$\left.\frac{I_{out_{T1}} - I_{out_{T2}}}{T1 - T2} = 85pA/^{\circ}\text{C}\right\} \qquad \textit{Differential} \tag{6.14}$$

The ISFETs source currents showed an increase from 10nA to approximately 20nA as the temperature increased from 32^oC to 42^oC following a decreasing trend as the temperature decreases from 42^oC to 32^oC. This happens due to the temperature dependence of the threshold voltage of the ISFET (Chapter 3) and thus of the drain current. This applies respectively to the decrease of the temperature leading to the decrease of the drain current of the ISFET. There was also observed a small offset in the measured ISFET currents of around 0.5nA to 1nA which can be explained due to the trapped charge [5] before heating

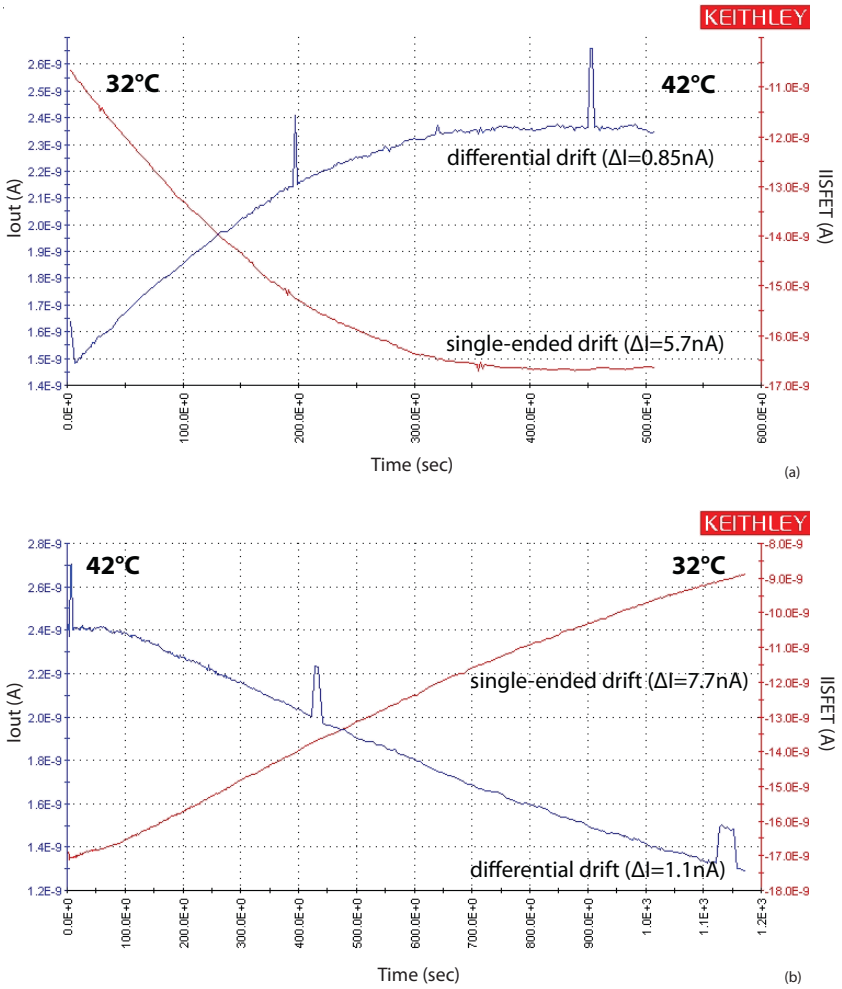


Figure 6.26: Temperature stability for a single ISFET in comparison to the differential output I_{out} for (a) ascending temperature from 32^{o}C to 42^{o}C and (b) descending temperature from 42^{o}C to 32^{o}C.

the sensors, charge that was potentially released after heating the chip.

It needs to be mentioned that keeping the temperature stable was one of the main constraints of using a hot plate that didn't exhibit a linear behaviour since the heating element was applied to the glass beaker and therefore to the total volume of the solution. As a result, the exponential temperature increase profile, as seen in Fig. 6.26, is not a result of the use of the Chemical Gilbert Cell but is due to the nonlinearity of the heater. This resulted to a significant time lag of several minutes between tuning the temperature manually and observing the actual change in the thermometer without exceeding the maximum/minimum targeted temperature value, which could explain the existence of spikes in Fig. 6.26 as well.

6.7 Summary

In this chapter, the idea of an ISFET based Chemical Gilbert Cell was presented, simulated, fabricated and finally integrated in a Lab-on-Chip implementation, demonstrating its ability for monitoring differentially derived changes in pH required for DNA amplification taking place in cases of existence of DNA methylation in the DNA target. The system's properties and performance are summarised in Table 6.4.

Simulation results showed the capability of the ISFET based Chemical Gilbert Cell for computing a differential current output amplified by a gain value, set by a gain parameter, A, allowing stable drift reduction. Simulations of the designed circuit based on real ISFET data demonstrated a capability for drift reduction, temperature stability and tunable amplification by the linearly dependent gain of the "Gilbert Gain Cell". These results highlighted an ideal application of the proposed circuit, such as applications where discrete pH changes occur due to a reaction taking place as a result of DNA amplification through methods such as Polymerase Chain Reaction (PCR) or Loop-Mediated Isothermal Amplification (LAMP), as has been explained in Chapter 4.

The theory behind the proposed circuit was then experimentally validated with the concept of the ISFET based Chemical Gilbert Cell proved by demonstrating its capabilities in the form of a fabricated system. Its capabilities mainly focus (a) on the ability to achieve continuous differential current-mode measurements of pH signals obtained from biochemical reactions of DNA amplification sensed by ISFET sensors, (b) on gain tunability through the use of an adjustable gain by tuning a single current with results confirming 15.56dB gain at 20nA of ISFET bias current, (c) on drift reduction reaching a ratio of 100:1 in favour of the

Table 6.4: System properties and performance characteristics

Technology	AMS 0.35μm 2P4M CMOS
Die dimensions	2.5mm × 2.81mm
Passivation Si_3N_4/SiO_2	1030nm/1000nm (about 120fF)
ISFET pixel: W×L (electrical)	200μm × 1μm
ISFET pixel: W×L (chemical)	34μm × 100μm
Sensing area	3400μm^2
Transistor sizes (W×L)	10μm × 10μm
Transistors per pixel	10
Power supply	3.3V
Chamber size	1mm × 0.4mm × 0.4mm
Chamber diameter	400μm
Chamber volume	0.3μl
pH sensitivity	45mV/pH
Gain @ (I_{DC}=20nA, I_{gain}=200nA)	15.56dB
Drift reduction	-37.8dB
Static ISFET drain current	20nA
Power consumption @ (I_{DC}=20nA, I_{gain}=10nA)	165nW

differential drift produced versus the single-ended drift derived from a single ISFET, making it ideal for robust, low power chemical measurement and (d) on temperature stability in favour of the differential output of the cell in comparison to a single ISFET output.

To achieve the cell's abilities mentioned above, a Lab-on-Chip interface was introduced with a microfluidic configuration developed, consisting of two micro-chambers, enabling the precise monitoring of chemical signals of certain pH produced by separate reactions generated in each chamber, therefore bringing the privilege of using two ISFETs independently. This allowed for differential monitoring of signals that could not be detected otherwise if a common "bucket solution" approach was chosen to be followed, exposing both ISFETs in the same buffer solution. In the current Lab-on-Chip interface, changes in the pH profile were applied in Ch 1, while Ch 2 was kept chemically stable, keeping the same pH solution in chamber. This resulted in the computation of differential current-mode output signals, proving the concept of the Chemical Gilbert Cell's operation.

The Chemical Gilbert Cell performed good, repeatable, differential operation, achieving a ΔI_{out} of around 7nA, for a given pH change, with a less than 10% variation in 15 repeats. The system's sensitivity was confirmed for 4 pH step changes for a given gain value achieving

a good differential pH sensitivity of 45mV/pH, derived from a chamber volume of 0.3μl. Moreover, the gain tunability of the system was tested, showing that the gain of the system can be efficiently tuned for a large range of pH, using only a single and adjustable current, I_{gain}, for very low current consumption. Finally, drift minimisation of continuously recorded pH signals was achieved leading to an almost 100 times reduction of drift in the differential current output produced by the cell compared to the drift derived by from a single ISFET's output current. The system achieved a measured low power consumption of 165nW due to the weak inversion operation regime.

The advantages of using a differential current-mode configuration as the Chemical Gilbert Cell can be exploited for any biomedical application, such as DNA methylation detection which includes the processing step of DNA amplification, which requires large scale integration especially when multiple genes need to be processed in parallel. It can also be combined with differential monitoring and ease of gain tunability combined with reduction of drift and high resolution. The use of such configuration can be a solution to several challenges found in DNA amplification and detection such as chemical noise, sensitivity of detection and good signal acquisition, facilitating its use for large scale integration. Looking forward into the future, we see many potential applications of using the Chemical Gilbert Cell for large sensing arrays in biomedical driven areas, such as in Single Nucleotide Polymorphism (SNP) detection, DNA sequencing and in general in low power Lab-on-Chip systems, with the potential of integration for ratiometric detection, as described in Chapter 5, the "Methylation Cell", to be one of these, improving the robustness of the approach by eliminating the effects of the non-idealities of ISFETs.

References

[1] C. Toumazou and P. Georgiou, "Bio-inspired semiconductors for early detection and therapy," *IEEE Asian Solid-State Circuits Conference (ASSCC)*, pp. 129–132, 2011.

[2] P. Georgiou and C. Toumazou, "Semiconductors for early detection and therapy," *Electronics letters*, vol. 47, no. 26, pp. S4–S6, 2011.

[3] J. Bausells, J. Carrabina, A. Errachid, and A. Merlos, "Ion-sensitive field-effect transistors fabricated in a commercial CMOS technology," *Sensors and Actuators B: Chemical*, vol. 57, no. 1-3, pp. 56–62, 1999.

[4] L. Shepherd and C. Toumazou, "Weak inversion ISFETs for ultra-low power biochemical sensing and real-time analysis," *Sensors and Actuators B: Chemical*, vol. 107, no. 1, pp. 468–473, 2005.

[5] P. Georgiou and C. Toumazou, "ISFET characteristics in CMOS and their application to weak inversion operation," *Sensors and Actuators B: Chemical*, vol. 143, no. 1, pp. 211–217, 2009.

[6] C. Z. Goh, P. Georgiou, T. Constandinou, T. Prodromakis, and C. Toumazou, "A CMOS-based ISFET chemical imager with auto-calibration capability," *IEEE Sensors*, vol. 11, no. 12, pp. 3253–3260, 2011.

[7] P. Georgiou and C. Toumazou, "Chemical bionics-a novel design approach using ion sensitive field effect transistors," pp. 229–232, 2008.

[8] W. Juffali, P. Georgiou, and C. Toumazou, "ISFET based urea: Creatinine translinear sensor," *Electronics letters*, vol. 46, no. 11, pp. 746–748, 2010.

[9] S. Purushothaman, C. Toumazou, and C. Ou, "Protons and single nucleotide polymorphism detection: a simple use for the Ion Sensitive Field Effect Transistor," *Sensors and Actuators B: Chemical*, vol. 114, no. 2, pp. 964–968, 2006.

[10] W. Wong, P. Georgiou, C.-P. Ou, and C. Toumazou, "PG-ISFET based DNA-logic for reaction monitoring," *Electronics letters*, vol. 46, no. 5, pp. 330–332, 2010.

[11] D. Garner, H. Bai, P. Georgiou, T. Constandinou, S. Reed, L. Shepherd, W. Wong, K. Lim, and C. Toumazou, "A multichannel DNA SoC for rapid point-of-care gene detection," *IEEE Conference on Solid-State Circuits (ISSCC)*, pp. 492–493, 2010.

[12] J. Rothberg, W. Hinz, T. Rearick, J. Schultz, W. Mileski, M. Davey, J. Leamon, K. Johnson, M. Milgrew, M. Edwards, *et al.*, "An integrated semiconductor device enabling non-optical genome sequencing," *Nature*, vol. 475, no. 7356, pp. 348–352, 2011.

[13] M. Kalofonou, P. Georgiou, C.-P. Ou, and C. Toumazou, "An ISFET based translinear sensor for DNA methylation detection," *Sensors and Actuators B: Chemical*, vol. 161, no. 1, pp. 156–162, 2012.

[14] M. Kalofonou and C. Toumazou, "Semiconductor technology for early detection of DNA methylation for cancer: From concept to practice," *Sensors and Actuators B: Chemical*, vol. 178, pp. 572–580, 2013.

[15] P. Bergveld, "Thirty years of ISFETOLOGY - what happened in the past 30 years and what may happen in the next 30 years," *Sensors and Actuators B: Chemical*, vol. 88, no. 1, pp. 1–20, 2003.

[16] J. Christen and A. Andreou, "Design, fabrication, and testing of a hybrid CMOS/PDMS microsystem for cell culture and incubation," *IEEE Transactions on Biomedical Circuits and Systems*, vol. 1, no. 1, pp. 3–18, 2007.

[17] L. Shepherd, P. Georgiou, and C. Toumazou, "A novel voltage-clamped CMOS ISFET sensor interface," pp. 3331–3334, IEEE, 2007.

[18] P. Bergveld, A. Van Den Berg, P. Van der Wal, M. Skowronska-Ptasinska, E. Sudhölter, and D. Reinhoudt, "How electrical and chemical requirements for REFETs may coincide," *Sensors and Actuators*, vol. 18, no. 3, pp. 309–327, 1989.

[19] E. Muller, P. Woias, P. Hein, and S. Koch, "Differential ISFET/REFET pairs as a reference system for integrated ISFET-sensor arrays," *International Conference on Solid-State Sensors and Actuators*, pp. 467–470, 1991.

[20] B. Palan, F. Santos, J. Karam, B. Courtois, and M. Husak, "New ISFET sensor interface circuit for biomedical applications," *Sensors and Actuators B: Chemical*, vol. 57, no. 1, pp. 63–68, 1999.

[21] L. Ravezzi, D. Stoppa, M. Corra, G. Soncini, G.-F. Dalla Betta, and L. Lorenzelli, "A CMOS ASIC for differential read-out of ISFET sensors," *IEEE International Conference on Electronics, Circuits and Systems (ICECS)*, vol. 3, pp. 1513–1516, 2001.

[22] V. Chodavarapu, A. Titus, and A. Cartwright, "CMOS ISFET microsystem for biomedical applications," *IEEE Sensors*, pp. 109–112, 2005.

[23] P. Hammond, D. Ali, and D. Cumming, "Design of a single-chip pH sensor using a conventional 0.6-μm cmos process," *IEEE Sensors*, vol. 4, no. 6, pp. 706–712, 2004.

[24] J. Wei, H. Yang, H. Sun, Z. Lin, and S. Xia, "A fully CMOS-integrated pH-ISFET interface circuit," *6th International Conference on ASIC (ASICON)*, vol. 1, pp. 365–367, 2005.

[25] V. Chodavarapu, A. Titus, and A. Cartwright, "Differential read-out architecture for CMOS ISFET microsystems," *Electronics Letters*, vol. 41, no. 12, pp. 698–699, 2005.

[26] Y. Ghallab, W. Badawy, and K. Kaler, "A novel pH sensor using differential ISFET current mode read-out circuit," *International Conference on MEMS, NANO and Smart Systems (ICMENS)*, pp. 255–258, 2003.

[27] Y. Ghallab and W. Badawy, "A new differential pH sensor current mode read-out circuit using two operational floating current conveyor," pp. S1.5–13–S1.5–16, 2004.

[28] P. Pookaiyaudom, C. Toumazou, and F. Lidgey, "The chemical current-conveyor: a new microchip biosensor," in *IEEE International Symposium on Circuits and Systems (ISCAS)*, pp. 3166–3169, IEEE, 2008.

[29] B. Gilbert, "A new wide-band amplifier technique," *IEEE Journal of Solid-State Circuits*, vol. 3, no. 4, pp. 353–365, 1968.

[30] B. Gilbert, "Current-mode circuits from a translinear viewpoint: A tutorial," *In Chapter 2 of Toumazou, C., Lidgey, F.J. and Haigh, D.G. eds., Analogue IC Design: the current-mode approach*, pp. 11–91, 1990.

[31] M. Kalofonou and C. Toumazou, "ISFET based chemical gilbert cell," *Electronics Letters*, vol. 47, pp. 903 –904, 4 2011.

[32] M. Kalofonou, P. Georgiou, and C. Toumazou, "An ISFET based chemical gilbert cell," pp. 365–368, IEEE, 2011.

[33] P. Georgiou, *Chemical Bionics - A novel design approach using Ion Sensitive Field Effect Transistors*. PhD thesis, Imperial College London, London, 2008.

[34] J.-C. Chou and C.-N. Hsiao, "Drift behavior of ISFETs with a-Si: H-SiO_2 gate insulator," *Materials Chemistry and Physics*, vol. 63, no. 3, pp. 270–273, 2000.

Chapter 7

Conclusion

This thesis introduced the application of semiconductor technology for detection of DNA methylation based biomarkers, laying down the foundation of a Point-of-Care (PoC) system for the early screening of cancer. A proof-of-concept approach was developed using a CMOS based ion sensor, the ISFET, enabling the detection of DNA methylation using the methods of pH-PCR and pH-LAMP, with the latter to be applied on a commercially available fully integrated System-on-Chip platform. Furthermore, the concept of real-time ratiometric detection of DNA methylation was developed and demonstrated using novel low power interfaces, integrating both electrical and chemical front-ends under a Lab-on-Chip (LoC) set-up. A hardware efficient system, referred to as the "Methylation Cell", able to compute the ratio of DNA methylation is designed, allowing real-time sensing of pH signals originated from DNA reactions. In addition to this, a novel differential monitoring system capable for differential reaction monitoring of pH signals combined with gain tunability and drift reduction, termed the ISFET based Chemical Gilbert Cell, was developed, achieving ultra low power operation.

Through the developments in this thesis, we are now one step closer into realising the technological vision introduced in Fig. 1.2 of Chapter 1, which sees a future where early screening of cancer will occur at a genetic level at the GP clinic, revolutionising the current methods of prevention of this disease.

7.1 Contributions

Chapter 2 introduces the field of epigenetics focusing on its significant role in cancer development. Emphasis is given on the role of DNA methylation as one of the most studied epigenetic events, with aberrations in DNA methylation patterns been actively involved in gene silencing contributing in the processes of tumour initiation and progression. Events of hypermethylation in the promoter regions of genes responsible for tumour suppression are also correlated with frequently reported cancer cases, used as credible diagnostic markers. Furthermore, an overview is given on the frequently used methods for DNA methylation detection at a genomic or genome-wide level, followed by other novel approaches with varying sensitivities and limitations based on the principles of detection, combined with computational tools used for enhancing the methylation signal resolution, providing a deeper analysis on the methylation information. The chapter concludes with thoughts on the current needs of DNA methylation based detection systems and the potential of CMOS based semiconductor technologies to satisfy these needs, due to their capabilities for development of large scale fully integrated platforms.

Chapter 3 presents the theory and fundamental principles behind the Ion-Sensitive Field-Effect Transistor (ISFET) as a CMOS based solid-state ion sensor, which provides the sensing capability for DNA methylation detection, as was shown in Chapter 4. Analysis of the ISFET model and its pH sensitivity characteristics is then described, followed by the principle behind the weak inversion region of operation used for low power chemical sensing and efficient analogue computation.

Chapter 4 describes the proof-of-concept approach of using commercially available ion-sensitive semiconductor technology for DNA methylation detection using the method of pH-PCR under thermocycling conditions. In addition to this, the first ISFET based label-free approach for DNA methylation detection was developed using the method of pH-LAMP under isothermal conditions, with results being demonstrated in real-time using the CMOS based System-on-Chip (SoC) platform for DNA detection. The platform was tested in two tumour suppressor genes ($DAPK1$ and $p16$), generating a strong signal, allowing clear differentiation of methylated from unmethylated DNA on-chip, bringing real-time amplification and detection of DNA methylation into a perspective of methylation analysis of multiple genes under a multiplexed highly integrated semiconductor platform.

Chapter 5 introduces the concept of a ratiometric approach for detecting DNA methy-

lation using the "Methylation Cell", a novel ISFET based readout as part of a hardware efficient system fabricated in CMOS due to the advantages of miniaturisation and low cost of fabrication. The "Methylation Cell" was integrated with a LoC set-up, allowing real-time sensing of pH signals derived from two isolated microfluidic chambers of the LoC, while performing continuous computation of the DNA methylation ratio. This was achieved by utilising the "translinear principle", a current-mode circuit technique applied to weakly inverted ISFETs, thus enabling the multiplication and division of currents for the computational analysis of DNA methylation ratio. The signals derived from the ISFETs were originated from DNA reactions occurring in presence of methylated DNA while being compared to the signals obtained as a result of no reactions taking place due to the absence of methylated DNA, with the ratio being used as an indication of the level of methylation existent in genes of interest. The "Methylation Cell" had also an additional feature of a comparison block capable of giving a discrete answer on the output in the form of a boolean value when methylation levels exceeded a threshold, which could further be used for epidemiological identification of DNA methylation ratios in real-time, given the dynamic nature of DNA methylation as an epigenetic marker.

Chapter 6 proposed a low power current-mode approach in CMOS, the ISFET based Chemical Gilbert Cell, for continuous differential reaction monitoring of pH changes derived from DNA amplification reactions taking place as result of the presence of DNA methylation in a DNA sample. The system was integrated with a LoC set-up combined with a microfluidic assembly that could offer separate control of reaction measurements and analysis combined with gain tunability through the use of a programmable gain term, achieving amplification of the output signal of the sensing cell. With respect to some non-idealities of ISFETs such as drift and temperature variation, the system achieved drift reduction reaching a ratio of 100:1 in favour of the differential ISFET front-end, opposed to the single-ended drift and stability in temperature, making it ideal for monitoring of reactions that require temperature control, sensitivity of detection and good differentiation of the reaction's signal from the background noise.

7.2 Recommendations for Future Work

Future recommendations based on the contributions of this work are proposed in the following sections. These include the prospects of realisation of large scale arrays for DNA methylation detection and analysis as well as of ISFET based Chemical Gilbert Cell arrays

for gain tunability control of multiple cells.

7.2.1 Large scale arrays for DNA methylation detection

Cancer susceptibility is related to hypermethylation of specific genes. Also, hypermethylation of a particular gene is usually specific to more than one cancer types generated from more than one organ sites. Multiplexed integration of in parallel analysis of methylation-specific gene assays using arrays of ISFET sensors is one of the main future objectives towards the realisation of a portable, lab-free DNA methylation based assay for screening of DNA methylation levels of tumour specific genes. The number of genes analysed per cancer type may considerably increase the sensitivity of detection, therefore parallel investigation of the methylation status of multiple genes is a desired feature for the identification of the stage of tumour progression. This could contribute in applying a personalised and effective treatment to the patient which could thus increase the chances for a better therapeutic targeting and a guided therapy using the epigenetic profile of the patient.

To accommodate this need, a CMOS ISFET based high reaction throughput platform technology needs to be utilised using integrated circuits scaled in arrays, with each array consisting of ISFET sensors under a flow cell, creating individually controlled chambers, offering a fast and simple way to monitor nucleotide incorporations generated by separate methylation specific reactions. This, in combination with targeted sequencing of methylation of specific areas and the use of computational analysis tools, such as the DNA methylation ratio, may allow for high-throughput DNA methylation analysis of a large range of samples at a sequence-specific level, since methylated patterns would be already differentiated from the unmethylated ones using bisulfite based DNA sample analysis.

7.2.2 Clinical validation of the system

As soon as the large scale realisation of DNA methylation analysis and monitoring is achieved, we aim to clinically validate the use of this technology in case groups of patients with firstly confirmed diagnosed cancer of all stages (I-IV) using a panel of genes correlated to chosen cancer types. A control group would also be needed consisting of healthy subjects with no previous history of malignancy occurrence. This will enable the use of DNA methylation as a biomarker for cancer screening, providing with the information for the tumour status (indolent or aggressive) and dependent on its aggressiveness, the possibility

of a tumour metastasis.

Matters related to the integration of the step of sample preparation and DNA extraction in the lab-free platform are to be investigated as well. Also possible ways for fast processing of data collected from the detection results are to be considered to provide maximum clinical benefit during several phases of cancer screening.

7.2.3 ISFET based Chemical Gilbert Cell arrays

The ISFET based Chemical Gilbert Cell, as presented in Chapter 6, was developed for differential monitoring of two reactions sensed by two ISFET sensors. For each differential output produced as a result of a given reaction, a fixed gain term was set, with the potential for maximum differential output signal to be achieved while tuning the gain of the cell at a range of values. Fabricating arrays of ISFET based Chemical Gilbert Cells could thus contribute in tuning independently the gain terms of all cells while minimising device mismatches, enhancing and matching the sensitivity of detection per cell, per array while acting as a calibration mechanism. This could also compensate for common non-idealities of ISFETs such as drift given the cell's inherent advantage for drift reduction, as has been proven in Chapter 6. Such arrangement would bring great benefits for in parallel monitoring of DNA amplification reactions, enhancing the amplification-specific output signals thus positively affecting the detection resolution. Potential future integration with the "Methylation Cell" can also be investigated.

Appendix A

Publications arising from this thesis

Journal Papers

- M. Kalofonou, P. Georgiou, C.-P. Ou and C. Toumazou, "An ISFET based translinear sensor for DNA methylation detection," *Sensors and Actuators B: Chemical*, vol. 161, no. 1, pp. 156-162, 2012.

- M. Kalofonou and C. Toumazou, "Semiconductor technology for early detection of DNA methylation for cancer: From concept to practice," *Sensors and Actuators B: Chemical*, vol. 178, pp. 572-580, 2013.

- M. Kalofonou and C. Toumazou, "A low power sub-μW Chemical Gilbert Cell for ISFET differential reaction monitoring," *IEEE Transactions on Biomedical Circuits and Systems*, 2013, in press.

Electronic Letters

- M. Kalofonou and C. Toumazou, "ISFET based chemical Gilbert cell," *Electronics Letters*, vol. 47, no. 16, pp. 903–904, 2011.

Conference Papers

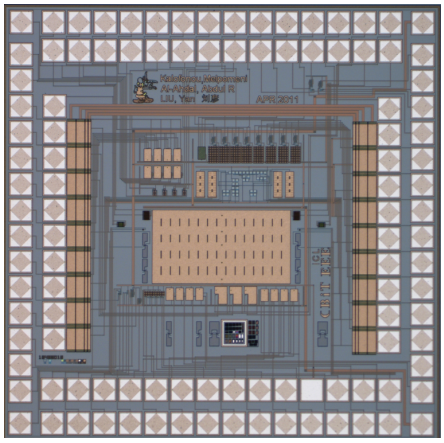
- M. Kalofonou, P. Georgiou and C. Toumazou, "An ISFET based Chemical Gilbert Cell," *IEEE Biomedical Circuits and Systems Conference (BioCAS)*, pp. 365–368, 2011.

Patent

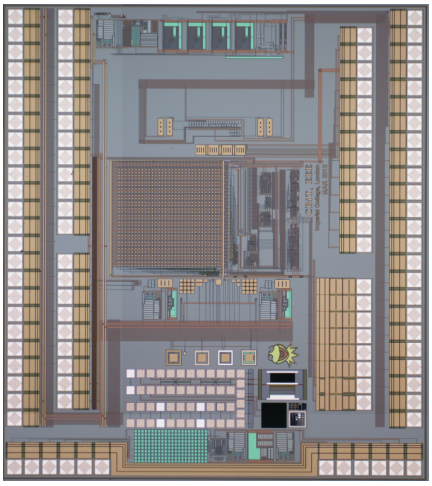
- C. Toumazou and M. Kalofonou, "Detection of methylated DNA," WO/2011/110873A1.

Appendix B

Fabricated Chips



AMS 0.35 µm
(1.73mm x 1.73mm)
Chemical sensor interface chip/Test
- Chemical Gilbert Cell
- "Methylation Cell"



AMS 0.35 µm
(2.5mm x 2.81mm)
Chemical sensor interface on a Lab-on-Chip
- Chemical Gilbert Cell
- "Methylation Cell"

Figure B.1: Chips fabricated during the course of this thesis.

Appendix C

CMOS ISFET Experimental set-up

For the device characterisation of the CMOS ISFET sensors, a semiconductor parameter analyser (Keithley 4200SCS) was used in combination with a switching matrix and three external source meter units as can be seen in Fig. C.1 or in more detail in Fig. C.2 for experiments where ISFETs were exposed in a common buffer solution.

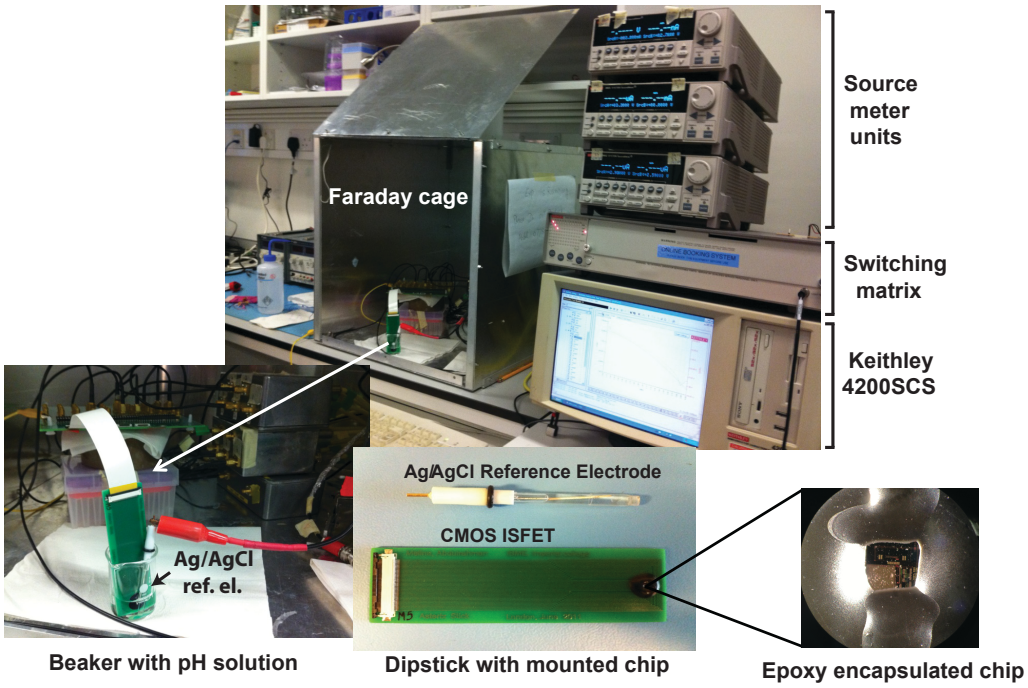


Figure C.1: Set-up for electrical characterisation of ISFETs using a glass beaker filled with pH buffer solution.

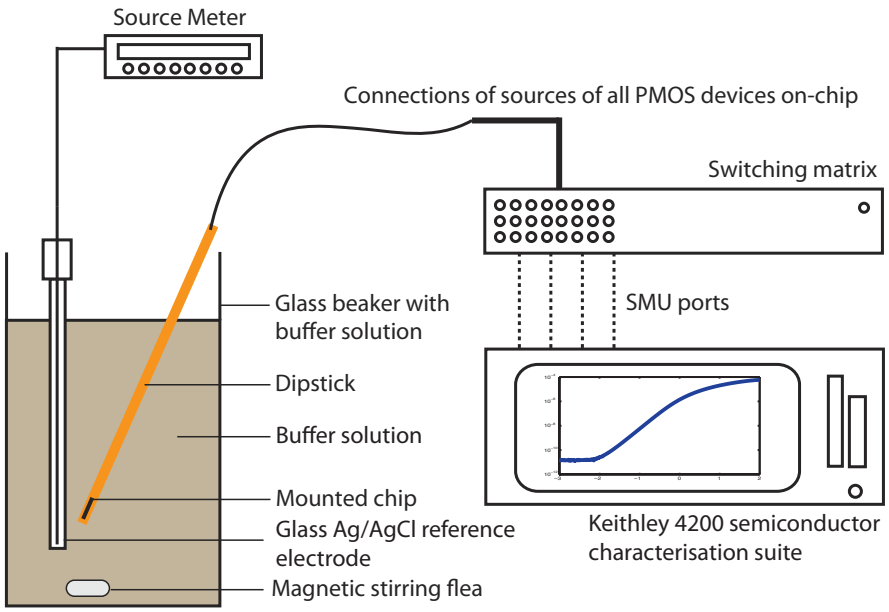


Figure C.2: Instrumentation set-up for electrical characterisation of ISFETs in a buffer solution.

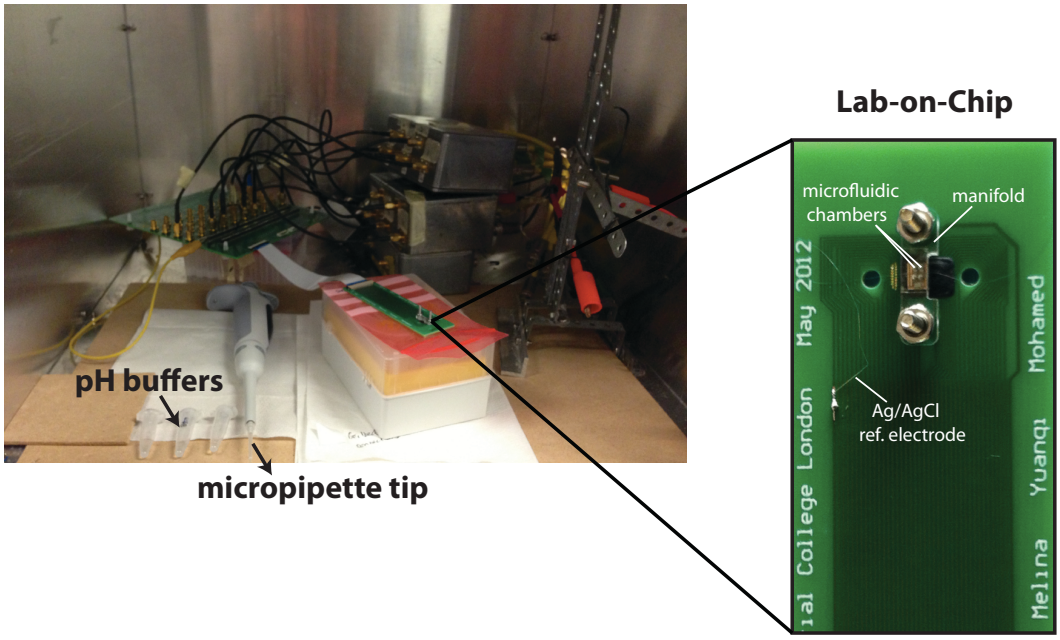


Figure C.3: Set-up for electrical characterisation of ISFETs using a microfluidic assembly in a Lab-on-Chip set-up.

The experimental set-up for the temperature stability test analysed in Section 6.6.6, Chapter 6 is shown below:

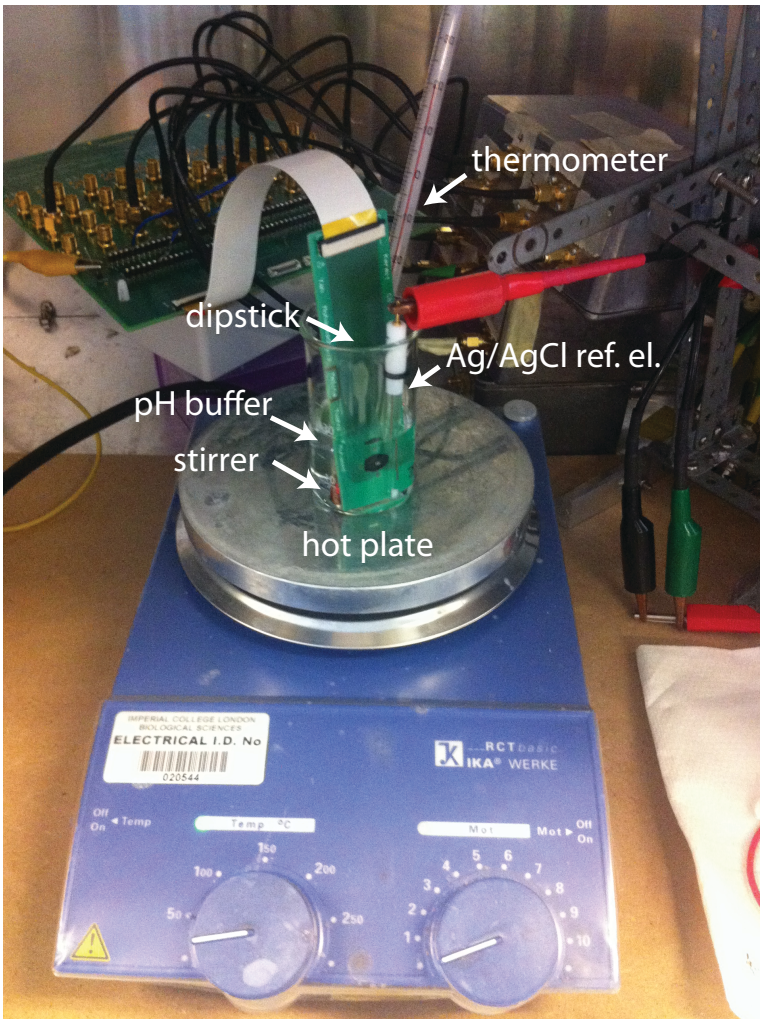


Figure C.4: Temperature stability experimental set-up

ISFET pH probe/Argus pH meter preparation

A pH measurement set-up consisting of a Sentron Argus pH-meter (Sentron Europe B.V.), in combination with a Sentron ISFET microelectrode (Sentron Europe B.V.) was used for the pH adjustments of the buffer solutions and DNA reaction mixtures in use during this thesis. Specifically, such a set-up was part of the experimental processes of pH-PCR and pH-LAMP as explained in Chapter 4 and for the electrical characterisation of ISFETs seen in Chapter 5 and Chapter 6.

Sentron pH microelectrodes have been reported to be very robust for laboratory use applications that involve highly accurate pH measurements of very small volumes, which can hardly be made by a conventional glass electrode, as well as fast and reliable for pH determination and temperature measurement. The Sentron sensing microelectrode is made of peek material, having a diameter of only 3 mm, with the measuring sensing part covering the tip of the electrode, a big advantage for small volume measurements. No inner buffer solution was used in that type of sensor design (Sentron Europe B.V.) compared to the conventional glass electrodes, with the whole microchip been embedded in plastic so that only the gate electrode would be in contact with the sample to be measured [1].

In more detail, the actual pH meter combines an ISFET pH sensor, a miniature Ag/AgCl reference electrode, a temperature sensor and a narrow tube [2], with the ISFET being able to monitor the pH of sample volumes. The coatings for the insulating layer of the pH sensor were Al_2O_3 based, as this has been reported to increase the selectivity of the sensor in $[H+]$ detection, and thus influencing the I_{DS} current, leaving the overall response of the pH probe directly related to the pH. This principle provides a considerably higher stability under light exposure and high electrostatic discharges.

Prior to the first use of the Argus system, the pH probe was placed in a buffer solution (preferably of pH 7.00) for 10 minutes, with the meter switched on, as an initiating time for the probe to set itself for use, therefore ensuring future stable readings. After the first use, it was advised by the manufacturer that the pH electrode was left dry, for an extended period of inactivity, or in saturated KCl solution for frequent use, so as to achieve maximum accuracy and stability in measurements. Prior to daily use, the pH meter was flushed with distilled water and then while laid on a soft sponge, it was cleaned with a soft toothbrush (provided with the Argus system), using a drop of a mild detergent, then rinsed again with distilled water and wiped using a soft cotton wipe. It was then placed in pH 7.00 for 10 min

(with the meter on) and was calibrated using pH buffers 7.00 and 4.00 at room temperature. Fresh buffer solutions were used for calibration to avoid any possibilities of contamination. Before calibration, the probe was rinsed with distilled water and then wiped. A 2-point calibration measurement was accordingly performed, using 2 buffers of close pH values. At first, a buffer solution of pH 7.00 was used, followed by a solution of pH 4.00, therefore targeting for increasing measurement accuracy over a certain pH range. After completing that step, the slope percentage was briefly displayed, with a resulting 98.0-105.0% slope (safe range), indicating that the probe is having the capability to perform at its maximum further on.

Appendix D

The multichannel pH-sensing SoC platform

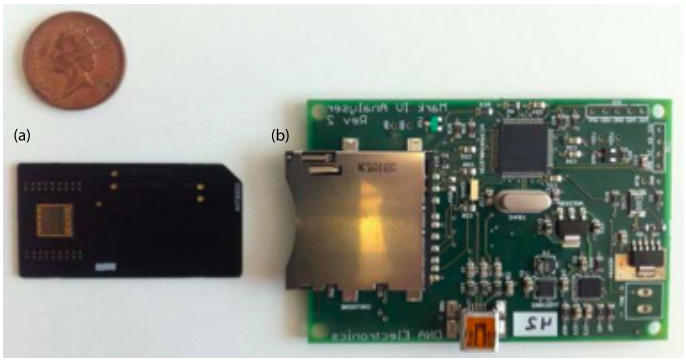


Figure D.1: The IC mounted on a test card (a) connected to an electronic analyser (b) [3]

The System-on-Chip (SoC) platform for DNA detection, as reported by [3, 4], consists of an integrated circuit combined with 40 ISFETs, 10 temperature sensors, heaters, signal processing and control circuitry all integrated on a single chip, fabricated using unmodified standard CMOS 0.35μm process. The Integrated Circuit (IC), sized 5.5mm x 4.8mm, is mounted on a disposable test card, as can be seen in Fig. D.1a, using an SD memory card format, connected to an electronic analyser, shown in Fig. D.1b, which is powering and controlling the IC, providing with a read-out interface for processing the reaction taking place on the CMOS chip, while transferring the results real-time to a tablet or PC. The IC is also combined with a microfluidic assembly through which the delivery of the reaction mixture for DNA amplification is performed through micro chambers and fitted access channels [3, 4].

Appendix E

DNA based methods

DNA separation - agarose gel electrophoresis

DNA separation was carried out by agarose gel electrophoresis using a $Power\ Pac^{TM}\ Bio-Rad$ unit in order to visualise the location of the small fragments of the base pairs of our DNA amplicon produced during a method of DNA amplification (i.e. PCR or LAMP), according to either one of the two universal templates (size markers), the $GeneRulerTM^{TM}$ $Low\ Range\ DNA\ ladder$ (25-700bp) or the $O'GeneRuler^{TM}\ Low\ Range\ DNA\ ladder$ (100-1000bp) (Thermo Fisher Scientific) [5, 6]. In most of the experiments the amplicon size that was expected to be seen was between 100 and 300bp and so the DNA ladder of the smaller bp range was preferred to be used when running the gel. What is more, a DNA loading dye was used, supplied by Thermo Fisher Scientific, combined with a $SYBR^{®}\ Green\ I$ nucleic acid gel stain, supplied by Invitrogen. Both the dye and the stain formed a loading buffer, giving colour and density to the sample, making it easy to be loaded into the wells. The dye is negatively charged in neutral buffers (TBE in our case) and thus moves in the same direction as the DNA (negatively charged) during electrophoresis, allowing us to monitor the progress of the gel. The more the voltage applied in the electrophoretic unit, the closer the fragments migrate in the gel.

1.8-2.0% agarose gels of around 100μl of 1xTBE buffer were employed, dependent on the experimental requirements. In each run, a gel was placed in a gel tank and submerged in 1xTBE buffer. 1μl of the DNA loading dye, for each sample, was mixed with a 10% of $SYBR^{®}\ Green\ I$ stain, of the relative loading dyes volume (most of the times the volume didnt exceed the amount of 0.1μl). The mixture of the loading dye and the $SYBR^{®}\ Green$

I stain was also added to the relative amount of the DNA ladder used (0.8-1.3μl). Then, 5μl of the DNA reaction mixture after PCR amplification or 0.5μl of the DNA reaction mixture after LAMP amplification (dependent upon the nature of the experiment) were added to the loading buffer. Upon mixing, the total volume of the sample mixtures was loaded into the wells of the gel. The gel was left running for around 12-15min with a constant voltage of 220-240V for PCR and around 20min with a constant voltage of 300V for LAMP. After checking that current was flowing in the gel tank, by checking the evolving gas (i.e. bubbles) in the tank, the gel was stopped when the blue loading dye had run 3/4 of the length of the gel. DNA bands from gel electrophoretic images were then visualised using a UV light-box and analysed using the image acquisition software *GeneSnap* [7].

Appendix F

Encapsulation Procedures

Epoxy Encapsulation

Epoxy encapsulation was used for the AMS 0.35μm technology die. The die was glued, using EPO-TEK H20E conductive epoxy on a commercially manufactured printed circuit board as shown in Fig. C.1. It was wirebonded using a 25μm wire consisting of 99% aluminium and 1% silicon. The bonded die was then encapsulated using glob topping epoxy by EPO-TEK (Ref: T7139), with only the chemically sensitive areas being exposed. The epoxy was cured in the oven at 120^{o}C for 60 minutes.

Appendix G

Supplementary Material

G.1 Chemical Gilbert Cell: Supplementary Experiments

Fig. G.1 shows supplementary results on the experimental analysis conducted in Fig. 6.21, Section 6.6.3, Chapter 6. These illustrate the transient response of the Chemical Gilbert Cell differential output I_{out} for different values of I_{gain} for 4 pH steps confirmed after three repeats. The 3rd repetition may not be entirely credible due to the evaporation of the solution in the reaction chambers.

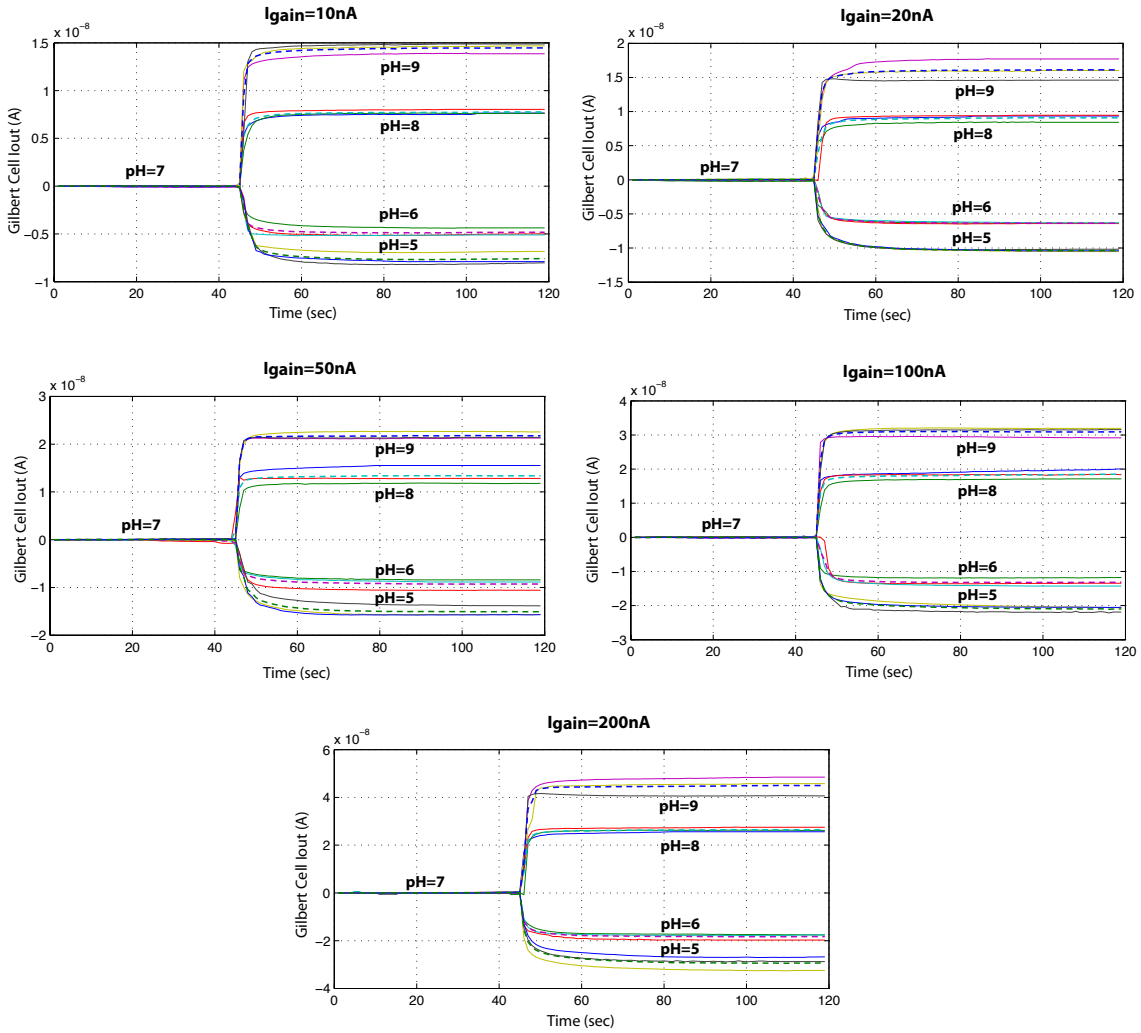


Figure G.1: Transient response of the Chemical Gilbert Cell's differential output I_{out} for different values of I_{gain} following 4 pH step changes. In both chambers a buffer of pH 7 was initially induced giving a differential output current of 0nA, followed by a step change of pH when pH buffers of 5, 6, 8 and 9 were induced. The experimental results shown are confirmed after three repeats. The average value is also displayed as a dotted line.

G.2 Ratiometric method: Supplementary Experiments

G.2.1 Voltage-mode switching

Fig. G.2 and Fig. G.3 show the results of voltage-mode switching for ascending and descending values of I_{perc} within the range of 1nA to 10nA, with both I_{meth} and I_{unmeth} fixed at 10nA and I_{gain} at 10nA. The point of switching of the inverter is indicated in both figures with the values of I_{ratio} been highlighted.

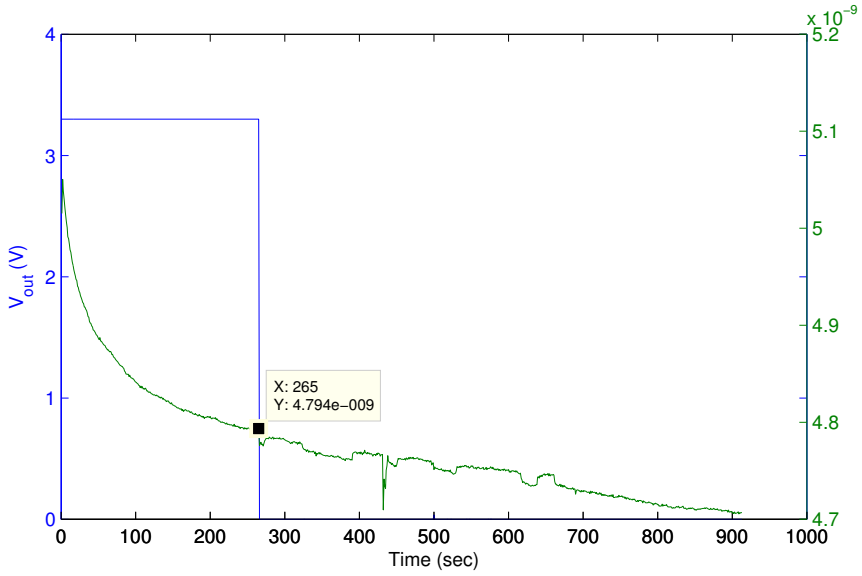


Figure G.2: Transient response of the voltage output, V_{out}, of the inverter and the current output, I_{ratio}, of the translinear cell in pH 7, for varying ascending values of I_{perc} starting from 1nA up to 10nA.

What is more, the transient response of the inverter, V_{out}, with respect to changes in I_{ratio} as results of changes in I_{meth} is shown in Fig. G.4. I_{perc} was set at 4.7nA based on the information acquired from the two previous experiments. As I_{meth} varies from 10nA to 40nA, the inverter switches after a delay, with the switching point indicated in the figure. After a period of some seconds, I_{meth} decreases from 40nA to 10nA and similarly the inverter switches with a relative delay. This shows that there was not given enough time to the node of the inverter to discharge, providing with a delay during switching.

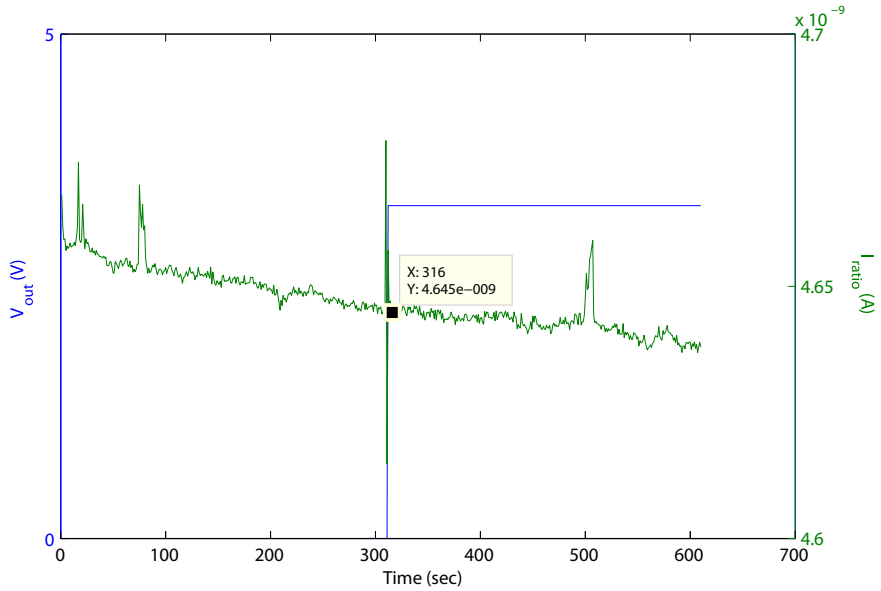


Figure G.3: Transient response of the voltage output, V_{out}, of the inverter and the current output, I_{ratio}, of the translinear cell in pH 7, for varying descending values of I_{perc} starting from 10nA down to 1nA.

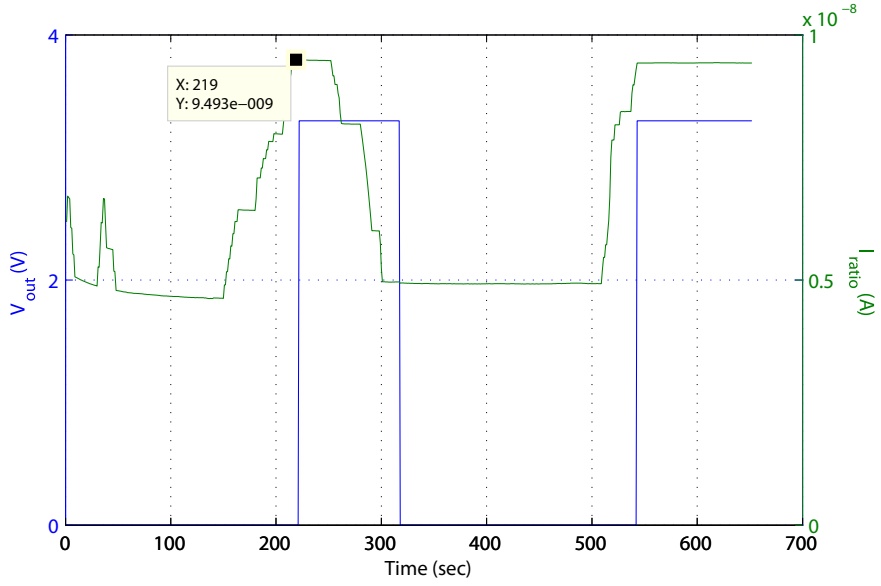


Figure G.4: Transient response of the voltage output, V_{out}, of the inverter and the current output, I_{ratio}, of the translinear cell in pH 7, while I_{meth} is electrically tuned from 10nA to 40nA and back to 10nA, for a given I_{unmeth}=10nA for an I_{gain} of 10nA.

G.2.2 I_{ratio} computation during pH 7-9

Shown is a supplementary table on the experimental analysis conducted in Section 5.5.2, Chapter 5. Additional experiments on the computation of I_{ratio} and I_{meth} with I_{unmeth} being constant were monitored during ascending and descending pH steps (pH 7-9) following two repeats, similar to the ones displayed in Table 5.4. This example is to show how I_{ratio} was affected by drift due to the lack of time given to the ISFETs to 'burn in' during the pH test.

Table G.1: Results of average and standard deviation values of two repeats of I_{ratio}, I_{meth} under given I_{unmeth} values during ascending and descending pH steps from pH 7 to pH 9 showing the effect of drift on I_{ratio}.

	pH=7	pH=8	pH=9	pH=8	pH=7
I_{meth}(nA)	100	113.5±0.707	132.5±4.949	122±5.656	105.5±6.363
I_{unmeth}(nA)	100	96.5±0.707	95±	93.5±0.707	91±
I_{ratio}(nA)	49.5±0.707	53±1.414	57.5±0.707	56±1.414	53±1.414

References

[1] "Sentron integrated sensor technology." [Online]. http://www.sentron.nl/.

[2] I. Schaepman, "pH measurement using ISFET technology," *Sentron Europe B.V-LabPlus International*, 2005.

[3] C. Toumazou, L. Shepherd, S. Reed, G. Chen, A. Patel, D. Garner, C.-J. Wang, C.-P. Ou, K. Amin-Desai, *et al.*, "Simultaneous DNA amplification and detection using a pH-sensing semiconductor system," *Nature Methods*, vol. 10, no. 7, pp. 641–646, 2013.

[4] D. Garner, H. Bai, P. Georgiou, T. Constandinou, S. Reed, L. Shepherd, W. Wong, K. Lim, and C. Toumazou, "A multichannel DNA SoC for rapid point-of-care gene detection," pp. 492–493, 2010.

[5] "Thermo Fisher Scientific: GeneRuler Low Range DNA Ladder 25-700 bp." [Online]. Available: http://www.thermoscientificbio.com, May 2013.

[6] "Thermo fisher scientific: O'GeneRuler DNA Ladder, Ready-to-Use 100-1000 bp." [Online]. Available: http://www.thermoscientificbio.com, May 2013.

[7] "Syngene: Image acquisition software *GeneSnap*." [Online]. Available: http://www.syngene.com/GeneSnap, May 2013.